CYCLODEXTRIN-BASED SUPRAMOLECULES

AS POTENTIAL MOLECULAR DEVICES

A thesis submitted for the degree of

Doctor of Philosophy of the Australian National University by

Lisa Randone

Australian National University

Research School of Chemistry

September 2021

AUTHOR'S DECLARATION

This is to declare that the work in this thesis represents original work that I have undertaken during my Ph.D. degree at the Research School of Chemistry, the Australian National University from 2014 to 2021, except that the crystal structures reported in Chapter 4 were obtained, solved and refined by Dr Michael Gardiner and Dr Paul D. Carr at the Australian National University. The conductivity experiments were carried out by me at Advanced Industrial Science and Technology (AIST) in Japan under the supervision of Dr Nobuko Fukuda.

To the best of my knowledge, the thesis does not contain material that has been published or written by another person or accepted for the award of any other degree or diploma in any other university or tertiary institution, unless due reference has been made in the text. All figures that do not cite permission to publish are my own work.

I give consent to this copy of my thesis, when deposited in the University library, being available for loan or photocopying.

Lisa Randone

September 2021

ACKNOWLEDGEMENTS

First and foremost I would like to express my sincere gratitude to Professor Chris Easton, who gave me the opportunity of undertake a Ph.D. in Australia. He has supported my project by sharing his knowledge in an accessible way and by enhancing the results of my research in a scientific context. On top of that, he has allowed me to extend my knowledge by supporting the undertaking of research experiments overseas.

I would also like to thank several individuals in the Easton group. Dr Hideki Onagi has been my mentor throughout my research project, which would not have been possible without his tireless assistance. Dr Lee Alissandratos has been an invaluable source of personal and scientific advice. I am honoured to have shared this experience with talented chemists, including Charlotte, Tom, Jeremy, and Louis and I am glad I was able to develop strong friendships with my group mates, in particular with Somayeh and Feiyu, who were at my side in the final stages of my research project.

I am grateful for the technical assistance I have received from the RSC staff, including Daniel Bartkus, Anithahini Jeyasingham, Chris Blake, Dr Anthony C. Willis, Dr Michael Gardiner, and Dr Paul Carr, and from other scientists I've been fortunate to work with, such as Dr Daniel Fankhauser and Dr Nobuko Fukuda.

I also wish to thank my friends in Canberra, who provided a much needed distraction from my Ph.D. studies.

Finally, special thanks to my family, in particular mum and dad for their constant confidence boost, Davide for his unconditional love, endless patience and support, and Kobe for his therapeutic smiles. Their encouragement really helped me out in this challenging journey.

ABSTRACT

The work presented in this Thesis focuses on the synthesis of cyclodextrin-based supramolecules and the investigation of their potential as molecular devices.

Daisy chains were initially targeted as a promising platform to build extended molecular muscles. Chapter 2 presents the synthesis of an oligomeric series of interlocked, cyclodextrin-based [*c*2]daisy chains through an innovative approach based on the direct self-assembly of cyclic dimeric complexes. The isolation and characterization of eight oligomeric species from this one pot reaction, as well as the photo-switching behaviour of some of these compounds, are discussed in this Chapter.

The next phase of this research was focused on rotaxanes because of their crucial role in the development of molecular devices. In particular, isomeric rotaxanes, generally resulting from the capping of an inclusion complex between an asymmetric macrocycle and a mono-capped guest, can exhibit different properties depending on the orientation of the host. Chapter 3 describes a complementary synthetic approach based on the desymmetrization of a pre-formed rotaxane. This work includes the synthesis of an α-CD [2]rotaxane and the subsequent preparation, separation and characterization of bromine-functionalised orientational isomers.

Finally, the behaviour of cyclodextrin-based rotaxanes as insulated molecular wires is investigated in Chapter 4. This work involved the discovery of the conductivity behaviour of crystals of two different α-CD rotaxanes showing π-π stacking aggregation in solution and in solid phase. The comparison with a blank experiment consisting of an α-CD crystal, the investigation of insulating properties of one of the rotaxanes, and some preliminary co-crystallisation experiments are also discussed as part of this study. This work identified the ability of self-assembled arrays of cyclodextrin-based rotaxanes to act as insulated molecular wires resembling coaxial cables.

Overall, this Thesis describes new synthetic approaches to prepare daisy chain oligomers and [2]rotaxanes and develops their respective abilities to act as molecular muscles and microelectronic devices.

ABBREVIATIONS

δ	chemical shift (ppm)
λ_{max}	wavelength absorption maximum
ρ	resistivity
σ	conductivity
Ω	ohm
°C	degrees Celsius
2D	two-dimensional
Å	angstrom
A	cross sectional area
*a*n	acyclic, n= number of repeating units
approx.	approximately
ATP	adenosine diphosphate
AU	arbitrary unit
azo	azobenzene
C	concentration
ca.	circa
calcd	calculated

CD	cyclodextrin
CD_3OD	deuterated methanol
$(CD_3)_2SO$	deuterated dimethyl sulfoxide
*c*n	cyclic, n= number of repeating units
COSY	correlation spectroscopy
CuAAC	copper(I)-catalysed azide–alkyne cycloaddition
d	diameter
D_2O	deuterated water
DCM	dichloromethane
dec.	decomposition
DFT	density functional theory
DMSO	dimethylsulphoxide
DMT-MM	4-(4,6-dimethoxy-1,3,5-triazin-2-yl)-4-
DNA	deoxyribonucleic acid
ESI	electrospray ionisation
et al.	et alia
Et_3N	triethylamine
EtOAc	Ethyl acetate
g	gram

h	hour
H	proton
HPLC	high performance liquid chromatography
HR	high resolution
HZ	hertz
I	current
ICD	induced circular dichroism
Id	source–drain current
IMW	Insulated molecular wire
IV	current-voltage
J	coupling constant
lit.	literature
l	lenght
M	moles per litre
M^+	molecular ion
MALDI	matrix assisted laser desorption ionization
Me	methyl
MeCN	acetonitrile
MeOH	methanol

MIM	mechanically interlocked molecule
mg	milligram
min	minutes
mL	millilitres
mol	moles
m.p.	melting point
MS	mass spectrometry
m/z	mass-to-charge ratio
nm	nanometre
NMR	nuclear magnetic resonance
NOE	nuclear overhauser effect
NOESY	nuclear overhauser effect spectroscopy
NP	nanoparticle
OFET	organic field effect transistor
PDV	poly(4,4′-diphenylene vinylene)
PF	polyfluorene
PM α-CD	permethylated α-cyclodextrin
ppm	parts per million
PPP	poly(*para*-phenylene)

R	resistance
R_f	retention factor
ROESY	rotating-frame Overhauser effect spectroscopy
RT	room temperature
S	siemens
THF	tetrahydrofuran
TFA	trifluoroacetic acid
TLC	thin layer chromatography
TOF	time-of-flight
t_R	retention time
UV-vis	ultraviolet-visible
v	volume
V	voltage
Vg	gate voltage
Vd	drain voltage
w	weight

CONTENTS

Chapter 1 - INTRODUCTION

1.1 Molecular devices and machines

Technological progress relies on the invention of novel devices; however, the progressive trend of miniaturization results in the necessity of producing always smaller components.[1] This method, called the "top-down approach", has severe limitations for dimensions smaller than 100 nm; therefore, as an alternative strategy for the construction of nanoscale devices, chemists have developed the "bottom-up approach", where molecules are used as building blocks to produce nanostructures[2] (Figure 1.1).

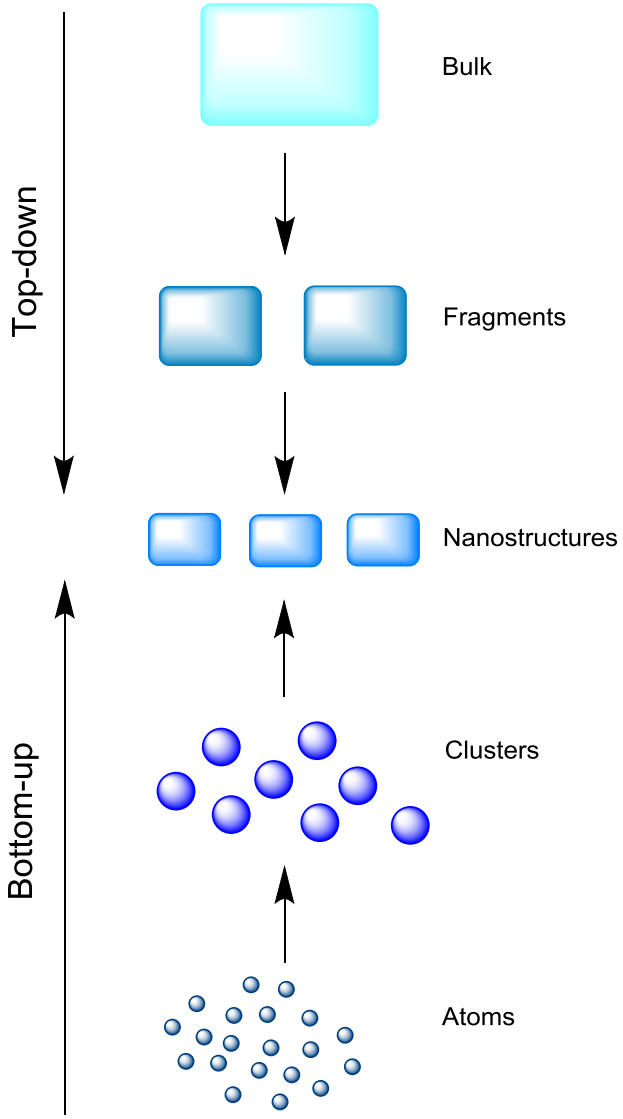

Fig. 1.1. Schematic representation of top-down and bottom-up approach.[3]

The concept of macroscopic devices operating in the real world can therefore be applied at the molecular level by adopting the molecule-by-molecule bottom-up strategy to design and synthesize chemical species able to perform specific functions.[4] Accordingly, a molecular device can be defined as an assembly of a variety of molecular components designed to perform a particular task. Each

component is responsible for a single act, and the cooperation of various components allows the whole system to realize a more complex function.[5]

Molecular machines are a subset of molecular devices, as they are functional molecular systems in which a controlled mechanical motion, activated by an external stimulus, allows a task to be performed.[6] According to this definition, undoubtedly, nature provides the most astonishing examples of molecular machines.[7] A number of biological systems can perform specific actions in response to certain biological stimuli.[8] The contraction of human muscles, for instance, is driven by the motion of cytoplasmic proteins, such as myosins, kinesins and dyesins, along acting filaments.[9] Furthermore, the synthesis and hydrolysis of adenosine 5′-triphosphate (ATP) is performed by ATP synthase through a unique rotatory motion.[10] On the basis of their motion-derived function, those two biological systems are defined as molecular motors and they represent the most extensively studied examples of molecular machines in nature.[11] In addition to molecular motors, other biological molecular machines, including helicases[12] and ribosomes,[13] exist when multiple movable parts in a biological system are specifically interlocked to achieve a directed motion. These biological molecular machines, as well as any chemical species connected by intermolecular bonds forming complex structurally organized and functionally integrated architectures, are the bedrock for what is now called “supramolecular chemistry”.[14]

1.2 Supramolecular chemistry

The first steps towards supramolecular science were taken in 1894 by Emil Fischer, who proposed the lock and key fit as a prerequisite to initiate a chemical reaction between an enzyme and a glycoside.[15] However, it was not until approximately forty years later that the concept of "Übermoleküle", literally supermolecule (or supramolecule), was introduced to describe the association of higher organization species.[16] Enormous advances in the field were then achieved by Charles J. Pedersen,[17] Jean-Marie Lehn[18] and Donald J. Cram[19] at the end of the 1960s and the beginning of the 1970s, with their pioneering studies on non-covalent interactions in host-guest chemistry. The impact of their work on the scientific community was recognised in 1987 with the award of the Nobel Prize in Chemistry. Inspired by the meaning of the Latin word *supra*, Jean-Marie Lehn firstly defined supramolecular chemistry in 1988 as "chemistry beyond the molecule", referring to the science that studies the association of chemical species by non-covalent interactions. Since then, supramolecular science has been a significant stimulus for chemists, leading to a further Nobel Prize in Chemistry in 2016, granted to Fraser Stoddart, Jean-Pierre Sauvage and Bernard Feringa, for their outstanding work on advanced molecular machines.[20] Being inspired by the variety of interactions governing nature, supramolecular science continues to attract much interest from a theoretical point of view, but it also shows promising applications in experimental chemistry.[14b, 21]

One of the main features characterising most supramolecular species is molecular recognition, which was defined by Jean-Marie Lehn in 1973 as "a process involving both binding and selection of substrate(s) by a given receptor molecule, as well as possibly a specific function".[22] Based on this concept, the arrangements of molecules and their related functions play a key role in the understanding of the potential of supramolecular species. Molecular recognition relies, for instance, upon self-assembly interactions. The self-assembly process involves different chemical species in equilibrium adopting the most energetically favoured arrangement through non-covalent, reversible interactions. The main intermolecular forces participating in the formation of self-assembled complexes are hydrogen bonding, electrostatic interactions, and Van der Waals forces. DNA base pairing represents an ideal example in nature showing molecular recognition based on self-assembly, being the DNA double helix held together by hydrogen bonds[23] (Figure 1.2).

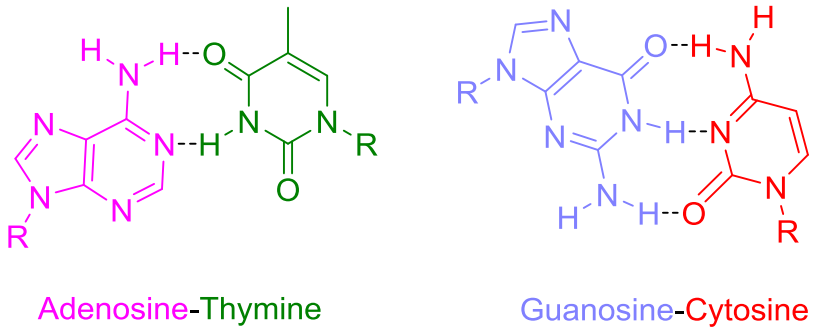

Fig. 1.2. Examples of hydrogen bonding between DNA bases.

Based on the molecular-level understanding of biological events, self-assembly and molecular recognition can be utilised to build supramolecular species and artificial molecular machines.[7, 24]

1.3 Cyclodextrins

Macrocycles are key building blocks in the construction of many supramolecular species. Among other macrocycles, cyclodextrins (CDs) have been widely adopted to synthesize molecular devices because of their selective self-assembly and molecular recognition properties. Initially observed in the bacterial fermentation of potato starch by Antoine Villiers in 1891,[25] CDs rapidly became of significant interest as building blocks for supramolecular chemistry. Their structure, consisting of D-(+)-glucopyranose units 1,4-α-linked in a cyclic oligosaccharide, was elucidated by Karl Freudenberg and Fritz Cramer in 1948.[26] α-CD, β-CD and γ-CD, composed of 6, 7 or 8 subunits respectively, are the most common CDs. As shown in Figure 1.3, their toroidal structure exhibits all the primary hydroxyl groups in the narrower end of a truncated cone (primary face), while secondary hydroxyl groups are located on the wider side of the cone (secondary face). All carbons of each glucopyranose ring are conventionally numbered from 1 to 6 in a clockwise direction.

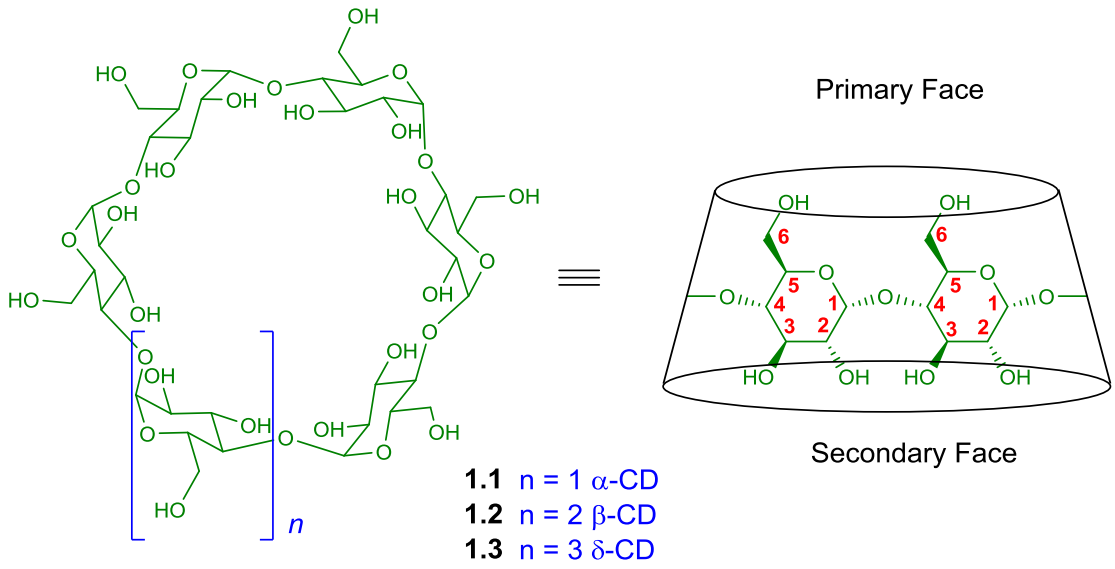

Fig. 1.3. Chemical structure of α-cyclodextrin **1.1**, β-cyclodextrin **1.2**, and γ-cyclodextrin **1.3** (left) and the schematic representation of a cyclodextrin as truncated cone (right).

Although CDs are soluble in water because of their hydrophilic exterior, the hydrogens linked to C3 and C5, as well as the ether-like oxygens, generate a less hydrophilic cavity. This feature provides CDs with the ability to host hydrophobic molecules to form inclusion complexes in aqueous media. This complexation process is enthalpically favoured due to the displacement of water molecules around the guest and within the cyclodextrin cavity (Figure 1.4).

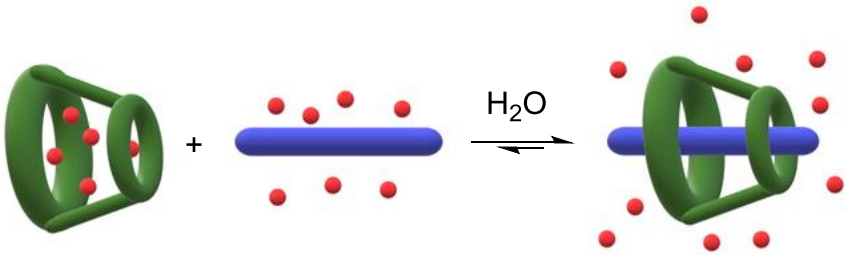

Fig. 1.4. A cartoon representation of a hydrophobic guest (blue) forming an inclusion complex with the hydrophobic cavity of a cyclodextrin (green) resulting in the displacement of water molecules (red).

CD inclusion complexes have been employed in a wide range of industrial processes and everyday products, including food, pharmaceuticals, cosmetics, agriculture and toiletries;[27] however, they are also becoming increasingly popular among supramolecular chemists for the construction of supramolecular structures and devices.[28]

1.4 Supramolecular species to build artificial molecular machines

Inspired by the performance of molecular machines in nature and with the aim of reproducing their behaviour, significant efforts have been made to design artificial molecular machines.[7, 24, 29] The first step towards the invention of artificial molecular machines was arguably taken in 1827 by the Scottish botanist Robert Brown, who observed under a microscope the incessant, irregular motion of small particles within pollen grains suspended in water.[30] The theory behind this

phenomenon, now known as Brownian motion,[31] was described in 1905 by Albert Einstein, who provided the kinetic explanation of the bombardment of particles by molecules causing the motion.[32] His theory was experimentally confirmed by Jean Perrin in 1923.[33] The understanding of the interplay between thermodynamic laws and Brownian motion led to an increasing awareness of the potential that synthetic molecular machines might hold.

A further achievement towards the construction of artificial molecular machines was the discovery of mechanically interlocked molecules (MIMs).[34] Catenanes and rotaxanes are arguably the best known examples of MIMs.[21a] The term catenane derives from the Latin word *catena*, meaning chain and, indeed, a catenane consists of a chain-like assembly of two or more macrocycles (Figure 1.5).[35]

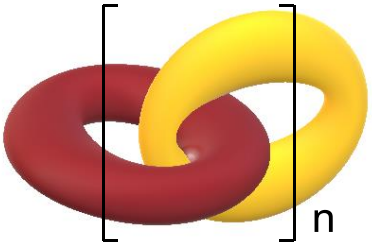

Fig. 1.5. A cartoon representation of a catenane.

One of the most remarkable examples of a catenane was provided in 1994 by two postdoctoral researchers, Anatoly Reder and David Amabilino, who synthesized a

pentacetenane and named it “olympiadane”, resembling the well-known symbol of the International Olympics (Figure 1.6).[36]

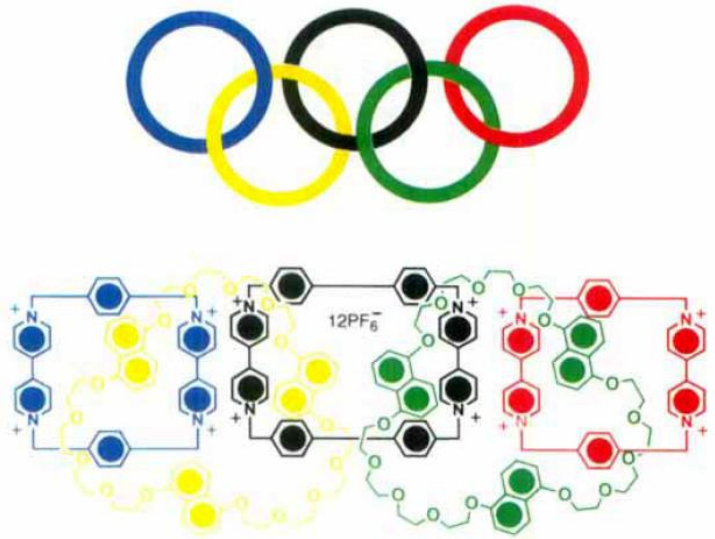

Fig. 1.6. The symbol of the International Olympics (top) and the structure of olympiadane (bottom).[36] Reproduced with permission from John Wiley and Sons.

Much longer polycatenanes have been prepared over the last few years. For example, in 2019 Taishi Higashi reported the synthesis and isolation of β-CD-based radial polycatenanes with over 10 cyclic components (Figure 1.7).[37]

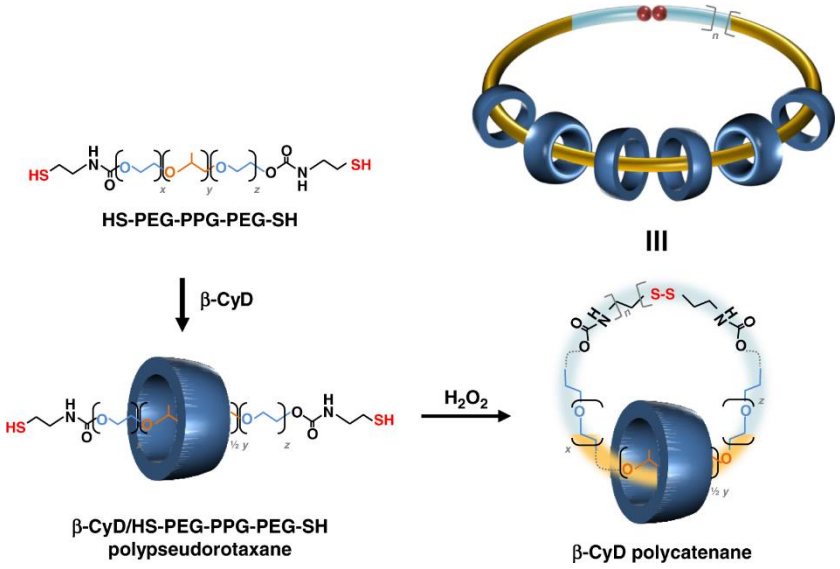

Fig. 1.7. Preparation of a β-cyclodextrin-based polycatenane.[37] Reproduced with permission from Springer Nature.

Catenanes have been employed in the construction of different molecular machines and switches. For example, David A. Leigh and his group designed a catenane-based molecular rotor, showing that sequential and unidirectional rotation of the rings forming a catenane can be induced in mechanically interlocked assemblies where one or two small rings move around one larger ring (Figure 1.8).[38]

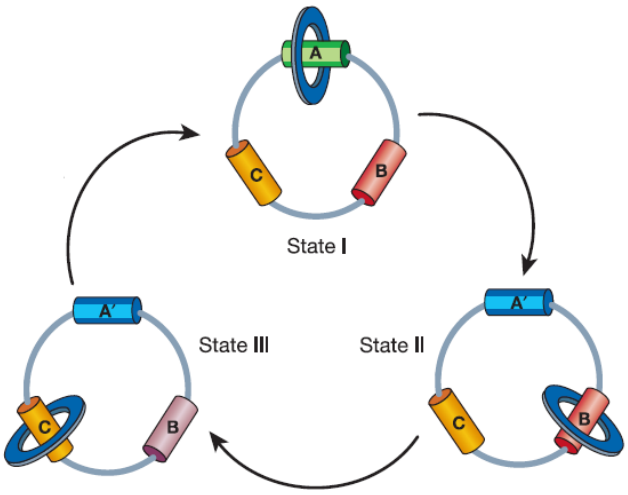

Fig. 1.8. Sequential movement of a macrocycle between three different binding sites in a [2]catenane.[38] Reproduced with permission from Springer Nature.

Pseudorotaxanes and rotaxanes are also considered key platforms to build artificial molecular machines. Deriving from the combination of the Latin words *rota* for wheel and *axis* for axle, these supramolecular structures are composed of a guest included in a macrocyclic host. As shown in Figure 1.9, rotaxanes are completely interlocked systems, where the macrocycle is trapped around a linear guest by bulky blocking groups, while pseudorotaxanes, according to the meaning of the prefix *pseudo*, are considered false rotaxanes due to the lack of big stoppers preventing the dethreading of the cyclic component that could occur under certain conditions, such as heating/cooling, irradiation, electrochemical stimuli, and/or solvent polarity changes.[39]

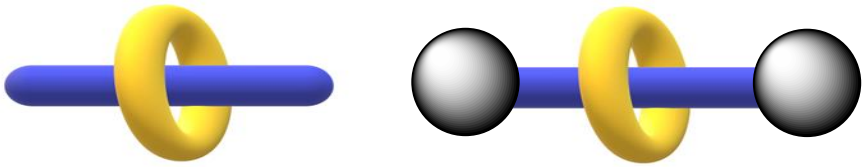

Fig. 1.9 Cartoon representation of a pseudorotaxane (left) and a rotaxane (right).

These compounds attracted interest among synthetic chemists in the late 1960s as an academic curiosity;[40] however, their appeal rapidly increased in the following years,[39] due to their large range of applications, including their ability to carry smaller molecules in their cavity. Unlike simple nano-carriers, rotaxanes and pseudorotaxanes can be used to build stimuli-responsive controlled release systems that are able to respond to intracellular environmental changes and external stimuli.[41] Starting from the statistical threading method introduced in 1967 by Ian T. Harrison and co-workers,[42] a number of synthetic techniques have been developed to prepare rotaxanes and pseudorotaxanes.[43]

Pseudorotaxanes are typically synthesized through direct self-assembly. For example, in 1991, Fraser Stoddart's group reported the preparation and characterization of a [2]pseudorotaxane consisting of a tetracationic cyclophane and a linear polyether, where the formation of the host-guest complex was driven by π-π stacking interactions between the bipyridinium units of the macrocycle and the axle and the hydroquinone ring of the axle, as well as by electrostatic edge to face interactions occurring within the cyclophane.[44] In more recent studies, CD-

based pseudorotaxanes have been incorporated in more complex structures, such as hydrogels,[45] nanofibers,[46] and polymer matrices.[47] The latter application was recently described by Sergii Sinelnikov,[47] who used β-CD pseudorotaxanes attached to polyacrylamide chains to build polymer cross-linked matrices (Figure 1.10), which demonstrated optimal drug release properties when 10 wt% β-CD-pseudorotaxane was included in the structure.

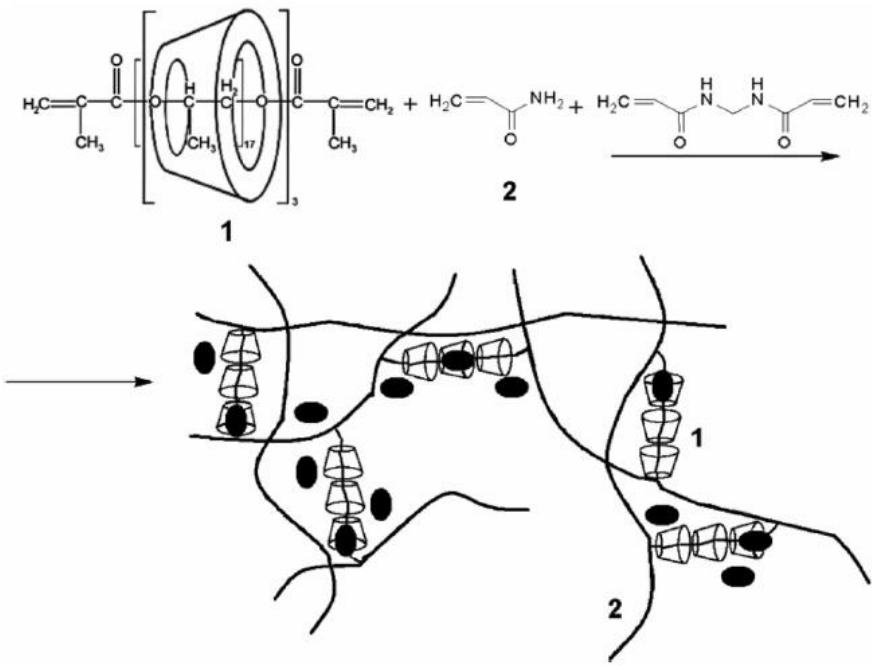

Fig. 1.10 Scheme for preparing polymeric matrices based on β-cyclodextrin pseudorotaxanes.[47] Reproduced with permission from John Wiley and Sons.

The wide application of pseudorotaxanes relies on their ability to perform different functions, such as in fluorescent sensors,[48] molecular logic gates,[49] molecular loops[50] and, most commonly, molecular switches.[51] In particular,

pseudorotaxanes enable two types of mobility under external stimuli. As illustrated in Figure 1.11, the host can either dissociate from the guest due to the lack of stoppers at the ends of the thread, or shuttle between two different stations of the axle due to changes in its interaction with the guest's binding sites. [39]

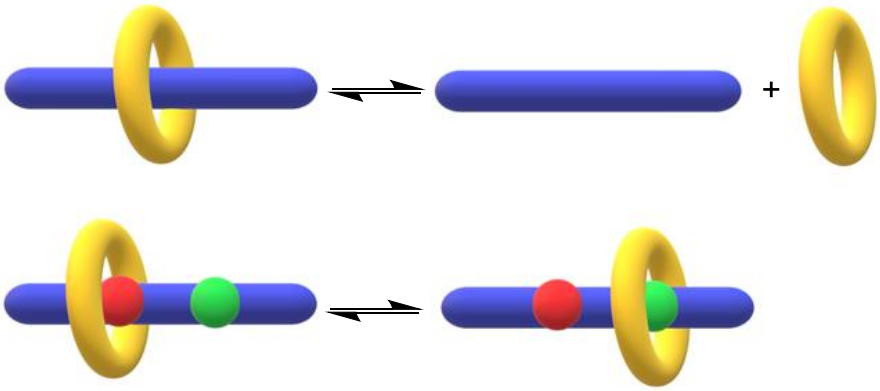

Fig. 1.11. Cartoon representation of two types of molecular mobilities of pseudorotaxanes: association/dissociation (top), and shuttling between two stations of the axle (bottom).

Fraser Stoddart's group, for instance, studied the switching behaviour of pseudorotaxanes attached to gold nanoparticles (AuNPs). The work showed that the ring reversibly associated or dissociated with the linear π-electron-rich recognition sites attached to the AuNPs upon addition of $Fe(ClO_4)_3$ or ascorbic acid (Figure 1.12).[52]

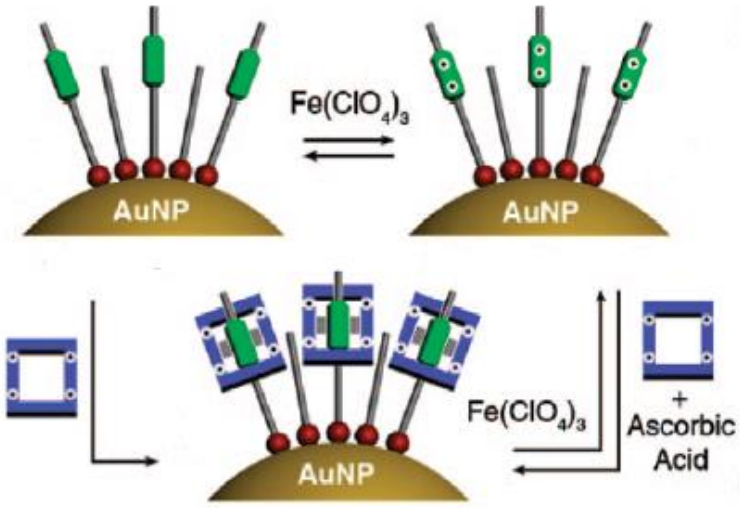

Fig. 1.12. Association and dissociation of pseudorotaxanes on a gold nanoparticle.[52] Reproduced with permission from the American Chemical Society.

An example of a pseudorotaxane exhibiting shuttling behaviour was provided by Wei Wu a few years ago.[53] In this system, the protonation and deprotonation of the terminal carboxylates of the linear guest promotes the shuttling of a cucurbit[7]uril macrocycle along a bispyridinium ethylene axle (Scheme 1.1).[53]

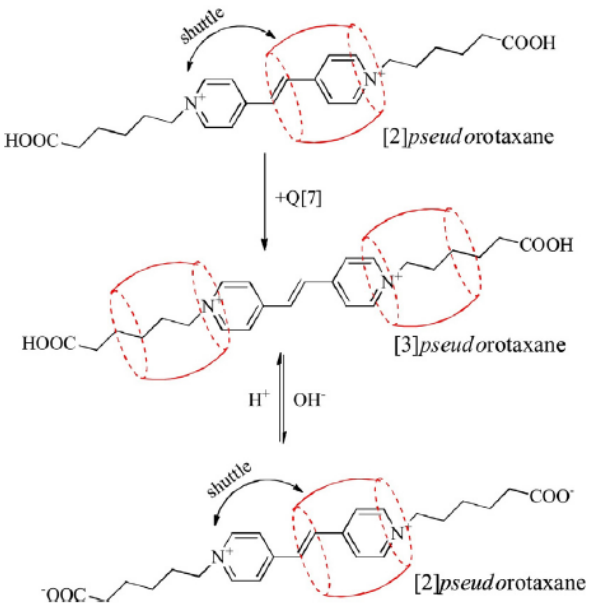

Scheme 1.1. Schematic representation of the shuttling of a cucurbit[7]uril wheel along the axle of a pseudorotaxane.[53] Reproduced with permission from Elsevier.

Great strides have also been made in the synthesis of rotaxanes by studying the interactions involved in their formation. These include metal-ion coordination,[54] π–π stacking,[55] hydrogen bonding,[56] hydrophobic interactions,[57] and anion templates.[58] However, the copper(I)-catalysed azide–alkyne cycloaddition (the CuAAC 'click' reaction) represents a breakthrough in rotaxane synthesis.[59] In this method, copper(I) catalyses the reaction between an alkyne and an azide to form a 5-membered heteroatom ring (Scheme 1.2).[60]

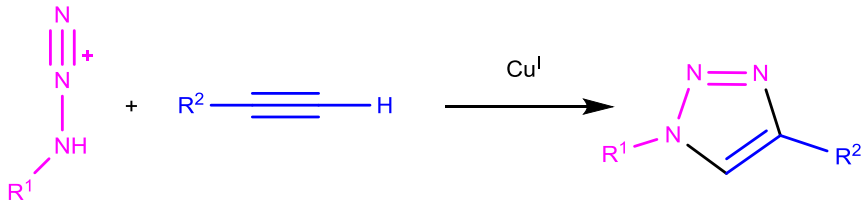

Scheme 1.2. Schematic representation of a copper(I)-catalyzed azide alkyne cycloaddition.[60]

'Click' chemistry has been widely used in the synthesis of rotaxanes due to the mild reaction conditions and simple execution.[61] For example, Costanza Casati *et al.* prepared a cyclodextrin-based [2]rotaxane by treating under click conditions a lactosyldecane azide and a hydroxylamino alkyne in the presence of α-CD (Scheme 1.3).[62]

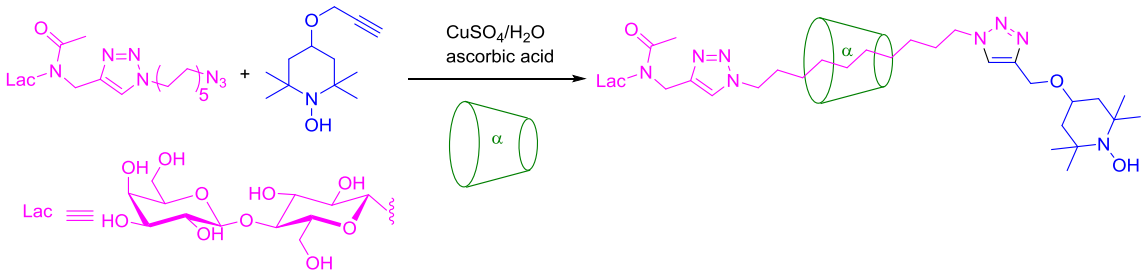

Scheme 1.3. Reaction of a lactosyldecane azide (pink) and a hydroxylamino alkyne (blue) in the presence of α-cyclodextrin (green).[62]

The increased accessibility of these compounds makes them a suitable platform to build artificial nanomachines.[63] In particular, as illustrated in Figure 1.13, two types of molecular motions may be envisaged under the influence of external

stimuli: rotation of the wheel around the axle and, similar to pseudorotaxanes, shuttling of the cyclic host along the guest. Thus, rotaxanes are good prototypes for the construction of rotary motors[64] and molecular shuttles.[65]

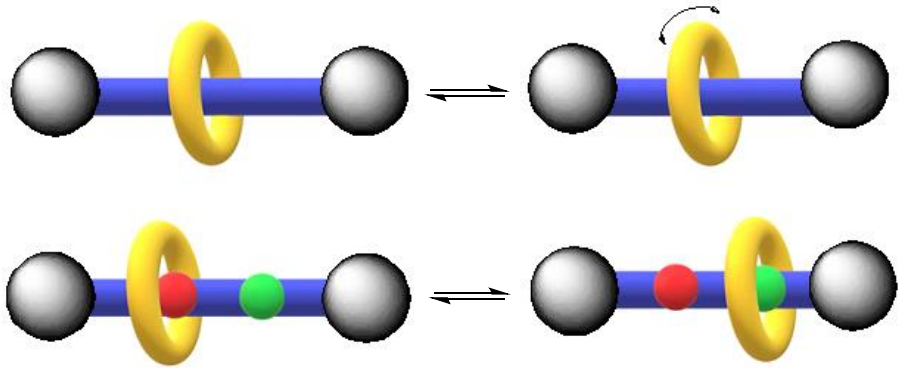

Fig. 1.13. Cartoon representation of two types of molecular mobilities of rotaxanes: rotation of the wheel around the axle (top), and shuttling between two stations (red and green) of the axle (bottom).

Rotaxane-based rotary motors were studied more than 20 years ago in Christopher J. Easton's group, who showed the rotation of an α-CD around a stilbene axle capped by trinitrobenzene capping groups (Figure 1.14).[66]

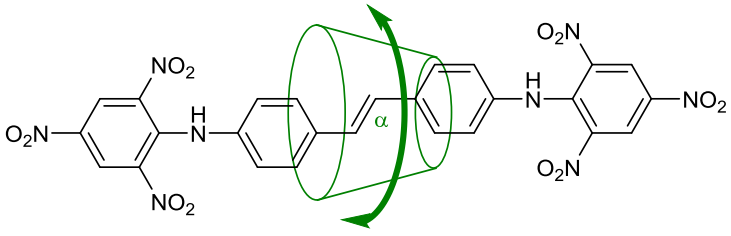

Fig. 1.14. [2]rotaxane showing rotation of the macrocycle around the axle.[66]

Christopher J. Easton's group also investigated the operation of an α-CD rotaxane as a molecular shuttle.[67] In this case, the host initially sits on the azobenzene moiety. Upon irradiation, the azobenzene isomerises to its *cis* configuration, resulting in the cyclodextrin being free to move between two propyl groups attached to the triazine blocking groups (Scheme 1.4).[67]

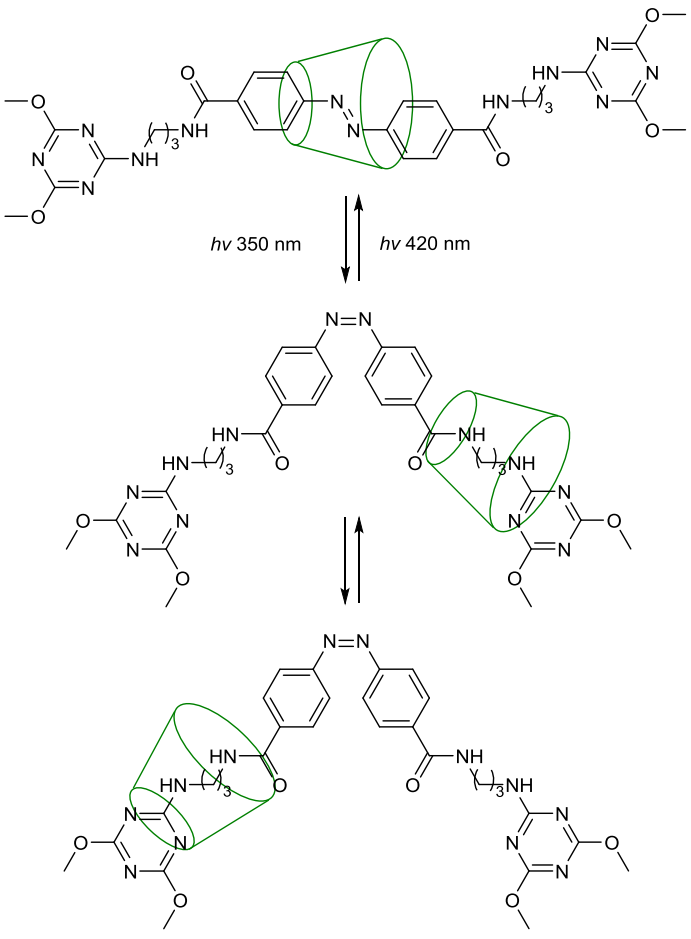

Scheme 1.4. Operation of a [2]rotaxane as a photochemical molecular shuttle.[67]

Following these preliminary studies, a number of rotaxane-based molecular machines have been studied and more complex structures are constantly under investigation. For example, Fraser Stoddart's group recently reported an electrochemically switchable bistable [2]rotaxane with one of the two stoppers acting as a fluorescent molecular rotor.[68] Upon oxidation of the tetrathiafulvalene recognition unit, the cyclobis(paraquat-p-phenylene) macrocycle shifts to a 8-phenyl-substituted boron dipyrromethene capping group (the rotor), driving changes in its excited-state properties, which result in fluorescence enhancement (Figure 1.15).[68]

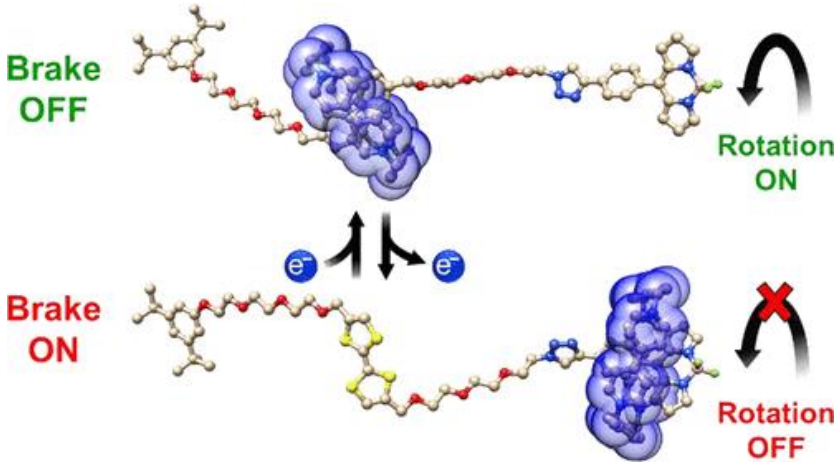

Fig. 1.15 Electrochemical switching of a molecular rotor embedded within a bistable rotaxane.[68] Reproduced with permission from the American Chemical Society.

Among other rotaxanes, daisy chains have gained special attention for the construction of artificial molecular machines. Resembling the distinctive assembly

of unique garlands of flowers, the term daisy chain was introduced in supramolecular chemistry to describe macromolecular assemblies formed by intermolecular linking of hermaphroditic monomers featuring complementary macrocyclic and linear units. Similar to the flower organization, molecular daisy chains arise by repeated threading of the axle of one monomer through the ring of the next one, with a blocking group preventing structural disassembly.[69] As illustrated in Figure 1.16, interlocked daisy chains can show either cyclic (*c*n) or acyclic (*a*n) molecular arrays, where n is the number of repeating units.

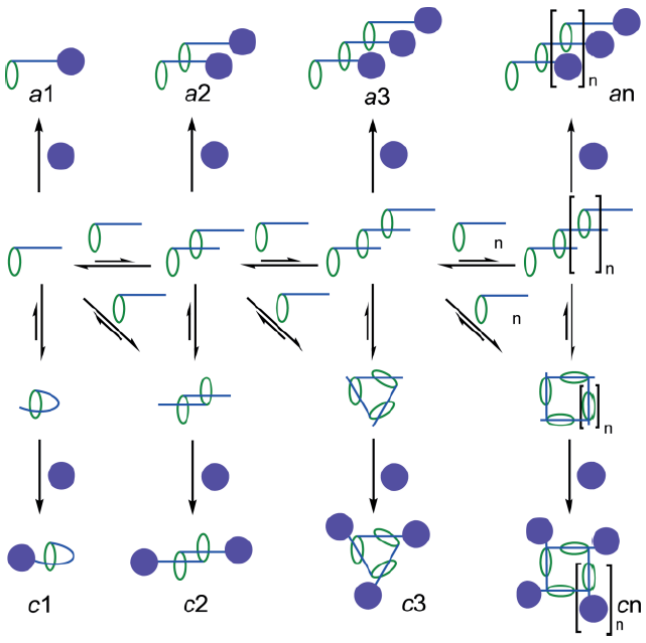

Fig. 1.16. Conceptual formation of linear and cyclic molecular daisy chains.[70]

Reproduced with permission from John Wiley and Sons.

With very few exceptions,[71] attempted synthesis of molecular daisy chains generally resulted in the formation of self-included monomers and cyclic dimers in preference to higher homologues.[24b, 72] This occurs because the corresponding *a*1 and [*c*2]daisy-chain complexes are thermodynamically favoured, based on considerations of entropy, as they contain the least number of monomers where every host and guest is in a complex.

Following the first synthesis of a [*c*2]daisy chain rotaxane described by Jean-Pierre Sauvage in 2000,[73] these complex molecules have attracted increasing interest among synthetic chemists and are even now the object of study due to their diverse applications.[74] For example, a recent study undertaken by Susumu Tsuda[74b] described the insulating properties of a [*c*2]daisy chain rotaxane. In this work, the monomer was synthesized by attaching a diarylacetylene moiety to a permethylated α-cyclodextrin (PM α-CD) and then used to generate a pseudo[2]rotaxane. Aniline blocking groups were then utilised to cap the [*c*2]daisy chain complex (Scheme 1.5). The PM α-CDs were able to insulate the diarylacetylene cores, as demonstrated by the unchanged maximum absorption wavelength of the [*c*2]daisy chain rotaxane in different solvents.

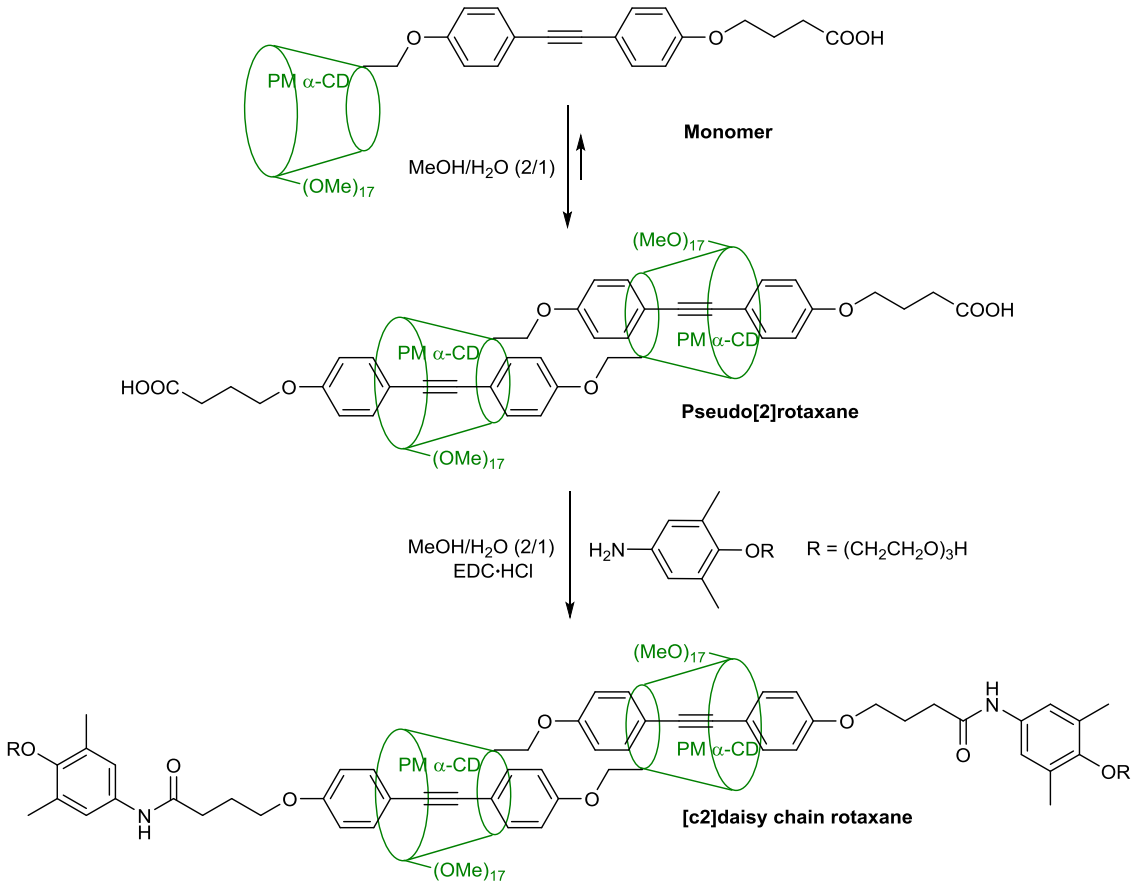

Scheme 1.5. Synthesis of [*c*2]daisy chain rotaxane.[74b]

As described below, daisy chains have been mainly adopted for the construction of muscle-based materials.[74a]

1.5 Daisy chain-based molecular muscles

Daisy chains are a key area of interest for supramolecular chemists due to their potential to allow alteration of macroscopic properties by switching mechanisms on a molecular scale. Mimicking the one-dimensional motion of biological muscles

upon chemical stimulation by ATP hydrolysis,[9] daisy chain structures can be contracted or expanded in response to different stimuli, including pH,[75] redox chemistry,[76] light,[24b, 77] solvent,[78] and metal complexation.[79] The possibility to control their molecular-level motion to generate force makes daisy chains a valuable platform to build the so-called molecular muscles, which are molecular mimics of the extension and contraction of natural fibers; whose switching properties are provided by an external stimulus.

The imitation of the myosin and actin filaments sliding motion in rotaxanes was pioneered by Jean-Pierre Sauvage's group,[75b, 76] who used transition metal ion templates to drive the expansion and contraction of a [*c*2]daisy chain. Bidentate phenanthroline and tridentate terpyridine ligands were included in one of the reported structures as metal binding sites.[73] The study showed that transition metals with different valencies could selectively pair with ring and thread ligands, generating different coordination geometries. An extended geometry resulted following the phenanthroline ligands of each component pairing up tetrahedrally around CuI ions, while ZnII ions formed a pentacoordinate complex involving terpyridine ligands, furnishing a contracted geometry (Figure 1.17).[73]

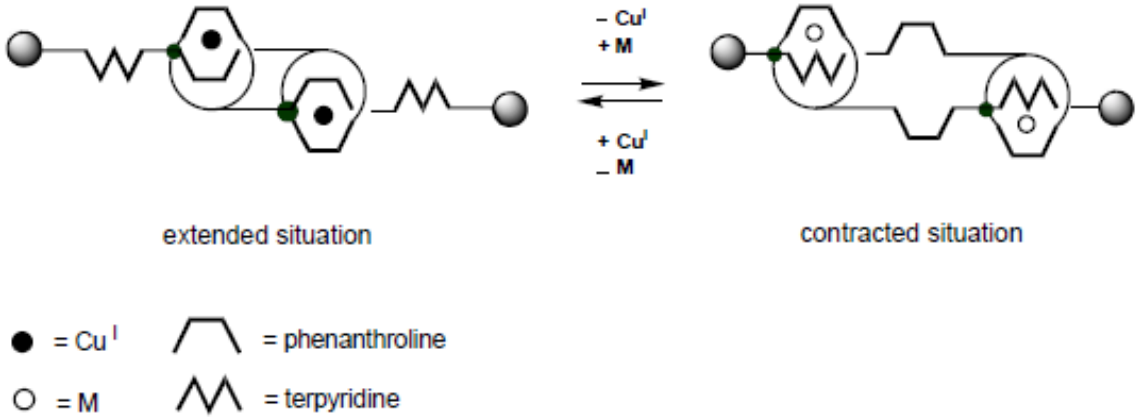

Fig. 1.17. Representation of expansion and contraction of a [*c*2]daisy chain driven by metal chelation.[73] Reproduced with permission from John Wiley and Sons.

Beside metal chelation, the recognition motif between crown ethers and secondary dialkylammonium salts is often exploited to drive conformational changes in [*c*2]daisy chains. In particular, pH driven switching can occur when, under basic conditions, cations acting as secondary stations displace the neutral amines within the rings. Bipyridinium[75a] and triazolium[75b] units have been often used as the permanent cations to operate the expansion and contraction of [*c*2]daisy chains. Following some key examples of pH-switchable [*c*2]daisy chain rotaxanes provided by Fraser Stoddart's,[75a, 80] Robert H. Grubbs',[81] and Frederic Coutrot's[75b] groups, Da-Hui Qu and HeTian more recently described a molecular switch with an interesting application.[82] In this case, the contraction and expansion motion of multiple daisy chain dimers anchored between two gold nanoparticles (Au NPs) allowed the manipulation of the distance between the Au NPs (Figure 1.18).[82]

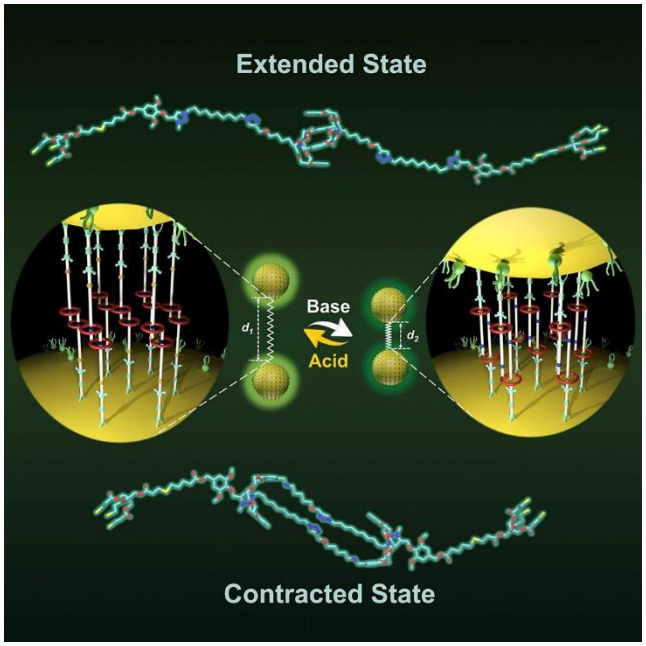

Fig. 1.18. Representation of expansion and contraction of pH-switchable [*c*2]daisy chains between two gold nanoparticles.[82] Reproduced with permission from Elsevier.

Within the past few years, redox-switchable donor-acceptor daisy chains have also been developed. Both neutral[76a] and multicationic[76b] [*c*2]daisy chains have been synthesized and actuated upon electrochemical reactions. For example, in 2014, Fraser Stoddart showed that the shuttling of a tetracationic cyclophane cyclobis(paraquat-p-phenylene) ring between the viologen and 1,5-dioxynaphthalene recognition units of a bistable daisy chain resulted in significant changes in molecular dimensions (Figure 1.19).[76b]

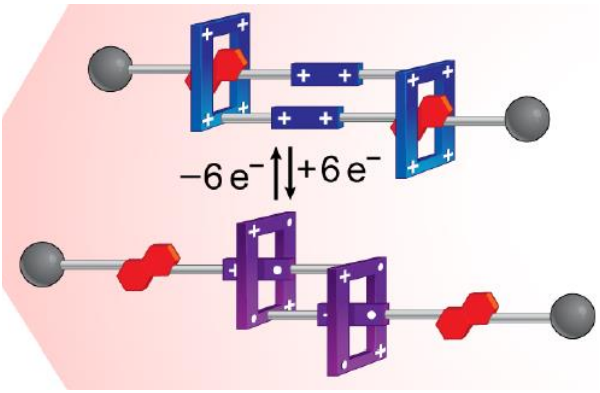

Fig. 1.19. Representation of expansion and contraction of a redox switchable [*c*2]daisy chain.[76b] Reproduced with permission from the American Chemical Society.

Akira Harada and co-workers[78] used solvents of different polarities to switch between contracted and extended states of a [*c*2]dimer. Their study showed that the cyclodextrin units, initially siting over the amide bonds of the cinnamide unit in DMSO, could shuttle to include the hexyl chain upon the addition of water to a 1:1 ratio (Figure 1.20). The switching to the apolar alkyl chain was a result of the thermodynamically unfavourable system generated by the presence of more polar solvent inside the apolar cyclodextrin cavity.

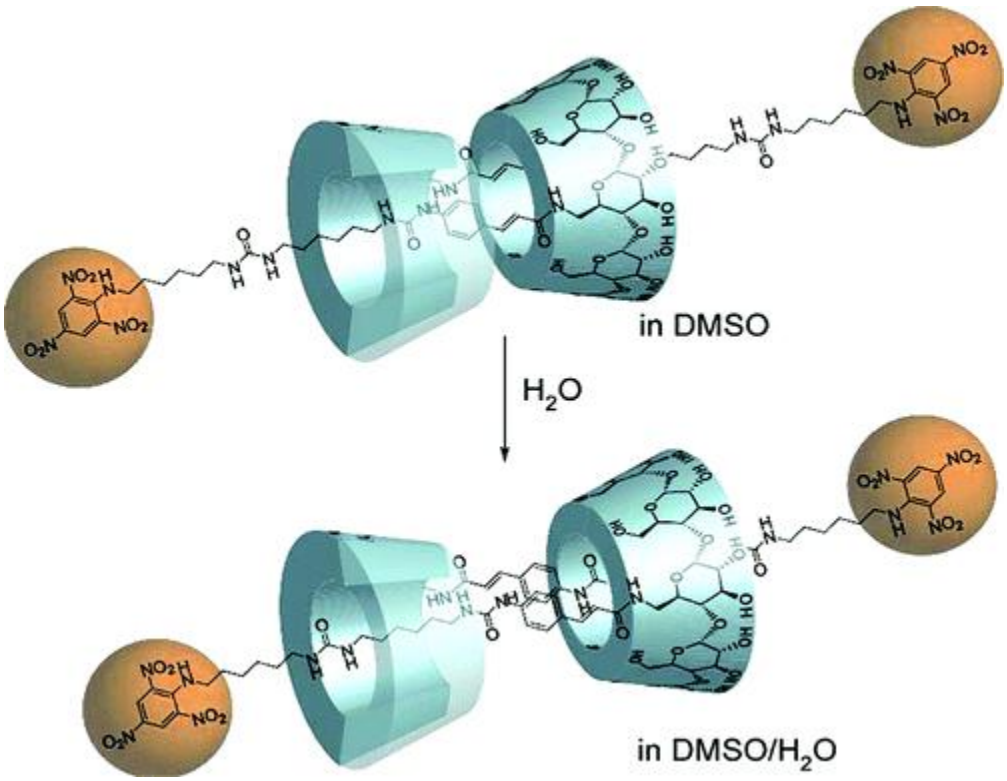

Fig. 1.20. Expansion and contraction of a solvent-sensitive [*c*2]daisy chain.[83]

Reproduced with permission from the American Chemical Society.

Finally, an example of a photo-switchable daisy chain has been previously reported in Christopher J. Easton's group.[24b] This work demonstrated that the ability to form inclusion complexes can be switched on and off via photoisomerization between *trans* and *cis* isomers. Naturally existing in its *trans* configuration, the stilbene included in the cyclodextrin to form a [*c*2]dimer, switched to the *cis* configuration upon photoisomerization. As a result of the new configuration, the shuttling of the host from the sterically bulky *cis* stilbene to the secondary, propyl guest station and resulting dimer contraction was observed (Scheme 1.6).[24b]

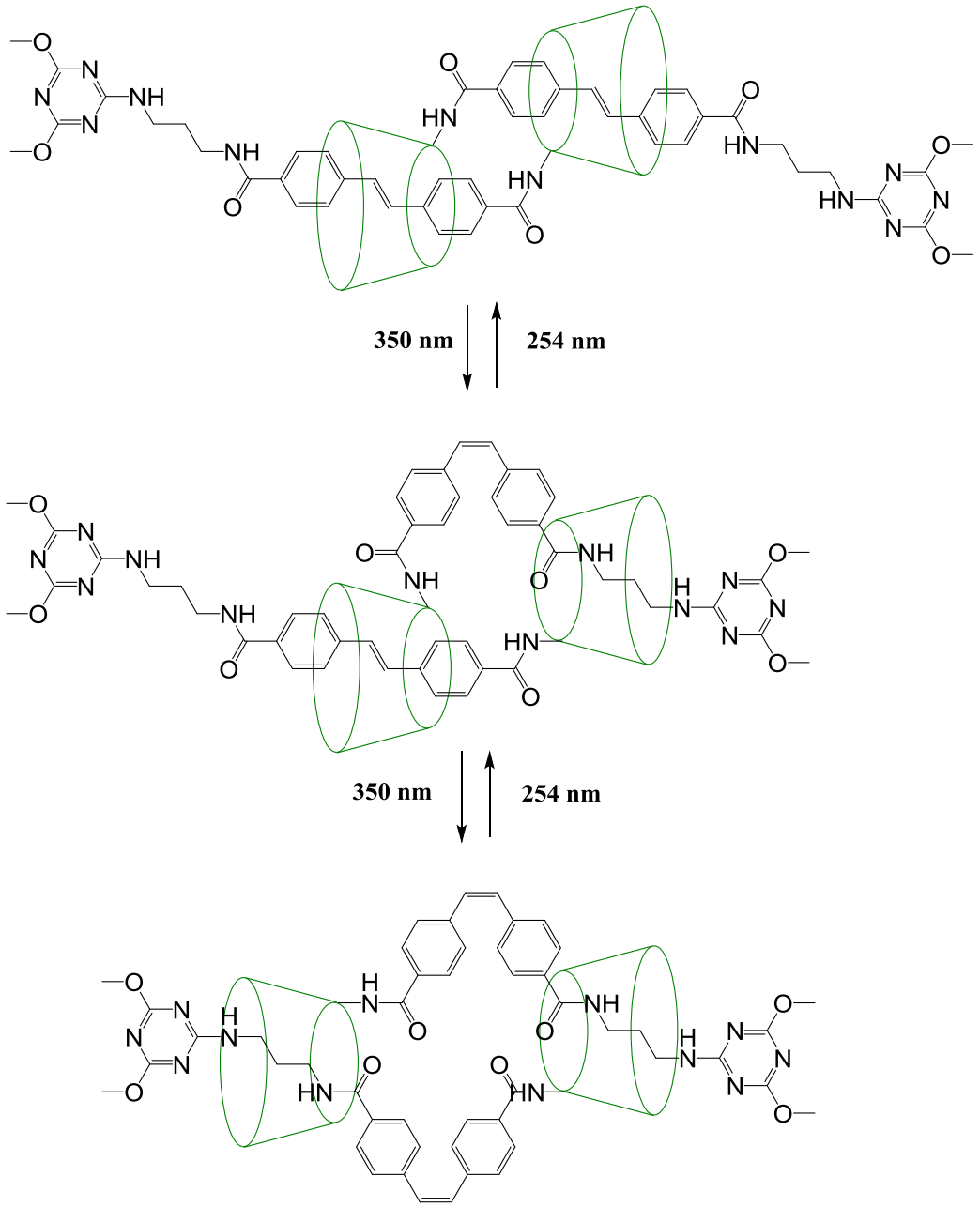

Scheme 1.6. Expansion and contraction of a photo-switchable [*c*2]daisy chain.[24b]

The just discussed works show that the synthesis and actuation of molecular muscles based on dimeric daisy chains has been extensively studied in the literature. However, the amplification of the switching behaviour in an oligomeric structure is

still a challenging target. Oligomerization of mechanically interlocked [*c*2]dimers can occur as a result of dynamic metal chelation[84] or hydrogen-bonding[85] of the blocking groups, or by their linkage through irreversible, covalent modification[77, 80-81, 86]. The last method was used by Takahiro Kaneda,[77] who prepared oligomeric series of up to 5 dimeric units. Later, Fraser Stoddart,[80, 86] employed acyclic diene metathesis and double Cu-catalyzed Huisgen 1,3-dipolar cycloaddition (Click chemistry) to give oligomers of [*c*2]daisy chains, having on average 7-9 and around 11 repeating units, respectively. Similarly, Robert H. Grubbs[81] applied the same Click chemistry on a [*c*2]dimer to grow a 22 units linear polymer. Linear daisy chain polymers of this configuration retain the inherently-flexible, rotaxane links, in some cases with switchable behaviour.

The macroscopic effects of the switching behaviour shown by daisy chain polymers have been further investigated over time and keep generating extraordinary results even in recent years. A remarkable example of this phenomenon was provided in 2005 by David A. Leigh's group, who managed to move a liquid droplet against the force of gravity by inducing changes in the surface properties following the shuttling of a surface-bond rotaxane.[87] In the same year, Fraser Stoddart observed the bending of a gold microcantilever beam by exploiting the contraction of a rotaxane based molecular actuator.[88] In a recent, seminal paper, Akira Harada reported the incorporation of a [*c*2]cyclodextrin-complex into a polymer gel network, and demonstrated photochemically-induced expansion and contraction of the gel driven by the conformational changes of the incorporated complex (Figure 1.21).[89]

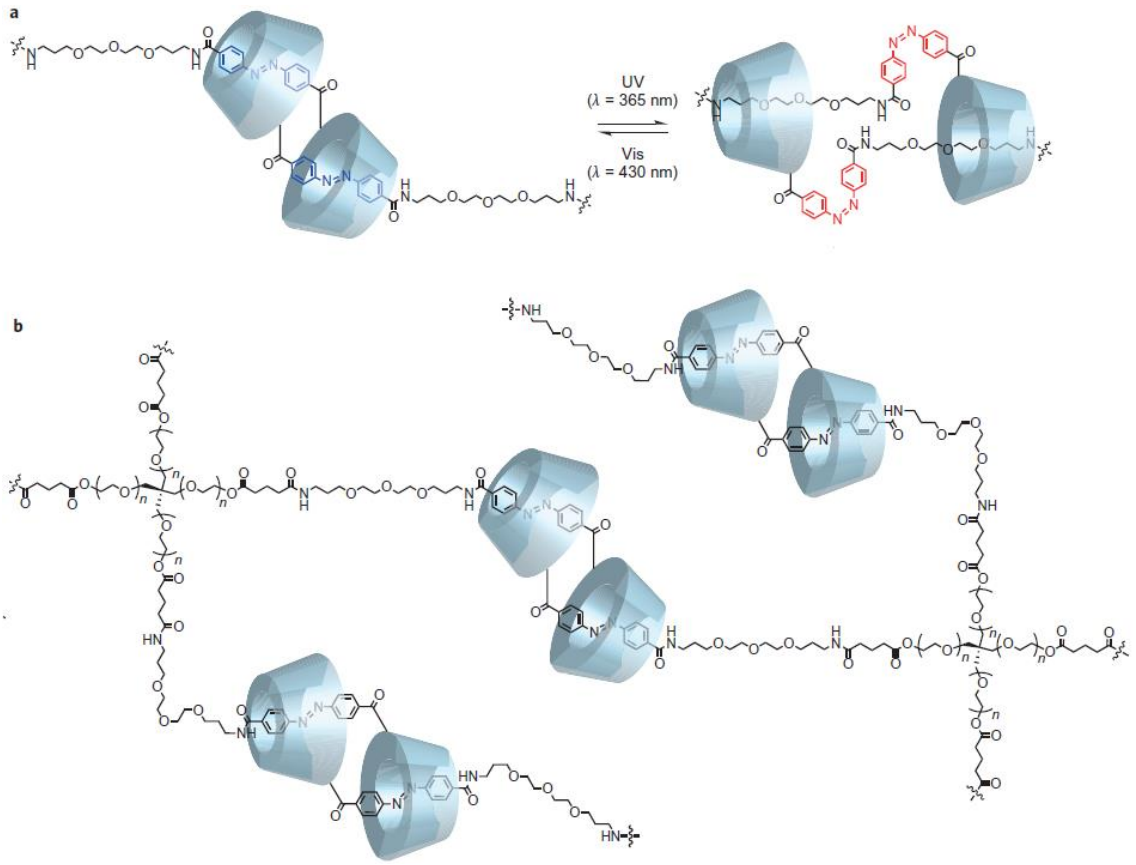

Fig. 1.21. a) Expansion and contraction of a photo-switchable [c2]daisy chain; and b) a [*c*2]daisy chain-based polymeric gel. Reproduced with permission from Springer Nature.

Even more recently, Nicolas Giuseppone described the integration of [*c*2]daisy chain rotaxanes in polymeric gel networks, able to extend or reduce their volume upon pH variation.[90] The examples described above demonstrate the wide application of daisy chains and their enormous potential as functional materials.

1.6 Rotaxane functionalisation

As previously discussed, daisy chains represent a convenient starting material to build functional devices, including molecular muscles. Similarly, rotaxanes represent a widely adopted interlocked system in supramolecular chemistry because of their versatility. Following the statistical threading method originally introduced by Ian T. Harrison and co-workers in 1967,[42] a number of strategies for the synthesis of rotaxanes have been developed in the course of the past 30 years, including template methods[91] and Click chemistry.[59] These synthetic methods, relying on the encapsulation of a symmetrical linear molecule in a guest, are now mature; however, the preparation and isolation of [2]rotaxanes can become more challenging when asymmetry is introduced in the structure. Asymmetry can be provided by the guest, the terminal groups, or a combination of these.[39] When macrocycles are symmetrical, as in the case of crown ethers, cucurbiturils, and pillararenes, two bulky stoppers can lead to an unsymmetrical structure. The complexity increases when the cyclic components are nonsymmetrical, such as with calixarenes and cyclodextrins, because an axle with different capping groups can insert into the cycle from both rims, thus resulting into two isomeric rotaxanes (Figure 1.22).

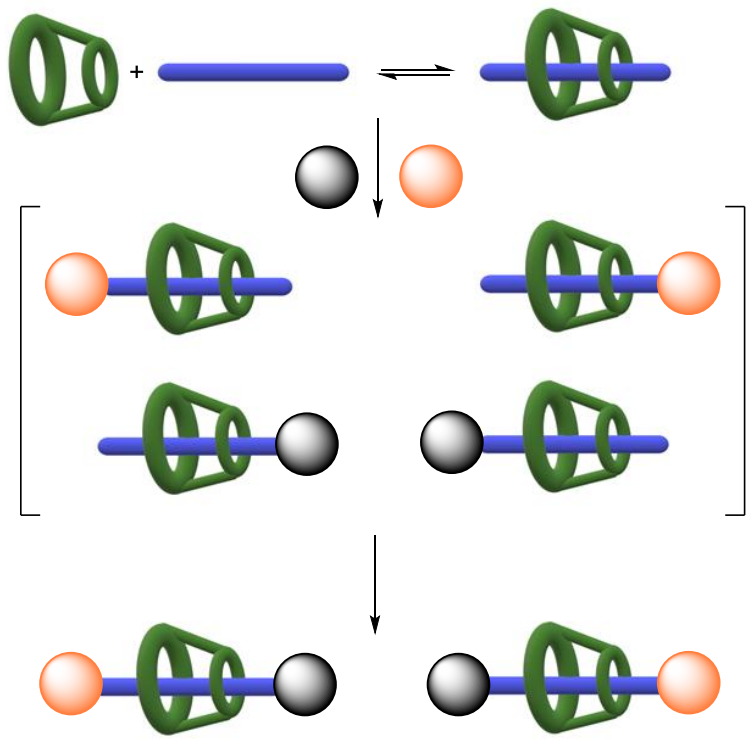

Fig. 1.22. Schematic representation of the synthesis of cyclodextrin-based [2]rotaxane orientational isomers.

Examples of these based on calixarenes[92] have been prepared, separated and individually characterized. Being asymmetric, CDs also show this behaviour.[62, 93] The first CD-based isomeric rotaxanes were observed by Angel E. Kaifer,[94] who obtained a mixture of isomers in a combined 15% isolated yield. However, the two species were not separated, therefore the individual properties were not investigated. Later, Harry L. Anderson[95] and He Tian[96] also made [2]rotaxanes comprising an asymmetric host (CD) and an asymmetric axle. Both studies, however, resulted in only a single orientational isomer. In fact, just a few examples of isolated and separated isomeric CD [2]rotaxane pairs have been reported.[93a-c]

Harry L. Anderson, for instance, prepared isomeric pairs of cyanine dyes based on α-CD rotaxanes (Figure 1.23).[93a, 93b] The two pairs of isomers were separated by reverse phase chromatography and structurally characterised by ^{1}H and ^{13}C NMR spectroscopy, while the relative orientations of the cyclodextrin were determined by NOESY experiments.

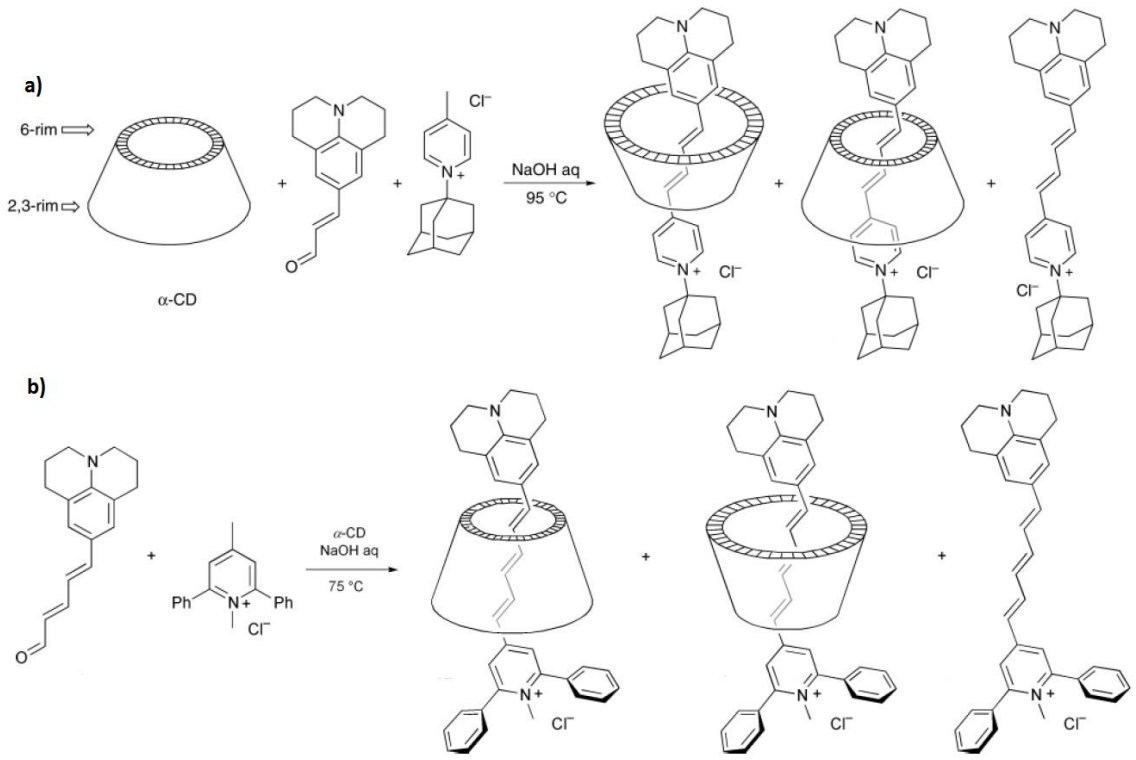

Fig. 1.23. Synthesis of cyclodextrin-based orientational isomers with a) adamantylpyridinium,[93a] and b) diphenylpyridinium.[93b] Reproduced with permission from the Royal Society of Chemistry.

A few years later, Joon W. Park and Hyun J. Song[93c] reported the synthesis, isolation and conformational analysis of two isomeric [2]rotaxanes composed of α-CD and

aliphatic chain linked carbazole-viologen (Figure 1.24). The orientation of the α-CD was determined by ^{1}H-^{1}H COSY and two-dimensional ROESY spectroscopy, and induced circular dichroism (ICD).

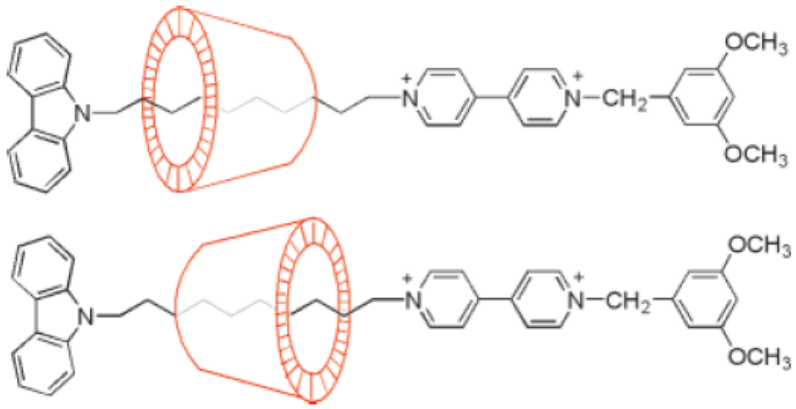

Fig. 1.24. Cyclodextrin-based orientational isomers.[93c] Reproduced with permission from the American Chemical Society.

Due to their strong potential as nanodevices, current research still focuses on the development of configurational isomers, especially those based on higher-order rotaxanes.[97]

1.7 Rotaxane-based insulated molecular wires

As part of the attempts of designing molecular devices with applications in the real world, the development of molecular electronic devices has drawn much attention over the last decades.[98] Among the basic components of electronic circuitry,

conductive polymers are of fundamental importance as they allow electrons to flow between different parts of the system.[99] Interest in conjugated polymers started during the 1940s, when it was wrongly believed that the π–π* energy gap of polyacetylene, close to zero because of the long polymer chain, resulted in metallic conductivity along the polymer backbone.[100] A few years later, a number of studies dispelled this inspirational misconception by looking at the absorption spectra of polyenes[101] and by developing the molecular orbital theory[102] and the concept of Peierls distortion,[103] which explained the bond-alternated structure of polyacetylene derived by the energy gap between the highest occupied state in the π band and the lowest unoccupied state in the π* band.[104] Another tipping point was reached in the 1960s, when metallic conductivity was found in polysulfurnitride[105] and cyanine dyes substituted polyacetylenes were suggested to be superconductors.[106] Since then, conjugated polymers have been extensively studied because of their potential application in molecular electronics, such as in light-emitting diodes,[107] field effect transistors,[108] photovoltaic cells,[109] and sensors.[110] Such polymers can exhibit semi-conducting or even metallic properties because of their electronic structure. Specifically, each carbon atom bears one unpaired electron (the p electron) because of the chemical bonding. Additionally, electron delocalization along the backbone of the polymer arises from the π bonding, between p orbitals of bonded carbon atoms (Figure 1.25).

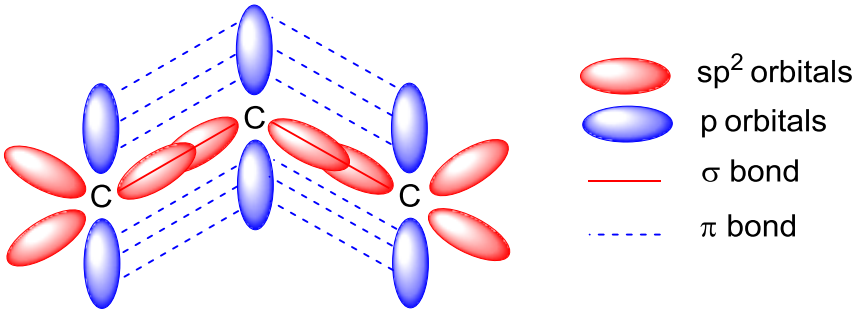

Fig. 1.25. Representation of σ and π bonds between orbitals of bonded carbon atoms.

The electron delocalization promotes the charge mobility along the chain; therefore, at molecular scale, a conjugated polymer can also be defined as a "molecular wire". The description of molecular wires as π-conjugated molecules aligned linearly to form a strand of conductive material led to further studies exploring the opportunity to insulate the wires in order to prevent signal crosstalk or leakage. Accordingly, if the molecular wire is encapsulated in a protective sheath preventing inter-chain interactions, then it can be said that the molecular wire is an Insulated Molecular Wire (IMW).[111] A wide variety of systems have been developed to build IMWs, thus showing the broad appeal of this topic. Pioneering studies in this area were performed in 1989 by Thomas Bein and co-workers,[112] who encapsulated conjugated polymers in zeolites and mesoporous hosts. While these solid hosts were ideal linear channels for isolating polymer chains, they caused the loss of solution processability, one of the main advantages of organic semi-conductors, compared to their inorganic counterparts. Aiming to preserve the molecularity of the wire, supramolecular structures, such as pseudopolyrotaxanes and polyrotaxanes, were

evaluated as potential candidates to build IMWs.[113] Similarly to the previously discussed pseudorotaxanes and rotaxanes, these systems arise from the inclusion complexes between conjugated π systems and macrocycles, however pseudopolyrotaxanes' and polyrotaxanes' guests are threated through more than one host to ensure full insulation for longer polymers (Figure 1.26).

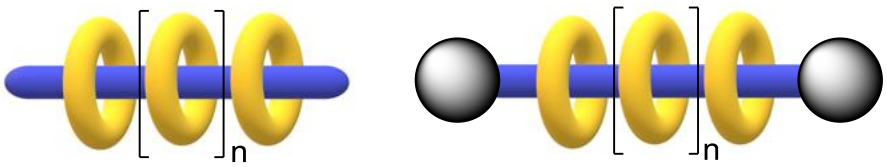

Fig. 1.26. Cartoon representation of a pseudopolyrotaxane (left) and a polyrotaxane (right).

Insulating molecules must fully include the molecular wire but should not be linked covalently to avoid potential signal crosstalk via the insulator. The formation of the inclusion complex is driven by non-covalent interactions between the linear polymer chain and the cyclic component, which needs to exhibit a hydrophobic interior, to allow the axle inclusion, and a hydrophilic exterior to be water-soluble. A number guests have been tested as conducting polymers, including polyheterocycles,[114] polyanilines,[115] polyaryleneimines,[116] polyarylenevinylenes[114] and polyarylenes.[114] Similarly, several macrocycles were tried as shell materials, but most of the synthesized insulated molecular wires are electrically insulated by a series of cyclodextrins. Pioneering work on cyclodextrin-threaded polymers was performed independently by Akira Harada and Mikiharu

Kamachi[117] and by Gerhard Wenz and Bruno Keller.[118] Akira Harada and Mikiharu Kamachi synthesized a cyclodextrin pseudopolyrotaxane exhibiting tightly packed macrocycles in a head-to-head arrangement along a polyethylene glycol chain. The reported complex was prepared as a crystalline precipitate, because of its poor solubility in water.[117] Instead, Gerhard Wenz and Bruno Keller prepared a water soluble pseudopolyrotaxane by threading cyclodextrins onto cationic polyelectrolytes. Unlike Akira Harada's pseudopolyrotaxane, the relative orientation of neighbouring cycle units was found to be random, due to the ammonium centres preventing the cyclodextrins from packing tightly together along the axle.[118]

Building upon the results of these seminal studies,[117-118] pseudopolyrotaxanes were further studied as a platform to build polyrotaxane-based IMWs.[111] In particular, Harry L. Anderson described a 3-steps approach to synthesize water-soluble conjugated rotaxanes.[113] As illustrated in Figure 1.27, the pseudorotaxane was initially formed by threading a conjugated backbone into a macrocycle; different monomeric units were then coupled to build a pseudopolyrotaxane, which was finally capped by bulky stoppers to yield a polyrotaxane.[113]

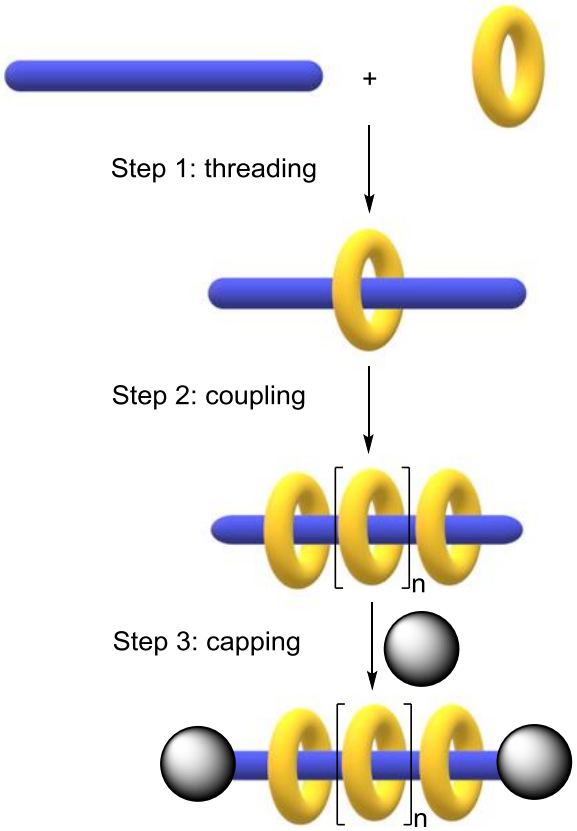

Fig. 1.27. Synthetic strategy to build insulated molecular wires.[113]

A number of compounds have been prepared by Harry L. Anderson's group using this method.[111, 113, 119] These include conjugated polymers, such as poly(para-phenylene) (PPP), poly(4,4′-diphenylene vinylene) (PDV) and polyfluorene (PF), incorporated in rotaxane complexes with α- and β-CDs (Figure 1.28).[119b]

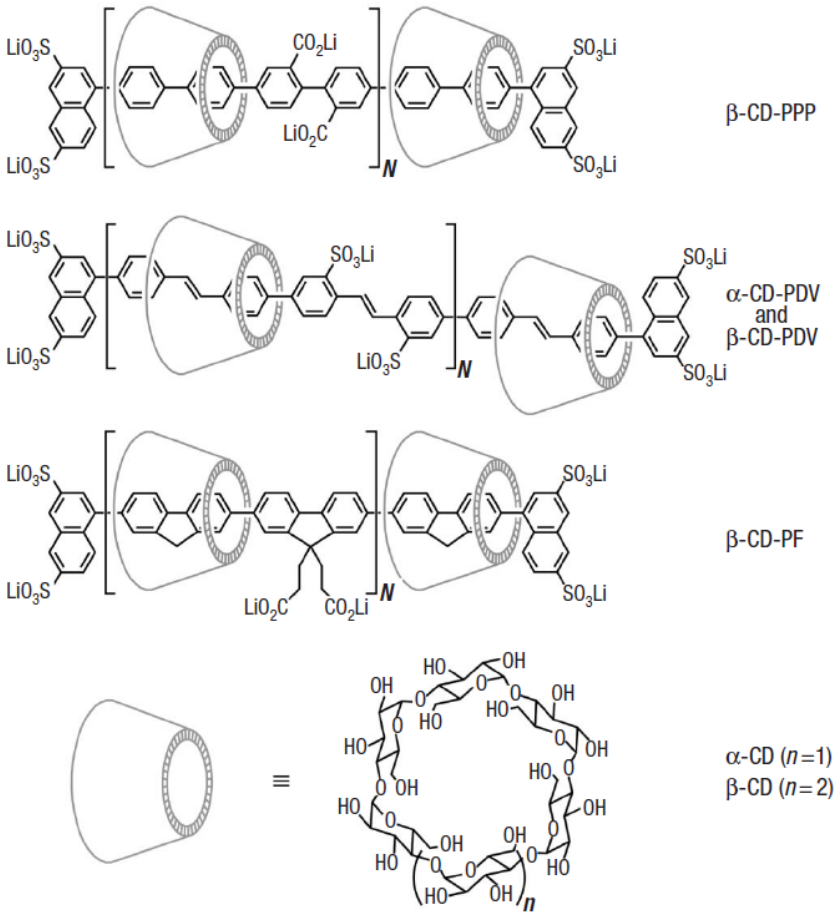

Fig. 1.28. The chemical structures of the cyclodextrin-threaded conjugated polyrotaxanes with poly(*para*-phenylene),and poly(4,4′-diphenylene vinylene) and polyfluorene cores.[119b] Reproduced with permission from Springer Nature.

The conductivity of insulated polymers has been investigated using various techniques. Takeshi Shimomura, for example, measured the conductivity of an α-CD/polyaniline nanotube by measuring the current through a single fiber placed between narrow-gap electrodes at different voltages.[120] Jun Terao utilised a combination of time-resolved microwave conductivity and transient absorption spectroscopy to measure the conductivity and hole mobility along a poly(phenylene

ethynylene) backbone insulated by a series of permethylated CDs.[121] More recently, a Brazilian research group synthesized a series of cyclodextrin-based poly(p-phenylene) polyrotaxanes (Figure 1.29) and investigated their electronic properties using Semiempirical and Density Functional Theory (DFT) calculations.[122] The poly(p-phenylene) oligomers showed conductive properties, which were maintained after the insulation with a series of β-CDs.[122]

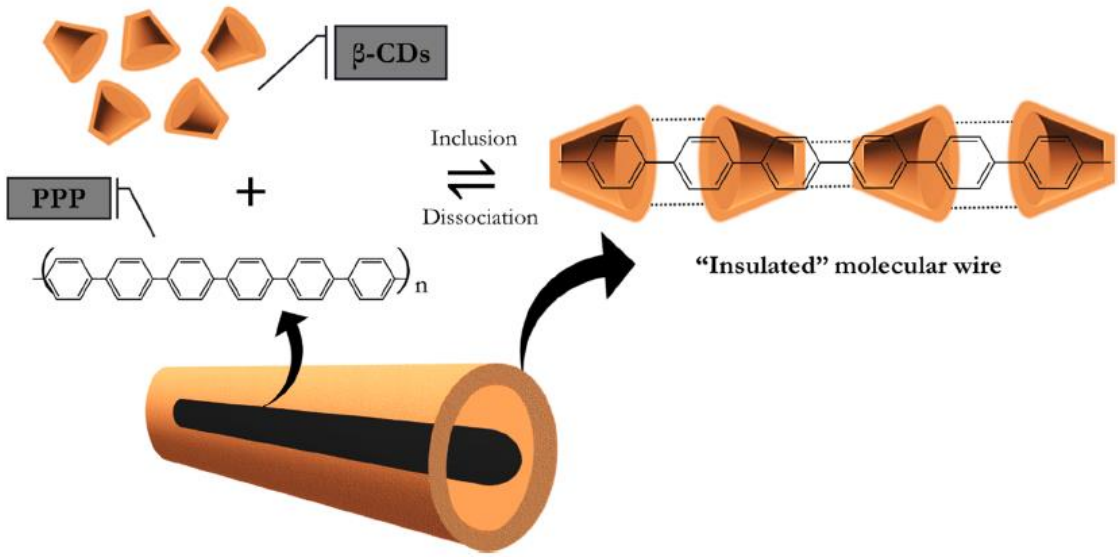

Fig. 1.29. Schematic representation of the cyclodextrin-based insulated molecular wires formation process.[122] Reproduced with permission from Elsevier.

Given the ongoing need for small components in electronic devices, new materials are constantly under development, and insulated molecular wires, being recognised as promising alternatives to silicon-based materials, are expected to provide a significant contribution to this research area.[123]

1.8 Aims of the project and overview

The aim of this project was to prepare different types of CD-based supramolecules and to explore the potential ability of some of them to act as molecular devices.

The work presented in Chapter 2 aimed at building interlocked [*c*2]daisy chain oligomers with the potential ability to act as molecular muscles. In the usual approach, monomers are not directly extended into polymers. Specifically, the reaction is carried out in two steps: initially the equilibrium between monomer and [*c*2]daisy chain is stopped by adding a capping group; subsequently the capped [*c*2]daisy chains are connected together through a linker to form a linear polymer.[52, 77, 81, 86] Although this method is convenient from a synthetic perspective, the need of two different steps to perform the polymerisation represents a limit. In order to overcome this drawback, an alternative approach consisting of the direct oligomerisation from the equilibrium between monomer and [*c*2]daisy chains was developed. Preliminary photoswitching experiments were also performed to investigate the muscle-like behaviour of these compounds.

Alongside daisy chains, rotaxanes were also studied as versatile supramolecular species. Despite remarkable achievements in rotaxanes synthesis and characterisation, the orientational rotaxane isomers still represent a challenging target.[124] The preparation and separation of [2]rotaxane orientational isomers was therefore the aim of the studies presented in Chapter 3. The usual approach to

synthesize isomeric rotaxanes is to cap an inclusion complex of a monocapped guest. This method was initially adopted in this work to introduce amino functionalities to a CD-rotaxane as they are excellent nucleophiles, able to form strong amide bonds to potentially allow the extension of the structure[125] or the anchorage to a surface.[126] Having observed significant limitations with this method, a complementary synthetic approach was developed. This new method involved the desymmetrization of a symmetric pre-formed [2]rotaxane by functionalization of a capping group, and was utilised to introduce bromine groups to the structure. Similarly to amines, they are a versatile functionality for a number of applications, including surface modification.[127]

Having investigated different synthetic procedures to build rotaxanes, the next phase of the research was focused on their application as molecular machines. In particular, the development of rotaxane-based insulated molecular wires and the analysis of their conductivity behaviour was the objective of the work described in Chapter 4. Insulated molecular wires have been previously prepared through the synthesis of polyrotaxanes.[111] In this work the formation of insulated molecular wires through rotaxane self-assembly was investigated. In particular, a previously reported cyclodextrin-based rotaxane[128] was initially tested because of its ability to build self-organised assemblies through π-π stacking, extended conjugation, and intra- and intermolecular co-planarity. Crystal engineering was then utilised to design and synthesize a new rotaxane in order to compare the conductivity behaviour of the species.

References

[1] a) L. Sun, Y. A. Diaz-Fernandez, T. A. Gschneidtner, F. Westerlund, S. Lara-Avila, K. Moth-Poulsen, *Chemical Society reviews* **2014**, *43*, 7378-7411. DOI: http://dx.doi.org/10.1039/C4CS00143E; b) A. H. J. Engwerda, S. P. Fletcher, *Nat Commun* **2020**, *11*, 4156. DOI: http://dx.doi.org/10.1038/s41467-020-17814-0.

[2] a) K. Konstas, S. J. Langford, M. J. Latter, *International journal of molecular sciences* **2010**, *11*, 2453-2472. DOI: http://dx.doi.org/http://dx.doi.org/10.3390/ijms11062453; b) V. Balzani, A. Credi, M. Venturi, *Chemistry – A European Journal* **2002**, *8*, 5524-5532. DOI: http://dx.doi.org/https://doi.org/10.1002/1521-3765(20021216)8:24<5524::AID-CHEM5524>3.0.CO;2-J; c) R. W. Keyes, *Proceedings of the IEEE* **2001**, *89*, 227-239. DOI: http://dx.doi.org/10.1109/5.915372.

[3] V. Galstyan, M. Bhandari, V. Sberveglieri, G. Sberveglieri, E. Comini, *Chemosensors* **2018**, *6*, 16. DOI: http://dx.doi.org/10.3390/chemosensors6020016.

[4] a) H. LI, J. XIANG, J. CHEN, X. YUE, X. YU, Z. XIAO, *Journal of Inorganic Materials* **2021**, *36*, 695-710. DOI: http://dx.doi.org/10.15541/jim20200443; b) V. Balzani, A. Credi, M. Venturi, *Chemistry (Weinheim an der Bergstrasse, Germany)* **2003**, *8*, 5524-5532. DOI: http://dx.doi.org/10.1002/1521-3765(20021216)8:24<5524::AID-CHEM5524>3.0.CO;2-J.

[5] a) M. Baroncini, M. Canton, L. Casimiro, S. Corra, J. Groppi, M. La Rosa, S. Silvi, A. Credi, *European Journal of Inorganic Chemistry* **2018**, *2018*, 4589-4603. DOI: http://dx.doi.org/https://doi.org/10.1002/ejic.201800923; b) V. Balzani, A. Credi, M. Venturi, *Nano Today* **2007**, *2*, 18-25. DOI: http://dx.doi.org/https://doi.org/10.1016/S1748-0132(07)70055-5.

[6] a) E. R. Kay, D. A. Leigh, F. Zerbetto, *Angewandte Chemie International Edition* **2007**, *46*, 72-191. DOI: http://dx.doi.org/10.1002/anie.200504313; b) Q. Wang, D. Chen, H. Tian, *Science China Chemistry* **2018**, *61*, 1261-1273. DOI: http://dx.doi.org/10.1007/s11426-018-9267-3.

[7] T. J. Huang, B. K. Juluri, *Nanomedicine : nanotechnology, biology, and medicine* **2008**, *3*, 107-124. DOI: http://dx.doi.org/http://dx.doi.org/10.2217/17435889.3.1.107.

[8] a) J. Howard, *Nature* **1997**, *389*, 561-567. DOI: http://dx.doi.org/10.1038/39247; b) T. Elston, H. Wang, G. Oster, *Nature* **1998**, *391*, 510-513. DOI: http://dx.doi.org/10.1038/35185.

[9] a) M. A. Geeves, *Nature* **2002**, *415*, 129-131. DOI: http://dx.doi.org/10.1038/415129a; b) K. Kitamura, M. Tokunaga, A. H. Iwane, T. Yanagida, *Nature* **1999**, *397*, 129-134. DOI: http://dx.doi.org/10.1038/16403.

[10] M. Palucki, J. P. Wolfe, S. L. Buchwald, *Journal of the American Chemical Society* **1996**, *118*, 10333-10334. DOI: http://dx.doi.org/10.1021/ja962408v.

[11] a) M. Schliwa, G. Woehlke, *Nature* **2003**, *422*, 759-765. DOI: http://dx.doi.org/10.1038/nature01601; b) R. Iino, K. Kinbara, Z. Bryant, *Chemical reviews* **2020**, *120*, 1-4. DOI: http://dx.doi.org/10.1021/acs.chemrev.9b00819.

[12] P. von Hippel, E. Delagoutte, *Cell* **2001**, *104*, 177-190. DOI: http://dx.doi.org/10.1016/S0092-8674(01)00203-3.

[13] A. S. Spirin, *FEBS Letters* **2002**, *514*, 2-10. DOI: http://dx.doi.org/https://doi.org/10.1016/S0014-5793(02)02309-8.

[14] a) J. M. Lehn, *Supramolecular chemistry*, VCH, Weinheim, **1995**; b) D. B. Amabilino, D. K. Smith, J. W. Steed, *Chemical Society reviews* **2017**, *46*, 2404-2420. DOI: http://dx.doi.org/10.1039/C7CS00163K.

[15] E. Fischer, *Berichte der deutschen chemischen Gesellschaft* **1894**, *27*, 2985-2993. DOI: http://dx.doi.org/10.1002/cber.18940270364.

[16] J. M. Lehn, *Angew. Chem. Int. Ed. Engl.* **1988**, *27*, 89-112. DOI: http://dx.doi.org/DOI 10.1002/anie.198800891.

[17] C. J. Pedersen, *Journal of the American Chemical Society* **1967**, *89*, 7017-7036. DOI: http://dx.doi.org/10.1021/ja01002a035.

[18] B. Dietrich, J. M. Lehn, J. P. Sauvage, *Tetrahedron Lett* **1969**, *10*, 2889-2892. DOI: http://dx.doi.org/https://doi.org/10.1016/S0040-4039(01)88300-3.

[19] D. J. Cram, J. M. Cram, *Complexes between organic compounds simulate the substrate selectivity of enzymes* **1974**, *183*, 803-809. DOI: http://dx.doi.org/10.1126/science.183.4127.803.

[20] B. L. Feringa, *Angewandte Chemie International Edition* **2017**, *56*, 11060-11078. DOI: http://dx.doi.org/https://doi.org/10.1002/anie.201702979.

[21] a) J. F. Stoddart, *Angewandte Chemie International Edition* **2017**, *56*, 11094-11125. DOI: http://dx.doi.org/https://doi.org/10.1002/anie.201703216; b) J. Chen, F. K.-c. Leung, M. C. A. Stuart, T. Kajitani, T. Fukushima, E. Van Der Giessen, B. L. Feringa, *Nature chemistry* **2018**, *10*, 132-138. DOI: http://dx.doi.org/http://dx.doi.org/10.1038/nchem.2887; c) S. Li, Q. Zou, Y. Li, C. Yuan, R. Xing, X. Yan, *Journal of the American Chemical Society* **2018**, *140*, 10794-10802. DOI: http://dx.doi.org/10.1021/jacs.8b04912; d) T. L. Mako, J. M. Racicot, M. Levine, *Chemical reviews* **2019**, *119*, 322-477. DOI: http://dx.doi.org/10.1021/acs.chemrev.8b00260; e) J. Li, J. Wang, H. Li, N. Song, D. Wang, B. Z. Tang, *Chemical Society reviews* **2020**, *49*, 1144-1172. DOI: http://dx.doi.org/10.1039/C9CS00495E; f) Y. Huang, R.-H. Gao, M. Liu, L.-X. Chen, X.-L. Ni, X. Xiao, H. Cong, Q.-J. Zhu, K. Chen, Z. Tao, *Angewandte Chemie International Edition* **2021**, *60*, 15166-15191. DOI: http://dx.doi.org/https://doi.org/10.1002/anie.202002666.

[22] J.-M. Lehn, Springer Berlin Heidelberg, Berlin, Heidelberg, **1973**, pp. 1-69.

[23] J. L. Sessler, C. M. Lawrence, J. Jayawickramarajah, *Chemical Society reviews* **2007**, *36*, 314-325. DOI: http://dx.doi.org/10.1039/B604119C.

[24] a) V. Balzani, A. Credi, S. Silvi, M. Venturi, *Chemical Society reviews* **2006**, *35*, 1135-1149. DOI: http://dx.doi.org/10.1039/B517102B; b) R. E. Dawson, S. F. Lincoln, C. J. Easton, *Chem. Commun.* **2008**, 3980–3982. DOI: http://dx.doi.org/10.1039/B809014A; c) M. N. Tasbas, E. Sahin, S. Erbas-Cakmak, *Coordination Chemistry Reviews* **2021**, *443*, 214039. DOI: http://dx.doi.org/https://doi.org/10.1016/j.ccr.2021.214039.

[25] A. Villiers, *Compt. Rend. Fr. Acad. Sci* **1891**, *112*, 435-438.

[26] K. Freudenberg, F. Cramer, *Zeitschrift für Naturforschung B* **1948**, *3*, 464-466.

[27] a) J. Szejtli, *Chemical reviews* **1998**, *98*, 1743-1754; b) W. Saenger, *Angewandte Chemie International Edition in English* **1980**, *19*, 344-362. DOI: http://dx.doi.org/10.1002/anie.198003441.

[28] A. Hashidzume, H. Yamaguchi, A. Harada, *Eur J Org Chem* **2019**, *2019*, 3344-3357. DOI: http://dx.doi.org/10.1002/ejoc.201900090.

[29] S. Erbas-Cakmak, D. A. Leigh, C. T. McTernan, A. L. Nussbaumer, *Chemical reviews* **2015**, *115*, 10081-10206. DOI: http://dx.doi.org/10.1021/acs.chemrev.5b00146.

[30] R. Brown, *The Philosophical Magazine* **1828**, *4*, 161-173. DOI: http://dx.doi.org/10.1080/14786442808674769.

[31] J. Topping, *Physics Bulletin* **1956**, *7*, 281-281. DOI: http://dx.doi.org/10.1088/0031-9112/7/10/012.

[32] A. Einstein, *Annalen der Physik* **1905**, *322*, 549-560. DOI: http://dx.doi.org/10.1002/andp.19053220806.

[33] J. Perrin, *Atoms (translated by D. Hammick)*, Constable & Co., London, **1923**.

[34] F. Raymo, J. F. Stoddart, *ChemInform* **1996**, *28*, 33-51.

[35] G. Schill, J. Boeckmann, *Catenanes, rotaxanes, and knots*, Academic Press, New York, **1971**.

[36] D. B. Amabilino, P. R. Ashton, A. S. Reder, N. Spencer, J. F. Stoddart, *Angewandte Chemie International Edition in English* **1994**, *33*, 1286-1290. DOI: http://dx.doi.org/https://doi.org/10.1002/anie.199412861.

[37] T. Higashi, K. Morita, X. Song, J. Zhu, A. Tamura, N. Yui, K. Motoyama, H. Arima, J. Li, *Communications Chemistry* **2019**, *2*, 78. DOI: http://dx.doi.org/10.1038/s42004-019-0180-x.

[38] D. A. Leigh, J. K. Y. Wong, F. Dehez, F. Zerbetto, *Nature* **2003**, *424*, 174-179. DOI: http://dx.doi.org/10.1038/nature01758.

[39] M. Xue, Y. Yang, X. Chi, X. Yan, F. Huang, *Chemical reviews* **2015**, *115*, 7398-7501. DOI: http://dx.doi.org/10.1021/cr5005869.

[40] G. Schill, H. Zollenkopf, *Liebigs Ann. Chem.* **1969**, *721*.

[41] C.-A. Cheng, T. Deng, F.-C. Lin, Y. Cai, J. I. Zink, *Theranostics* **2019**, *9*, 3341-3364. DOI: http://dx.doi.org/10.7150/thno.34576.

[42] I. T. Harrison, S. Harrison, *Journal of the American Chemical Society* **1967**, *89*, 5723-5724. DOI: http://dx.doi.org/10.1021/ja00998a052.

[43] H.-L. Sun, H.-Y. Zhang, Z. Dai, X. Han, Y. Liu, *Chemistry – An Asian Journal* **2017**, *12*, 265-270. DOI: http://dx.doi.org/https://doi.org/10.1002/asia.201601545.

[44] P. R. Ashton, D. Philip, N. Spencer, J. F. Stoddart, *Journal of the Chemical Society, Chemical Communications* **1991**, 1677-1679. DOI: http://dx.doi.org/10.1039/C39910001677.

[45] P. L. Chee, A. Prasad, X. Fang, C. Owh, V. J. J. Yeo, X. J. Loh, *Materials Science and Engineering: C* **2014**, *39*, 6-12. DOI: http://dx.doi.org/https://doi.org/10.1016/j.msec.2014.02.026.

[46] G. Narayanan, R. Aguda, M. Hartman, C.-C. Chung, R. Boy, B. Gupta, A. Tonelli, *Biomacromolecules* **2015**, *17*. DOI: http://dx.doi.org/10.1021/acs.biomac.5b01379.

[47] S. Sinelnikov, L. Orel, L. Kobrina, V. Boiko, S. Riabov, V. Shtompel, O. Povnitsa, S. Zagorodnya, *J Appl Polym Sci* **2021**, *138*, 50554. DOI: http://dx.doi.org/https://doi.org/10.1002/app.50554.

[48] N. L. Strutt, R. S. Forgan, J. M. Spruell, Y. Y. Botros, J. F. Stoddart, *Journal of the American Chemical Society* **2011**, *133*, 5668-5671. DOI: http://dx.doi.org/10.1021/ja111418j.

[49] A. Credi, V. Balzani, S. J. Langford, J. F. Stoddart, *Journal of the American Chemical Society* **1997**, *119*, 2679-2681. DOI: http://dx.doi.org/10.1021/ja963572l.

[50] W. S. Jeon, E. Kim, Y. H. Ko, I. Hwang, J. W. Lee, S.-Y. Kim, H.-J. Kim, K. Kim, *Angewandte Chemie International Edition* **2005**, *44*, 87-91. DOI: http://dx.doi.org/10.1002/anie.200461806.

[51] M. Han, H.-Y. Zhang, L.-X. Yang, Q. Jiang, Y. Liu, *Organic Letters* **2008**, *10*, 5557-5560. DOI: http://dx.doi.org/10.1021/ol802376k.

[52] R. Klajn, L. Fang, A. Coskun, M. A. Olson, P. J. Wesson, J. F. Stoddart, B. A. Grzybowski, *Journal of the American Chemical Society* **2009**, *131*, 4233-4235. DOI: http://dx.doi.org/10.1021/ja9001585.

[53] W. Wu, S. Song, X. Cui, T. Sun, J.-X. Zhang, X.-L. Ni, *Chinese Chemical Letters* **2018**, *29*, 95-98. DOI: http://dx.doi.org/https://doi.org/10.1016/j.cclet.2017.08.049.

[54] J. C. Chambron, V. Heitz, J. P. Sauvage, *Journal of the American Chemical Society* **1993**, *115*, 12378-12384. DOI: http://dx.doi.org/10.1021/ja00079a019.

[55] M. Asakawa, P. R. Ashton, R. Ballardini, V. Balzani, M. Bělohradský, M. T. Gandolfi, O. Kocian, L. Prodi, F. M. Raymo, J. F. Stoddart, M. Venturi, *Journal of the American Chemical Society* **1997**, *119*, 302-310. DOI: http://dx.doi.org/10.1021/ja961817o.

[56] C. A. Schalley, T. Weilandt, J. Brüggemann, F. Vögtle, in *Templates in Chemistry I: -/-* (Eds.: C. A. Schalley, F. Vögtle, K. H. Dötz), Springer Berlin Heidelberg, Berlin, Heidelberg, **2004**, pp. 141-200.

[57] S. A. Nepogodiev, J. F. Stoddart, *Chemical reviews* **1998**, *98*, 1959-1976. DOI: http://dx.doi.org/10.1021/cr970049w.

[58] M. R. Sambrook, P. D. Beer, M. D. Lankshear, R. F. Ludlow, J. A. Wisner, *Organic & Biomolecular Chemistry* **2006**, *4*, 1529-1538. DOI: http://dx.doi.org/10.1039/B518178J.

[59] K. D. Hänni, D. A. Leigh, *Chemical Society reviews* **2010**, *39*, 1240-1251. DOI: http://dx.doi.org/10.1039/B901974J.

[60] L. Liang, D. Astruc, *Coordination Chemistry Reviews* **2011**, *255*, 2933-2945. DOI: http://dx.doi.org/https://doi.org/10.1016/j.ccr.2011.06.028.

[61] O. Š. Miljanić, W. R. Dichtel, I. Aprahamian, R. D. Rohde, H. D. Agnew, J. R. Heath, J. Fraser Stoddart, *QSAR & Combinatorial Science* **2007**, *26*, 1165-1174. DOI: http://dx.doi.org/https://doi.org/10.1002/qsar.200740070.

[62] C. Casati, P. Franchi, R. Pievo, E. Mezzina, M. Lucarini, *J. Am. Chem. Soc.* **2012**, *134*, 19108-19117. DOI: http://dx.doi.org/10.1021/ja3073484.

[63] M. Baroncini, L. Casimiro, C. de Vet, J. Groppi, S. Silvi, A. Credi, *ChemistryOpen* **2018**, *7*, 169-179. DOI: http://dx.doi.org/https://doi.org/10.1002/open.201700181.

[64] M. Linke, J.-C. Chambron, V. Heitz, J.-P. Sauvage, V. Semetey, *Chemical Communications* **1998**, 2469-2470. DOI: http://dx.doi.org/10.1039/A805746J.

[65] P. L. Anelli, N. Spencer, J. F. Stoddart, *Journal of the American Chemical Society* **1991**, *113*, 5131-5133. DOI: http://dx.doi.org/10.1021/ja00013a096.

[66] C. J. Easton, S. F. Lincoln, A. G. Meyer, H. Onagi, *Journal of the Chemical Society, Perkin Transactions 1* **1999**, 2501-2506. DOI: http://dx.doi.org/10.1039/A902176K.

[67] R. E. Dawson, S. Maniam, S. F. Lincoln, C. J. Easton, *Organic & Biomolecular Chemistry* **2008**, *6*, 1814-1821. DOI: http://dx.doi.org/10.1039/B802229A.

[68] Y. Wu, M. Frasconi, W.-G. Liu, R. M. Young, W. A. Goddard, M. R. Wasielewski, J. F. Stoddart, *Journal of the American Chemical Society* **2020**, *142*, 11835-11846. DOI: http://dx.doi.org/10.1021/jacs.0c03701.

[69] P. R. Ashton, I. Baxter, S. J. Cantrill, M. C. T. Fyfe, P. T. Glink, J. F. Stoddart, A. J. P. White, D. J. Williams, *Angew Chem Int Edit* **1998**, *37*, 1294-1297. DOI: http://dx.doi.org/Doi 10.1002/(Sici)1521-3773(19980518)37:9<1294::Aid-Anie1294>3.0.Co;2-F.

[70] L. Randone, H. Onagi, S. F. Lincoln, C. J. Easton, *Eur J Org Chem* **2019**, *2019*, 3495-3502. DOI: http://dx.doi.org/https://doi.org/10.1002/ejoc.201900136.

[71] a) J. C. Chang, S. H. Tseng, C. C. Lai, Y. H. Liu, S. M. Peng, S. H. Chiu, *Nature chemistry* **2017**, *9*, 128-134. DOI: http://dx.doi.org/10.1038/Nchem.2608; b) K. Takahiro, Y. Takashi, F. Tatsuhiko, S. Yoshiteru, *Chem Lett* **2001**, *30*, 1264-1265. DOI: http://dx.doi.org/doi:10.1246/cl.2001.1264; c) T. Hoshino, M. Miyauchi, Y. Kawaguchi, H. Yamaguchi, A. Harada, *Journal of the American Chemical Society* **2000**, *122*, 9876-9877. DOI: http://dx.doi.org/10.1021/ja0018264.

[72] a) M. C. Jimenez, C. Dietrich-Buchecker, J. P. Sauvage, *Angew. Chem. Int. Ed. Engl.* **2000**, *39*, 3284-3287. DOI: http://dx.doi.org/https://doi.org/10.1002/1521-3773(20000915)39:18<3284::AID-ANIE3284>3.0.CO;2-7; b) H. Onagi, C. J. Easton, S. F. Lincoln, *Organic Letters* **2001**, *3*, 1041-1044. DOI: http://dx.doi.org/10.1021/ol015607e; c) D. Cao, C. Wang, M. A. Giesener, Z. Liu, J. F. Stoddart, *Chemical Communications* **2012**, *48*, 6791-6793. DOI: http://dx.doi.org/10.1039/C2CC32499G.

[73] M. C. Jiménez, C. Dietrich-Buchecker, J.-P. Sauvage, *Angewandte Chemie International Edition* **2000**, *39*, 3284-3287. DOI: http://dx.doi.org/https://doi.org/10.1002/1521-3773(20000915)39:18<3284::AID-ANIE3284>3.0.CO;2-7.

[74] a) E. Moulin, L. Faour, C. C. Carmona-Vargas, N. Giuseppone, *Adv Mater* **2020**, *32*, 1906036. DOI: http://dx.doi.org/https://doi.org/10.1002/adma.201906036; b) S. Tsuda, Y. Komai, S.-i. Fujiwara, Y. Nishiyama, *Chemistry – A European Journal* **2021**, *27*, 1966-1969. DOI: http://dx.doi.org/https://doi.org/10.1002/chem.202004505; c) W.-J. Li, W. Wang, X.-Q. Wang, M. Li, Y. Ke, R. Yao, J. Wen, G.-Q. Yin, B. Jiang, X. Li, P. Yin, H.-B. Yang, *Journal of the American Chemical Society* **2020**, *142*, 8473-8482. DOI: http://dx.doi.org/10.1021/jacs.0c02475.

[75] a) J. Wu, K. C.-F. Leung, D. Benítez, J.-Y. Han, S. J. Cantrill, L. Fang, J. F. Stoddart, *Angewandte Chemie International Edition* **2008**, *47*, 7470-7474. DOI: http://dx.doi.org/10.1002/anie.200803036; b) F. Coutrot, C. Romuald, E. Busseron, *Organic Letters* **2008**, *10*, 3741-3744. DOI: http://dx.doi.org/10.1021/ol801390h.

[76] a) C. J. Bruns, J. Li, M. Frasconi, S. T. Schneebeli, J. Iehl, H.-P. Jacquot de Rouville, S. I. Stupp, G. A. Voth, J. F. Stoddart, *Angewandte Chemie International Edition* **2014**, *53*, 1953-1958. DOI: http://dx.doi.org/10.1002/anie.201308498; b) C. J. Bruns, M. Frasconi, J. Iehl, K. J. Hartlieb, S. T. Schneebeli, C. Cheng, S. I. Stupp, J. F. Stoddart, *Journal of the American Chemical Society* **2014**, *136*, 4714-4723. DOI: http://dx.doi.org/10.1021/ja500675y.

[77] S. Tsuda, Y. Aso, T. Kaneda, *Chem. Commun.* **2006**, 3072-3074. DOI: http://dx.doi.org/10.1039/B604033K.

[78] S. Tsukagoshi, A. Miyawaki, Y. Takashima, H. Yamaguchi, A. Harada, *Org. Lett.* **2007**, *9*, 1053-1055. DOI: http://dx.doi.org/10.1021/ol063078e.

[79] a) Z. Zhang, C. Han, G. Yu, F. Huang, *Chem Sci* **2012**, *3*, 3026-3031. DOI: http://dx.doi.org/10.1039/C2SC20728A; b) M. C. Jimenez-Molero, C. Dietrich-Buchecker, J.-P. Sauvage, *Chemical Communications* **2003**, 1613-1616. DOI: http://dx.doi.org/10.1039/B302326P.

[80] L. Fang, M. Hmadeh, J. Wu, M. A. Olson, J. M. Spruell, A. Trabolsi, Y. W. Yang, M. Elhabiri, A. M. Albrecht-Gary, J. F. Stoddart, *J. Am. Chem. Soc.* **2009**, *131*, 7126-7134. DOI: http://dx.doi.org/10.1021/ja900859d.

[81] P. G. Clark, M. W. Day, R. H. Grubbs, *J. Am. Chem. Soc.* **2009**, *131*, 13631-13633. DOI: http://dx.doi.org/10.1021/ja905924u.

[82] Q. Zhang, S.-J. Rao, T. Xie, X. Li, T.-Y. Xu, D.-W. Li, D.-H. Qu, Y.-T. Long, H. Tian, *Chem* **2018**, *4*, 2670-2684. DOI: http://dx.doi.org/https://doi.org/10.1016/j.chempr.2018.08.030.

[83] S. Tsukagoshi, A. Miyawaki, Y. Takashima, H. Yamaguchi, A. Harada, *Org Lett* **2007**, *9*, 1053-1055. DOI: http://dx.doi.org/10.1021/ol063078e.

[84] a) G. Du, E. Moulin, N. Jouault, E. Buhler, N. Giuseppone, *Angewandte Chemie International Edition* **2012**, *51*, 12504-12508. DOI: http://dx.doi.org/10.1002/anie.201206571; b) L. Gao, Z. Zhang, B. Zheng, F. Huang, *Polymer Chemistry* **2014**, *5*, 5734-5739. DOI: http://dx.doi.org/10.1039/C4PY00733F.

[85] a) A. Goujon, G. Du, E. Moulin, G. Fuks, M. Maaloum, E. Buhler, N. Giuseppone, *Angewandte Chemie* **2016**, *55*, 703-707. DOI: http://dx.doi.org/10.1002/anie.201509813; b) X. Fu, R.-R. Gu, Q. Zhang, S.-J. Rao, X.-L. Zheng, D.-H. Qu, H. Tian, *Polymer Chemistry* **2016**, *7*, 2166-2170. DOI: http://dx.doi.org/10.1039/C6PY00309E.

[86] E. N. Guidry, J. Li, J. F. Stoddart, R. H. Grubbs, *J. Am. Chem. Soc.* **2007**, *129*, 8944-8945. DOI: http://dx.doi.org/10.1021/ja0725100.

[87] J. Berná, D. A. Leigh, M. Lubomska, S. M. Mendoza, E. M. Pérez, P. Rudolf, G. Teobaldi, F. Zerbetto, *Nat. Mater.* **2005**, *4*, 704-710. DOI: http://dx.doi.org/10.1038/nmat1455.

[88] Y. Liu, A. H. Flood, P. A. Bonvallet, S. A. Vignon, B. H. Northrop, H.-R. Tseng, J. O. Jeppesen, T. J. Huang, B. Brough, M. Baller, S. Magonov, S. D. Solares, W. A. Goddard, C.-M. Ho, J. F. Stoddart, *Journal of the American Chemical Society* **2005**, *127*, 9745-9759. DOI: http://dx.doi.org/10.1021/ja051088p.

[89] K. Iwaso, Y. Takashima, A. Harada, *Nature chemistry* **2016**, *8*, 625-632. DOI: http://dx.doi.org/10.1038/nchem.2513.

[90] A. Goujon, G. Mariani, T. Lang, E. Moulin, M. Rawiso, E. Buhler, N. Giuseppone, *J Am Chem Soc* **2017**, *139*, 4923-4928. DOI: http://dx.doi.org/10.1021/jacs.7b00983.

[91] D. B. Amabilino, J. F. Stoddart, *Chemical reviews* **1995**, *95*, 2725-2828. DOI: http://dx.doi.org/10.1021/cr00040a005.

[92] a) A. Arduini, F. Ciesa, M. Fragassi, A. Pochini, A. Secchi, *Angew. Chem. Int. Edit.* **2005**, *44*, 278-281. DOI: http://dx.doi.org/10.1002/anie.200461336; b) A. Arduini, R. Bussolati, A. Credi, G. Faimani, S. Garaudee, A. Pochini, A. Secchi, M. Semeraro, S. Silvi, M. Venturi, *Chem. – Eur. J.* **2009**, *15*, 3230-3242. DOI: http://dx.doi.org/10.1002/chem.200801926; c) H. X. Wang, Z. Meng, J. F. Xiang, Y. X. Xia, Y. H. Sun, S. Z. Hu, H. Chen, J. N. Yao, C. F. Chen, *Chem. Sci.* **2016**, *7*, 469-474. DOI: http://dx.doi.org/10.1039/c5sc03511b; d) V. Zanichelli, G. Ragazzon, A. Arduini, A. Credi, P. Franchi, G. Orlandini, M. Venturi, M. Lucarini, A. Secchi, S. Silvi, *Eur. J. Org. Chem.* **2016**, 1033-1042. DOI: http://dx.doi.org/10.1002/ejoc.201501522; e) P. La Manna, C. Talotta, C. Gaeta, A. Soriente, M. De Rosa, P. Nerie, *J. Org. Chem.* **2017**, *82*, 8973-8983. DOI: http://dx.doi.org/10.1021/acs.joc.7b01388.

[93] a) J. E. H. Buston, J. R. Young, H. L. Anderson, *Chem. Commun.* **2000**, 905-906. DOI: http://dx.doi.org/10.1039/B001812k; b) J. E. H. Buston, F. Marken, H. L. Anderson, *Chem. Commun.* **2001**, 1046-1047. DOI: http://dx.doi.org/10.1039/B102068o; c) J. W. Park, H. J. Song, *Org. Lett.* **2004**, *6*, 4869-4872. DOI: http://dx.doi.org/10.1021/ol048079q; d) A. J. Baer, D. H. Macartney, *Supramol Chem* **2007**, *19*, 537-546. DOI: http://dx.doi.org/10.1080/10610270601185200.

[94] a) R. Isnin, A. E. Kaifer, *J. Am. Chem. Soc.* **1991**, *113*, 8188-8190. DOI: http://dx.doi.org/10.1021/Ja00021a067; b) R. Isnin, A. E. Kaifer, *Pure Appl. Chem.* **1993**, *65*, 495-498. DOI: http://dx.doi.org/10.1351/pac199365030495.

[95] M. R. Craig, M. G. Hutchings, T. D. W. Claridge, H. L. Anderson, *Angew. Chem. Int. Edit.* **2001**, *40*, 1071-1074. DOI: http://dx.doi.org/10.1002/1521-3773(20010316)40:6<1071::Aid-Anie10710>3.0.Co;2-5.

[96] Q. C. Wang, X. Ma, D. H. Qu, H. Tian, *Chem. - Eur. J.* **2006**, *12*, 1088-1096. DOI: http://dx.doi.org/10.1002/chem.200500415.

[97] M. Bazzoni, L. Andreoni, S. Silvi, A. Credi, G. Cera, A. Secchi, A. Arduini, *Chem Sci* **2021**, *12*, 6419-6428. DOI: http://dx.doi.org/10.1039/D1SC00279A.

[98] B. Chen, K. Xu, *Nano* **2019**, *14*, 1930007. DOI: http://dx.doi.org/10.1142/s179329201930007x.

[99] N. K, C. S. Rout, *RSC Advances* **2021**, *11*, 5659-5697. DOI: http://dx.doi.org/10.1039/D0RA07800J.

[100] J. E. Lennard-Jones, *Proceedings of the Royal Society of London. Series A - Mathematical and Physical Sciences* **1937**, *158*, 280-296. DOI: http://dx.doi.org/doi:10.1098/rspa.1937.0020.

[101] H. Kuhn, *The Journal of chemical physics* **1949**, *17*, 1198-1212. DOI: http://dx.doi.org/10.1063/1.1747143.

[102] H. C. Longuet-Higgins, L. Salem, *Proceedings of the Royal Society of London. Series A. Mathematical and Physical Sciences* **1959**, *251*, 172-185. DOI: http://dx.doi.org/doi:10.1098/rspa.1959.0100.

[103] R. E. Peierls, *Quantum Theory of Solids*, Clarendon Press, **1996**.

[104] A. J. Heeger, *Angew. Chem. Int. Ed. Engl.* **2001**, *40*, 2591-2611.

[105] a) M. Goehring, *Quarterly Reviews, Chemical Society* **1956**, *10*, 437-450. DOI: http://dx.doi.org/10.1039/QR9561000437; b) D. Chapman, R. J. Warn, A. G. Fitzgerald, A. D. Yoffe, *Transactions of the Faraday Society* **1964**, *60*, 294-300. DOI: http://dx.doi.org/10.1039/TF9646000294; c) M. M. Labes, P. Love, L. F. Nichols, *Chemical reviews* **1979**, *79*, 1-15. DOI: http://dx.doi.org/10.1021/cr60317a002.

[106] W. A. Little, *Physical Review* **1964**, *134*, A1416-A1424. DOI: http://dx.doi.org/10.1103/PhysRev.134.A1416.

[107] a) R. H. Friend, R. W. Gymer, A. B. Holmes, J. H. Burroughes, R. N. Marks, C. Taliani, D. D. C. Bradley, D. A. D. Santos, J. L. Brédas, M. Lögdlund, W. R. Salaneck, *Nature* **1999**, *397*, 121; b) A. Kraft, A. C. Grimsdale, A. B. Holmes, *Angewandte Chemie International Edition* **1998**, *37*, 402-428. DOI: http://dx.doi.org/10.1002/(sici)1521-3773(19980302)37:4<402::aid-anie402>3.0.co;2-9.

[108] a) H. Sirringhaus, N. Tessler, R. H. Friend, *Science* **1998**, *280*, 1741-1744. DOI: http://dx.doi.org/10.1126/science.280.5370.1741; b) C. D. Dimitrakopoulos, P. R. L. Malenfant, *Adv Mater* **2002**, *14*, 99-117. DOI: http://dx.doi.org/10.1002/1521-4095(20020116)14:2<99::aid-adma99>3.0.co;2-9.

[109] a) K. M. Coakley, M. D. McGehee, *Chem Mater* **2004**, *16*, 4533-4542. DOI: http://dx.doi.org/10.1021/cm049654n; b) M. Granström, K. Petritsch, A. C. Arias, A. Lux, M. R. Andersson, R. H. Friend, *Nature* **1998**, *395*, 257-260. DOI: http://dx.doi.org/10.1038/26183.

[110] a) A. Rose, Z. Zhu, C. F. Madigan, T. M. Swager, V. Bulović, *Nature* **2005**, *434*, 876-879. DOI: http://dx.doi.org/10.1038/nature03438; b) J. H. Wosnick, T. M. Swager, *Current opinion in chemical biology* **2000**, *4*, 715-720.

[111] M. J. Frampton, H. L. Anderson, *Angew. Chem. Int. Ed. Engl.* **2007**, *46*, 1028-1064. DOI: http://dx.doi.org/10.1002/anie.200601780.

[112] a) P. Enzel, T. Bein, *The Journal of Physical Chemistry* **1989**, *93*, 6270-6272. DOI: http://dx.doi.org/10.1021/j100354a004; b) T. Bein, P. Enzel, *Angewandte Chemie International Edition in English* **1989**, *28*, 1692-1694. DOI: http://dx.doi.org/10.1002/anie.198916921; c) P. Enzel, T. Bein, *Journal of the Chemical Society, Chemical Communications* **1989**, 1326-1327. DOI: http://dx.doi.org/10.1039/C39890001326.

[113] S. Anderson, R. T. Aplin, T. D. W. Claridge, T. Goodson Iii, A. C. Maciel, G. Rumbles, J. F. Ryan, H. L. Anderson, *J. Chem. Soc., Perkin Trans. 1* **1998**, 2383-2398. DOI: http://dx.doi.org/10.1039/A802680G.

[114] T. A. Skotheim, J. R. Reynolds, *Handbook of conducting polymers*, **2007**.

[115] N. Gospodinova, L. Terlemezyan, *Progress in Polymer Science* **1998**, *23*, 1443-1484. DOI: http://dx.doi.org/https://doi.org/10.1016/S0079-6700(98)00008-2.

[116] M. Grigoras, C. O. Catanescu, *Journal of Macromolecular Science, Part C* **2004**, *44*, 131-173. DOI: http://dx.doi.org/10.1081/MC-120034152.

[117] A. Harada, M. Kamachi, *Macromolecules* **1990**, *23*, 2821-2823. DOI: http://dx.doi.org/10.1021/ma00212a039.

[118] G. Wenz, B. Keller, *Angewandte Chemie International Edition in English* **1992**, *31*, 197-199. DOI: http://dx.doi.org/10.1002/anie.199201971.

[119] a) P. N. Taylor, M. J. O'Connell, L. A. McNeill, M. J. Hall, R. T. Aplin, H. L. Anderson, *Angewandte Chemie International Edition* **2000**, *39*, 3456-3460. DOI: http://dx.doi.org/10.1002/1521-3773(20001002)39:19<3456::aid-anie3456>3.0.co;2-0; b) F. Cacialli, J. S. Wilson, J. J. Michels, C. Daniel, C. Silva, R. H. Friend, N. Severin, P. Samori, J. P. Rabe, M. J. O'Connell, P. N. Taylor, H. L. Anderson, *Nat. Mater.* **2002**, *1*, 160-164. DOI: http://dx.doi.org/10.1038/nmat750; c) J. J. Michels, M. J. O'Connell, P. N. Taylor, J. S. Wilson, F. Cacialli, H. L. Anderson, *Chemistry – A European Journal* **2003**, *9*, 6167-6176. DOI: http://dx.doi.org/10.1002/chem.200305245; d) G. Sforazzini, A. Kahnt, M. Wykes, J. K. Sprafke, S. Brovelli, D. Montarnal, F. Meinardi, F. Cacialli, D. Beljonne, B. Albinsson, H. L. Anderson, *The Journal*

of Physical Chemistry C **2014**, *118*, 4553-4566. DOI: http://dx.doi.org/10.1021/jp500624q; e) M. M. Mróz, G. Lanzani, T. Virgili, S. O. Mc Donnell, M. J. Frampton, H. L. Anderson, *Phys Rev B* **2009**, *80*, 045111. DOI: http://dx.doi.org/10.1103/PhysRevB.80.045111.

[120] T. Shimomura, T. Akai, M. Fujimori, S. Heike, T. Hashizume, K. Ito, *Synthetic Met* **2005**, *153*, 497-500. DOI: http://dx.doi.org/https://doi.org/10.1016/j.synthmet.2005.07.305.

[121] J. Terao, Y. Tanaka, S. Tsuda, N. Kambe, M. Taniguchi, T. Kawai, A. Saeki, S. Seki, *Journal of the American Chemical Society* **2009**, *131*, 18046-18047. DOI: http://dx.doi.org/10.1021/ja908783f.

[122] P. Henrique S. Paulino, C. F. Silva, W. B. De Almeida, L. Guimarães, C. S. Nascimento, *Computational and Theoretical Chemistry* **2021**, *1197*, 113157. DOI: http://dx.doi.org/https://doi.org/10.1016/j.comptc.2021.113157.

[123] P.-O. Morin, T. Bura, M. Leclerc, *Materials Horizons* **2016**, *3*, 11-20. DOI: http://dx.doi.org/10.1039/C5MH00164A.

[124] M. Xue, Y. Yang, X. D. Chi, X. Z. Yan, F. H. Huang, *Chem. Rev.* **2015**, *115*, 7398-7501. DOI: http://dx.doi.org/10.1021/cr5005869.

[125] A. Harada, A. Hashidzume, H. Yamaguchi, Y. Takashima, *Chem. Rev.* **2009**, *109*, 5974-6023. DOI: http://dx.doi.org/10.1021/cr9000622.

[126] S. E. Brown, C. J. Easton, J. B. Kelly, *J. Incl. Phenom. Macro.* **2003**, *46*, 167-173. DOI: http://dx.doi.org/Doi 10.1023/A:1026311003881.

[127] C. Wendeln, I. Singh, S. Rinnen, C. Schulz, H. F. Arlinghaus, G. A. Burley, B. J. Ravoo, *Chem Sci* **2012**, *3*, 2479-2484. DOI: http://dx.doi.org/10.1039/C2SC20555F.

[128] S. Maniam, M. M. Cieslinski, S. F. Lincoln, H. Onagi, P. J. Steel, A. C. Willis, C. J. Easton, *Org. Lett.* **2008**, *10*, 1885-1888. DOI: http://dx.doi.org/10.1021/ol8002145.

Chapter 2 - DIRECT SYNTHESIS OF AN OLIGOMERIC SERIES OF INTERLOCKED, CYCLODEXTRIN-BASED [*c*2]DAISY CHAINS

2.1 Foreword

As discussed in the Introduction, one of the objectives of the work described in this thesis was to prepare an oligomeric series of interlocked [*c*2]daisy-chains with potential to act as functional materials.* Molecular daisy chains can be acyclic [*a*n] or cyclic [*c*n]. Between the two, cyclic daisy chains are thermodynamically more stable. In particular, the formation of cyclic dimers [*c*2] is entropically favourable, as it maximizes the number of host-guest complexes with the minimum number of constituents. Their synthesis and switching behaviour have therefore been extensively explored in the literature.* Following these studies, the oligomerisation of [*c*2]daisy-chains has become an appealing challenge for supramolecular chemists because the oligomers can potentially extend the molecular motions observed in the dimers.* In the usual approach for the synthesis of interlocked [*c*2]daisy-chain oligomers, monomers are not directly extended into oligomers. Instead, the reaction is carried out in two steps: initially monomers are locked into [*c*2]daisy-chains by adding capping groups; subsequently the capped [*c*2]daisy-chains are connected together through linkers to form linear oligomers of the dimers. This method has the advantage that, after the capping, relatively harsh conditions can be applied to

the system in order to optimise the reaction yield; however the need for two different steps to complete the oligomerisation is a limitation. The aim of the work presented in this Chapter was therefore to develop an alternative approach in order to overcome this drawback. To this end a linear oligomerisation was directly performed from a monomer and its cyclic dimer that formed spontaneously in equilibrium in solution. The reaction resulted in the formation of eight individual supramolecular species, which were isolated and fully characterised. In addition, preliminary photochemical experiments were performed to analyse their switching behaviour.

This research has been reported in a publication in the European Journal of Organic Chemistry, issue 21, pages 3495-3502, 2019, entitled *'Direct Synthesis of an Oligomeric Series of Interlocked, Cyclodextrin-Based [c2]Daisy Chains'*, which is copied on the following pages. This work is particularly innovative because it represents a one-pot condensation of up to sixteen molecular components, resulting in discrete interlocked compounds consisting of two to five dimeric complexes.

*Literature citations are provided in the following manuscript.

2.2 Manuscript

Australian National University

Statement of Contribution

I declare that the research published in this multi-authored paper represents original work that I carried out during my candidature at the Australian National University, except for contributions by other authors as specified in this Statement of Contribution.

Title: Direct Synthesis of an Oligomeric Series of Interlocked, Cyclodextrin-Based [c2]Daisy Chains

Authors: Lisa Randone, Hideki Onagi, Stephen F. Lincoln and Christopher J. Easton

Publication outlet: European Journal of Organic Chemistry

Current status of paper: Published

Contribution to paper:

I carried out all the experiments and assisted with the preparation of the manuscript.

H. Onagi, S. Lincoln and C. Easton supervised the research and assisted in preparation of the manuscript.

Senior author or collaborating authors endorsement:

Prof. Chris J. Easton		20/09/2021
C. Easton	Signature	Date
Hideki Onagi		20/09/2021
H. Onagi	Signature	Date
Prof. Stephen F. Lincoln		21/09/2021
S. Lincoln	Signature	Date
Lisa Randone		20/09/2021
L. Randone - Candidate	Signature	Date

Endorsed

Prof. Chris J. Easton		20/09/2021
Primary Supervisor – Print Name	Signature	Date
Luke Connal		24- sept- 2021
Delegated Authority – Print Name	Signature	Date

ChemPubSoc Europe
DOI: 10.1002/ejoc.201900136
EurJOC European Journal of Organic Chemistry
Full Paper

SPECIAL ISSUE

Molecular Daisy Chains

Direct Synthesis of an Oligomeric Series of Interlocked, Cyclodextrin-Based [c2]Daisy Chains

Lisa Randone,[a] Hideki Onagi,[a] Stephen F. Lincoln,[b] and Christopher J. Easton*[a]

Abstract: Despite their anticipated utility and aesthetic appeal, attempts to prepare extended molecular daisy chains have been thwarted by preferential formation of cyclic dimers ([c2]-rotaxanes). Previously, to circumvent this limitation, an alternative type of molecular chain has been synthesized by linking pre-prepared [c2]rotaxanes already interlocked with bulky capping groups. Instead of this stepwise approach, here we describe the direct self-assembly of dimeric complexes and their in situ oligomerization, which simultaneously interlocks the dimers so that no prior capping of the complexes is required. Eight individual supramolecular species, including a tetramer, hexamer, octamer and decamer series, have been isolated and characterized. The decamer is derived from 16 molecular components, through ten highly selective reactions of six equivalents of the bifunctional linking reagent with five self-assembled dimeric cyclodextrin inclusion complexes, all in one pot.

Introduction

Mechanically-interlocked, molecular daisy chains have attracted considerable attention as challenging targets for synthesis, due to their aesthetic appeal and potential utility as components of functional materials.[1–5] Conceptually, they are comprised of hermaphroditic monomer units having both host and guest recognition sites, assembled into linear and cyclic chains, and physically blocked to prevent dissociation of the components (Figure 1). Although these arrangements are simple to imagine, in practice and with very few exceptions,[5–7] related syntheses generally produce only [c2]-species.[8–11] This occurs because the corresponding cyclic-dimeric complexes are formed in preference to those that would lead to [cn]- (n > 2) and acyclic (*a*n) chains. This bias results from the greater thermodynamic stability of complexes having the least number of monomer units that still allow every guest component to be included in a host and every host moiety to have an included guest.

An alternative type of molecular chain may be prepared without this limitation, by linking [c2]rotaxanes that are already mechanically interlocked with covalently-attached, bulky capping groups (Figure 2).[4,12–21] In various cases that have been reported, oligomerization of dimers of this type has been accomplished through covalent modification of the blocking groups,[4,12–14] while dynamic metal chelation[15,16] and hydrogen-bonding[17–20] have been used for their polymerization. As an example of the former of these methods, Kaneda et al.,[12] produced the tetrameric, hexameric, octameric and decameric cyclodextrin derivatives **2a-d** (*n* = 1–4) in the ratio 33:14:4:2 from the dimer **1** (Scheme 1). In a similar way, Grubbs and Stoddart et al.,[4,13,14] employed acyclic-diene metathesis and double-Cu-catalyzed-Huisgen 1,3-dipolar cycloaddition (Click chemistry), to give mixtures of oligomerized [c2]rotax-

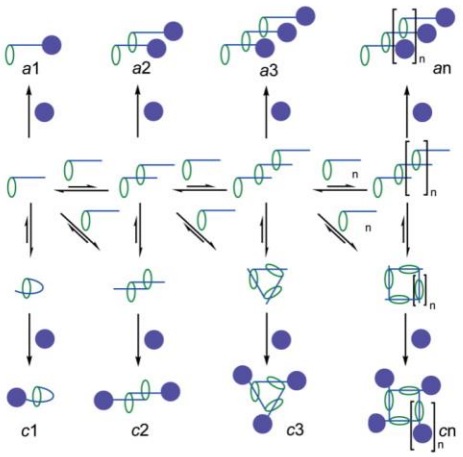

Figure 1. Conceptual formation of linear and cyclic, molecular daisy chains, and related species.

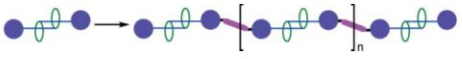

Figure 2. Representation of the production of molecular chains from pre-prepared, capped [c2]rotaxanes.

[a] Research School of Chemistry, The Australian National University, Canberra ACT 2601, Australia
E-mail: Chris.Easton@anu.edu.au
https://chemistry.anu.edu.au
[b] Department of Chemistry, The University of Adelaide, Adelaide SA 5005, Australia
Supporting information and ORCID(s) from the author(s) for this article are available on the WWW under https://doi.org/10.1002/ejoc.201900136.

ChemPubSoc Europe
EurJOC European Journal of Organic Chemistry
Full Paper

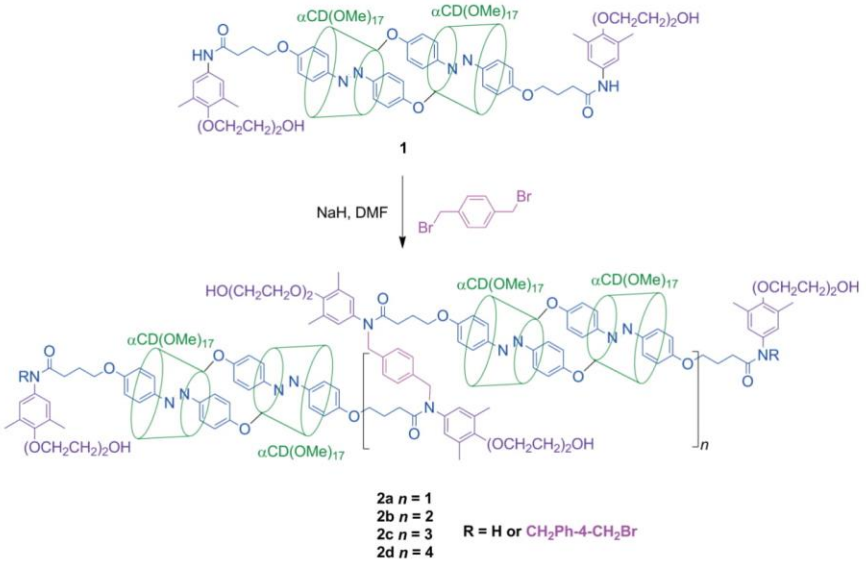

Scheme 1. Preparation of oligomeric chains of [c2]rotaxanes reported by Kaneda et al.[12]

anes. Molecular chains of this configuration retain the inherently-flexible rotaxane units, in some cases with switchable behavior.[12–19]

In a recent, seminal paper, Harada et al.,[22] reported the incorporation of a dimeric cyclodextrin complex into a polymer gel network and demonstrated photochemically-induced expansion and contraction of the gel in accord with the corresponding realignment of the incorporated complex. More recently, Guiseppone and Buhler et al.,[23] used Click chemistry to prepare chemical gels incorporating cyclodextrin dimers. Their gels expanded and contracted in response to pH changes. Here, we describe a related strategy for the direct synthesis of a homologous series of interlocked, cyclodextrin-based [c2]daisy-chains. It involves self-assembly of dimeric complexes and their in situ oligomerization, which simultaneously interlocks the dimers to produce the [c2]rotaxane moieties (Figure 3). Unlike previous reports,[4,12–20] it does not require prior synthesis of a capped [c2]rotaxane. It produces discrete molecular entities, including a cyclodextrin tetramer, hexamer, octamer and decamer, which have been separated and individually characterized. In the case of the decamer, its formation constitutes the condensation of 16 molecular components, through self-assembly of ten cyclodextrin derivatives into five dimeric complexes, and their interlocking through ten covalent bond forming reactions with six bifunctional linking reagents.

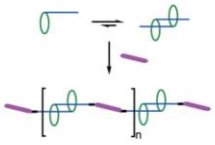

Figure 3. Representation of the direct synthesis of molecular chains of [c2]rotaxanes, by linking and simultaneously interlocking self-assembled dimeric complexes.

Results and Discussion

In developing this direct synthesis of daisy-chain oligomers, we first tried a variety of alternatives that were unsuccessful, but they highlight the challenges faced. An aqueous medium is normally required to accomplish cyclodextrin host-guest complexation, and therefore the linking reagents had to be compatible with this solvent. This had not been necessary in the indirect synthesis reported previously by Kaneda et al.,[12] where the complexation and linking were performed separately, so the synthesis of their [c2]rotaxane was performed in aqueous methanol and their subsequent oligomerization employed NaH in DMF. Earlier, we had prepared the cyclodextrin [c2]rotaxanes **4a,b** through reaction of the hermaphroditic monomers **3a,b** with 2-chloro-4,6-dimethoxy-1,3,5-triazine in water (Scheme 2),[10,24] so our initial attempts involved the monomer **3a** and bifunctional triazine variants such as 2,4-dichloro-6-methoxy-1,3,5-triazine as potential linkers. However, these reactions were all ineffective due to competing hydrolysis of the triazines and their side reactions with cyclodextrin hydroxyl groups.

Takata et al.,[25,26] used 2-bromo- and 3,5-dimethyl-phenyl-isocyanate as capping reagents to produce the [3]rotaxanes **5a**

ChemPubSoc Europe
EurJOC European Journal of Organic Chemistry
Full Paper

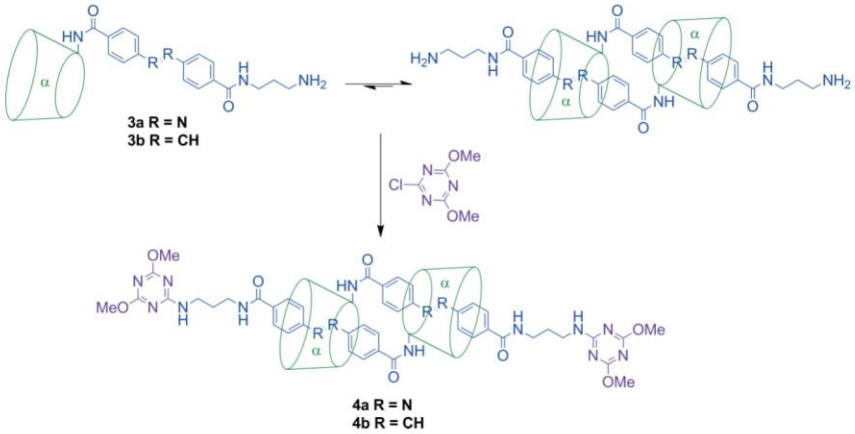

Scheme 2. Synthesis of the [*c*2]rotaxanes **4a,b**.[10,24]

and **5b**, respectively (Figure 4). While we reproduced the synthesis of **5b** without difficulty, attempts to adapt that method using 4-bromo-2,6-dimethylphenylisocyanate gave only very small amounts of the analogue **5c**, as determined by HPLC and MALDI-TOF mass spectrometry, even after extended reaction times and with large excesses of the isocyanate. Likewise, treatment of the monomer **3a** with 4-bromo-2,6-dimethylphenylisocyanate afforded only a trace of the [*c*2]rotaxane **6**. In principal, this material could have been elaborated to chains of [*c*2]rotaxanes, but its synthesis on any useful scale proved to be impractical. Instead, we next focused on the reaction of the cyclodextrin derivative **3a** with 1,4-phenyldiisocyanate. This afforded small amounts of species that were isolated by HPLC and tentatively identified, on the basis of their MALDI-TOF mass spectra, as a linear tetramer, cyclic dimer and cyclic tetramer having structures analogous to those representing **9a**, **11** and **12** in Figure 5. Other water-soluble products were monomeric and trimeric. In addition, a relatively large amount of precipitate formed in the reaction mixture, which appeared to be derived from the production of carbamates through reaction of cyclodextrin hydroxyl groups with the diisocyanate. In an attempt to avoid this, we prepared the permethylated cyclodextrin analogue of the monomer **3a**, but the MALDI-TOF mass spectrum of the product of its reaction with the diisocyanate again showed only traces of dimer, trimer and tetramer, but no evidence of higher oligomers. Experimental details are provided in the Supporting Information.

We also investigated several bis-activated dicarboxylic acids as possible linking reagents. Generally, these also afforded complex product mixtures, complicated by reagent hydrolysis and side reactions with the cyclodextrin **3a**, until we tried the suberic acid derivative **7** (Sigma-Aldrich Chem. Co.). It is water-

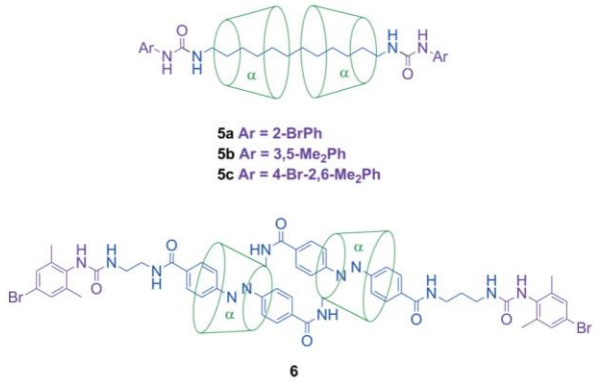

Figure 4. Structures of the [*c*2]rotaxanes **5a**,[25,26] **5b**,[25,26] **5c** and **6**.

ChemPubSoc Europe
EurJOC European Journal of Organic Chemistry
Full Paper

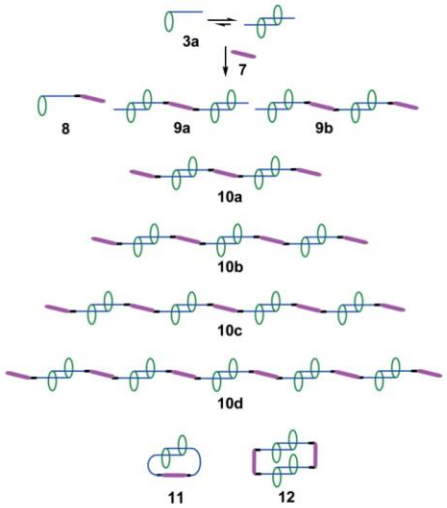

Figure 5. Representation of the production of interlocked [*c*2]daisy chains shown in Scheme 3.

soluble and known to react selectively with primary amines, under mild conditions, in aqueous media.[27,28] Consequently, it has been used extensively in biological chemistry, as a cross-linking agent to prepare protein-protein, receptor-ligand and hapten-carrier molecule conjugates. With the cyclodextrin **3a**, it finally afforded a series of oligomers of interlocked [*c*2]daisy-chains (Scheme 3, Figure 5).

A representative reaction was carried out with the cyclodextrin **3a** (120 mM) and the linking reagent **7** (0.6 equiv.), at room temperature in pH 9.5 carbonate buffer. This pH was chosen so as to maintain the amino group of the cyclodextrin **3a** as the nucleophilic free base, while minimizing deprotonation and therefore reactivity of the cyclodextrin hydroxyl groups. At 1 mM concentration and higher, aqueous solutions of the cyclodextrin **3a** show concentration-independent ^{1}H NMR spectra with cross-correlations in the ROESY NMR spectra between cyclodextrin and azobenzene proton resonances, indicating effectively complete formation of a symmetric host-guest complex. A 20 mM concentration of the cyclodextrin **3a** was used in the synthesis of **4a**.[10,24] Therefore, the concentration of **3a** used here greatly exceeds that required to expect full self-assembly into a dimeric complex and [*c*2]rotaxane formation.

After 24 h, fractionation of the reaction mixture using HPLC afforded pure samples of each of the major components; the tetrameric species **9a** and **9b**, as well as the starting monomer **3a** and its suberic acid derivative **8** (See Supporting Information for details). Further reaction occurred with extended reaction times until, after 3 days, only a trace of the unreacted monomer **3a** remained and the tetramer **9a** was no longer detected using the same reverse-phase analytical method. Instead, normal-phase HPLC analysis (Figure 6), suitable for larger and more polar species, showed that the major components of the product mixture after this time were the derivatized monomer **8**, some of the tetramer **9b**, and an oligomeric series of linearly-linked [*c*2]daisy chains, of which the tetramer **10a**, hexamer **10b**, octamer **10c** and decamer **10d** were each separated by HPLC. Samples of the cyclic dimer **11** and of a species that was tentatively identified as the cyclic tetramer **12** were also isolated.

Each of the separated compounds **8**, **9a,b**, **10a-d** and **11** was characterized using HPLC, mass spectrometry and NMR spectroscopy (See Supporting Information for details). HPLC analysis with a photodiode array detector showed a single component in every case, with a λ_{max} at 332 nm for compound **8**, but near 340–345 nm for the others. These wavelengths are typical of *trans*-azobenzene moieties, with the shift to higher wavelength for **9a,b**, **10a-d** and **11** being characteristic of inclusion in a cyclodextrin.[29,30] The mass spectra all displayed diagnostic $[M + Na]^+$ ions. More detailed information was provided by the NMR spectra. In particular, the relative integrals for the azobenzene (δ7.6–8.6 ppm), propyl $CONHCH_2C\mathbf{H}_2CH_2NHCO$- (ca. δ1.85–2.00 ppm) and $-CONHCH_2C\mathbf{H}_2CH_2NH_2$ (ca. δ2.10 ppm), and octyl $-C\mathbf{H}_2CH_2CH_2CO$- (ca. δ1.30–1.45 ppm), $-CH_2C\mathbf{H}_2CH_2CO$- (ca. δ1.55–1.75 ppm), $-CH_2CH_2C\mathbf{H}_2CONH$- (ca. δ2.25–2.35 ppm) and $-CH_2CH_2C\mathbf{H}_2CO_2H$ (ca. δ2.40–2.45 ppm) proton resonances uniquely define each structure, including the extent of substitution of the terminal groups with suberic acid. Each of the compounds **8**, **9a,b**, **10a-d** and **11** showed a very similar, single set of aromatic proton resonances, indicating that all the azobenzenes are in the same type of environment. Cross-peaks in ROESY NMR spectra established that this is when the azobenzene moieties are included in cyclodextrin cavities. In the case of the monomer **8**, the inclusion is consistent with the formation of a dimeric complex under the conditions used to record the NMR spectra in D_2O. This inclusion is not reflected in the HPLC data because very little complexation occurs in the much more dilute aqueous acetonitrile solution eluting from the HPLC column. For **9a**,**b**, **10a-d** and **11**, the simplicity of their NMR spectra only matches oligomers of [*c*2]rotaxanes and there was no evidence of the formation of other [*c*n]- or [*a*n]-species. It was only practical to isolate a small sample of compound **12** but its λ_{max} at 345 nm and MALDI-TOF mass spectrum (*m*/*z* 5420, $[M + Na]^+$) are diagnostic of the assigned structure. The HPLC retention times of the cyclic dimer **11** and tetramer **12** are strikingly dissimilar (Figure 6). Under the normal-phase conditions of this analysis, the dimer **11** has a much longer retention time and therefore appears to be significantly more polar. A possible reason for this is that geometric constraints in this small ring system force the cyclodextrin units out of alignment and expose more of their hydroxyl groups to solvent.

The production of compounds **9a,b**, **10a-d**, **11** and **12** involves an intricate balance of competing processes. Formation of **9a** occurs through a dimeric inclusion complex of the cyclodextrin **3a** reacting with a second complex formed between **3a** and the product of the reaction of **3a** with the bifunctional linking reagent **7**. A competing cyclization of this asymmetric complex leads to **11**. The symmetric and asymmetric complexes are in dynamic equilibrium and **3a** may be either free or in-

ChemPubSoc Europe
EurJOC European Journal of Organic Chemistry
Full Paper

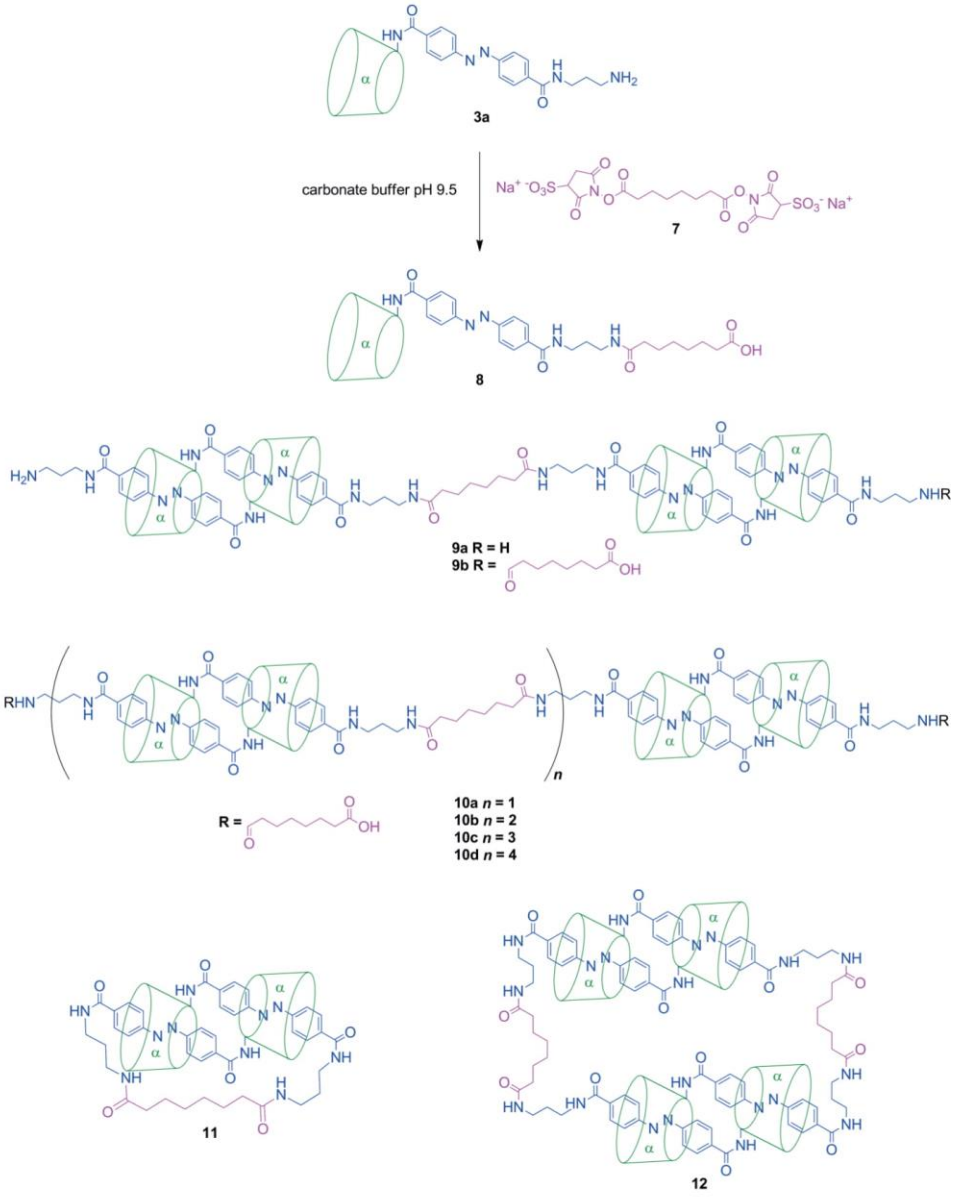

Scheme 3. Synthesis of interlocked [c2]daisy chains through reaction of the cyclodextrin **3a** with the suberic acid derivative **7**.

cluded when it reacts with **7**. One possible route to **9b** and **10a** is through sequential reactions of **9a** with **7**, followed by hydrolysis of the end-groups, but there are various other pathways. Indeed, some hydrolysis of **7** is likely to occur even before

ChemPubSoc Europe

EurJOC European Journal of Organic Chemistry

Full Paper

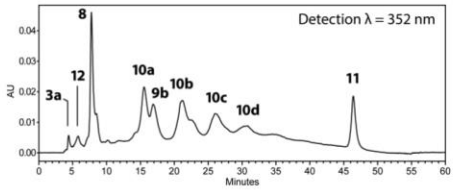

Figure 6. HPLC analysis of the mixture of products obtained from reaction of the cyclodextrin **3a** with the suberic acid derivative **7** after 3 days.

its attachment to a cyclodextrin. Consequently, **9b** and **10a** are likely to be formed in multiple ways, from **3a**, **8** and the hydroxysuccinimide ester of **8**, and the range of their inclusion complexes. The situation with **10b-d** is even more complex. With **10d**, for example, it could be produced either through coupling of various dimeric and octameric cyclodextrin species or from tetramers reacting with hexamers. Formation of **12** results from cyclization of the hydroxysuccinimide ester of **9b**, which would be in competition with oligomerization of this ester and its hydrolysis to give **9b**. An obvious consequence of this competition is that the relative proportion of **12** in the product mixture increases by a factor of around 10 when the concentration of the cyclodextrin **3a** used in the reaction is reduced from 120 mM to 30 mM.

The interlocked species **9a,b**, **10a-d** and **11** exhibit switchable behavior characteristic of *cis*-*trans* isomerization of azobenzenes.[22,24,31] In preliminary photochemical experiments (see Supporting Information for details), irradiation at 350 nm of methanol solutions of all-*trans* **10a**, **10d** and **11** resulted in 50, 55 and 60 % *trans* to *cis* conversion at the photostationary state, which was reached after around 15, 2 and 60 minutes, respectively. Species **10a** and **10d** fully reverted to their *trans*-forms on irradiation at 420 nm for 10 min. At the same wavelength, the cyclic dimer **11** only reverted from 60 % *cis* to 50 % even after longer periods of irradiation, but when the methanol was removed and replaced with water, the *trans* form was quantitatively restored. Aqueous solutions of **10a**, **10d** and **11** irradiated at 350 nm showed lower degrees of isomerization at the photostationary state, with respective *trans* to *cis* conversions of 40, 30 and 20 %. In this solvent, all three species showed full reversion to the *trans*-isomers after irradiation for 10 min at 420 nm. It was impractical to study the conformational changes associated with interconversions such as these, due to *cis*- to *trans*-azobenzene conversion occurring spontaneously in the dark at room temperature.

Conclusions

In summary, compounds **9a,b**, **10a-d**, **11** and **12** are produced through self-assembly of dimeric cyclodextrin complexes and their in situ oligomerization in competition with cyclization and hydrolysis. The oligomerization (or cyclization in the case of **11**) also serves to mechanically interlock the dimers, so that no prior capping of the complexes is required. Instead, the direct syntheses of these chains of [c2]rotaxanes rely on the high thermodynamic stability of the complexes in water, used as the reaction solvent, and the marked selectivity of the reaction of hydroxysuccinimide esters with amines in preference to both the cyclodextrin hydroxyl groups and water. Considering the decamer **10d**, as an example, it is formed by self-assembly of ten modules of the cyclodextrin derivative into five dimeric complexes and their interlocking with six modules of the bifunctional linking reagent. This one-pot condensation of sixteen molecular components involves ten reactions between hydroxysuccinimide ester and amino moieties, during which there are only two competing ester hydrolysis reactions that produce the carboxylic acid end groups. Initial photochemical experiments illustrate the potential utility of this class of compounds in functional supramolecular assemblies and materials.

Experimental Section

(*E*)-4-((4-((6^A-Deoxy-α-cyclodextrin-6^A-yl)carbamoyl)phenyl)diazenyl) benzoic acid

A solution of 6^A-amino-6^A-deoxy-α-cyclodextrin[32] (1.60 g, 1.65 mmol) and Et_3N (0.2 mL, 1.4 mmol) in anhydrous DMF (20 mL) was added dropwise over 0.5 h to a solution of azobenzene-4,4′-dicarboxylic acid (1.78 g, 6.6 mmol), BOP (1.06 g, 2.4 mmol) and Et_3N (3.2 mL, 23 mmol) in anhydrous DMF (24 mL), under nitrogen. The resultant mixture was stirred overnight at room temperature, before it was added dropwise into ice-cooled acetone (0.5 L), with stirring. The orange precipitate that formed was separated by centrifugation, washed with acetone (6 × 50 mL) then Et_2O (2 × 50 mL), and dried under vacuum, before it was dissolved in water (0.5 L). The solution was acidified to pH ca. 2 with HCl before it was applied to a Diaion HP-20 column (185 × 45 mm). The column was then eluted with water that had been acidified with HCl to pH ca. 2 (3 L), until the eluate was free of the starting aminocyclodextrin, as determined by TLC. A gradient of methanol-acidified water was then applied, and the title compound eluted with 30–40 % methanol (ca. 10 L). Fractions containing this material were combined and lyophilized to give an orange powder (1.11 g, 55 %). R_f = 0.55 (*n*-butanol/ethanol/water, 5:4:3); m.p. 228–231 °C (dec.); ^{1}H NMR (400 MHz, D_2O): δ = 8.51 (d, *J* = 8.2 Hz, 2H), 8.40 (d, *J* = 8.2 Hz, 2H), 7.74 (d, *J* = 8.2 Hz, 2H), 7.70 (d, *J* = 8.2 Hz, 2H), 5.16–4.96 (m, 6H), 4.32–3.25 (m, 36H); HRMS (ESI): *m/z* calcd. for $C_{50}H_{69}N_3O_{32}Na$ [M + Na]$^+$ 1246.3762, found 1246.3738; HPLC: t_R 9.7 min (column: YMC ODS-AQ, 250 × 20 mm, eluent MeCN/H_2O (0.1 % TFA) 1:4, flow rate 15 mL min^{-1}).

(*E*)-*tert*-Butyl (3-(4-((4-((6^A-deoxy-α-cyclodextrin-6^A-yl)carbamoyl) phenyl)diazenyl)benzamido)propyl)carbamate

A solution of (*E*)-4-((4-((6^A-deoxy-α-cyclodextrin-6^A-*yl*)carbamoyl)-phenyl) diazenyl)benzoic acid (1.11 g, 0.91 mmol), *tert*-butyl (3-aminopropyl) carbamate (0.25 g, 1.4 mmol), BOP (0.49 g, 1.1 mmol) and Et_3N (0.1 mL, 0.72 mmol) in anhydrous DMF (15 mL) was stirred overnight at room temperature, before it was added dropwise into ice-cooled acetone (0.5 L), with stirring. The orange precipitate that formed was separated by centrifugation, washed with acetone (5 × 200 mL), and dried under vacuum, before it was dissolved in water (0.5 L). The solution was applied to a Diaion HP-20 column (185 × 45 mm). The column was then eluted with water (1 L), followed by a gradient of methanol/water. The starting material eluted with 5–40 % methanol, while the title compound eluted with 45–80 % methanol. Fractions containing this material were combined and lyophilized to give an orange powder (1.02 g, 81 %). R_f = 0.74

ChemPubSoc Europe

EurJOC European Journal of Organic Chemistry

Full Paper

(*n*-butanol/ethanol/water, 5:4:3); ^{1}H NMR (400 MHz, D_2O): δ = 8.52 (d, *J* = 8.0 Hz, 2H), 8.19 (d, *J* = 8.0 Hz, 2H), 7.74 (d, *J* = 8.2 Hz, 2H), 7.69 (d, *J* = 8.2 Hz, 2H), 5.16–4.87 (m, 6H), 4.31–3.14 (m, 40H), 1.88 (m, 2H), 1.47 (s, 9H); HRMS (ESI): *m/z* calcd. for $C_{58}H_{86}N_5O_{33}$ $[M + H]^+$ 1380.5205, found 1380.5212.

(*E*)-*N*-(3-Aminopropyl)-4-((4-((6^A-deoxy-α-cyclodextrin-6^A-yl)-carbamoyl)phenyl)diazenyl)benzamide (3a)

A solution of (*E*)-*tert*-butyl (3-(4-((4-((6^A-deoxy-α-cyclodextrin-6^A-*yl*)carbamoyl)phenyl)diazenyl)benzamido)propyl)carbamate (0.20 g, 0.15 mmol) in TFA (10 mL) cooled to 5 °C was stirred for 1.5 h, before it was concentrated under vacuum to dryness, to give a red film. The film was washed with diethyl ether (3 × 5 mL) to obtain a fine precipitate, which was dried under vacuum overnight, to give the trifluoroacetate salt of the title compound as an orange powder (170 mg, 81 %). R_f = 0.14 (*i*-propanol/ethanol/water/acetic acid 5:4:3:2); m.p. 219–223 °C (dec.); ^{1}H NMR (400 MHz, D_2O): δ = 8.53 (d, *J* = 8.0 Hz, 2H), 8.20 (d, *J* = 8.0 Hz, 2H), 7.74 (d, *J* = 8.2 Hz, 2H), 7.69 (d, *J* = 8.2 Hz, 2H), 5.16–4.86 (m, 6H), 4.32–2.81 (m, 40H), 2.12–2.00 (m, 2H); HRMS (ESI): *m/z* calcd. for $C_{53}H_{78}N_5O_{31}$ $[M + H]^+$ 1280.4681, found 1280.4688; HPLC: t_R 18.1 min (column: Agilent Zorbax SB C18 3.5 µm, 150 × 4.6 mm, eluent gradient MeCN/H_2O (0.1 % TFA)/MeCN 5 % 0–3 min, 5–47 % 3–20 min, 47 % 20–30 min, flow rate 1 mL min^{-1}); HPLC: t_R 4.2 min (column: Grace Prevail Carbohydrate ES 9 µm, 300 × 20 mm, eluent gradient MeCN/H_2O (0.1 % TFA)/MeCN 70–60 % 0–40 min, 60–30 % 40–45 min, 30 % 45–60 min, flow rate 10 mL min^{-1}).

Reaction of (*E*)-*N*-(3-aminopropyl)-4-((4-((6^A-deoxy-α-cyclodextrin-6^A-yl)carbamoyl)phenyl)diazenyl)-benzamide (3a) with suberic acid bis(3-sulfonato-*N*-hydroxysuccinimide ester) disodium salt (7)

In a representative reaction, the trifluoroacetate salt of the cyclodextrin **3a** (80 mg, 62 µmol, 120 mM) was added to pH 9.5 carbonate buffer (0.5 mL, 100 mM), and the mixture was stirred at room temperature for 15 min. The suberic acid derivative **7** (22 mg, 38 µmol, 0.6 equiv.) was then added, and stirring was continued at room temperature for 3 days. HPLC analysis of the product mixture (Figure 6) after that time showed the presence of the unreacted starting material **3a**, its suberic acid derivative **8**, the cyclodextrin tetramers **9b** and **10a**, the oligomers **10b**, **10c** and **10d**, the cyclic dimer **11** and a tetrameric species **12**. Samples of **8**, **9b**, **10a**–**10d**, **11** and **12** were isolated using preparative HPLC. When the reaction product was analyzed after 1 day instead of 3, HPLC analysis showed the presence of **3a**, **8**, and the cyclodextrin tetramers **9a** and **9b**. A sample of **9a** was also isolated using preparative HPLC. HPLC was carried out using a Grace Prevail Carbohydrate ES 9 µm (300 × 20 mm) column, with a gradient eluent of MeCN/H_2O (0.1 % TFA)/MeCN 70–60 % 0–40 min, 60–30 % 40–45 min, 30 % 45–60 min, at a flow rate of 10 mL min^{-1}, monitoring at 352 nm.

Cyclodextrin monomer 8. HPLC: t_R 8.0 min, λ_{max} 332 nm; ^{1}H NMR (400 MHz, D_2O): δ = 8.52 (d, *J* = 8.1 Hz, 2H), 8.19 (d, *J* = 8.1 Hz, 2H), 7.74 (d, *J* = 8.1 Hz, 2H), 7.69 (d, *J* = 8.1 Hz, 2H), 5.20–4.90 (m, 6H), 4.40–2.90 (m, 40H), 2.41 (t, *J* = 7.3 Hz, 2H, -$CH_2CH_2CH_2CO_2H$), 2.30 (t, *J* = 7.3 Hz, 2H, -$CH_2CH_2CH_2CONH$-), 1.95–1.85 (m, 2H, -$CONHCH_2CH_2CH_2NHCO$-), 1.71–1.58 (m, 4H, -$CH_2CH_2CH_2CO$-), 1.40–1.33 (m, 4H, -$CH_2CH_2CH_2CO$-); MALDI-TOF MS: *m/z* calcd. for $C_{61}H_{89}N_5O_{34}Na$ $[M + Na]^+$ 1459, found 1460; HRMS (ESI): *m/z* calcd. for $C_{61}H_{88}N_5O_{34}$ $[M - H]^-$ 1434.5316, found 1434.5312.

Linear tetrameric daisy chain 9a. HPLC: t_R 16.2 min, λ_{max} 342 nm; ^{1}H NMR (600 MHz, D_2O): δ = 8.55 (d, *J* = 8.2 Hz, 8H), 8.23 (d, *J* = 8.2 Hz, 8H), 7.77 (d, *J* = 8.2 Hz, 8H), 7.72 (d, *J* = 8.2 Hz, 8H), 5.21–4.87 (m, 24H), 4.34–2.99 (m, 160H), 2.34 (t, *J* = 7.4 Hz, 4H, -$CH_2CH_2CH_2CONH$-), 2.13–2.08 (m, 4H, -$CONHCH_2CH_2CH_2NH2$), 1.97–1.91 (m, 4H, -$CONHCH_2CH_2CH_2NHCO$-), 1.72–1.65 (m, 4H, -$CH_2CH_2CH_2CO$-), 1.42–1.38 (m, 4H, -$CH_2CH_2CH_2CO$-); MALDI-TOF MS: *m/z* calcd. for $C_{220}H_{318}N_{20}O_{126}Na$ $[M + Na]^+$ 5282, found 5286; HRMS (ESI): *m/z* calcd. for $C_{220}H_{319}N_{20}O_{126}$ $[M + H]^+$ 5259.9264, found 5259.9455.

Linear tetrameric daisy chain 9b. HPLC: t_R 16.9 min, λ_{max} 340 nm; ^{1}H NMR (600 MHz, D_2O): δ = 8.55 (d, *J* = 8.0 Hz, 8H), 8.23 (d, *J* = 8.0 Hz, 8H), 7.77 (d, *J* = 8.0 Hz, 8H), 7.72 (d, *J* = 8.0 Hz, 8H), 5.20–4.88 (m, 24H), 4.40–3.00 (m, 160H), 2.44 (t, *J* = 7.4 Hz, 2H, -$CH_2CH_2CH_2CO_2H$), 2.34 (t, *J* = 7.4 Hz, 6H, -$CH_2CH_2CH_2CONH$-), 2.13–2.08 (m, 2H, -$CONHCH_2CH_2CH_2NH_2$), 1.97–1.91 (m, 6H, -$CONHCH_2CH_2CH_2NHCO$-), 1.72–1.65 (m, 8H, -$CH_2CH_2CH_2CO$-), 1.42–1.38 (m, 8H, -$CH_2CH_2CH_2CO$-); MALDI-TOF MS: *m/z* calcd. for $C_{228}H_{330}N_{20}O_{129}Na$ $[M + Na]^+$ 5438, found 5437; HRMS (ESI): *m/z* calcd. for $C_{228}H_{331}N_{20}O_{129}$ $[M + H]^+$ 5416.0051, found 5416.0273.

Linear tetrameric daisy chain 10a. HPLC: t_R 15.7 min, λ_{max} 343 nm; ^{1}H NMR (400 MHz, D_2O): δ = 8.52 (d, *J* = 8.0 Hz, 8H), 8.20 (d, *J* = 8.0 Hz, 8H), 7.74 (d, *J* = 8.0 Hz, 8H), 7.68 (d, *J* = 8.0 Hz, 8H), 5.20–4.88 (m, 24H), 4.36–2.97 (m, 160H), 2.40 (t, *J* = 7.4 Hz, 4H, -$CH_2CH_2CH_2CO_2H$), 2.30 (t, *J* = 7.4 Hz, 8H, -$CH_2CH_2CH_2CONH$-), 1.95–1.86 (m, 8H, -$CONHCH_2CH_2CH_2NHCO$-), 1.70–1.58 (m, 12H, -$CH_2CH_2CH_2CO$-), 1.42–1.31 (m, 12H, -$CH_2CH_2CH_2CO$-); MALDI-TOF MS: *m/z* calcd. for $C_{236}H_{342}N_{20}O_{132}Na$ $[M + Na]^+$ 5594, found 5591; HRMS (ESI): *m/z* calcd. for $C_{236}H_{343}N_{20}O_{132}$ $[M + H]^+$ 5572.0830, found 5572.0961.

Linear hexameric daisy chain 10b. HPLC: t_R 21.7 min, λ_{max} 342 nm; ^{1}H NMR (400 MHz, D_2O): δ = 8.52 (d, *J* = 8.0 Hz, 12H), 8.19 (d, *J* = 8.0 Hz, 12H), 7.73 (d, *J* = 8.0 Hz, 12H), 7.68 (d, *J* = 8.0 Hz, 12H), 5.20–4.88 (m, 36H), 4.33–2.95 (m, 240H), 2.40 (t, *J* = 7.4 Hz, 4H, -$CH_2CH_2CH_2CO_2H$), 2.31 (t, *J* = 7.4 Hz, 12H, -$CH_2CH_2CH_2CONH$-), 1.95–1.87 (m, 12H, -$CONHCH_2CH_2CH_2NHCO$-), 1.70–1.58 (m, 16H, -$CH_2CH_2CH_2CO$-), 1.41–1.32 (m, 16H, -$CH_2CH_2CH_2CO$-); MALDI-TOF MS: *m/z* calcd. for $C_{350}H_{506}N_{30}O_{196}Na$ $[M + Na]^+$ 8293, found 8290; HRMS (ESI): *m/z* calcd. for $C_{350}H_{507}N_{30}O_{196}$ $[M + H]^+$ 8270.0746, found 8270.0883.

Linear octameric daisy chain 10c. HPLC: t_R 26.7 min, λ_{max} 342 nm; ^{1}H NMR (400 MHz, D_2O): δ = 8.52 (d, *J* = 8.0 Hz, 16H), 8.19 (d, *J* = 8.0 Hz, 16H), 7.73 (d, *J* = 8.0 Hz, 16H), 7.68 (d, *J* = 8.0 Hz, 16H), 5.16–4.93 (m, 48H), 4.33–2.95 (m, 320H), 2.40 (t, *J* = 7.4 Hz, 4H, -$CH_2CH_2CH_2CO_2H$), 2.30 (t, *J* = 7.4 Hz, 16H, -$CH_2CH_2CH_2CONH$-), 1.95–1.86 (m, 16H, -$CONHCH_2CH_2CH_2NHCO$-), 1.70–1.59 (m, 20H, -$CH_2CH_2CH_2CO$-), 1.42–1.33 (m, 20H, -$CH_2CH_2CH_2CO$-); MALDI-TOF MS: *m/z* calcd. for $C_{464}H_{670}N_{40}O_{260}Na$ $[M + Na]^+$ 10991, found 10986; HRMS (ESI): *m/z* calcd. for $C_{464}H_{671}N_{40}O_{260}$ $[M + H]^+$ 10968.0676, found 10968.1170.

Linear decameric daisy chain 10d. HPLC: t_R 32.0 min, λ_{max} 341 nm; ^{1}H NMR (400 MHz, D_2O): δ = 8.51 (d, *J* = 8.0 Hz, 20H), 8.19 (d, *J* = 8.0 Hz, 20H), 7.73 (d, *J* = 8.0 Hz, 20H), 7.68 (d, *J* = 8.0 Hz, 20H), 5.16–4.93 (m, 60H), 4.33–2.94 (m, 400H), 2.40 (t, *J* = 7.4 Hz, 4H, -$CH_2CH_2CH_2CO_2H$), 2.30 (t, *J* = 7.4 Hz, 20H, -$CH_2CH_2CH_2CONH$-), 1.95–1.85 (m, 20H, -$CONHCH_2CH_2CH_2NHCO$-), 1.70–1.58 (m, 24H, -$CH_2CH_2CH_2CO$-), 1.42–1.33 (m, 24H, -$CH_2CH_2CH_2CO$-); MALDI-TOF MS: *m/z* calcd. for $C_{578}H_{834}N_{50}O_{324}Na$ $[M + Na]^+$ 13690, found 13689.

Cyclic dimeric daisy chain 11. HPLC: t_R 46.7 min, λ_{max} 342 nm; ^{1}H NMR (600 MHz, D_2O): δ = 8.55 (d, *J* = 8.0 Hz, 4H), 8.23 (d, *J* = 8.0 Hz, 4H), 7.77 (d, *J* = 8.0 Hz, 4H), 7.72 (d, *J* = 8.0 Hz, 4H), 5.16–4.93 (m, 12H), 4.36–2.98 (m, 80H), 2.34 (t, *J* = 7.0 Hz, 4H, -$CH_2CH_2CH_2CONH$-), 1.97–1.91 (m, 4H, -$CONHCH_2CH_2CH_2NHCO$-), 1.72–1.64 (m, 4H,

ChemPubSoc Europe

EurJOC European Journal of Organic Chemistry

Full Paper

-CH_2C**H**$_2$$CH_2$CO-), 1.43–1.37 (m, 4H, -C**H**$_2$$CH_2$$CH_2$CO-); MALDI-TOF MS: *m/z* calcd. for $C_{114}H_{164}N_{10}O_{64}Na$ $[M + Na]^+$ 2721, found 2722.

Cyclic tetrameric daisy chain 12. HPLC: t_R 5.8 min, λ_{max} 345 nm; MALDI-TOF MS: *m/z* calcd. for $C_{228}H_{328}N_{20}O_{128}Na$ $[M + Na]^+$ 5420, found 5420.

Photochemical Experiments

Solutions of **10a**, **10d** and **11** in methanol or water in a 1 cm quartz cuvette, prepared to an absorbance of around 0.5 at 340 nm, were irradiated at 25 °C in a Luzchem photoreactor fitted with Hitachi FL8BL-B 8 Watt lamps (350 nm) or Luzchem LZC-420 8 Watt lamps (420 nm). Reactions monitored using UV/Visible spectroscopy showed decreases or increases in the absorbance near 340–345 nm, characteristic of *trans*-azobenzenes, and corresponding increases or decreases in the absorbance near 270 nm, characteristic of *cis*-azobenzenes, related in each case through an isosbestic point near 290 nm.[22,24,29] The ratios of *cis*- and *trans*-azobenzenes in mixtures were calculated from the percentage change in the absorbance at the λ_{max} of the *trans*-isomers, assuming negligible absorbance of the *cis*-isomers at that wavelength.

Acknowledgments

The authors gratefully acknowledge financial assistance provided by the Australian Research Council.

Keywords: Cyclodextrins · Rotaxanes · Daisy chains · Oligomers · Inclusion complexes

[1] P. R. Ashton, I. Baxter, S. J. Cantrill, M. C. T. Fyfe, P. T. Glink, J. F. Stoddart, A. J. P. White, D. J. Williams, *Angew. Chem. Int. Ed.* **1998**, *37*, 1294–1297; *Angew. Chem.* **1998**, *110*, 1344–1347.
[2] G. Wenz, B.-H. Han, A. Müller, *Chem. Rev.* **2006**, *106*, 782–817.
[3] J. Rotzler, M. Mayor, *Chem. Soc. Rev.* **2013**, *42*, 44–62.
[4] E. N. Guidry, J. Li, J. F. Stoddart, R. H. Grubbs, *J. Am. Chem. Soc.* **2007**, *129*, 8944–8945.
[5] J.-C. Chang, S.-H. Tseng, C.-C. Lai, Y.-H. Liu, S.-M. Peng, S.-H. Chiu, *Nat. Chem.* **2017**, *9*, 128–134.
[6] T. Kaneda, T. Yamada, T. Fujimoto, Y. Sakata, *Chem. Lett.* **2001**, *30*, 1264–1265.
[7] T. Hoshino, M. Miyauchi, Y. Kawaguchi, H. Yamaguchi, A. Harada, *J. Am. Chem. Soc.* **2000**, *122*, 9876–9877.
[8] M. C. Jiménez, C. Dietrich-Buchecker, J.-P. Sauvage, *Angew. Chem. Int. Ed.* **2000**, *39*, 3284–3287; *Angew. Chem.* **2000**, *112*, 3422–3425.
[9] H. Onagi, S. F. Lincoln, C. J. Easton, *Org. Lett.* **2001**, *3*, 1041–1044.
[10] R. E. Dawson, S. F. Lincoln, C. J. Easton, *Chem. Commun.* **2008**, 3980–3982.
[11] D. Cao, C. Wang, M. A. Giesener, Z. Liu, J. F. Stoddart, *Chem. Commun.* **2012**, *48*, 6791–6793.
[12] S. Tsuda, Y. Aso, T. Kaneda, *Chem. Commun.* **2006**, 3072–3074.
[13] L. Fang, M. Hmadeh, J. Wu, M. A. Olson, J. M. Spruell, A. Trabolsi, Y.-W. Yang, M. Elhabiri, A.-M. Albrecht-Gary, J. F. Stoddart, *J. Am. Chem. Soc.* **2009**, *131*, 7126–7134.
[14] P. G. Clark, M. W. Day, R. H. Grubbs, *J. Am. Chem. Soc.* **2009**, *131*, 13631–13633.
[15] G. Du, E. Moulin, N. Jouault, E. Buhler, N. Giuseppone, *Angew. Chem. Int. Ed.* **2012**, *51*, 12504–12508; *Angew. Chem.* **2012**, *124*, 12672–12676.
[16] L. Gao, Z. Zhang, B. Zheng, F. Huang, *Polym. Chem.* **2014**, *5*, 5734–5739.
[17] A. Goujon, G. Du, E. Moulin, G. Fuks, M. Maaloum, E. Buhler, N. Giuseppone, *Angew. Chem. Int. Ed.* **2016**, *55*, 703–707; *Angew. Chem.* **2016**, *128*, 713–717.
[18] A. Goujon, G. Mariani, T. Lang, E. Moulin, M. Rawiso, E. Buhler, N. Giuseppone, *J. Am. Chem. Soc.* **2017**, *139*, 4923–4926.
[19] G. Mariani, A. Goujon, E. Moulin, M. Rawiso, N. Giuseppone, E. Buhler, *Nanoscale* **2017**, *9*, 18456–18466.
[20] X. Fu, R.-R. Gu, Q. Zhang, S.-J. Rao, X.-L. Zheng, D.-H. Qu, H. Tian, *Polym. Chem.* **2016**, *7*, 2166–2170.
[21] X. Yan, B. Zheng, F. Huang, *Polym. Chem.* **2013**, *4*, 2395–2399.
[22] K. Iwaso, Y. Takashima, A. Harada, *Nat. Chem.* **2016**, *8*, 625–632.
[23] A. Goujon, T. Lang, G. Mariani, E. Moulin, G. Fuks, J. Raya, E. Buhler, N. Giuseppone, *J. Am. Chem. Soc.* **2017**, *139*, 14825–14828.
[24] R. E. Dawson, J. Zhang, C. J. Easton, *Australian National University*, unpublished results.
[25] Y. Akae, H. Okamura, T. Koyama, T. Arai, T. Takata, *Org. Lett.* **2012**, *14*, 2226–2229.
[26] Y. Akae, Y. Koyama, H. Sogawa, Y. Hayashi, S. Kawauchi, S. Kuwata, T. Takata, *Chem. Eur. J.* **2016**, *22*, 5335–5341.
[27] G. Hermanson, *Bioconjugate Techniques 3rd ed.*, Academic Press, **2013**.
[28] C. Schmidt, C. V. Robinson, *Nat. Protocols* **2014**, *9*, 2224–2236.
[29] P. Bortolus, S. Monti, *J. Phys. Chem.* **1987**, *91*, 5046–5050.
[30] A. Abou-Hamdan, P. Bugnon, C. Saudan, P. G. Lye, A. E. Merbach, *J. Am. Chem. Soc.* **2000**, *122*, 592–602.
[31] R. E. Dawson, S. Maniam, S. F. Lincoln, C. J. Easton, *Org. Biomol. Chem.* **2008**, *6*, 1814–1821.
[32] S. E. Brown, J. H. Coates, D. R. Coghlan, C. J. Easton, S. J. van Eyk, W. Janowski, A. Lepore, S. F. Lincoln, Y. Luo, B. L. May, D. S. Schiesser, P. Wang, M. L. Williams, *Aust. J. Chem.* **1993**, *46*, 953–958.

Received: January 26, 2019

Supporting Information

Direct Synthesis of an Oligomeric Series of Interlocked, Cyclodextrin-Based [*c*2]Daisy Chains

Lisa Randone, Hideki Onagi, Stephen F. Lincoln, and Christopher J. Easton*

ejoc201900136-sup-0001-SupMat.pdf

Table of Contents

1. General Information

Proton Nuclear Magnetic Resonance (^{1}H NMR) spectra were acquired on a Bruker Avance 400 spectrometer and a Bruker Avance 600 spectrometer. Spectra were recorded at 400 or 600 MHz, respectively, using D_2O as solvent. 3-(Trimethylsilyl)-3,3,2,2-tetradeuteropropionic acid sodium salt (TSPA-d_4) was used as an external standard. The multiplicity of signals is abbreviated as follows: d = doublet, m = multiplet, s = singlet. NMR solvents with purity of at least 99.8% were purchased from Cambridge Isotope Laboratories Inc. High resolution electrospray ionisation (HR-ESI) mass spectra were recorded using a Waters LCT premier TM XE orthogonal acceleration time-of-flight (oa-TOF) mass spectrometer or ThermoFisher Scientific Orbitrap Elite™ Hybrid Ion Trap-Orbitrap Mass Spectrometer at 240k resolution. Matrix-Assisted Laser Desorption/Ionization (MALDI) mass spectra were acquired on an AB SCIEX 4800 MALDI-TOF mass spectrometer, using 2,5-dihydroxybenzoic acid (DHB) as matrix. Thin layer chromatography (TLC) was carried out on aluminium backed 0.2 mm EMD Millipore silica gel 60 F_{254} plates purchased from Merck. Developed plates were visualized either using UV light (254 nm) or by staining with a naphthalene-1,3-diol solution (0.1% w/v) in ethanol:water:H_2SO_4 (200:157:43), followed by heating for detecting cyclodextrins. The R_f values are reported relative to the solvent front. High performance liquid chromatography (HPLC) was carried out with a Waters 600 Controller, a Waters 717 Plus Autosampler and a Waters 2996 Photodiode Array Detector, controlled with Empower Pro Empower 2 software. HPLC solvents were purchased from Merck and ultrapure water (resistivity >15 MΩ cm^{-1}) was prepared using a Milli-Q® reagent system.

2. Compound Characterization

2.1 (*E*)-4-((4-((6^A-Deoxy-α-cyclodextrin-6^A-yl)carbamoyl)phenyl)diazenyl)benzoic acid

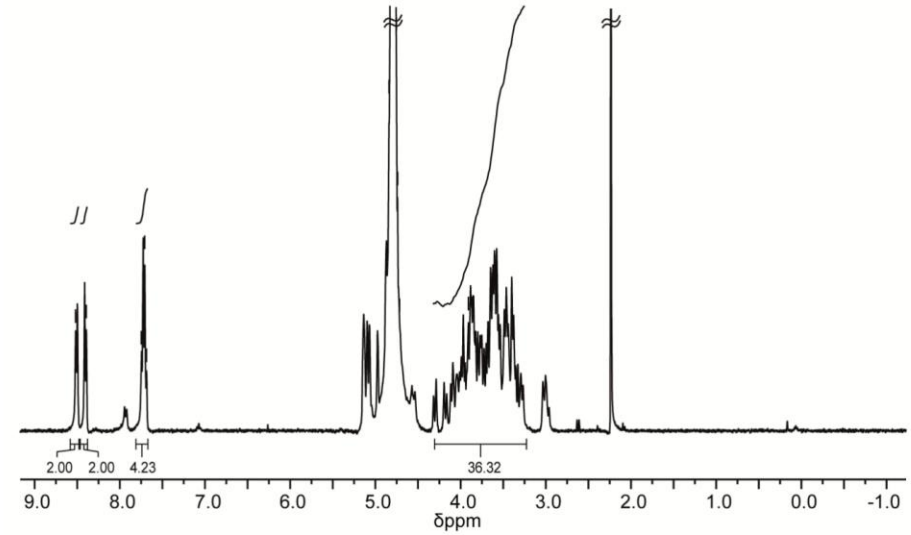

Figure S1. ^{1}H NMR spectrum (400 MHz, 298 K, D_2O).

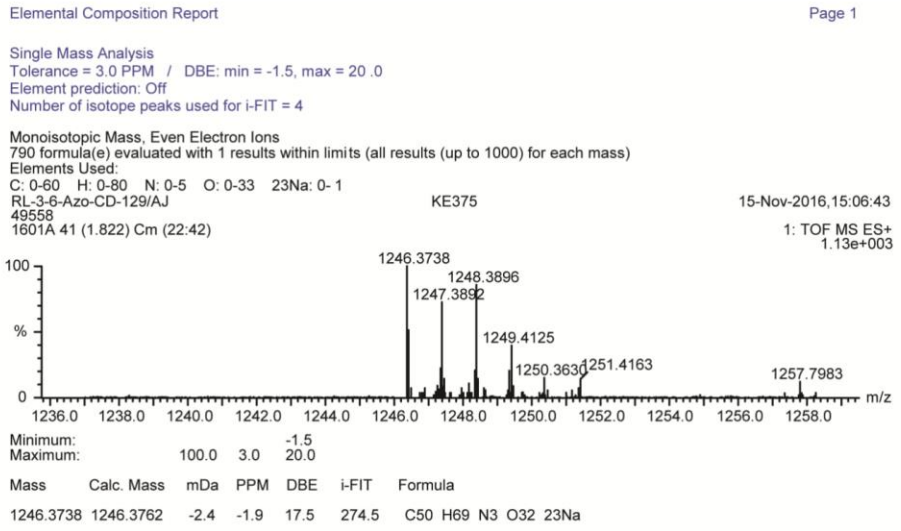

Figure S2. HR ESI spectrum.

2.2 (*E*)-*tert*-Butyl (3-(4-((4-((6^A-deoxy-α-cyclodextrin-6^A-yl)carbamoyl)phenyl)diazenyl)-benzamido)propyl)carbamate

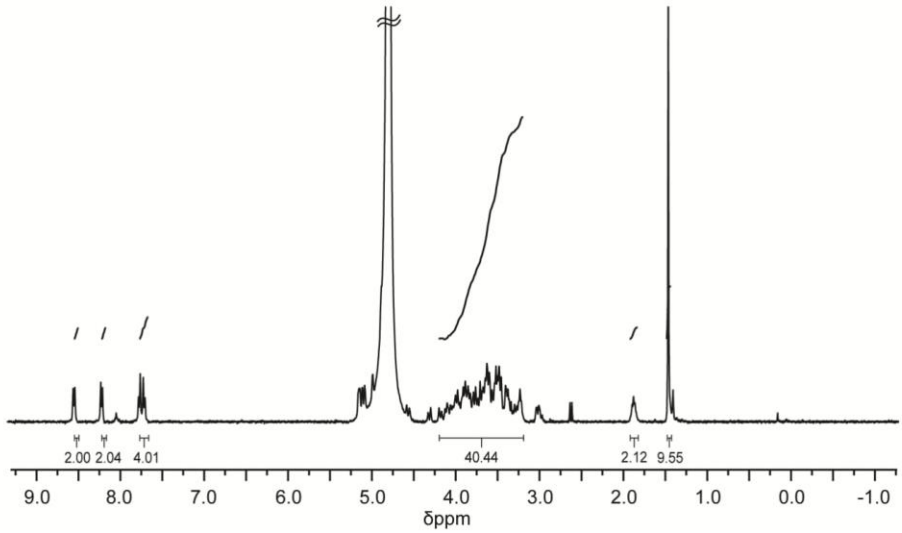

Figure S3. ^{1}H NMR spectrum (400 MHz, 298 K, D_2O).

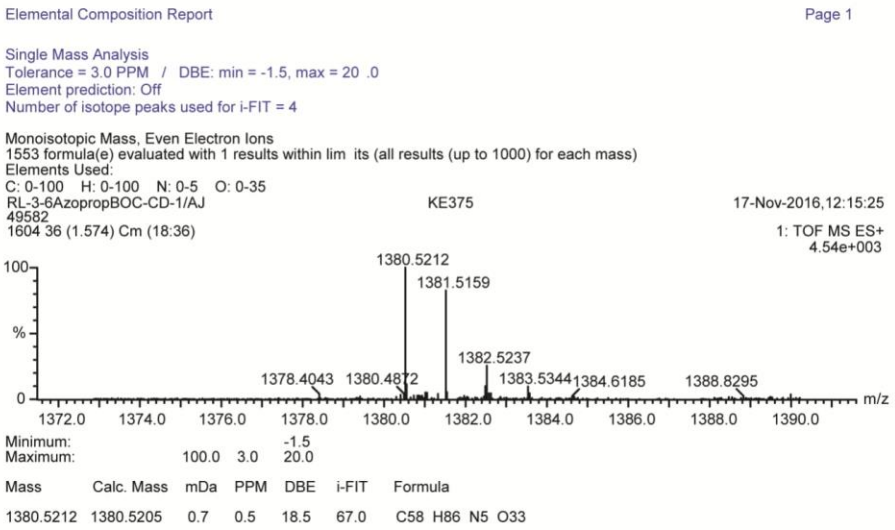

Figure S4. HR ESI spectrum.

2.3 (*E*)-*N*-(3-Aminopropyl)-4-((4-((6^A-deoxy-α-cyclodextrin-6^A-yl)carbamoyl)phenyl)-diazenyl)benzamide (3a)

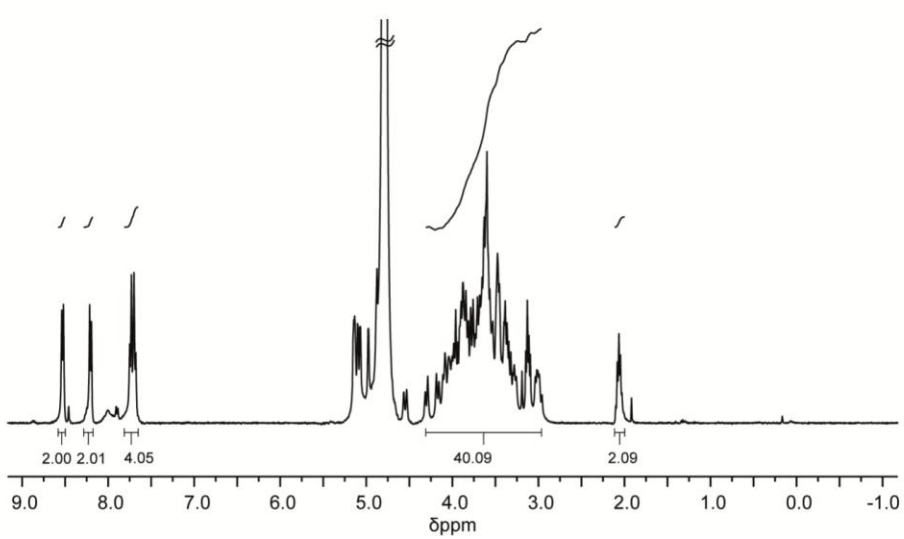

Figure S5. ^{1}H NMR spectrum (400 MHz, 298 K, D_2O).

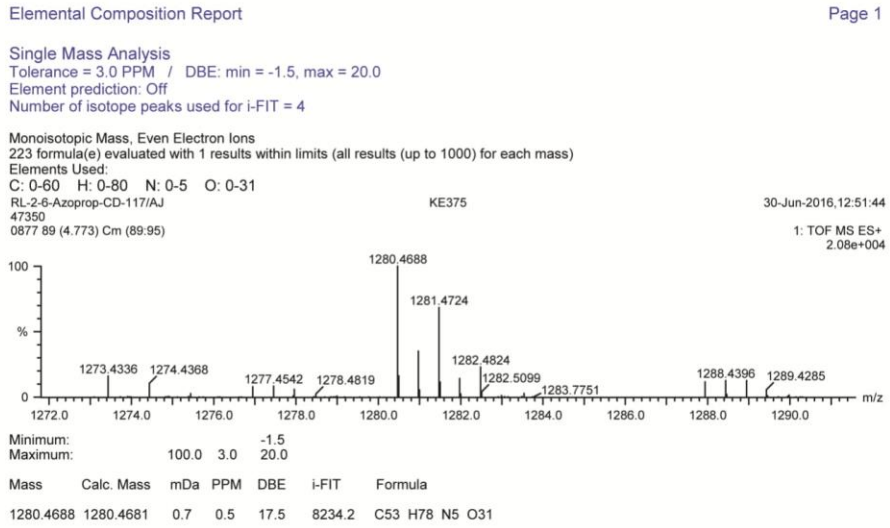

Figure S6. HR ESI spectrum.

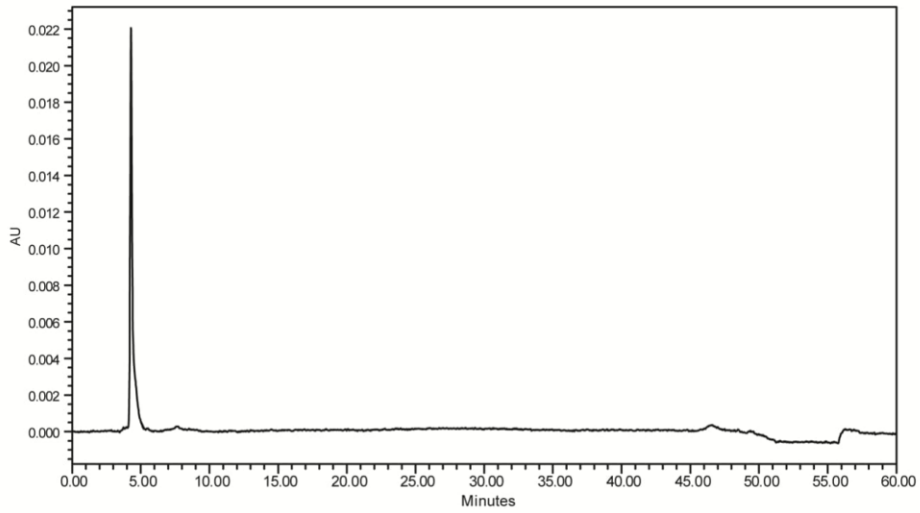

Figure S7. HPLC trace (Grace Prevail Carbohydrate column).

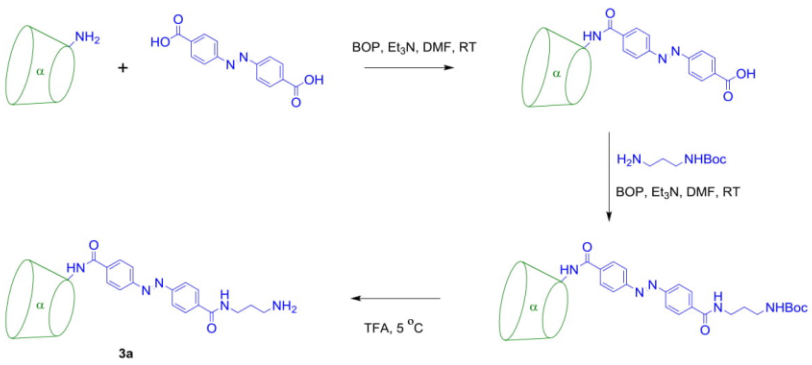

Scheme S1. Reaction scheme for the preparation of compound **3a** from 6^A-amino-6^A-deoxy-α-cyclodextrin.

2.4 Compounds isolated from reaction of the cyclodextrin monomer 3a with suberic acid bis(3-sulfonato-*N*-hydroxysuccinimide ester) disodium salt (7)

2.4.1 Cyclodextrin Monomer 3a

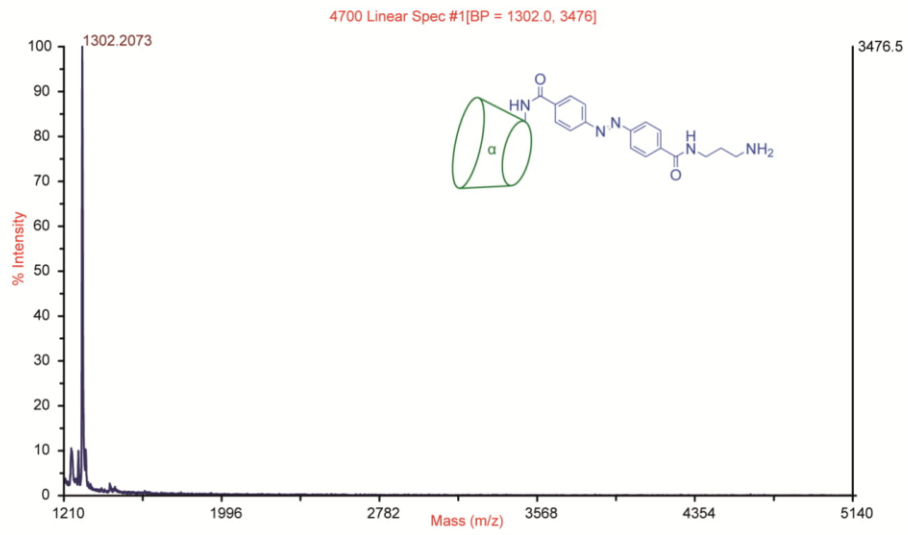

Figure S8. MALDI mass spectrum.

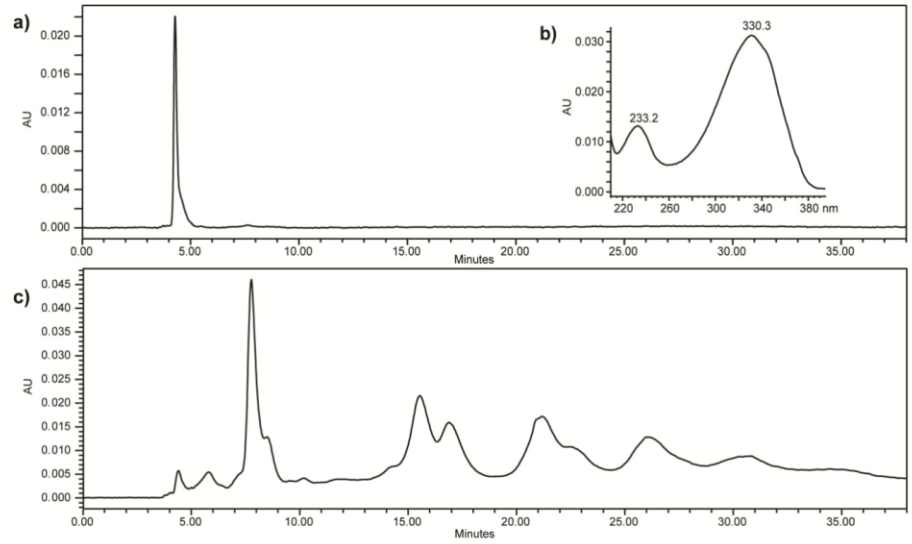

Figure S9. Comparison of a) the HPLC trace of the separated cyclodextrin monomer **3a** with b) the diode array detector response and c) the HPLC trace of the crude reaction mixture.

2.4.2 Cyclodextrin Monomer 8

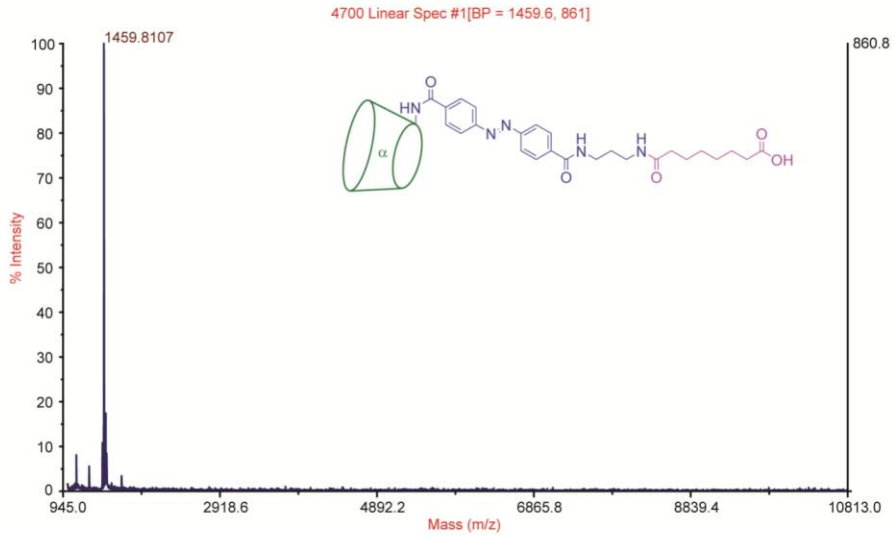

Figure S10. MALDI mass spectrum.

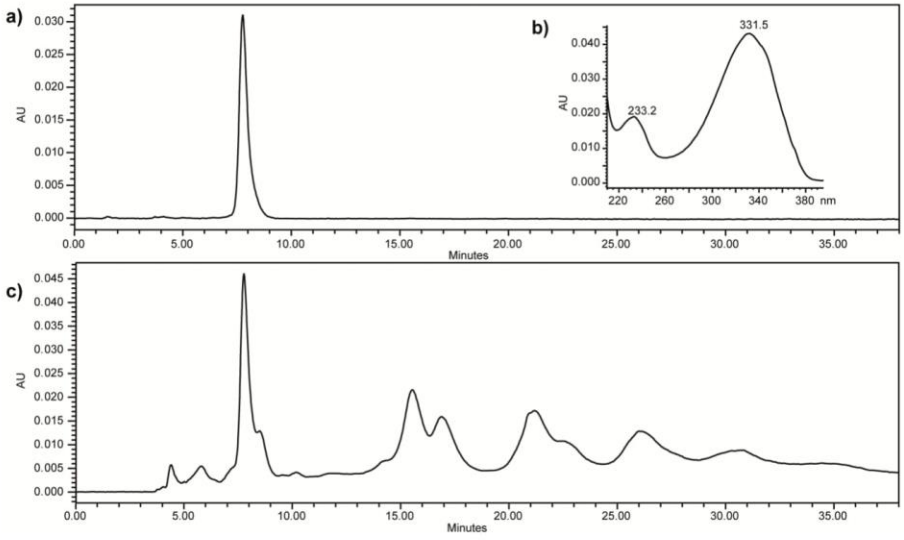

Figure S11. Comparison of a) the HPLC trace of the separated cyclodextrin monomer **8** with b) the diode array detector response and c) the HPLC trace of the crude reaction mixture.

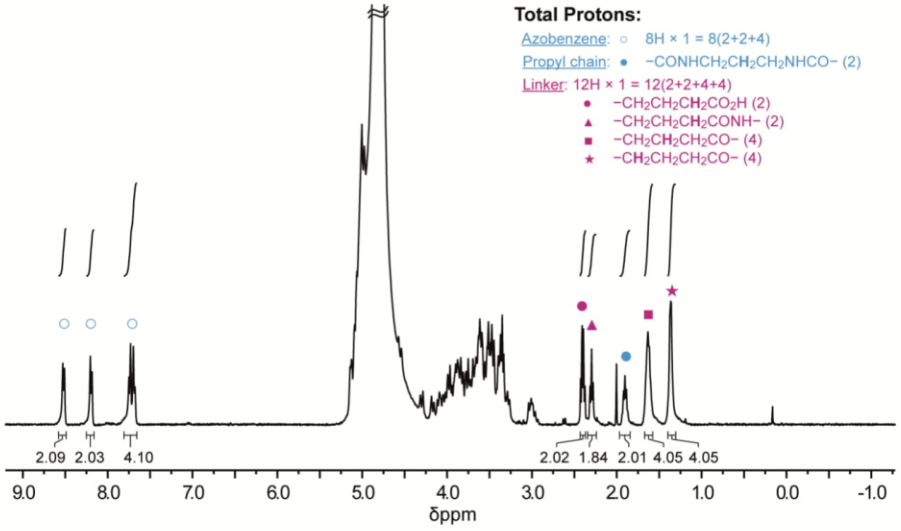

Figure S12. ^{1}H NMR spectrum (400 MHz, 298 K, D_2O).

2.4.3 Linear Tetrameric Daisy Chain 9a

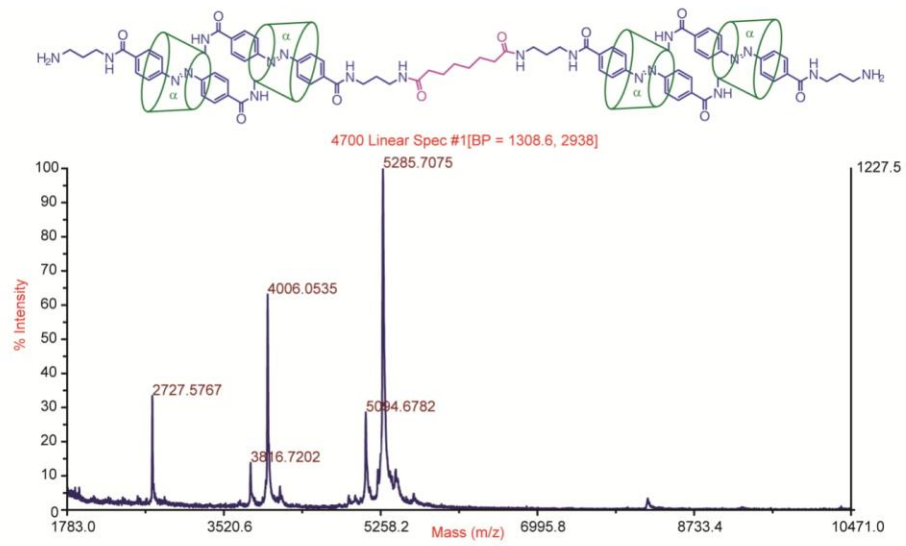

Figure S13. MALDI mass spectrum.

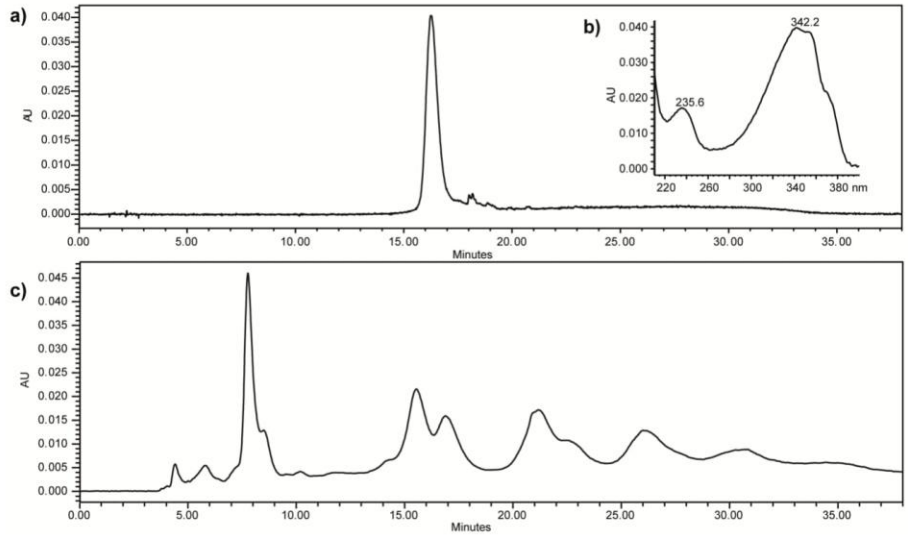

Figure S14. Comparison of a) the HPLC trace of the separated linear tetrameric daisy chain **9a** with b) the diode array detector response and c) the HPLC trace of the crude reaction mixture.

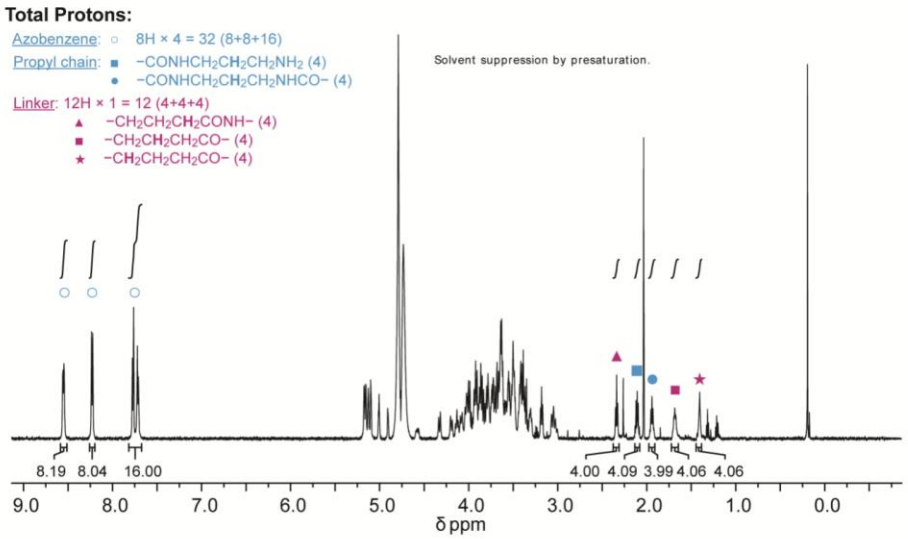

Figure S15. ^{1}H NMR spectrum (600 MHz, 298 K, D_2O).

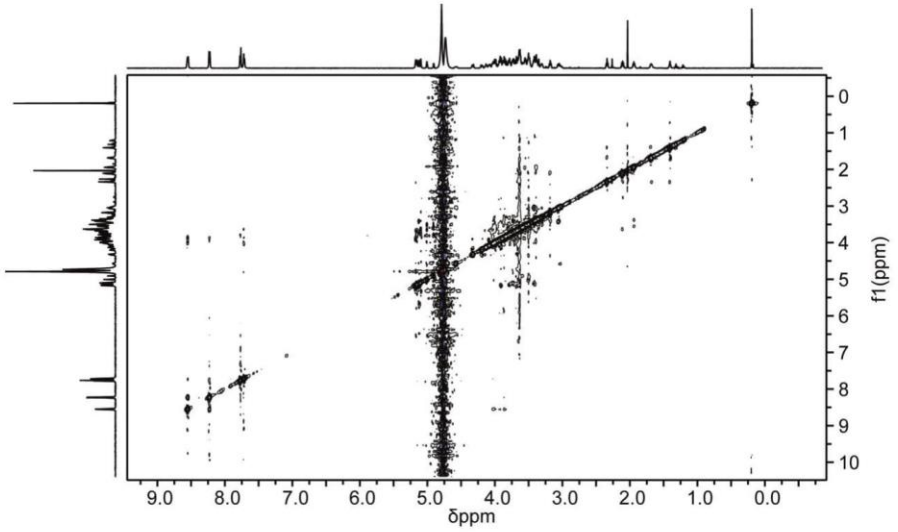

Figure S16. ROESY NMR spectrum (600 MHz, 298 K, D_2O).

2.4.4 Linear Tetrameric Daisy Chain 9b

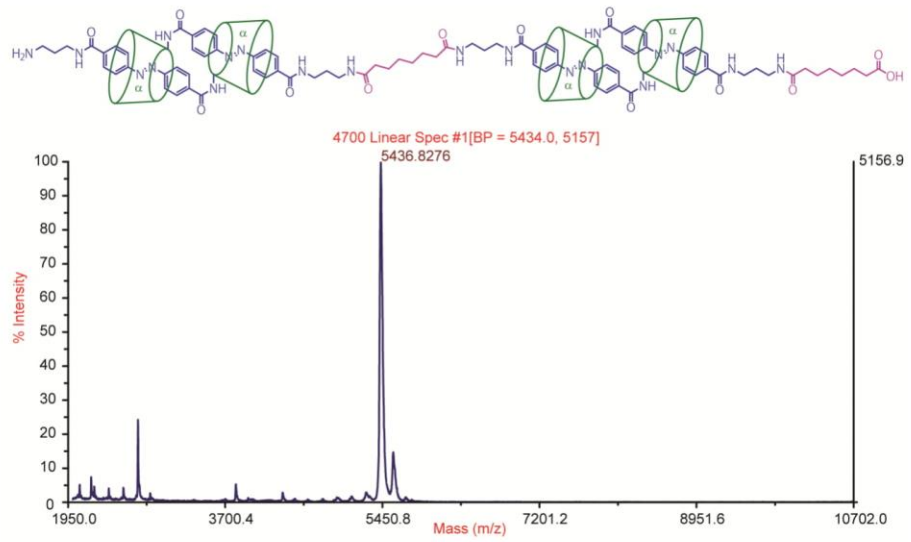

Figure S17. MALDI mass spectrum.

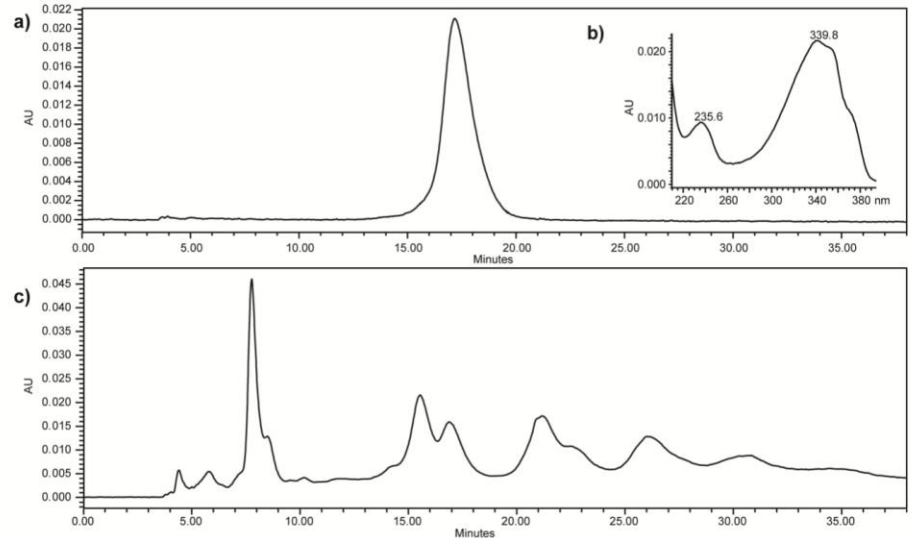

Figure S18. Comparison of a) the HPLC trace of the separated linear tetrameric daisy chain **9b** with b) the diode array detector response and c) the HPLC trace of the crude reaction mixture.

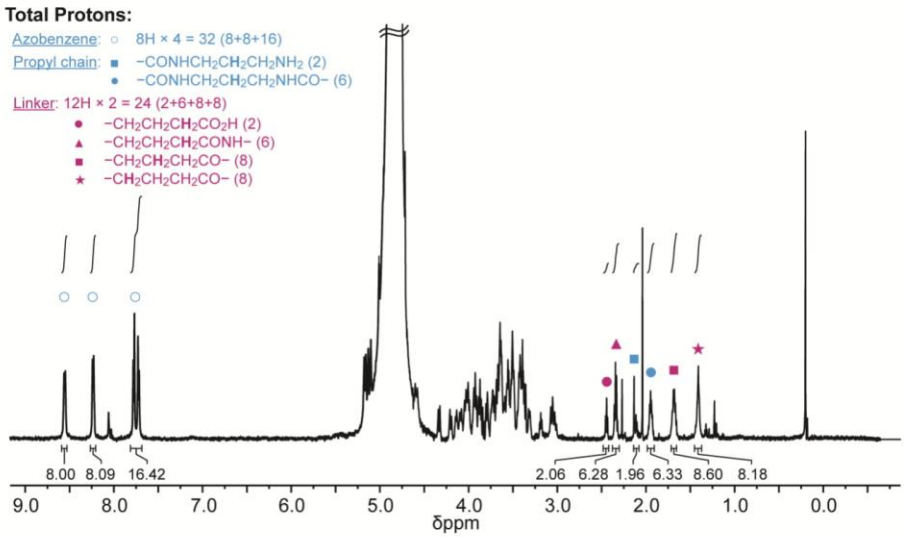

Figure S19. ^{1}H NMR spectrum (600 MHz, 298 K, D_2O).

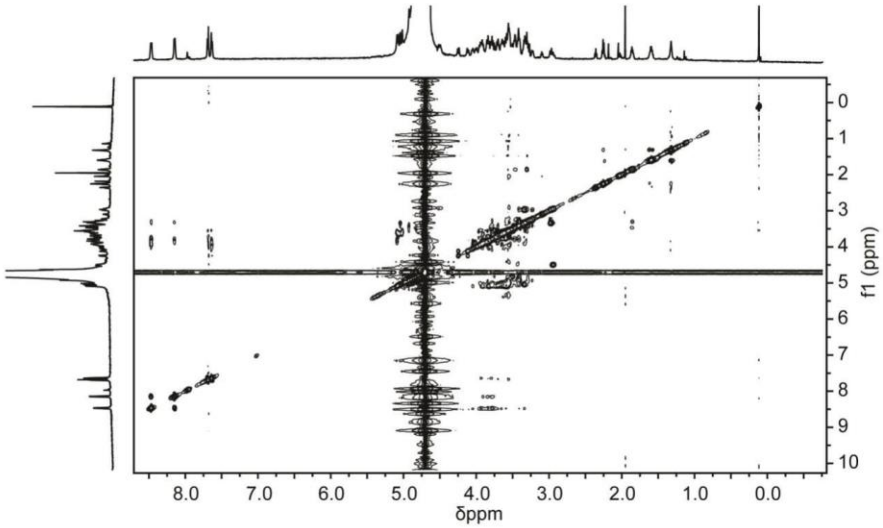

Figure S20. ROESY NMR spectrum (600 MHz, 298 K, D_2O).

2.4.5 Linear Tetrameric Daisy Chain 10a

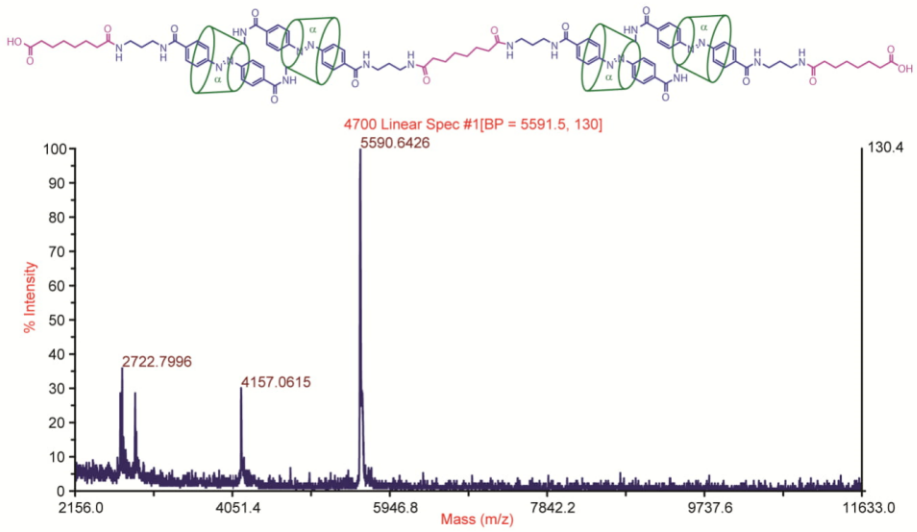

Figure S21. MALDI mass spectrum.

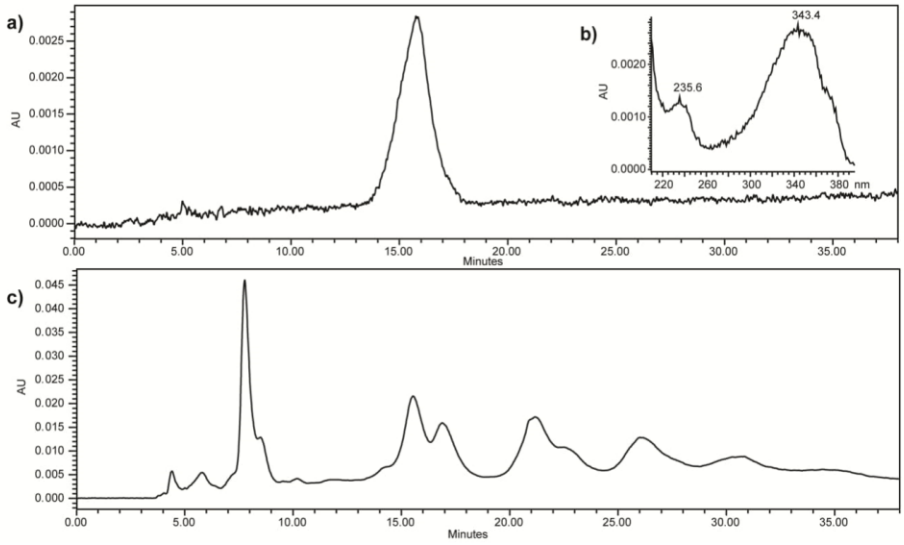

Figure S22. Comparison of a) the HPLC trace of the separated linear tetrameric daisy chain **10a** with b) the diode array detector response and c) the HPLC trace of the crude reaction mixture.

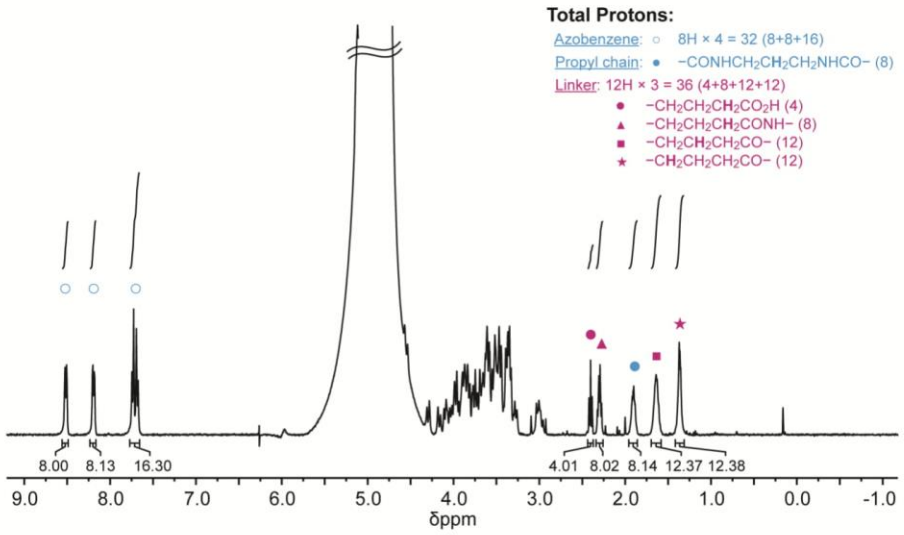

Figure S23. ^{1}H NMR spectrum (400 MHz, 298 K, D_2O).

S15

2.4.6 Linear Hexameric Daisy Chain 10b

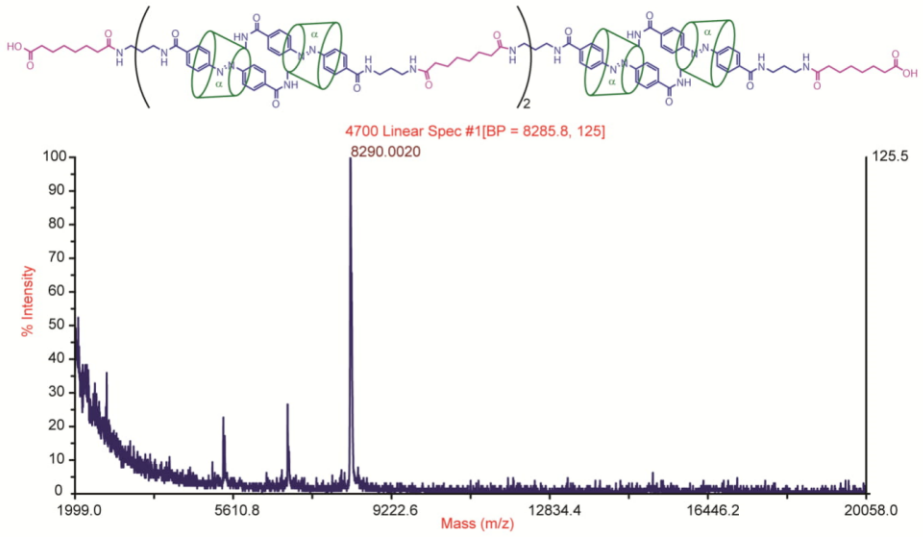

Figure S24. MALDI mass spectrum.

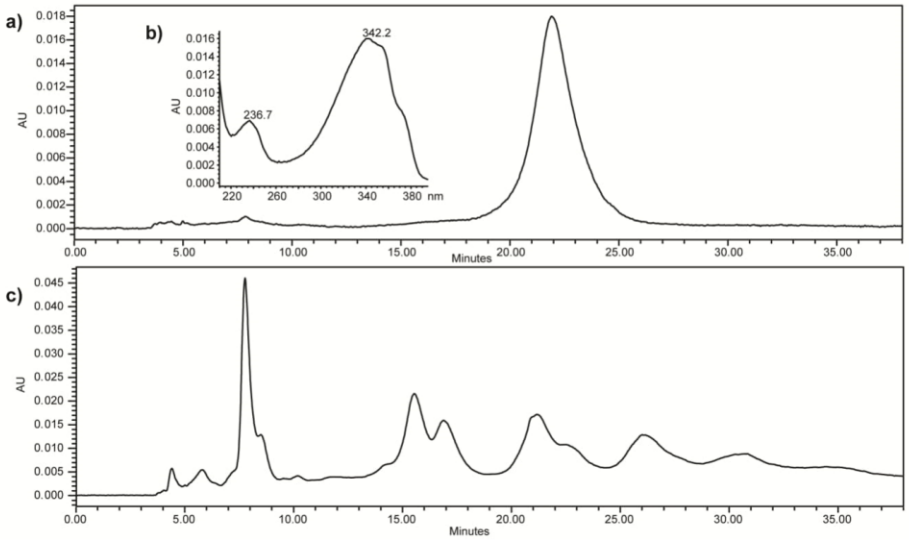

Figure S25. Comparison of a) the HPLC trace of the separated linear tetrameric daisy chain **10b** with b) the diode array detector response and c) the HPLC trace of the crude reaction mixture.

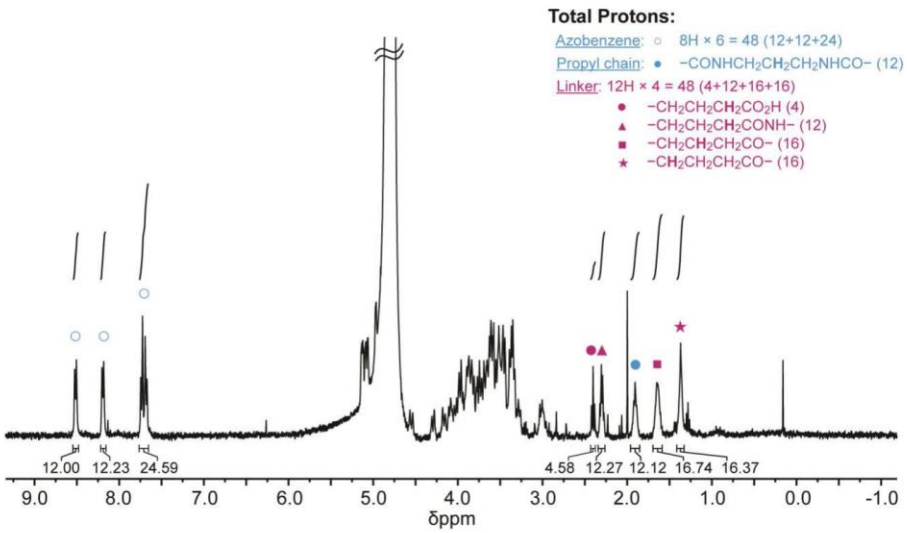

Figure S26. ^{1}H NMR spectrum (400 MHz, 298 K, D_2O).

S17

2.4.7 Linear Octameric Daisy Chain 10c

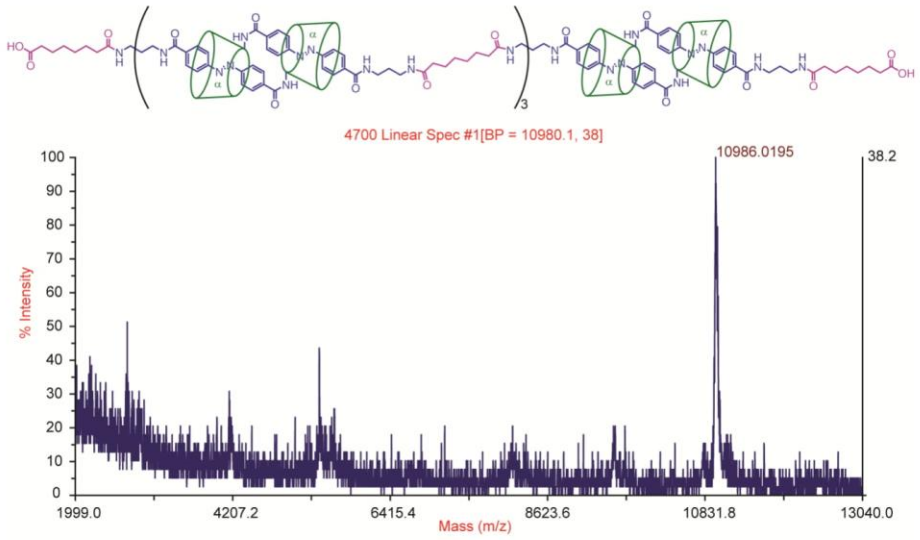

Figure S27. MALDI mass spectrum.

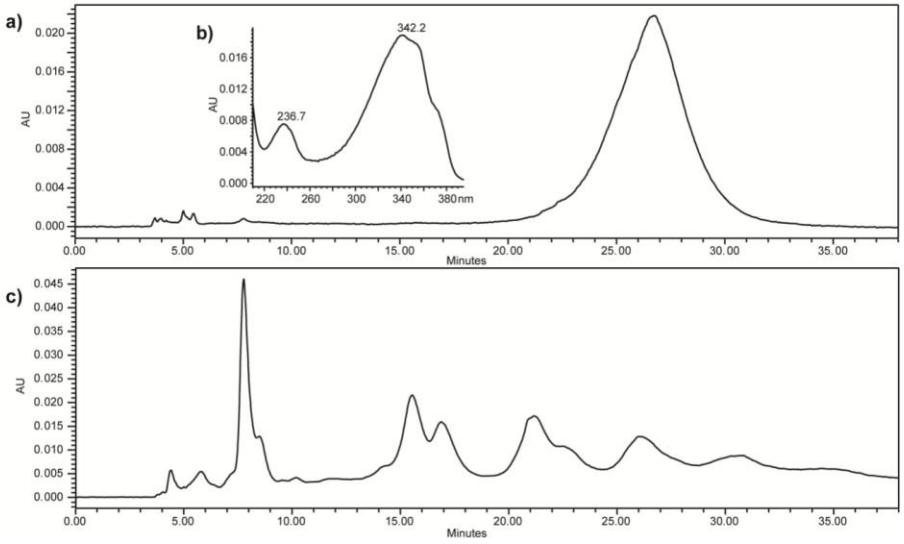

Figure S28. Comparison of a) the HPLC trace of the separated linear tetrameric daisy chain **10c** with b) the diode array detector response and c) the HPLC trace of the crude reaction mixture.

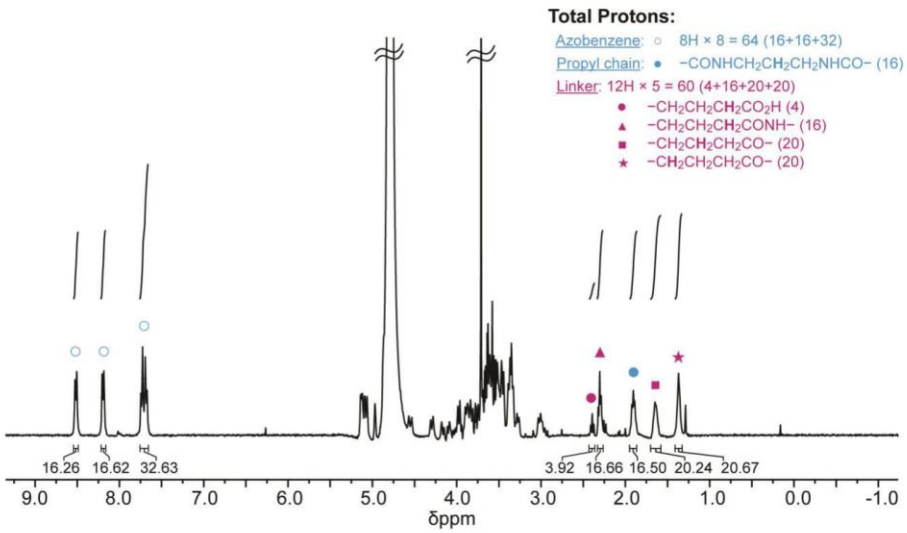

Figure S29. ^{1}H NMR spectrum (400 MHz, 298 K, D_2O).

2.4.8 Linear Decameric Daisy Chain 10d

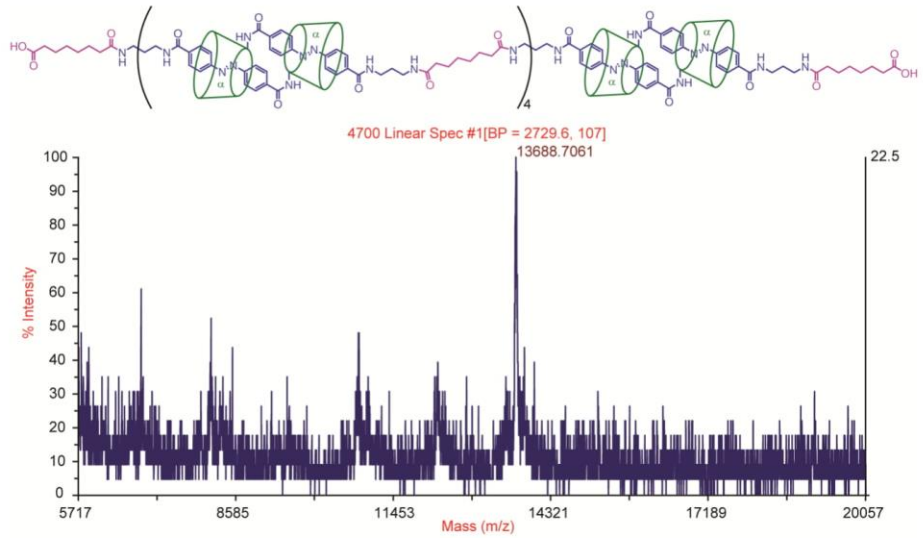

Figure S30. MALDI mass spectrum.

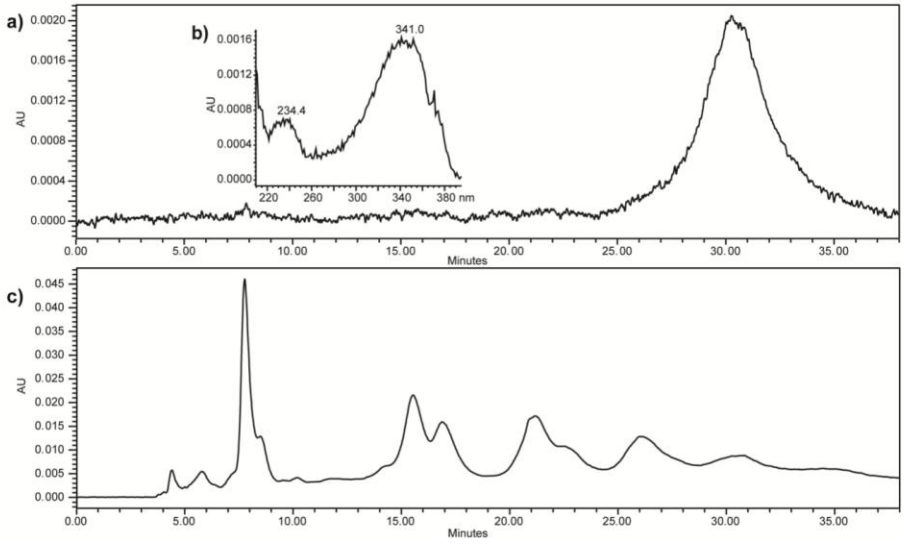

Figure S31. Comparison of a) the HPLC trace of the separated linear tetrameric daisy chain **10d** with b) the diode array detector response and c) the HPLC trace of the crude reaction mixture.

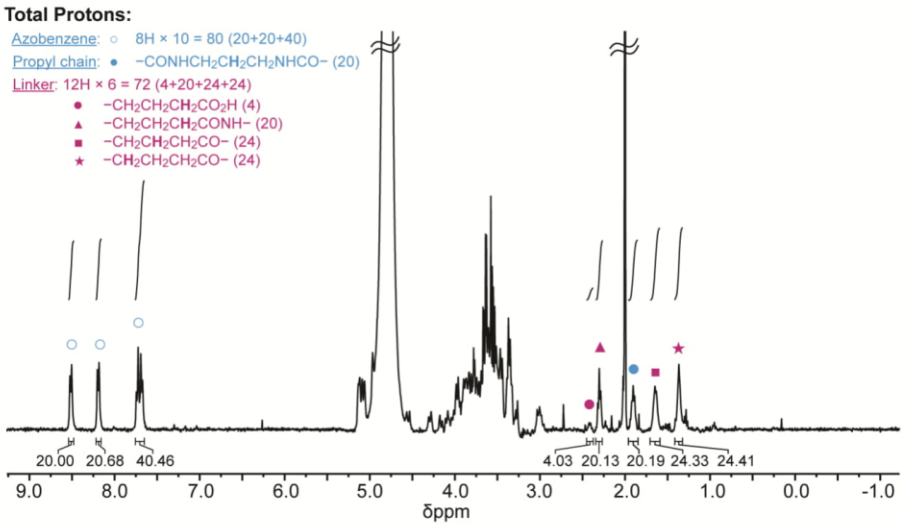

Figure S32. ^{1}H NMR spectrum (400 MHz, 298 K, D_2O).

S21

2.4.9 Cyclic Dimeric Daisy Chain 11

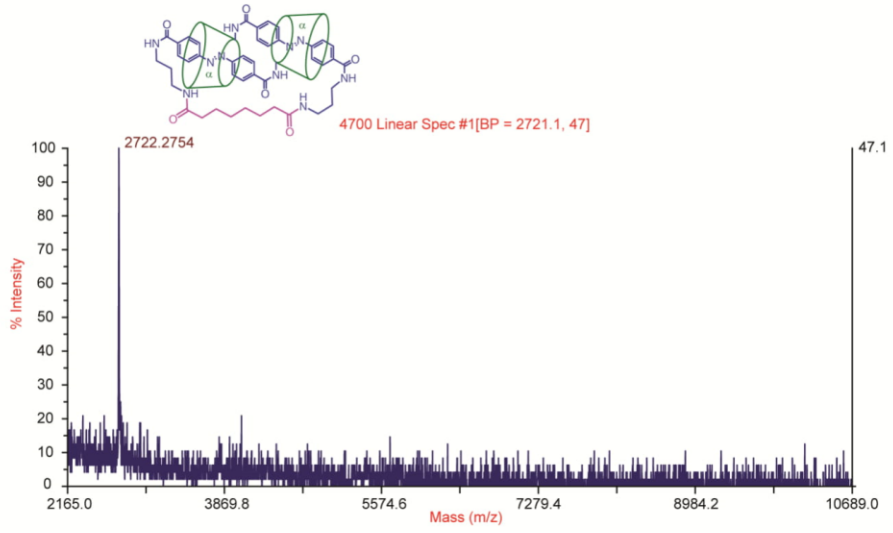

Figure S33. MALDI mass spectrum.

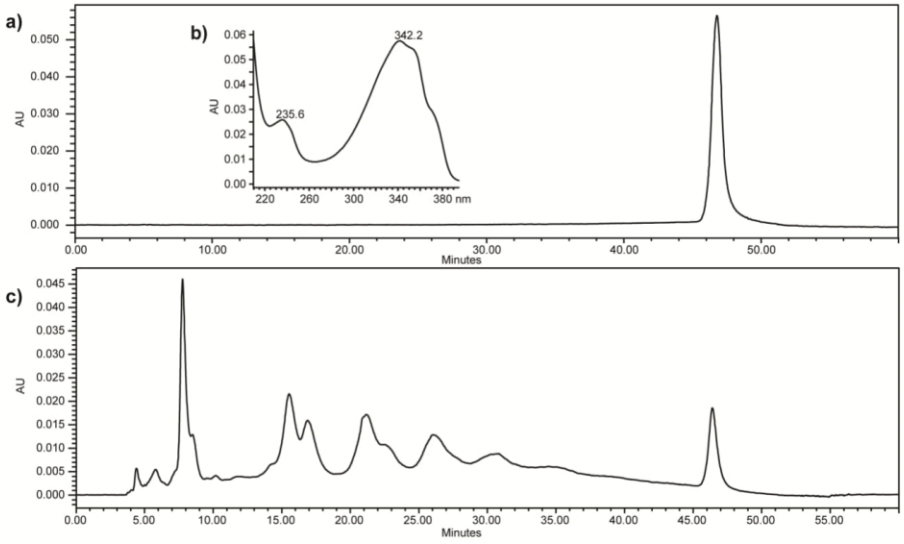

Figure S34. Comparison of a) the HPLC trace of the separated linear tetrameric daisy chain **11** with b) the diode array detector response and c) the HPLC trace of the crude reaction mixture.

S22

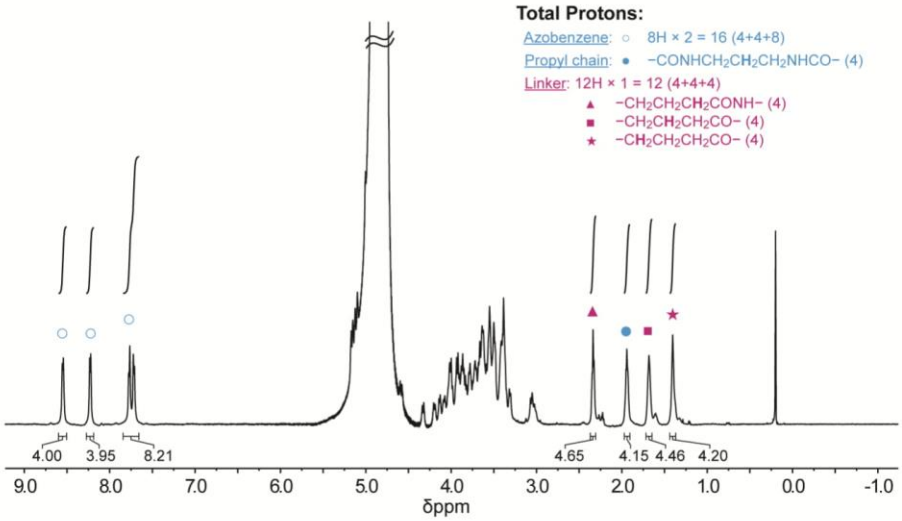

Figure S35. ^{1}H NMR spectrum (600 MHz, 298 K, D_2O).

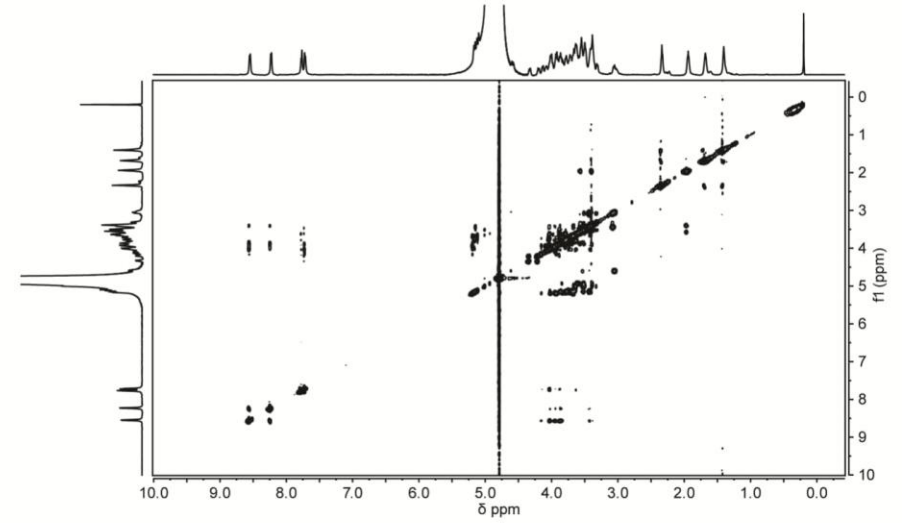

.**Figure S36.** ROESY NMR spectrum (600 MHz, 298 K, D_2O).

2.4.10 Cyclic Tetrameric Daisy Chain 12

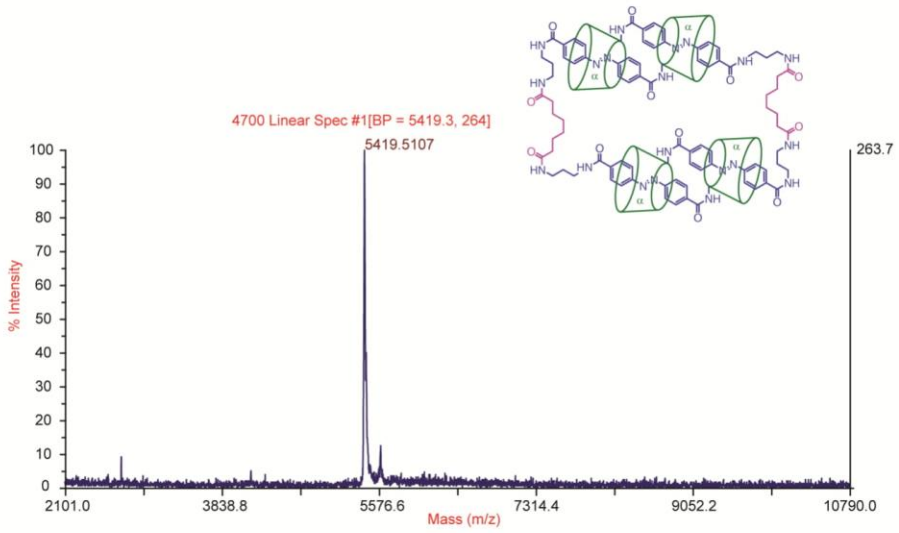

Figure S37. MALDI mass spectrum.

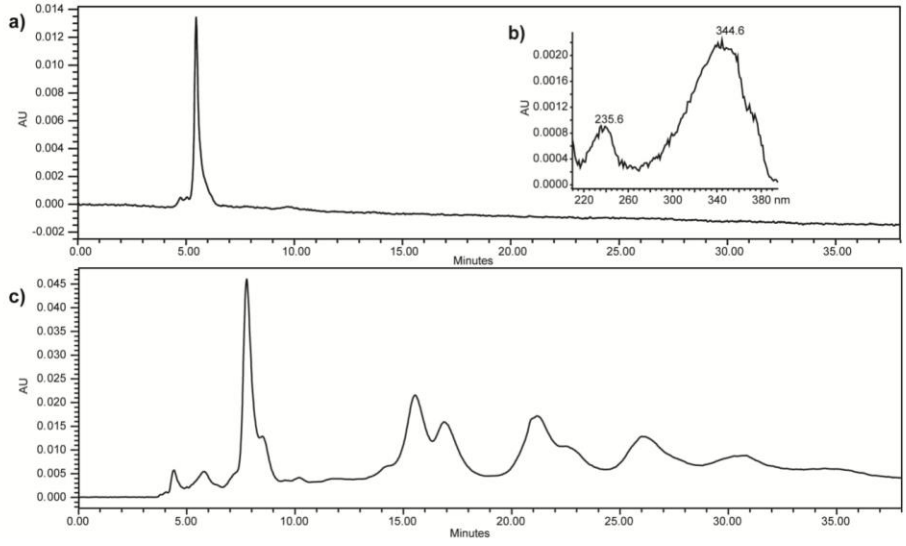

Figure S38. Comparison of a) the HPLC trace of the separated linear tetrameric daisy chain **12** with b) the diode array detector response and c) the HPLC trace of the crude reaction mixture.

2.5 HPLC analysis of the mixture of products obtained from reaction of the cyclodextrin 3a with the suberic acid derivative 7 after 24 h

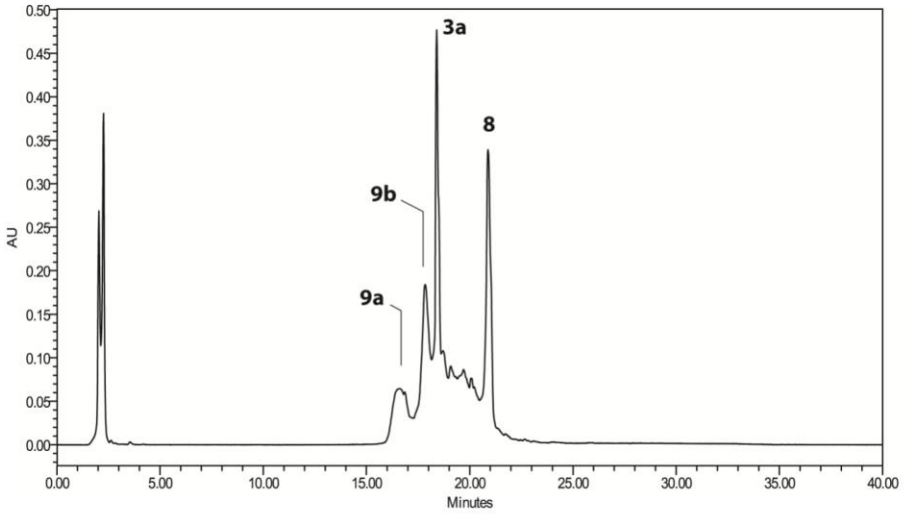

Figure S39. HPLC was carried out using an Agilent Zorbax SB C18 3.5 μm (150 × 4.6 mm) column, with a gradient eluent of MeCN/H_2O (0.1% TFA) – MeCN 5% 0-3 min, 5-47% 3-20 min, 47% 20-30 min, at a flow rate of 1 mL min^{-1}, monitoring at 352 nm. Note that these reverse-phase conditions are different to the normal-phase analysis described in the text, and illustrated in Figure 6 of the text, for the reasons outlined in the text.

2.6 Absorption spectra of 10a, 10d and 11, in methanol and water, initially, after irradiation at 350 nm until the photostationary state was attained, and after further irradiation at 420 nm for 10 min

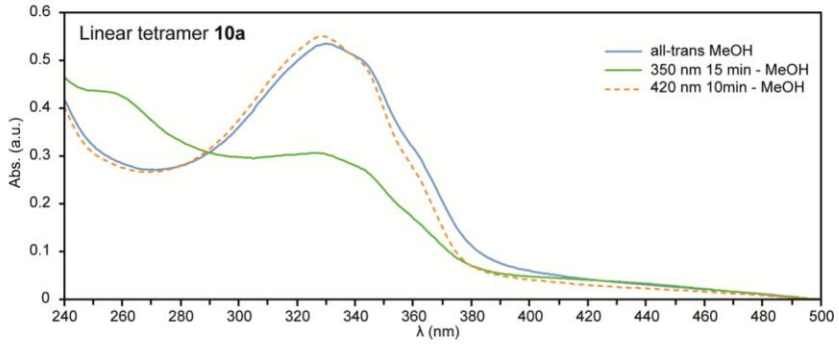

Figure S40. Absorption spectra of **10a** in methanol.

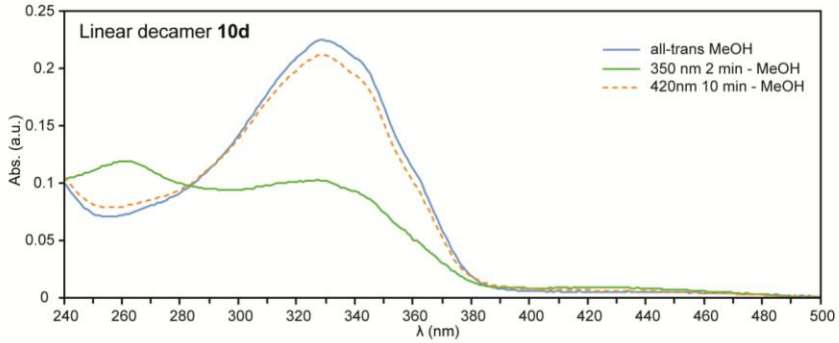

Figure S41. Absorption spectra of **10d** in methanol.

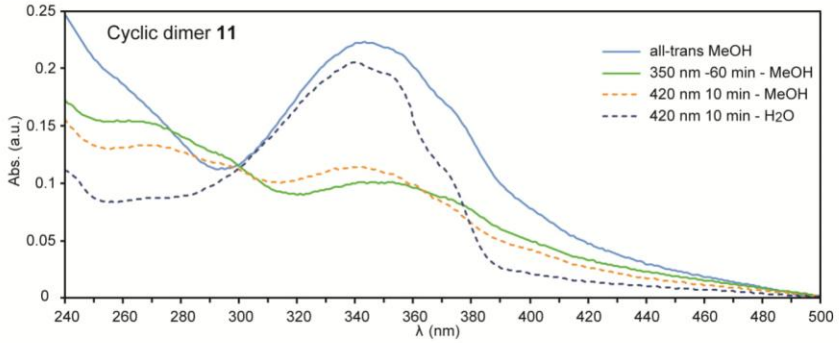

Figure S42. Absorption spectra of **11** in methanol, and after methanol was replaced with water.

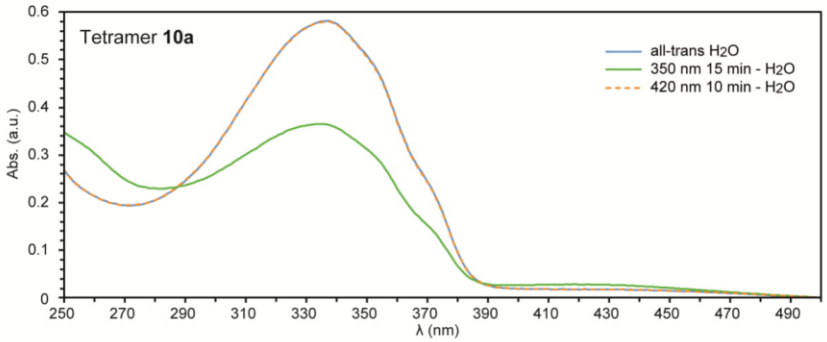

Figure S43. Absorption spectra of **10a** in water.

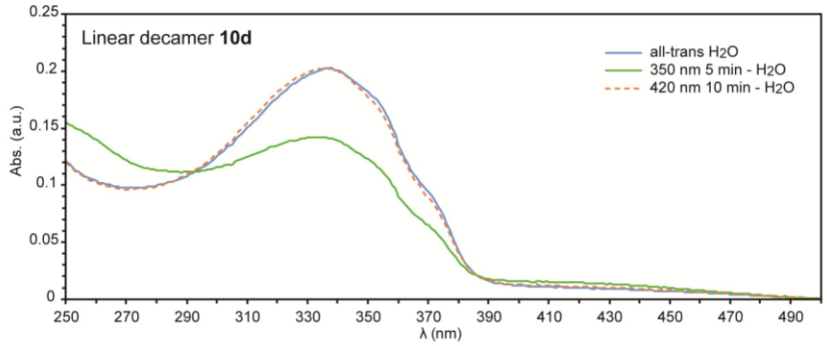

Figure S44. Absorption spectra of **10d** in water.

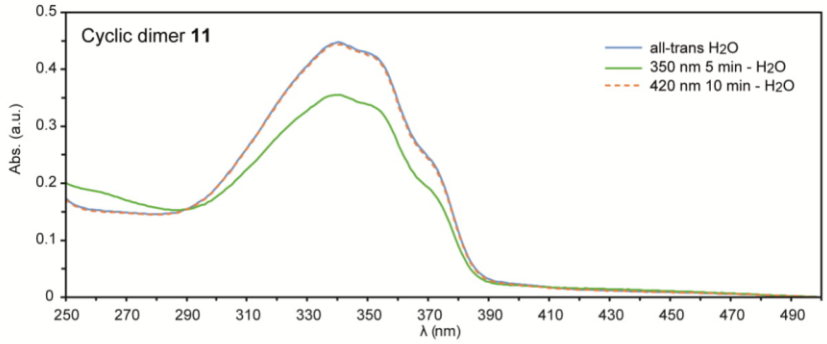

Figure S45. Absorption spectra of **11** in water.

3. Reaction of (*E*)-*N*-(3-aminopropyl)-4-((4-((6^A-deoxy-α-cyclodextrin-6^A-yl)carb-amoyl)phenyl)diazenyl)benzamide (3a) with 1,4-phenyldiisocycanate

In a representative reaction, a solution of the trifluoroacetate salt of the cyclodextrin **3a** (12 mg, 9.4 μmol) in water (0.75 mL) was adjusted to pH 9.5 with Et_3N, before 1,4-phenyldiisocyanate (8 mg, 50 μmol) was added, and the mixture was stirred at RT for 24 h. Centrifugation of the resultant suspension afforded a clear supernatant and colourless solid. An HPLC analysis (Phenomenex Luna C18 5 μm (250 x 10 mm) with a gradient eluent of MeCN/H_2O (0.1% TFA) - MeCN 10-20% 0-50 min, 80% 51-60 min, at a flow rate of 4 mL min^{-1}, monitoring at 352 nm) of the supernatant is shown below (Figure S46).

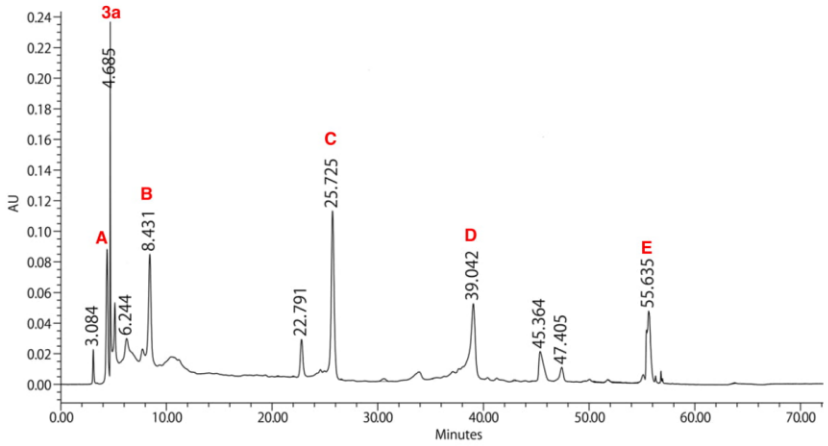

Figure S46. HPLC analysis of the mixture of products in the supernatant obtained from reaction of the cyclodextrin **3a** with 1,4-phenyldiisocyanate.

Samples of the unreacted starting material **3a** and each of the compounds corresponding to the peaks designated **A-E** were isolated and analysed using MALDI-TOF mass spectrometry. Plausible structures for these compounds are illustrated below, along with comparisons of the found and calculated mass spectrometry data.

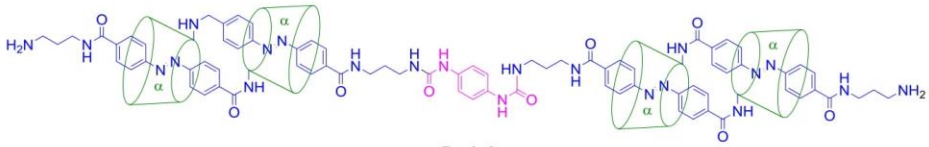

Peak A

MALDI-TOF MS: *m/z* calcd for $C_{220}H_{312}N_{22}O_{126}Na$ $[M + Na]^+$, 5300.9; found 5301.1

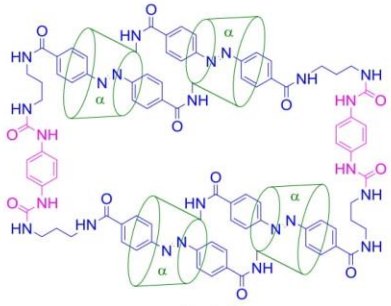

Peak B

MALDI-TOF MS: *m/z* calcd for $C_{228}H_{316}N_{24}O_{128}Na$ $[M + Na]^+$, 5460.9; found 5461.5

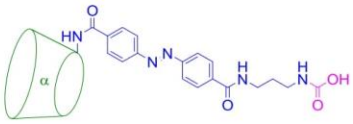

Peak C

MALDI-TOF MS: *m/z* calcd for $C_{54}H_{77}N_5O_{33}Na$ $[M + Na]^+$, 1346.4; found 1347.7

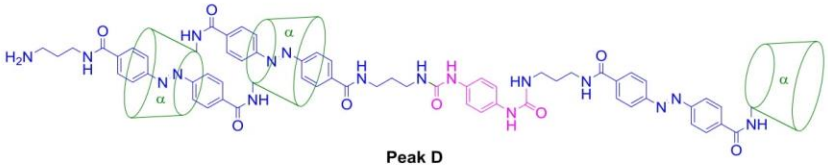

Peak D

MALDI-TOF MS: *m/z* calcd for $C_{167}H_{235}N_{17}O_{95}Na$ $[M + Na]^+$, 4021.4; found 4022.2

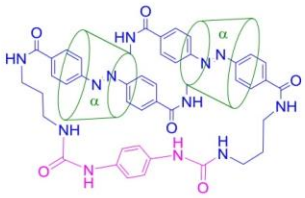

Peak E

MALDI-TOF MS: *m/z* calcd for $C_{114}H_{158}N_{12}O_{64}Na$ $[M + Na]^+$, 2741.9; found 2743.1

S29

Chapter 3 - SYNTHESIS OF [2]ROTAXANE ORIENTATIONAL ISOMERS THROUGH DESYMMETRISATION

3.1 Foreword

Having developed a new method to build daisy chains potentially able to act as molecular muscles, another aim was to design new synthetic procedures to prepare rotaxanes because, as mentioned in the Introduction, they also represent a key platform for the preparation of molecular machines. In particular, we set out to synthesize [2]rotaxane orientational isomers using alternative approaches.

This work is presented in the following pages as a draft manuscript for publication. However, it has not been submitted because the data acquired with the characterisation experiments did not allow the distinction between orientational isomers. It is expected that this information will be obtained through X-ray crystallographic analysis of the compounds, but preliminary crystallization experiments have so far not been successful.

3.2 Introduction

Rotaxanes are among the fundamental building blocks of supramolecular chemistry.[1] The simplest examples are [2]rotaxanes, which consist of a macrocycle

encompassing an axle that is capped with bulky groups at each end to prevent dissociation of the components. Typically, these constituents form a unique, symmetric assembly (Fig. 3.1a), the exception being when both the macrocycle and capped axle are asymmetric; then there is the possibility of orientational isomers (Fig. 3.1b).

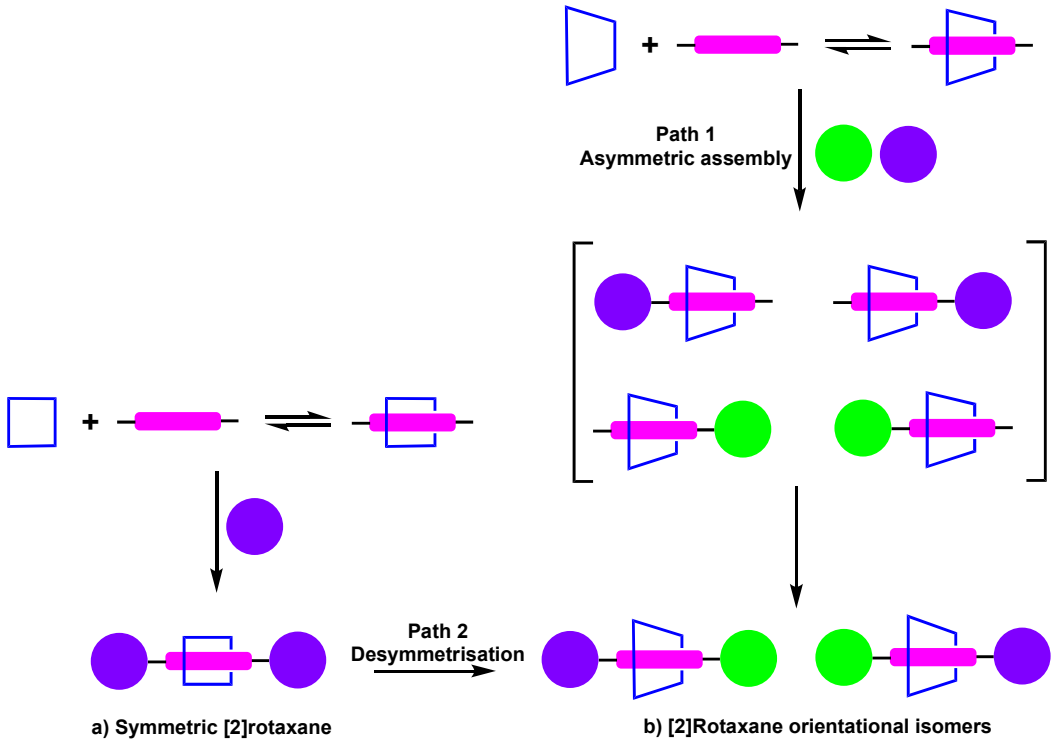

Fig. 3.1. Schematic representation of methods for the synthesis of [2]rotaxane orientational isomers.

Examples of these with a calixarene[2] or a cyclodextrin[3] as the macrocycle have been reported. In some cases, the isomeric pairs have been separated or at least distinguished in mixtures.[3a-g] With other examples of [2]rotaxanes comprising a

cyclodextrin macrocycle and an asymmetric capped axle, orientational isomers are conceivable but only one has been reported.[3h, 3i]

Apart from being conceptually attractive, [2]rotaxane orientational isomers are intrinsically interesting where they have properties that are different from those of each other and those of the individual components.[3a-c] Therefore, their synthesis continues to be topical.[3j] In all of the preparations reported to date, the methodology has involved asymmetric assembly, through capping an inclusion complex of a mono-capped guest (Fig. 3.1, Path 1). Here we report an alternative approach, through desymmetrisation of a preformed, symmetric [2]rotaxane. We also compare this with the conventional route.

3.3 Results and Discussion

The compounds initially targeted in this study were the [2]rotaxanes **6a,b** and **7a,b**, because the amino and bromo substituents were intended to provide opportunities for further elaboration. However, attempts to produce these compounds following the typical route (Fig. 3.1, Path 1) were not successful. The procedures were adapted from those that had been used for the synthesis of the closely related rotaxane **5a** (Scheme 3.1).[4]

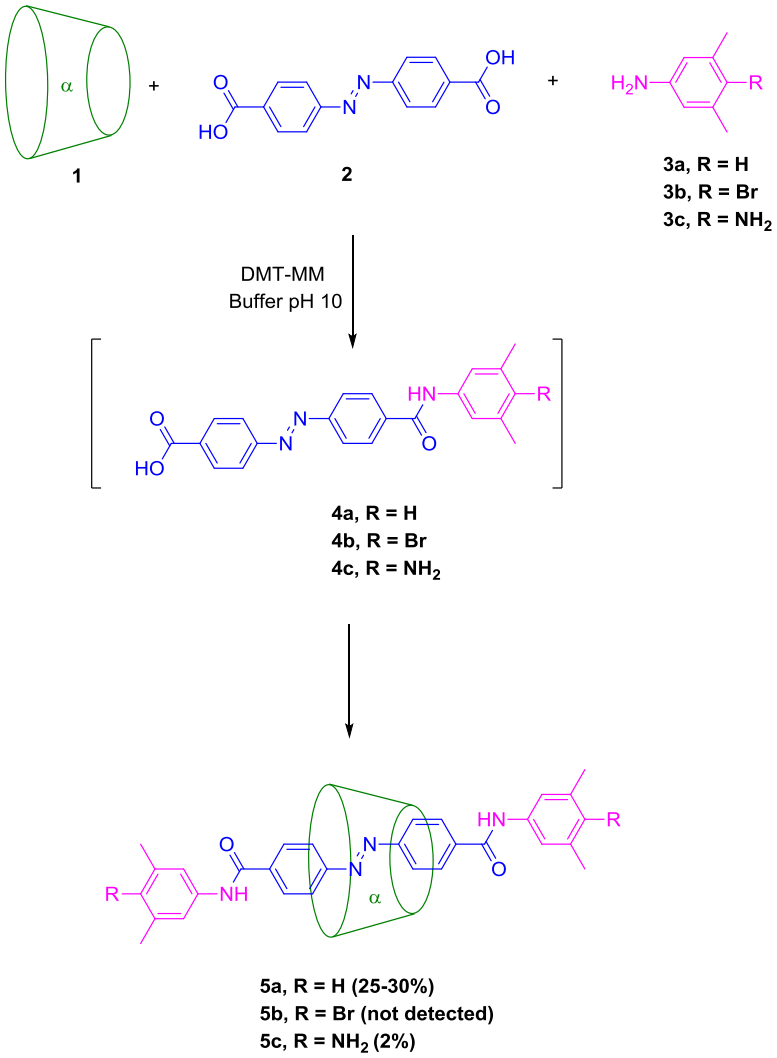

Scheme 3.1. Synthesis of symmetric [2]rotaxanes.

In that case, the azobenzene **2** and the aniline **3a** were treated with DMT-MM, in an aqueous solution of α-cyclodextrin (**1**) that had been basified with either Et_3N or carbonate buffer. That reaction proceeds *via in situ* production of the mono-capped axle **4a**. In the present work, this species was instead preformed and treated with either of the anilines **3b** or **3c**, under otherwise analogous reaction conditions (Scheme 3.2).

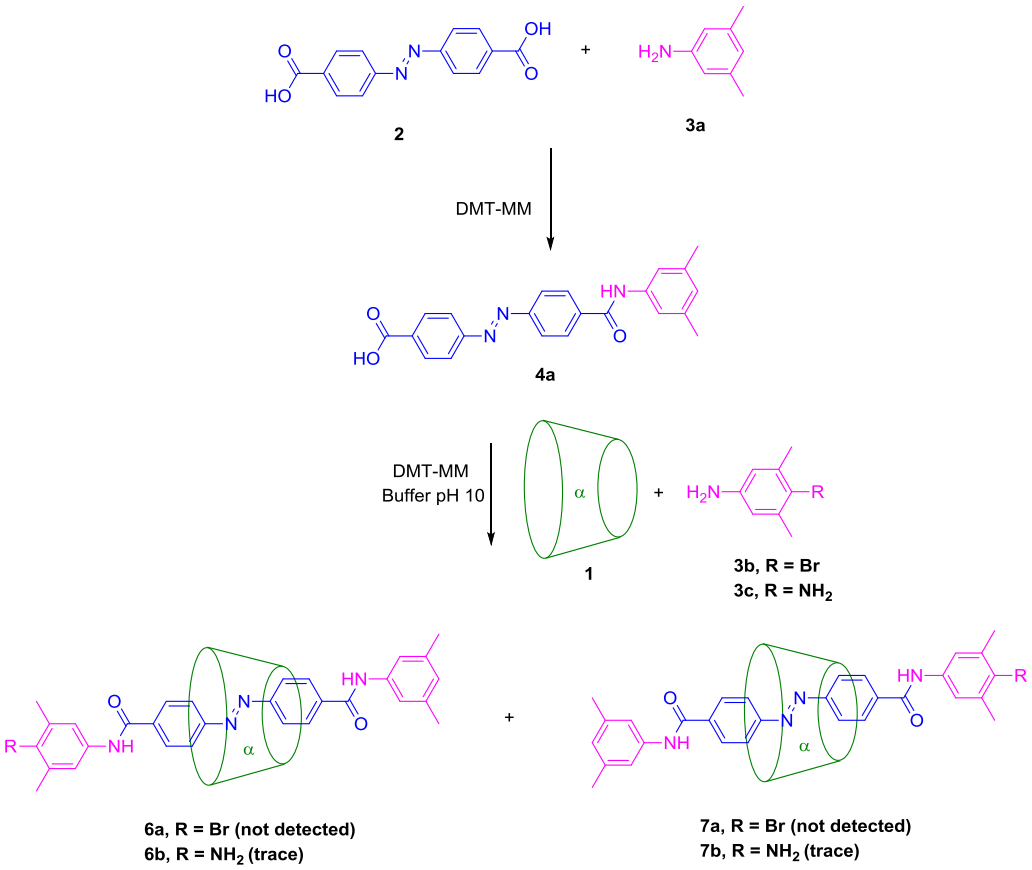

Scheme 3.2. Attempted asymmetric assembly of [2]rotaxane orientational isomers.

The objective of this modification was to simplify the process, in order to avoid competing formation of rotaxanes having the same blocking group at each end of the axle, and to require only one capping reaction rather than two. Even so, reactions with the bromoaniline **3b** showed no evidence of formation of the rotaxanes **6a** or **7a**. With the diamine **3c**, species were obtained and isolated by HPLC that had mass spectra consistent with the amines **6b** and **7b**, but they were formed in only trace amounts insufficient for adequate characterisation.

These results indicate that coupling of the inclusion complex of the capped axle **4a** with either of the substituted anilines **3b** or **3c** is much less efficient than the corresponding reaction of **3a**. Consistent with this observation, whereas the [2]rotaxane **5a** forms reproducibly in *ca.* 25-30% yield from α-cyclodextrin (**1**), the azobenzene **2** and the aniline **3a**, none of the dibromo-[2]rotaxane **5b** was detected in the corresponding reaction of the bromide **3b**, and the diamino-[2]rotaxane **5c** was obtained in only 2% yield using the aniline **3c**. It is not clear why the outcomes of these reactions are so different, since the factors affecting them are complicated, but the solubility and basicity of the various anilines **3a-c**, their relative tendencies to form non-productive complexes with α-cyclodextrin (**1**) and their reactivities towards inclusion complexes of DMT-MM-activated azobenzenes, are all possible contributing factors.

Given the lack of success in the attempted syntheses of the bromides **5b**, **6a** and **7a**, described above, the alternative approach of accessing them through functionalisation of the [2]rotaxane **5a** was evaluated (Scheme 3.3).

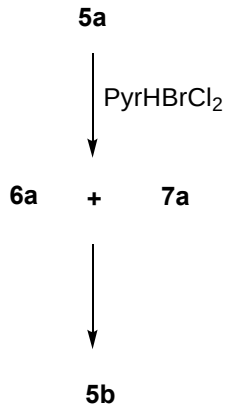

Scheme 3.3. Functionalisation of the [2]rotaxane **5a** and synthesis of the orientational isomers **6a** and **7a** through desymmetrisation.

Pyridinium dichlorobromate (**8**) was selected as the brominating agent since it has previously been employed in electrophilic aromatic substitution reactions in the presence of cyclodextrins.[5] Using a two-fold molar excess, the reaction in methanol overnight at room temperature afforded the dibromide **5b**, in 67% yield. With less of the dichlorobromate **8** or shorter reaction times, the monobromides **6a** and **7a** were also observed as intermediates. Analyses of crude reaction mixtures (Fig. 3.2) showed that they are produced in a ratio of *ca.* 1:1, and build up to a maximum proportion of about 30% each, before being consumed in subsequent reactions to give the dibromide **5b** faster than they continue to be formed. This behaviour indicates similar bromination rates of the dimethylphenyl-capping groups of the rotaxanes **5a**, **6a** and **7a**.

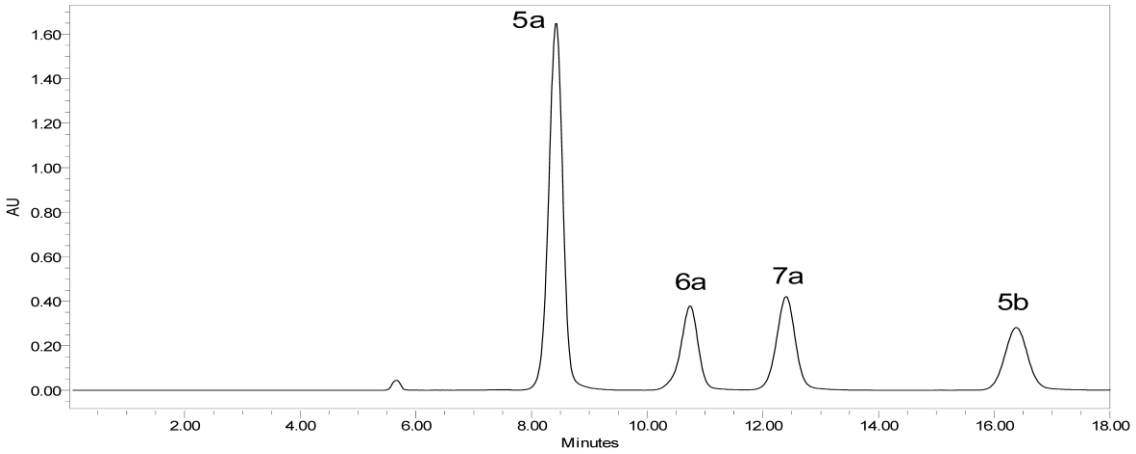

Fig. 3.2. An HPLC analysis of the reaction of the [2]rotaxane **5a** with the dichlorobromate **8**.

Each of the monobromides **6a** and **7a** was isolated by HPLC and, as with the dibromide **5b**, characterised using mass spectrometry and NMR spectroscopy. Using their COSY and ROESY NMR spectra, it was possible to correlate the azobenzene and cyclodextrin proton resonances, as illustrated in Fig. 3.3, and show that the cyclodextrins are positioned over the centres of the azobenzene axles. However, there was nothing in the spectra that enabled distinction between the orientational isomers **6a** and **7a**, so the structural assignments may be as illustrated or the reverse. It is anticipated that this ambiguity will be resolved using X-ray crystallographic analysis but, to date, attempts to obtain suitable crystals of either **6a** or **7a** have not been successful. This is not atypical for cyclodextrin-based rotaxanes because of their complex crystal packing in the solid state and their unpredictable solubility profiles.

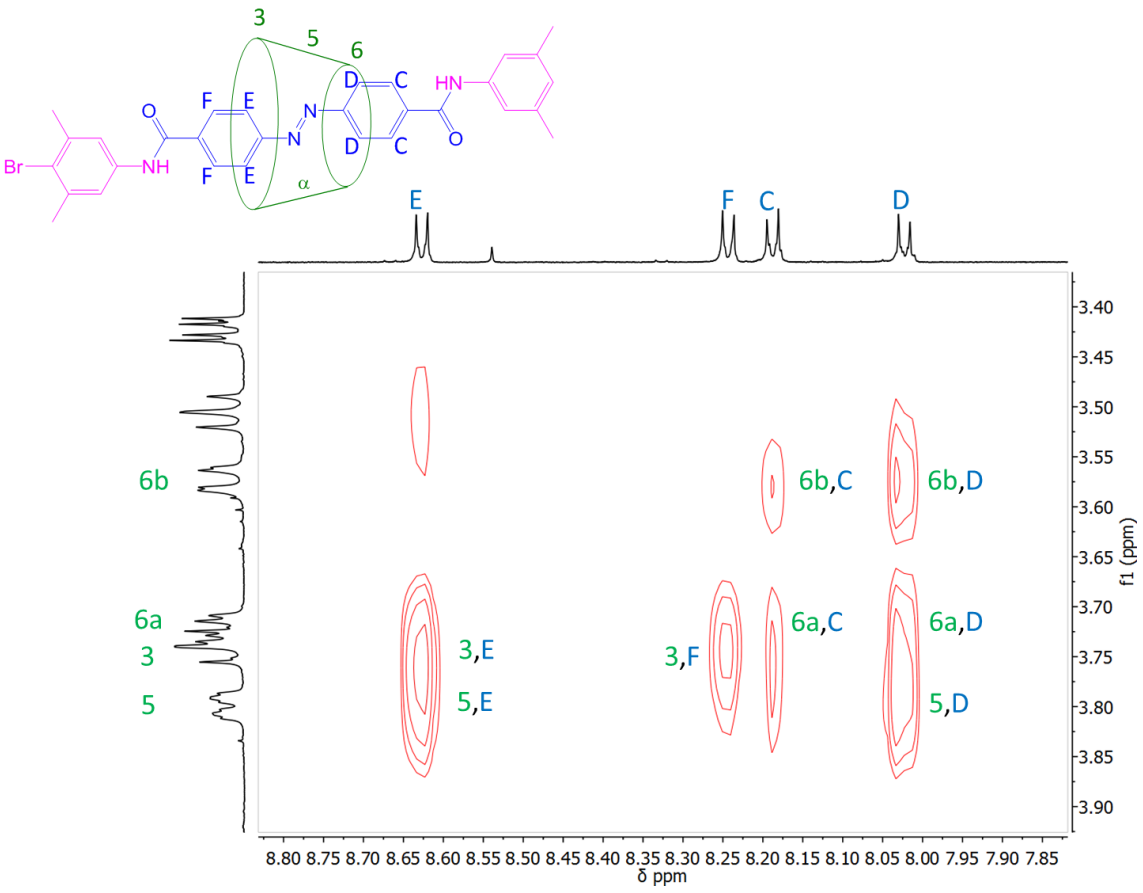

Fig. 3.3. A portion of the ROESY NMR spectrum of the rotaxane **6a**, showing proton assignments and correlations between azobenzene and cyclodextrin proton resonances.

In any event, desymmetrisation of the [2]rotaxane **3a** through bromination provided an alternative route (Fig. 3.1, Path 2) for the synthesis of the monobromides **6a** and **7a**, where the normal method of preparation of such orientational isomers involving capping an inclusion complex of a mono-capped guest (Fig. 3.1, Path 1) had failed.

3.4 Conclusions

Functionalisation of the [2]rotaxane **5a** has been achieved through reaction with pyridinium dichlorobromate (**8**), to produce the dibromorotaxane **5b**, as well as the isomeric monobromides **6a** and **7a**. Preparation of the latter compounds constitutes a new approach for the synthesis of such orientational isomers, through desymmetrisation of a symmetric precursor. Although this method is likely to have only limited general applicability, compared to the conventional route of asymmetric assembly, it is a complementary option that is worth considering when the assembly process affords either mixtures that are too complicated to separate or only one of the isomers (if both are, or the other one is, required), or where the assembly process simply fails, as was the case with **6a** and **7a**. The yields of **6a** and **7a** are modest, but similar to those typically obtained for the synthesis of rotaxanes through self-assembly, and infinitely greater in this particular example. Further work may include crystallography experiments to allow the identification of the isomers **6a** and **7a**.

3.5 Experimental

General Experimental Procedures

α-Cyclodextrin (**1**) was purchased from Nihon Shokuhin Kako Co., Japan, in 99.1% purity, and dried over P_2O_5 under reduced pressure to a constant weight before use. Reported procedures were used to prepare the rotaxane **5a**,[4] the aniline **3b**[6] and

pyridinium dichlorobromate (**8**).[7] Other chemicals, including the azobenzene **2** and the corresponding diacyl chloride, and the anilines **3a** and **3c**, were purchased from commercial suppliers and used as received. HPLC was carried out with a Waters 600 Controller, a Waters 717 Plus Autosampler and a Waters 2996 Photodiode Array Detector, controlled with Empower Pro Empower 2 software. NMR spectra were acquired on Bruker Avance 400 and 600 spectrometers, using $(CD_3)_2SO$ and CD_3OD as solvents, and 3-(trimethylsilyl)-3,3,2,2-tetradeuteropropionic acid sodium salt as an external standard. The multiplicity of signals is reported as singlet (s), doublet (d) and multiplet (m). High resolution electrospray ionisation (HR-ESI) mass spectra were recorded using a Waters LCT premier TM XE orthogonal acceleration time-of-flight (oa-TOF) mass spectrometer or ThermoFisher Scientific Orbitrap Elite™ Hybrid Ion Trap-Orbitrap Mass Spectrometer at 240k resolution.

*Synthesis of trans-4'-(3,5-Dimethylphenylcarbamoyl)azobenzene-4-carboxylic acid (**4a**)*

A solution of 3,5-dimethylaniline (**3a**) (63 mg, 0.52 mmol) in dry DCM (60 mL) was added dropwise over 30 min to a solution of azobenzene-4,4'-dicarbonyl dichloride (200 mg, 0.65 mmol) in dry DCM (15 mL), under a N_2 atmosphere, while the temperature was maintained below 5°C using a sodium chloride ice-salt bath. Et_3N (80 mg, 0.79 mmol) was then added and the mixture was stirred at room temperature for 2 h, before it was concentrated under reduced pressure. THF/water (150 mL, 2:1) was added to the residue and the mixture was sonicated at 50°C for 1 h. The resulting solution was concentrated under reduced pressure, then the residue

was dissolved in MeOH/DCM 1:99 (5 mL) and subjected to flash column chromatography on silica gel (200 g) using MeOH/DCM as eluent, to give the title compound **4a** as an orange powder (155 mg, 80 %). M.p. 268-269°C (dec). δ_H (400 MHz, $(CD_3)_2SO$) 10.36 (s, 1H, NHCO), 8.19 (d, *J* 8.0 Hz, 2H), 8.15 (d, *J* 8.0 Hz, 2H), 8.02 (d, *J* 8.0 Hz, 2H), 7.97 (d, *J* 8.0 Hz, 2H), 7.45 (s, 2H), 6.77 (s, 1H), 2.27 (s, 6H). HRMS ESI *m/z* 372.1351; calc. for $C_{22}H_{18}N_3O_3$ $[M-H]^-$ 372.1426.

*Treatment of the anilines **3b** and **3c** with α-cyclodextrin (**1**) and the azobenzene **2***

Each of the anilines **3b** and **3c** was treated with α-cyclodextrin (**1**) and the azobenzene **2**, using the procedure reported for the synthesis of the rotaxane **5a** from the aniline **3a**.[4] Accordingly, in the case of **3c**, a solution of the azobenzene **2** (50 mg, 0.19 mmol), α-cyclodextrin (**1**) (1.0 g, 1.05 mmol) and Et_3N (40 μL, 0.29 mmol) in water (20 mL) was equilibrated for 1 h at room temperature. After then heating the solution to 50°C, DMT-MM (110 mg, 0.40 mmol), 1,4-diamino-2,6-dimethylbenzene dihydrochloride **3c** (96 mg, 0.46 mmol) and Et_3N (120 μL, 0.86 mmol) were added, and the mixture was stirred at 50°C overnight. The resulting suspension was concentrated under reduced pressure and the residue was dissolved in 1 M NaOH (50 mL). The solution was washed with EtOAc (3 x 50 mL), concentrated and subjected to reverse-phase preparative HPLC, to give **5c** as an orange powder (2.4 mg, 2 %).

When the process was carried out using **3b** instead of **3c**, under otherwise identical conditions, none of the dibromorotaxane **5b** was detected in the product mixture,

despite the availability of an authentic sample for comparison, obtained as described below.

*Data for [trans-4,4'-Bis(4-amino-3,5-dimethylphenylcarbamoyl) azobenzene]-[α-cyclodextrin]-[2]rotaxane (**5c**)*

HPLC t_R = 5.6 min [Waters XBridge Prep C18 5 µm, 150 x 19 mm. Flow = 8 mL min^{-1}. Gradient MeCN (0.1 % TFA)/H_2O (0.1 % TFA) – 0-10 % MeCN (0.1% TFA), 0-10 min. Detection wavelength 352 nm]. δ_H (400 MHz, CD_3OD) 8.63 (d, *J* 8.3 Hz, 2H), 8.23 (d, *J* 8.3 Hz, 2H), 8.18 (d, *J* 8.3 Hz, 2H), 8.01 (d, *J* 8.3 Hz, 2H), 7.33 (s, 2H), 7.25 (s, 2H), 4.99–4.90 (m, 6H), 3.96–3.39 (m, 36H), 2.22 (s, 12H). HRMS ESI *m/z* 1479.5688; calc. for $C_{66}H_{91}N_6O_{32}Na$ $[M+H]^+$ 1479.5678.

*Functionalisation of the rotaxane **5a** with pyridinium dichlorobromate **8***

A solution of pyridinium dichlorobromate (**8**) (6.0 mg, 28.0 µmol) in MeOH (5 mL) was added to a solution of the rotaxane **5a** (20 mg, 14.0 µmol) in MeOH (10 mL) and the mixture was stirred at room temperature overnight, before it was concentrated under reduced pressure. The residue was dissolved in water (200 mL) and the solution was applied to a Diaion HP-20 column (120 x 40 mm), eluting with a water-methanol gradient. Elution with 50-90 % methanol afforded the dibromorotaxane **5b** as a yellow powder (15 mg, 67 %).

When the process was carried out using less pyridinium dichlorobromate **8** (2.2 mg, 9.7 µmol) and the mixture was stirred for only 2 h before work-up, but under

otherwise analogous conditions, reverse phase HPLC of the crude product afforded the rotaxanes **6a** (1.2 mg, 8 %) and **7a** (2.7 mg, 18 %) as orange powders.

*Data for [trans-4,4'-Bis(4-bromo-3,5-dimethylphenylcarbamoyl) azobenzene]-[α-cyclodextrin]-[2]rotaxane (**5b**)*

HPLC t_R = 17.8 min [Waters XBridge Prep C18 5 µm, 150 x 19 mm. Flow = 10 mL min^{-1}. Isocratic MeOH / H_2O; 70:30. Detection wavelength 352 nm]. δ_H (400 MHz, CD_3OD) 8.64 (d, J 8.2 Hz, 2H), 8.25 (d, J 8.2 Hz, 2H), 8.20 (d, J 8.2 Hz, 2H), 8.04 (q, J 8.2 Hz, 2H), 7.64 (s, 2H), 7.57 (s, 2H), 4.96–4.87 (m, 6H), 3.84–3.40 (m, 36H), 2.45 (s, 6H), 2.44 (s, 6H). HRMS ESI *m/z* 1605.3674; calc. for $C_{66}H_{87}{}^{79}Br_2N_4O_{32}$ $[M+H]^+$ 1605.3670; 1627.3484; calc. for $C_{66}H_{86}Br_2N_4O_{32}Na$ $[M+Na]^+$ 1627.3490.

*Data for [trans-4-(4-Bromo-3,5-dimethylphenylcarbamoyl)-4'-(3,5-dimethylphenyl-carbamoyl)azobenzene]-[α-cyclodextrin]-[2]rotaxane orientational isomers **6a** and **7a***

For **6a**: HPLC t_R = 10.9 min [Waters XBridge Prep C18 5 µm, 150 x 19 mm. Flow = 10 mL min^{-1}. Isocratic MeOH / H_2O; 70:30. Detection wavelength 352 nm]. δ_H (400 MHz, CD_3OD) 8.64 (d, J 8.4 Hz, 2H), 8.25 (d, J 8.4 Hz, 2H), 8.20 (d, J 8.4 Hz, 2H), 8.03 (q, J 8.4 Hz, 2H), 7.64 (s, 2H), 7.36 (s, 2H), 6.86 (s, 1H), 4.96–4.87 (m, 6H), 3.83 – 3.40 (m, 36H), 2.46 (s, 6H), 2.34 (s, 6H). HRMS ESI *m/z* 1549.4386; calc. for $C_{66}H_{87}{}^{79}BrN_4O_{32}Na$ $[M+Na]^+$ 1549.4384.

For **7a**: HPLC t_R = 12.5 min [Waters XBridge Prep C18 5 μm, 150 x 19 mm. Flow = 10 mL min^{-1}. Isocratic MeOH / H_2O; 70:30. Detection wavelength 352 nm]. δ_H (400 MHz, CD_3OD) 8.64 (d, J 8.4 Hz, 2H), 8.25 (d, J 8.4 Hz, 2H), 8.20 (d, J 8.4 Hz, 2H), 8.03 (q, J 8.4 Hz, 2H), 7.56 (s, 2H), 7.45 (s, 2H), 6.87 (s, 1H), 4.96–4.87 (m, 6H), 3.83–3.41 (m, 36H), 2.44 (s, 6H), 2.35 (s, 6H). HRMS ESI *m/z* 1549.4415; calc. for $C_{66}H_{87}{}^{79}BrN_4O_{32}Na$ $[M+Na]^+$ 1549.4384.

References

[1] J.-P. Sauvage, *Eur J Org Chem* **2019**, *2019*, 3287-3288. DOI: http://dx.doi.org/10.1002/ejoc.201900723.

[2] a) A. Arduini, F. Ciesa, M. Fragassi, A. Pochini, A. Secchi, *Angew. Chem. Int. Edit.* **2005**, *44*, 278-281. DOI: http://dx.doi.org/10.1002/anie.200461336; b) A. Arduini, R. Bussolati, A. Credi, G. Faimani, S. Garaudee, A. Pochini, A. Secchi, M. Semeraro, S. Silvi, M. Venturi, *Chem. – Eur. J.* **2009**, *15*, 3230-3242. DOI: http://dx.doi.org/10.1002/chem.200801926; c) H. X. Wang, Z. Meng, J. F. Xiang, Y. X. Xia, Y. H. Sun, S. Z. Hu, H. Chen, J. N. Yao, C. F. Chen, *Chem. Sci.* **2016**, *7*, 469-474. DOI: http://dx.doi.org/10.1039/c5sc03511b; d) V. Zanichelli, G. Ragazzon, A. Arduini, A. Credi, P. Franchi, G. Orlandini, M. Venturi, M. Lucarini, A. Secchi, S. Silvi, *Eur. J. Org. Chem.* **2016**, 1033-1042. DOI: http://dx.doi.org/10.1002/ejoc.201501522; e) P. La Manna, C. Talotta, C. Gaeta, A. Soriente, M. De Rosa, P. Nerie, *J. Org. Chem.* **2017**, *82*, 8973-8983. DOI: http://dx.doi.org/10.1021/acs.joc.7b01388.

[3] a) J. E. H. Buston, J. R. Young, H. L. Anderson, *Chem. Commun.* **2000**, 905-906. DOI: http://dx.doi.org/10.1039/B001812k; b) J. E. H. Buston, F. Marken, H. L. Anderson, *Chem. Commun.* **2001**, 1046-1047. DOI: http://dx.doi.org/10.1039/B102068o; c) J. W. Park, H. J. Song, *Org. Lett.* **2004**, *6*, 4869-4872. DOI: http://dx.doi.org/10.1021/ol048079q; d) C. Casati, P. Franchi, R. Pievo, E. Mezzina, M. Lucarini, *J. Am. Chem. Soc.* **2012**, *134*, 19108-19117. DOI: http://dx.doi.org/10.1021/ja3073484; e) R. Isnin, A. E. Kaifer, *J. Am. Chem. Soc.* **1991**, *113*, 8188-8190. DOI: http://dx.doi.org/10.1021/Ja00021a067; f) R. Isnin, A. E. Kaifer, *Pure Appl. Chem.* **1993**, *65*, 495-498. DOI: http://dx.doi.org/10.1351/pac199365030495; g) A. J. Baer, D. H. Macartney, *Supramol Chem* **2007**, *19*, 537-546. DOI: http://dx.doi.org/10.1080/10610270601185200; h) M. R. Craig, M. G. Hutchings, T. D. W. Claridge, H. L. Anderson, *Angew. Chem. Int. Edit.* **2001**, *40*, 1071-1074. DOI: http://dx.doi.org/10.1002/1521-3773(20010316)40:6<1071::Aid-Anie10710>3.0.Co;2-5; i) Q. C. Wang, X. Ma, D. H. Qu, H. Tian, *Chem. - Eur. J.* **2006**, *12*, 1088-1096. DOI: http://dx.doi.org/10.1002/chem.200500415; j) M. Xue, Y. Yang, X. Chi, X. Yan, F. Huang, *Chemical reviews* **2015**, *115*, 7398-7501. DOI: http://dx.doi.org/10.1021/cr5005869.

[4] S. Maniam, M. M. Cieslinski, S. F. Lincoln, H. Onagi, P. J. Steel, A. C. Willis, C. J. Easton, *Org. Lett.* **2008**, *10*, 1885-1888. DOI: http://dx.doi.org/10.1021/ol8002145.

[5] P. G. Dumanski, C. J. Easton, S. F. Lincoln, J. S. Simpson, *Aust J Chem* **2003**, *56*, 1107-1111. DOI: http://dx.doi.org/10.1071/CH03102.

[6] E. Zysman-Colman, K. Arias, J. Siegel, *Can. J. Chem.* **2009**, *87*, 440-447. DOI: http://dx.doi.org/10.1139/V08-176.

[7] H. A. Muathen, *Synthesis-Stuttgart* **2002**, 169-171.

3.6 Supplementary material

*trans-4'-(3,5-Dimethylphenylaminocarbonyl)azobenzene-4-carboxylic acid (**4a**)*

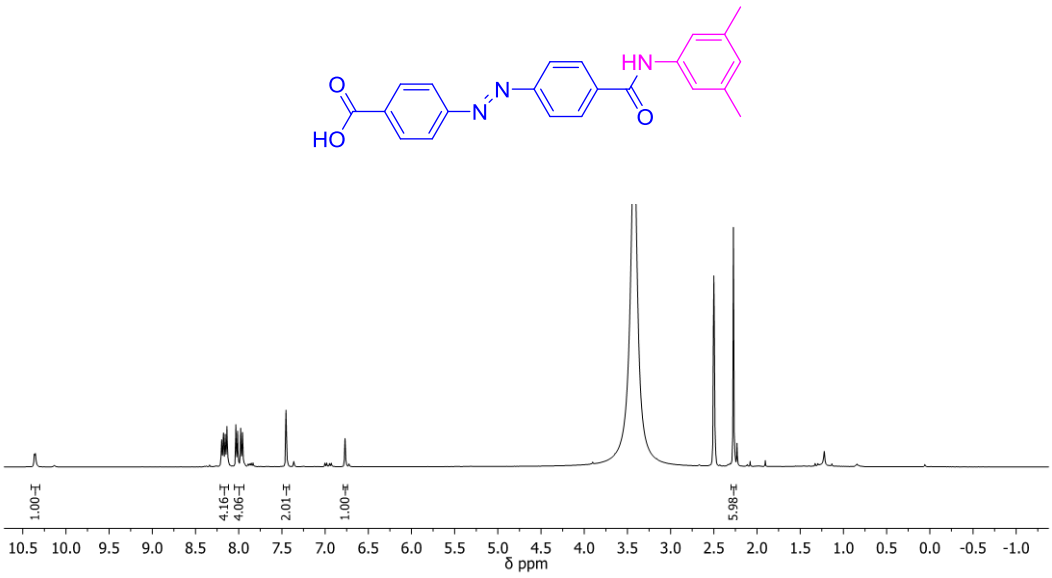

Figure S3.1. ^{1}H NMR spectrum (400 MHz, 298 K, $(CD_3)_2SO$)) of **4a**.

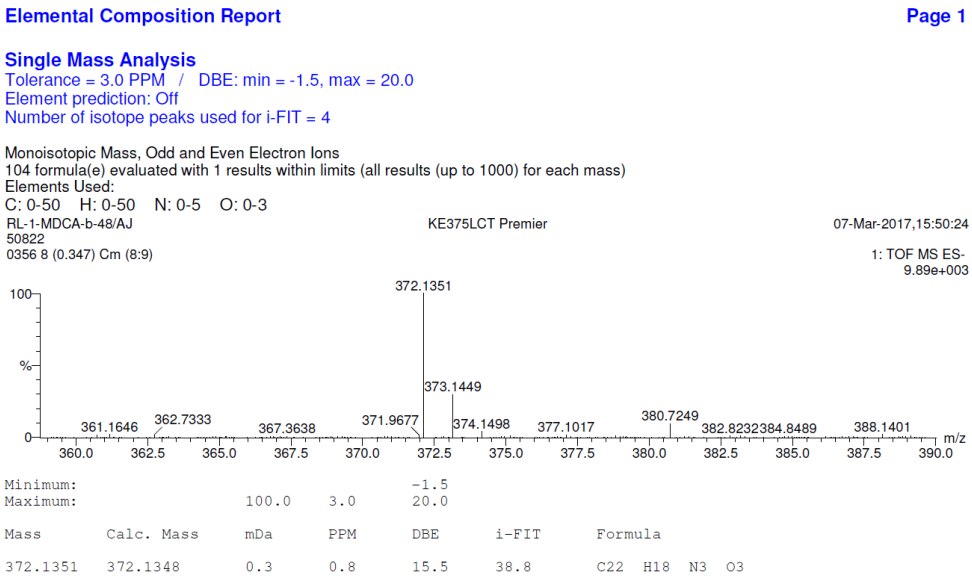

Figure S3.2. HR ESI spectrum of **4a**.

*trans-4,4'-Bis(4-bromo-3,5-dimethylphenylaminocarbonyl)azobenzene]-[α-cyclodextrin]-[2]rotaxane (**5b**)*

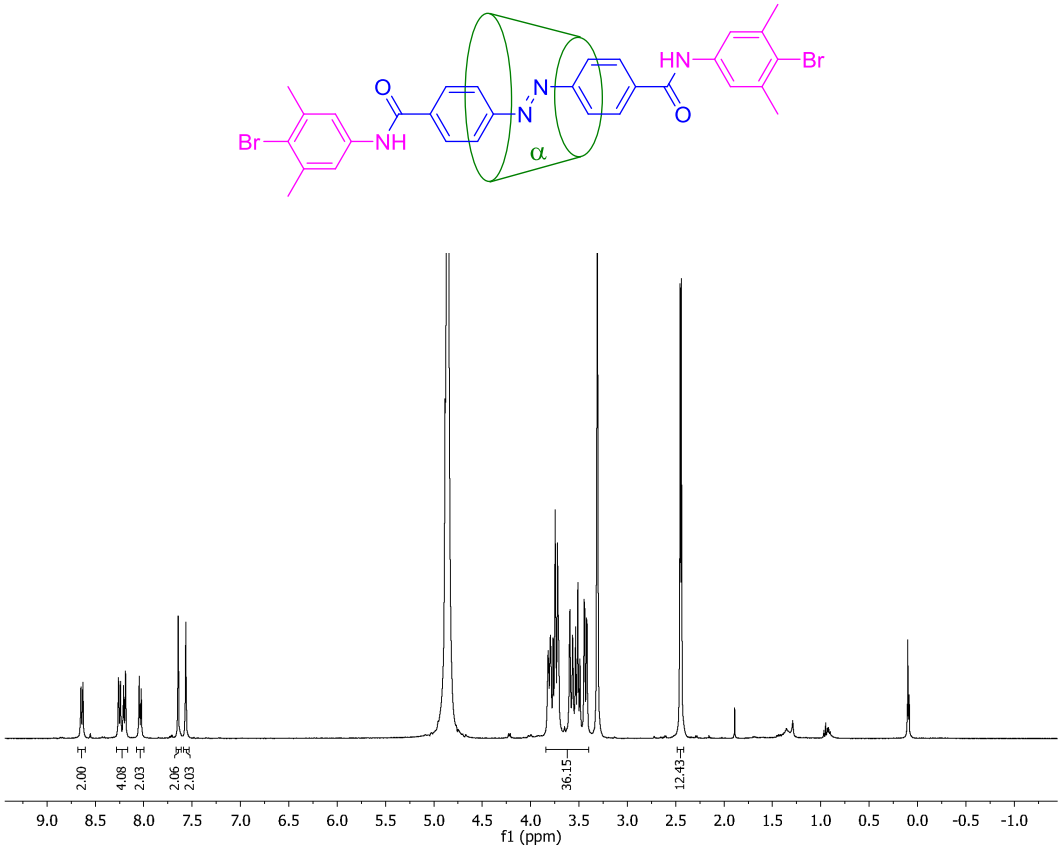

Figure S3.3. ^{1}H NMR spectrum (400 MHz, 298 K, CD_3OD) of **5b**.

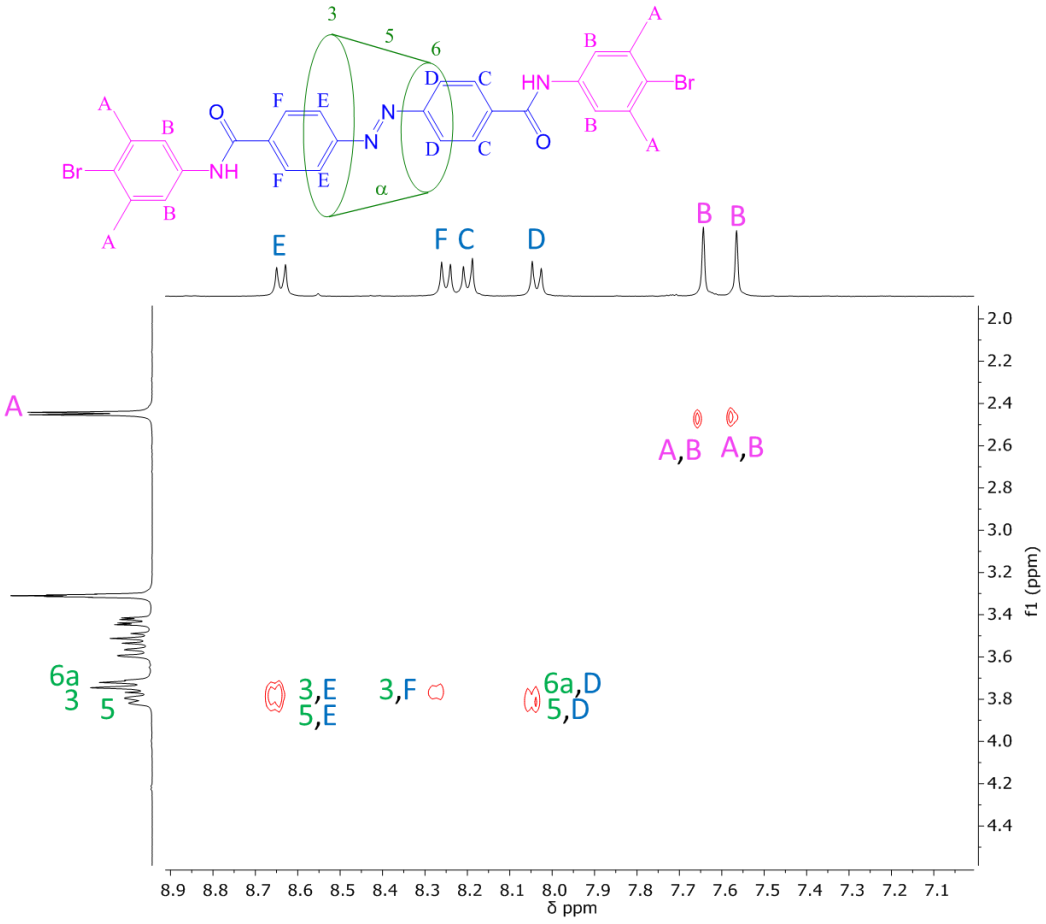

Figure S3.4. Section of ROESY NMR spectrum (600 MHz, 298 K, CD_3OD) of **5b**.

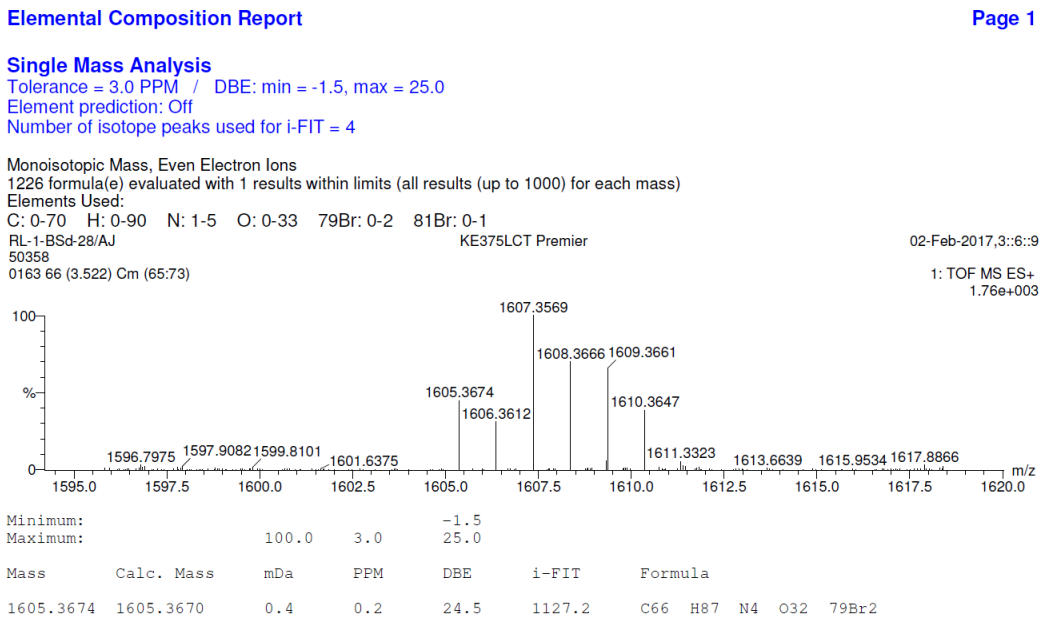

Figure S3.5. HR ESI spectrum of **5b** showing $[M+H]^+$.

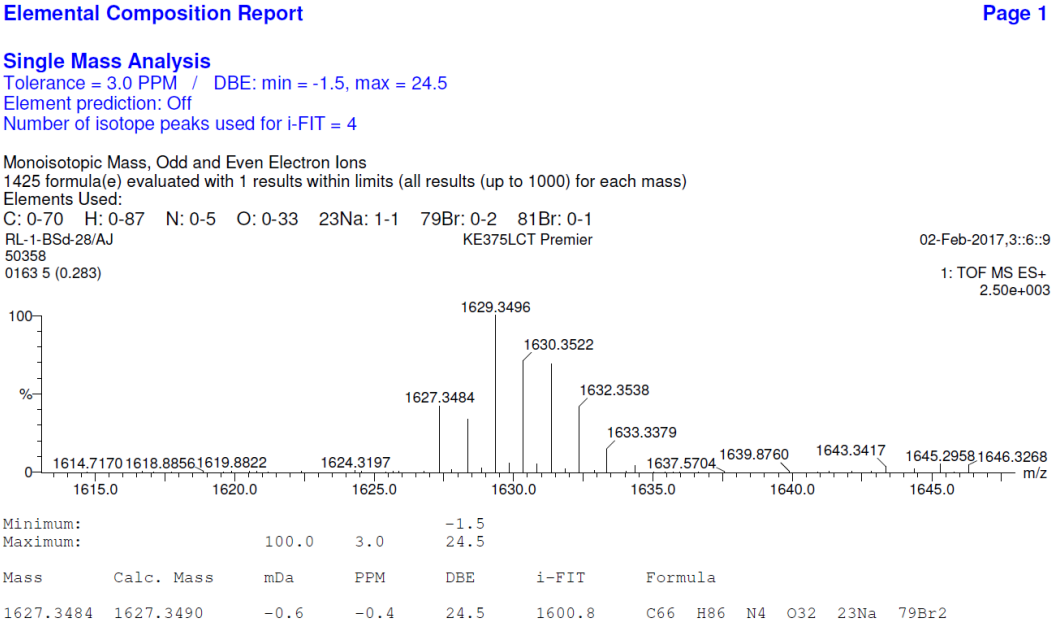

Figure S3.6. HR ESI spectrum of **5b** showing $[M+Na]^+$.

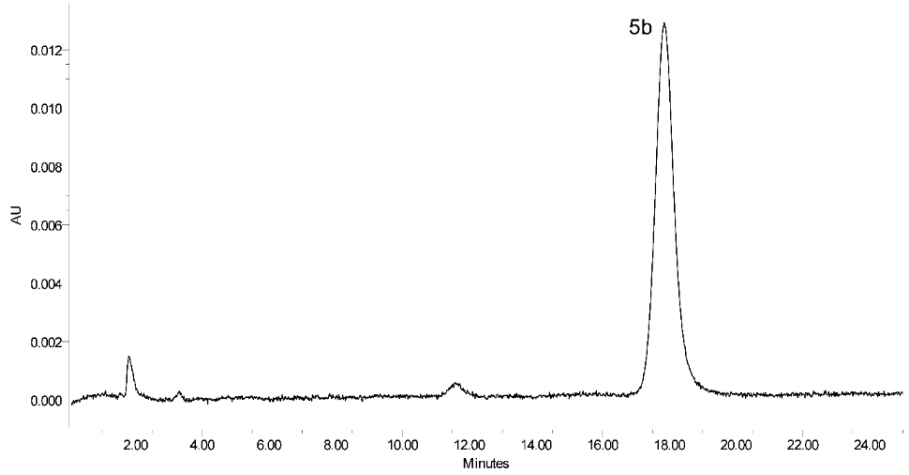

Figure S3.7. HPLC trace of **5b**.

*[trans-4,4'-Bis(4-amino-3,5-dimethylphenylaminocarbonyl)azobenzene]-[α-cyclodextrin]-[2]rotaxane (**5c**)*

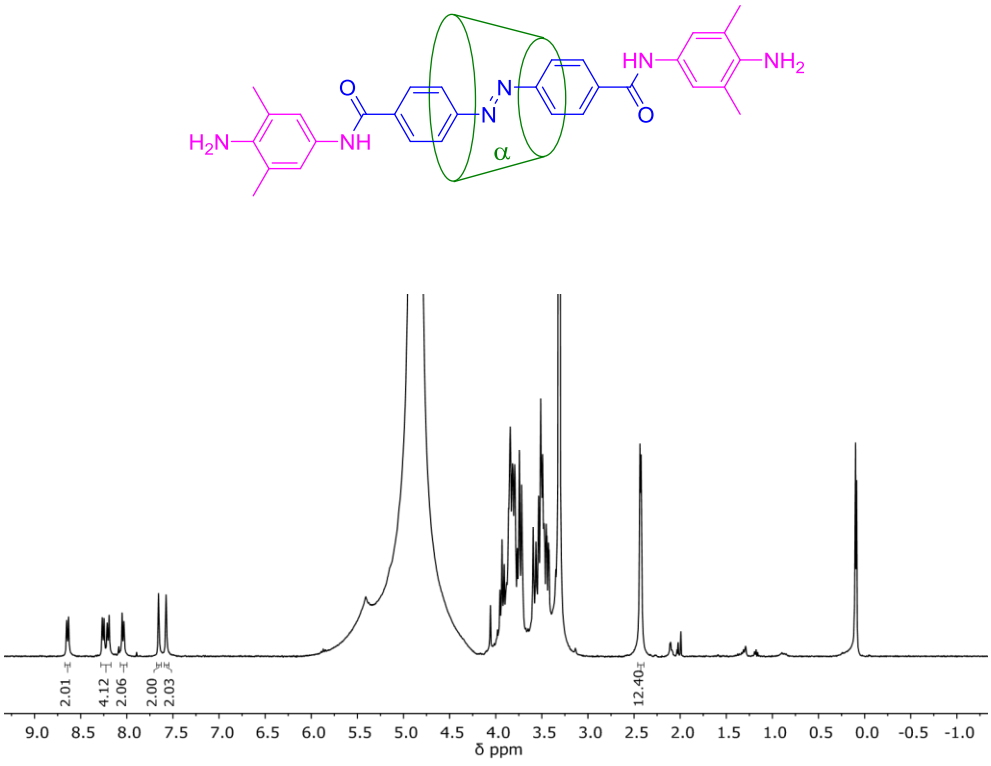

Figure S3.8. ^{1}H NMR spectrum (400 MHz, 298 K, CD_3OD) of **5c**.

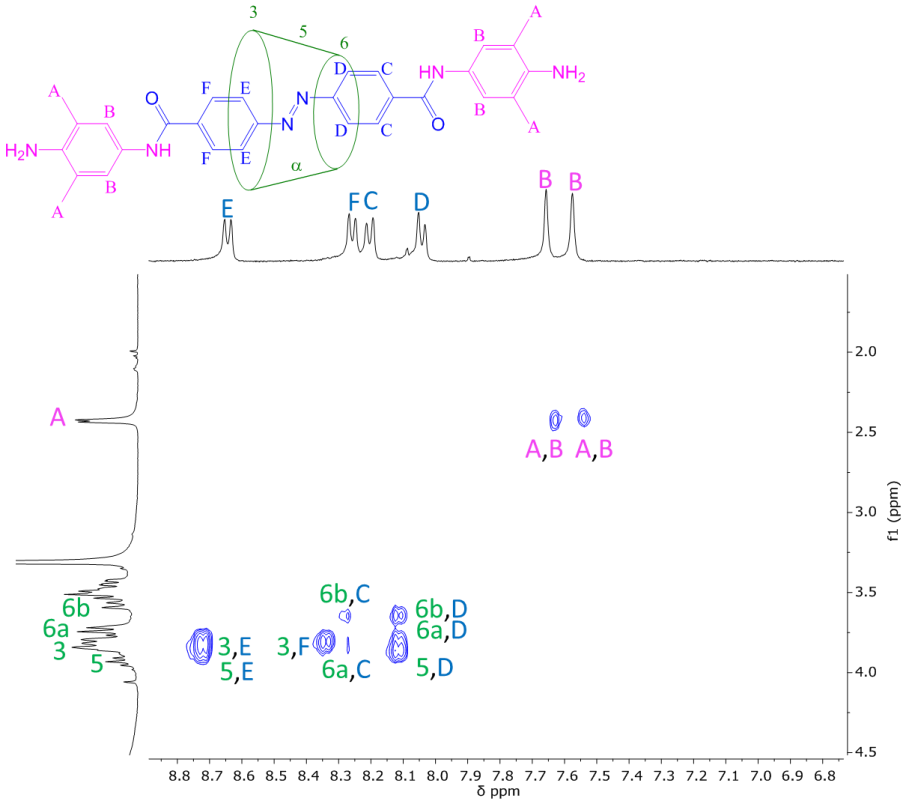

Figure S3.9. Section of ROESY NMR spectrum (600 MHz, 298 K, CD_3OD) of **5c**.

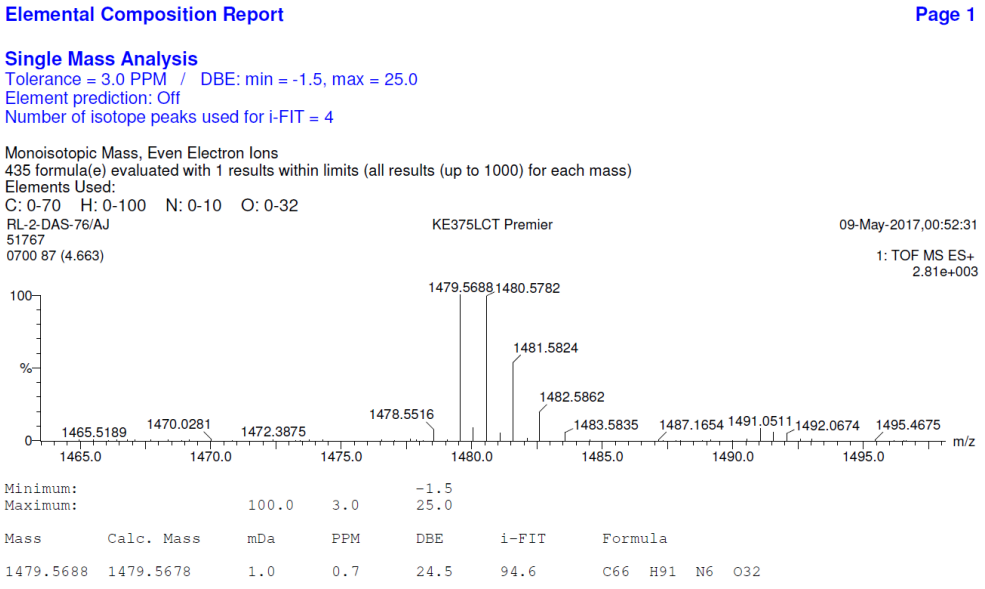

Figure S3.10. HR ESI spectrum of **5c**.

*[trans-4'-(4-Bromo-3,5-dimethylphenylaminocarbonyl)-4-(3,5-dimethylphenylaminocarbonyl)azobenzene]-[α-cyclodextrin]-[2]rotaxane isomers (**6a**, **7a**)*

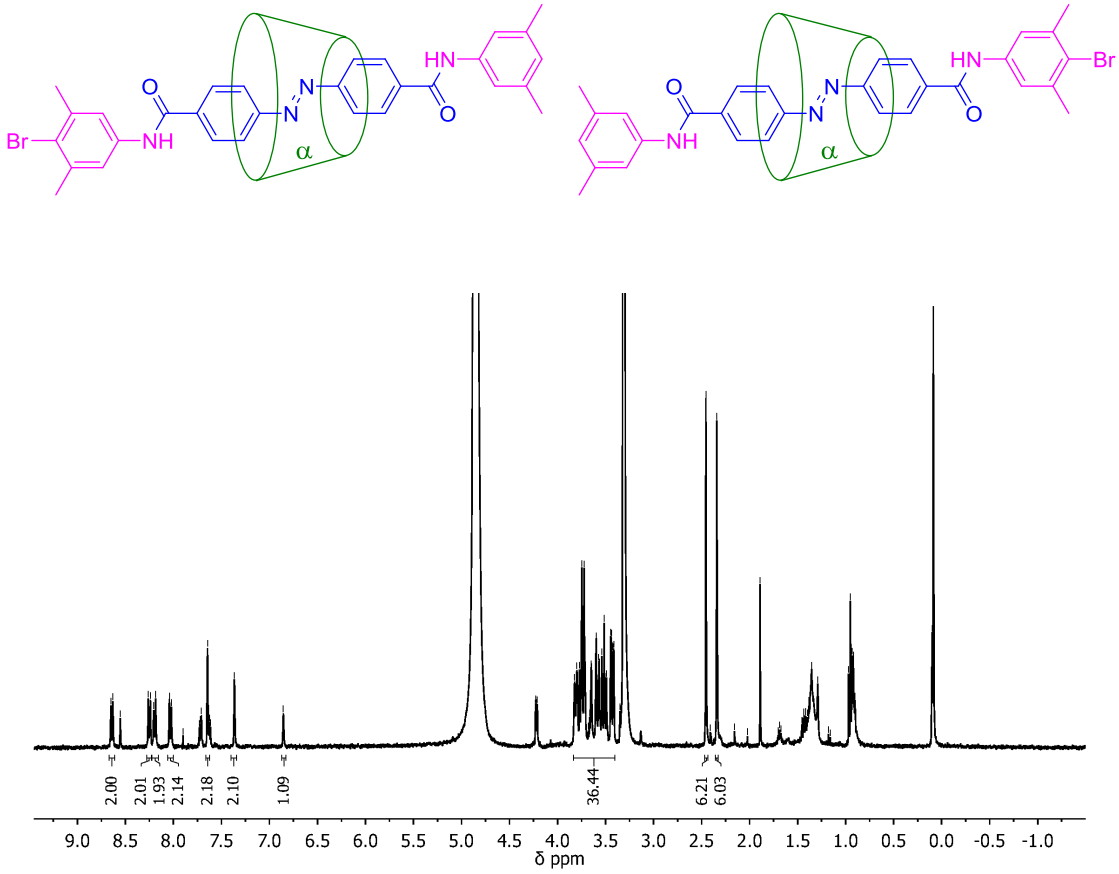

Figure S3.11. ^{1}H NMR spectrum (400 MHz, 298 K, CD_3OD) of **6a**.

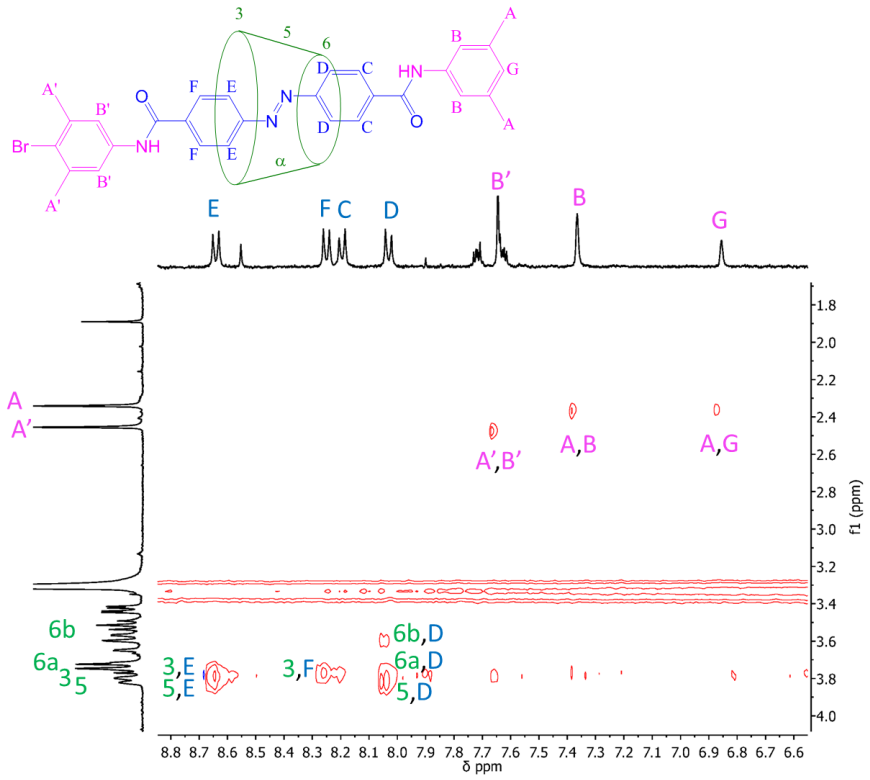

Figure S3.12. Section of ROESY NMR spectrum (600 MHz, 298 K, CD_3OD) of **6a**.

Elemental Composition Report **Page 1**

Single Mass Analysis
Tolerance = 3.0 PPM / DBE: min = -1.5, max = 30.0
Element prediction: Off
Number of isotope peaks used for i-FIT = 3

Monoisotopic Mass, Odd and Even Electron Ions
80 formula(e) evaluated with 1 results within limits (all results (up to 1000) for each mass)
Elements Used:
C: 0-75 H: 0-95 N: 4-4 O: 30-32 23Na: 1-1 79Br: 0-1 81Br: 0-1

RL-1-BS-16/EO KE375 30-Jul-2014 11:13:57
33925
1177 21 (0.945) Cm (21:25) 1: TOF MS ES+
2.67e+004

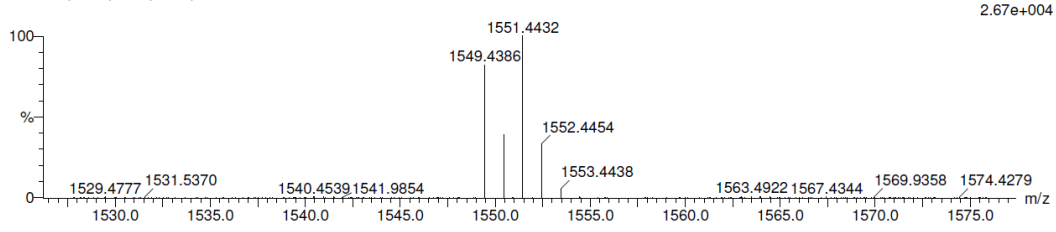

Minimum:				-1.5		
Maximum:		5.0	3.0	30.0		
Mass	Calc. Mass	mDa	PPM	DBE	i-FIT	Formula
1549.4386	1549.4384	0.2	0.1	24.5	8423.0	C66 H87 N4 O32 23Na 79Br

Figure S3.13. HR ESI spectrum of **6a**.

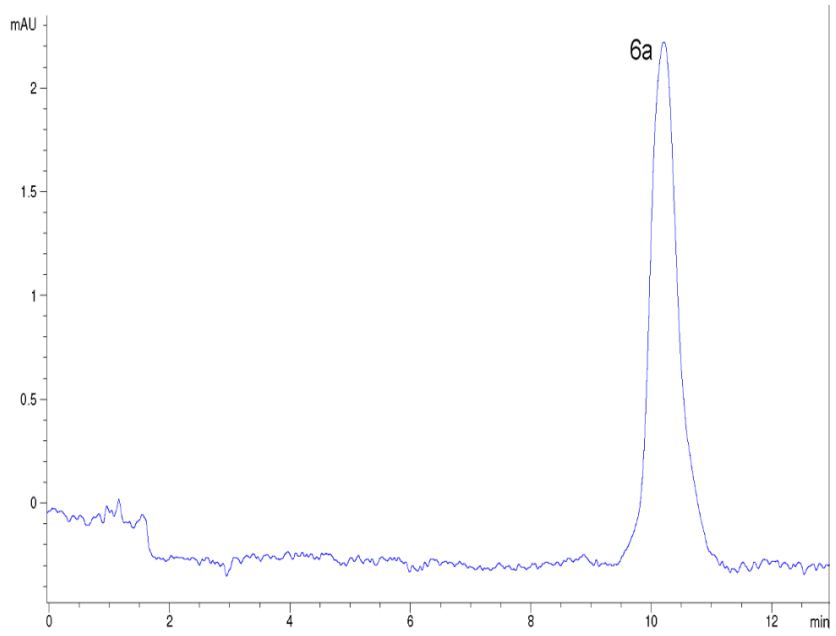

Figure S3.14. HPLC trace of **6a**.

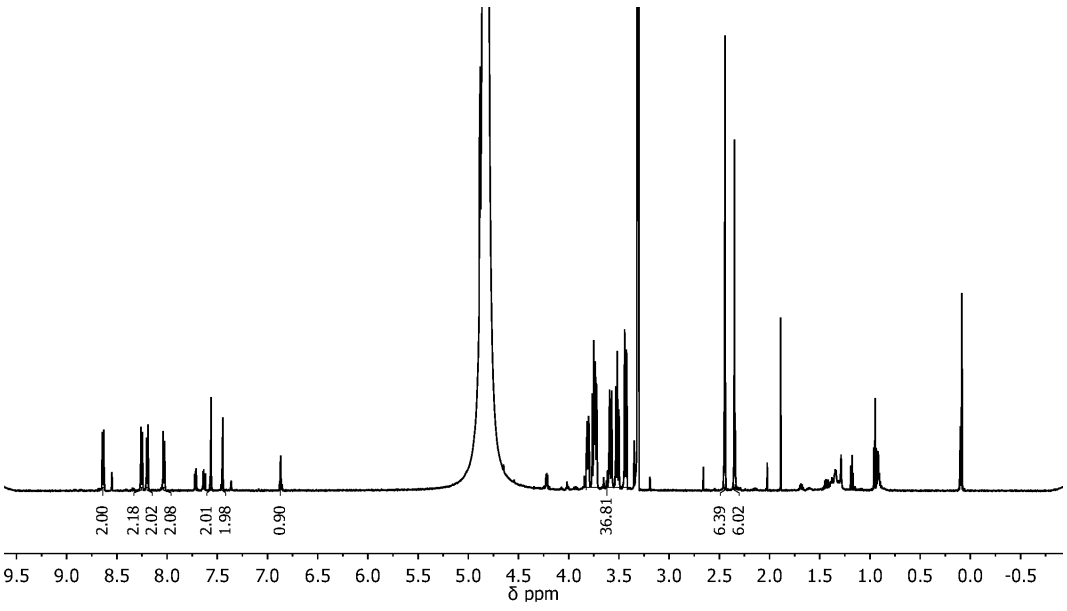

Figure S3.15. ^{1}H NMR spectrum (400 MHz, 298 K, CD_3OD) of **7a**.

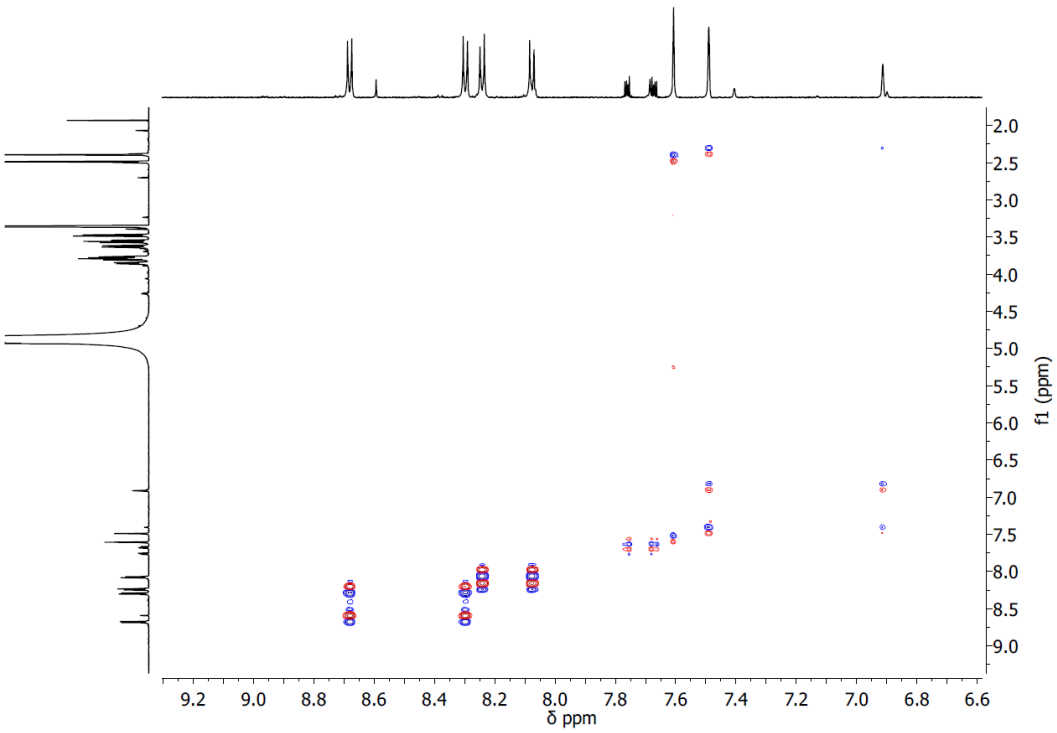

Figure S3.16. Section of COSY NMR spectrum (600 MHz, 298 K, CD_3OD) of **7a**.

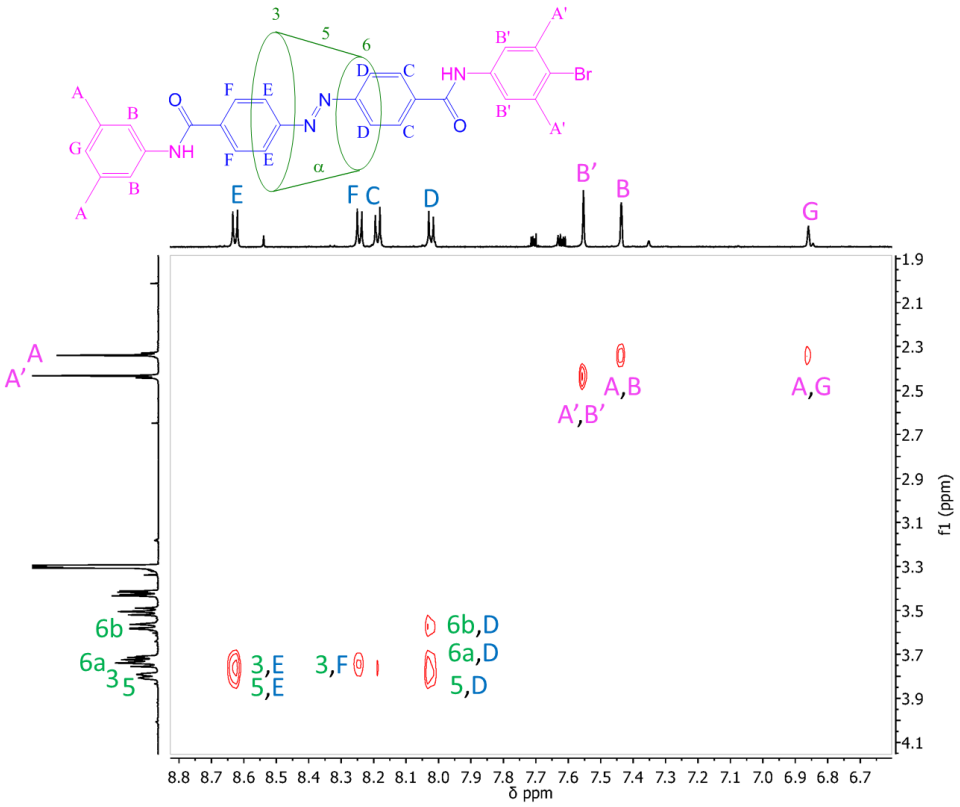

Figure S3.17. Section of ROESY NMR spectrum (600 MHz, 298 K, CD_3OD) of **7a**.

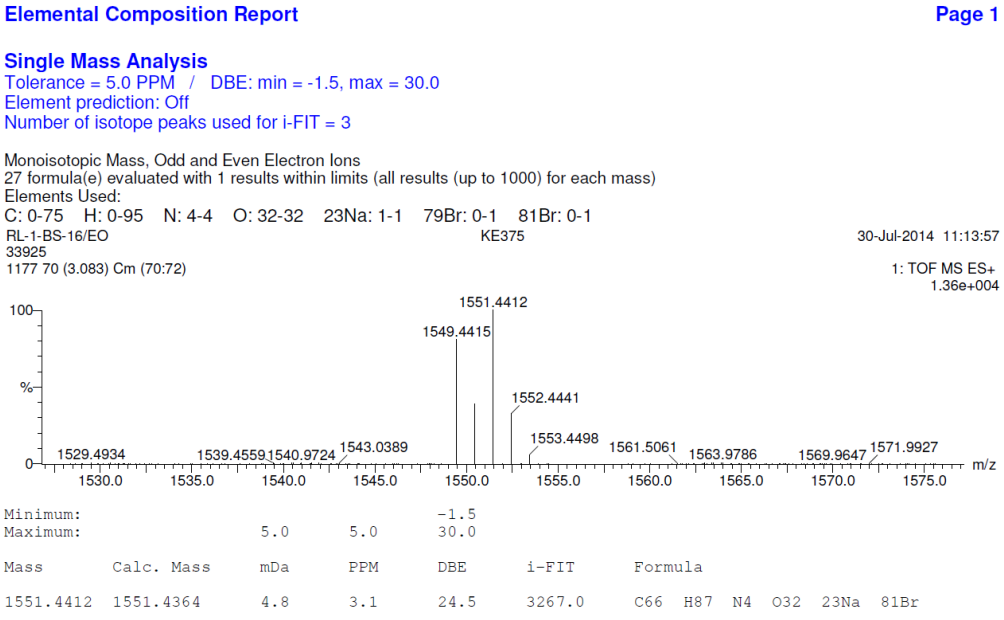

Figure S3.18. HR ESI spectrum of **7a**.

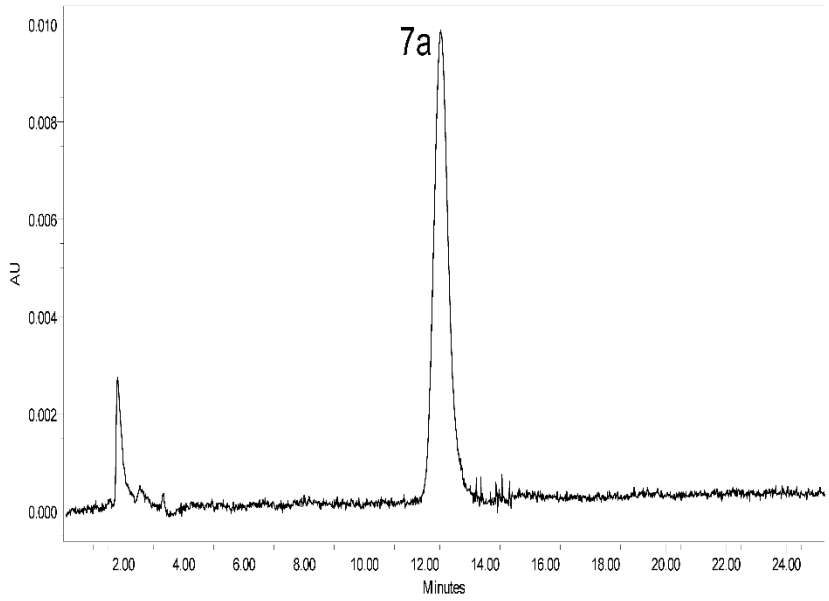

Figure S3.19. HPLC trace of **7a**.

Chapter 4 - INSULATED MOLECULAR WIRES FROM CYCLODEXTRIN [2]ROTAXANE SELF-ASSEMBLIES

4.1 Introduction

The advancements presented in Chapter 2 on the preparation of daisy chains and their potential application as molecular muscles, as well as the investigation of novel synthetic techniques to prepare rotaxanes discussed in Chapter 3, identified significant development opportunities in the field of mechanically interlocked molecules and set the stage for further studies on their application as molecular devices. As discussed in Chapter 1, rotaxanes were initially studied as an academic curiosity more than fifty years ago;[1] however, since then they have attracted increasing interest as the basis of many molecular machines.[2] Cyclodextrin-based examples have included shuttles,[3] ratchets,[4] muscles,[5] sensors[6] and microelectronic devices.[7] The latter applications have involved fabrication of polyrotaxanes into insulated molecular wires, where the cyclodextrins sheath the axles and shield them from each other and the surrounding environment.[7] The Easton group were interested in developing related systems using [2]rotaxanes which, being discrete supramolecular entities rather than complex mixtures, offer potential advantages such as in the straightforward and controlled fabrication of devices through crystallisation. Initially, they observed that each of the cyclodextrin-based rotaxanes **4.1a-4.1d** spontaneously crystallizes as a self-assembly of molecular fibers aligned on a single axis (Figure 4.1).[8] The dumbbells are oriented

along the fibers, with the trinitrophenyl blocking groups of adjacent units displaying π-π interactions. Between the fibers, the dumbbells are isolated from each other by the cyclodextrin components. This arrangement is reminiscent of insulated coaxial cables and the individual strands might have been expected to behave as electronic wires, were it not for the fact that the trinitrophenyl blocking groups are twisted approximately 90° out of conjugation with the stilbene axles.

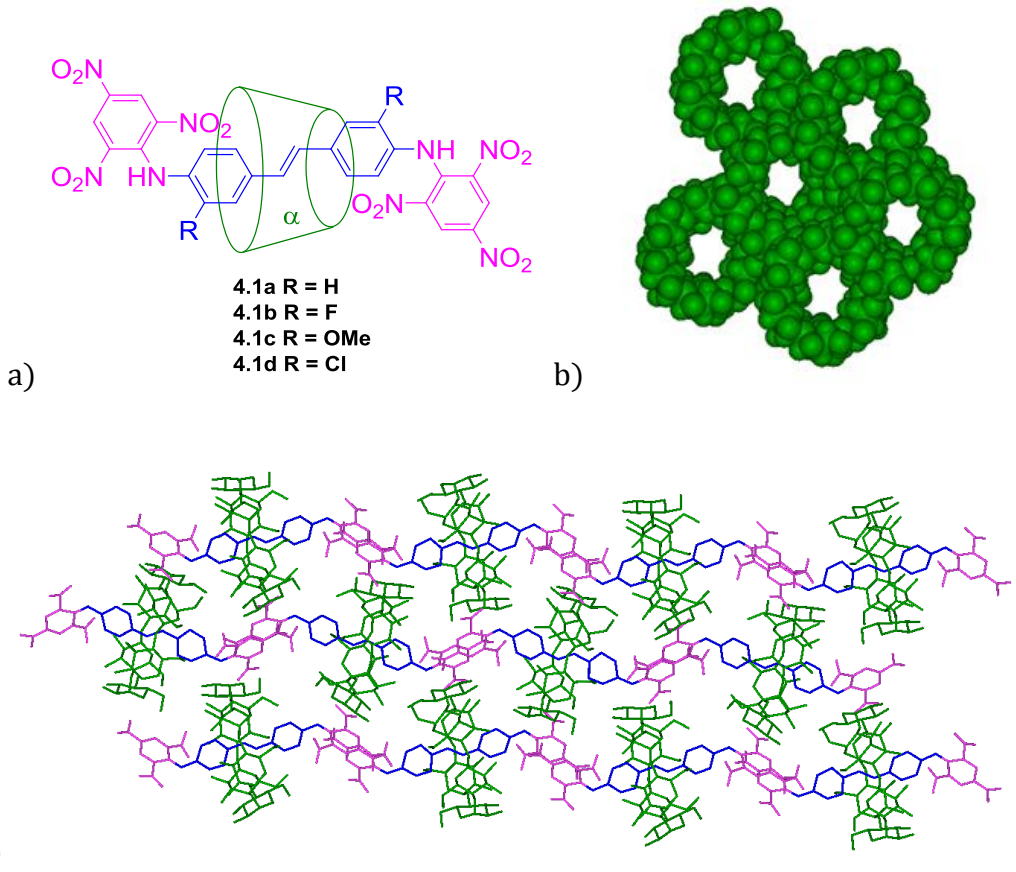

Fig. 4.1. a) Structures of **4.1a-4.1d**; b) the alignment of the cyclodextrins in the crystal structure of **4.1a**; and c) a representation of the crystal structure of **4.1a**.

Of the other [2]rotaxanes that have been subsequently analysed in the solid state,[9] only the 3,5-dimethylaniline-capped rotaxane **4.2** shows features similar to **4.1a-4.1d**;[9a] it displays a network of molecular fibers aligned on one axis, with the blocking groups of adjacent rotaxane units being coplanar and separated by 3.461 Å in an arrangement characteristic of the most common type of π-π interactions (Figure 4.2).[8] However, unlike **4.1a-4.1d**, in this case the dumbbell is almost planar, with a twist angle of less than 5% between the axle and the blocking groups, so there is extended conjugation along the length of each fiber.[9a] The spectroscopic analysis of rotaxane **4.2** in water shows deviation from Beer's law, i.e., a direct correlation between the concentration of a solution and its absorbance. In particular, for concentrations of rotaxane **4.2** higher than 10 μM, the increase in absorbance is not proportional to the increase in concentration. In addition, absorbances at wavelengths higher than those characteristic of an azobenzene are observed at high concentrations. This behaviour, along with the fluorescence emitted by an irradiated solution, is a clear indication of the assembly of π-π stacked aggregates in water, similar to those observed in the solid state.[9a] In comparison, [2]rotaxanes **4.3** and **4.4** also crystallize to form molecular strands with fully conjugated dumbbells, but the strands are not all lined up in one direction.[9b, 9c] Instead, those oriented on one axis are interspersed by others arranged at right angles (Figure 4.2). A similarly interposed assembly of fibers forms on crystallization of the 2,6-dimethylaniline-capped rotaxane **4.5** and those dumbbells are not fully conjugated (Figure 4.2).[9a]

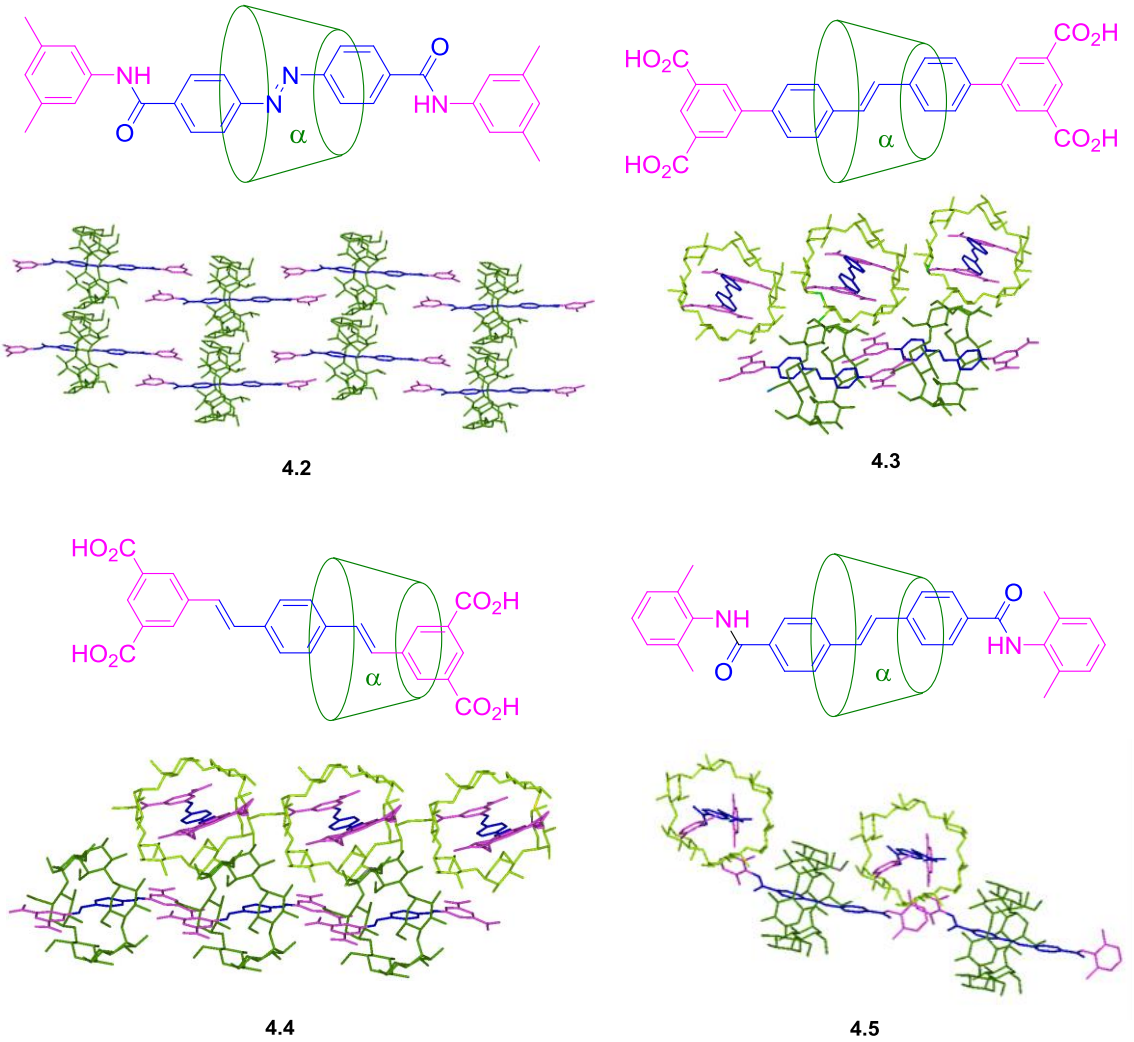

Fig. 4.2. Structures and corresponding representations of the crystal structures of **4.2-4.5**.

Rotaxanes **4.2** and **4.5** differ in two respects; whether the capping groups are 3,5- or 2,6-dimethylanilino groups and whether the axle is an azobenzene or a stilbene. Consequently, additional [2]rotaxanes **4.6-4.9** have been prepared in the Easton

group[9d] (Figure 4.3), so that the effects of the individual variables could be assessed.

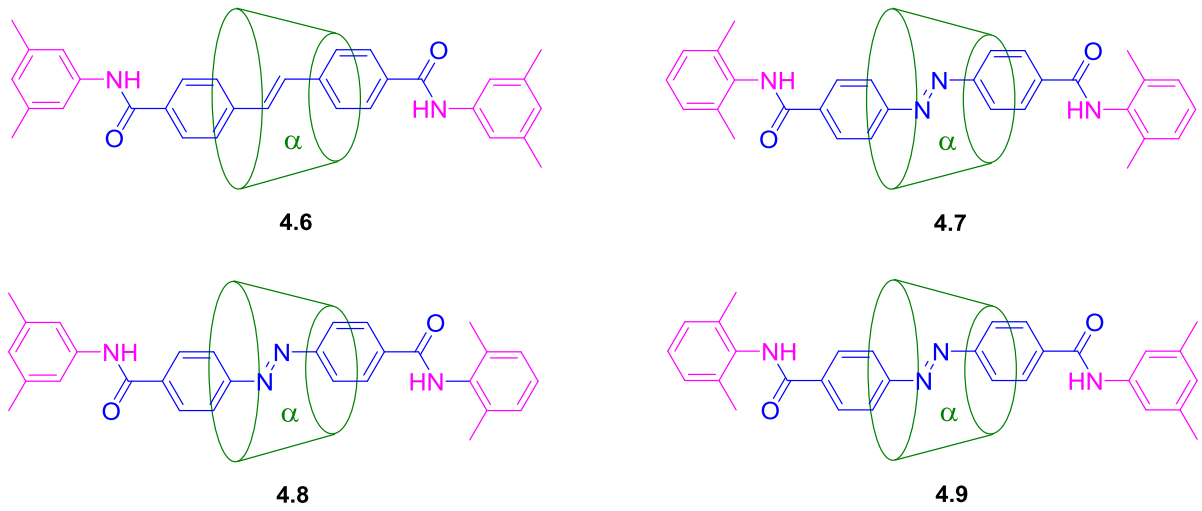

Fig. 4.3. Structures of **4.6-4.9**.[9d]

The solid state structures of rotaxanes **4.6-4.9** were analysed by X-ray crystallography and compared with those of the previous species. The crystal structures of **4.5** and **4.7** are strikingly similar, so the substitution of the stilbene with the azobenzene appears to make very little difference. The planes of both 2,6-dimethylaniline blocking groups are twisted approximately 90° from that of the stilbene of **4.5** and the azobenzene of **4.7**, consistent with steric interactions between the methyl substituents and the oxygens of the amide groups. Both **4.2** and **4.6** align as molecular fibers on a single axis but, in contrast to the coplanar arrangement of the blocking groups and azobenzene of **4.2**, the dimethylanilino groups of **4.6** are each twisted out of the plane of the stilbene by approximately 30°. The result is that

the dumbbell of **4.6** is much less conjugated. Similar to **4.6**, the dumbbells of rotaxanes **4.8** and **4.9** are not conjugated, but rather than both end groups being twisted out of the plane of the axle, here the 3,5-dimethylaniline group is coplanar, while the 2,6-dimethylaniline group is twisted at 90°. Among all the rotaxanes previously synthesized, rotaxane **4.2**, showing intra- and inter-molecular dumbbell co-planarity, extended conjugation and π-π stacking between adjacent molecules, was the obvious starting point for further investigation into the development of solid-state self-assemblies of rotaxanes as coaxial molecular wires.

4.2 Results and Discussion

Rotaxane **4.2** was synthesized by adapting the procedure of Maniam *et al.* [9a] As shown in Scheme 4.1, azobenzene-4,4'-dicarboxylic acid **4.10** and α-CD **4.11** were equilibrated in water in the presence of Et_3N; DMT-MM and 3,5-dimethylaniline **4.12** were then added to the reaction mixture, which was stirred at room temperature overnight.

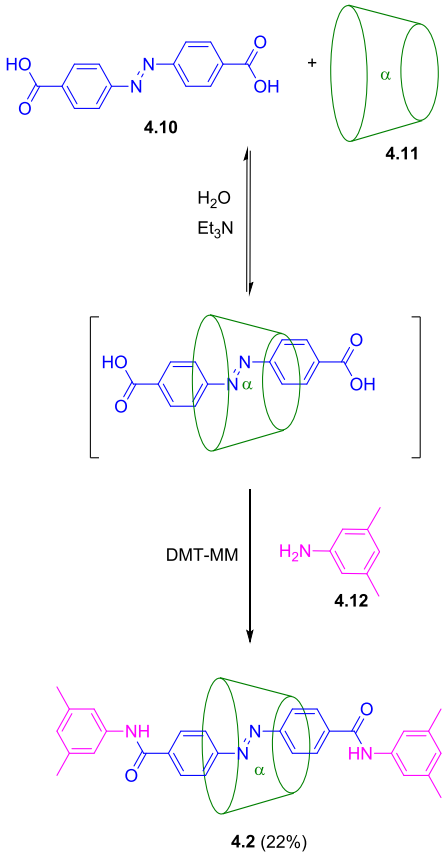

Scheme 4.1. Synthesis of rotaxane **4.2**.

The product was isolated in 22% yield through reverse phase HPLC chromatography and characterised by mass spectrometry and NMR spectroscopy. The ESI spectrum showed an ion at *m/z* 1471, which corresponds to the sodiated ion of the rotaxane **4.2**, while the ^{1}H NMR spectrum confirmed the purity of the compound, as well as the key components of the rotaxane, including the azobenzene, the cyclodextrin and the dimethylaniline (Figure 4.4).

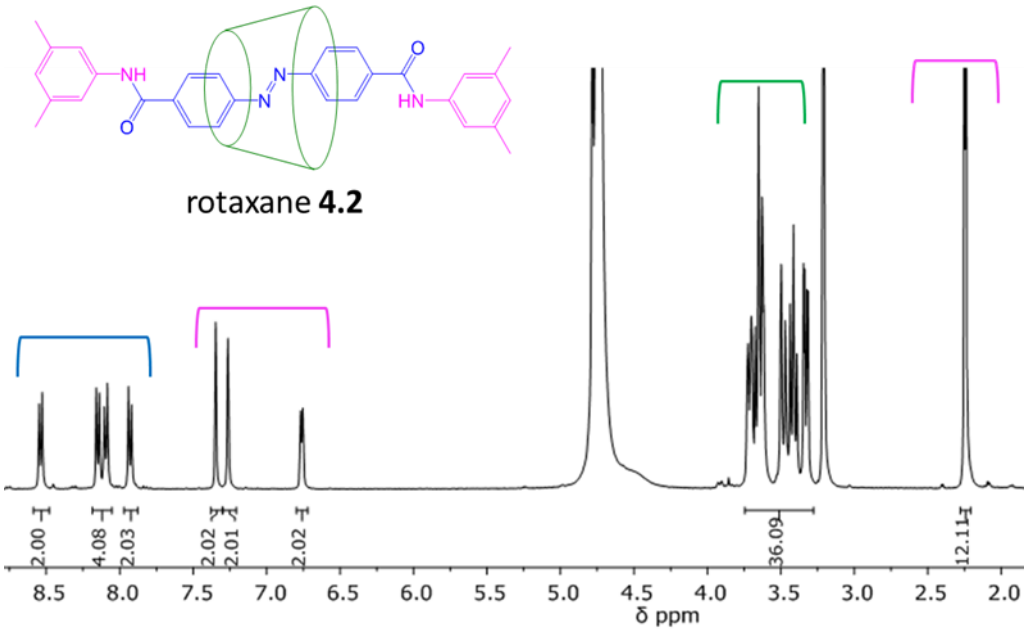

Fig. 4.4. ^{1}H NMR spectrum (400 MHz, 298 K, CD_3OD) of rotaxane **4.2**.

Having prepared rotaxane **4.2**, the next aim was to test its conductivity properties in the solid state. While the rotaxane **4.2** had been observed to form fibers resembling coaxial cables in the solid state, its ability to function as a molecular wire had not been examined. Crystal growth experiments on rotaxane **4.2** were performed based on previous studies undertaken in the group, which demonstrated that the crystal morphology could be manipulated by changing the concentration of the solution where the rotaxane was dissolved.[9d] Following UV-vis spectroscopic studies to identify the saturation concentration of rotaxane **4.2** at different temperatures, two supersaturated solutions of rotaxane **4.2**, respectively at 25 μM and 250 μM, were prepared to grow crystals. In both cases, amorphous material, which is typically more soluble than the crystalline material, was added to water, the mixture was then heated to below boiling point to achieve dissolution of the amorphous material, and

finally the solutions were left to stand at room temperature to promote crystallization. After a few days needle-shaped crystals formed. Comparing the size of the crystals obtained from the two batches, no significant difference was observed in terms of width, while the length was significantly different, with much longer crystals from the more concentrated solution. Following the reported procedure,[9d] a 250 μM solution of rotaxane **4.2** was again prepared by dissolving the amorphous material in water, heating the mixture up to 95 °C and then leaving it to stand at room temperature to allow crystal formation. Over one week, needle-shaped crystals up to 1 mm long formed. According to previous crystal engineering studies undertaken in the Easton group,[9d] the formation of long and thin needle-shaped crystals of rotaxane **4.2** is due to kinetically favoured π-π stacking between the dumbbells, leading to preferential growth along one axis. This suggests that the direction of the strands of π-overlapped guest molecules is along the long axis of the needles. In order to verify this hypothesis, the correlation between the crystal structure and the crystal morphology was explored by X-ray crystallography. The face indexing analysis showed that the long axis of the needle corresponds to the b axis, which is also the direction of the strands of π-overlapped guest molecules (Figure 4.5).

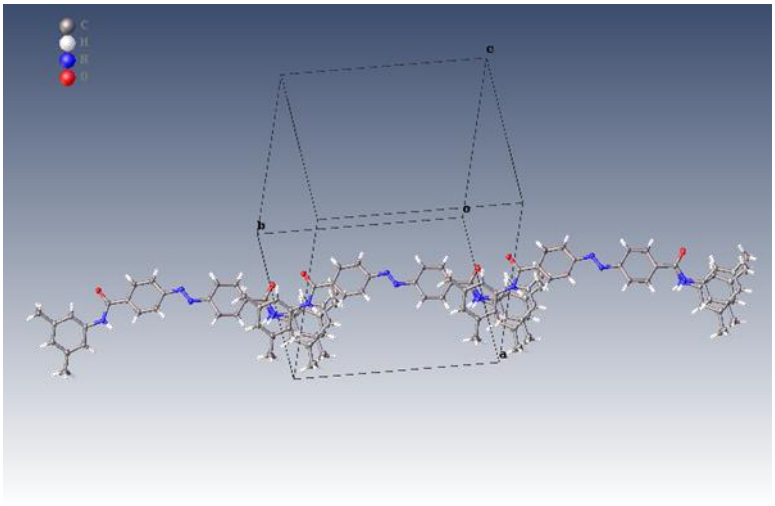

Fig. 4.5. Olex2 (OlexSys) representation of the crystal structure of rotaxane **4.2** showing the strands of guest molecules extending along the crystal unit cell (host and water molecules omitted for clarity).

This result is consistent with the crystal engineering studies previously undertaken in the Easton group,[9d] and provided key information for the design of conductivity experiments. Given the alignment between the long axis of the crystal and the rotaxane axle, the measurement of the conductivity along the needle was the key experiment to evaluate the ability of electrons to flow through the π-π stacked dumbbells of the compound. An established method to determine the conductivity of a material relies on the measurement of its current-voltage (IV) characteristics.[10] This analysis can be performed by positioning a crystal between a source and a drain electrode and applying different voltages to the contacts. The device can be operated in bottom- or top-contact mode. In the first case the electrodes are attached on the surface of an insulating plate and the material is placed on top of them, while in the second layout the material is firstly laid over the

insulating plate, and then the electrodes are placed at either end of the substrate (Figure 4.6).[11] The top contact mode has been widely adopted in the fabrication of nanoscale electronic devices because it provides better electronic performance compared to the bottom contact approach.[11]. Initially, the conductivity experiments were therefore performed in a top contact configuration, where silicon plates were used as the insulator and gold films, acting as the source and drain electrodes, were positioned at both ends of needle-shaped crystals of rotaxane **4.2**.

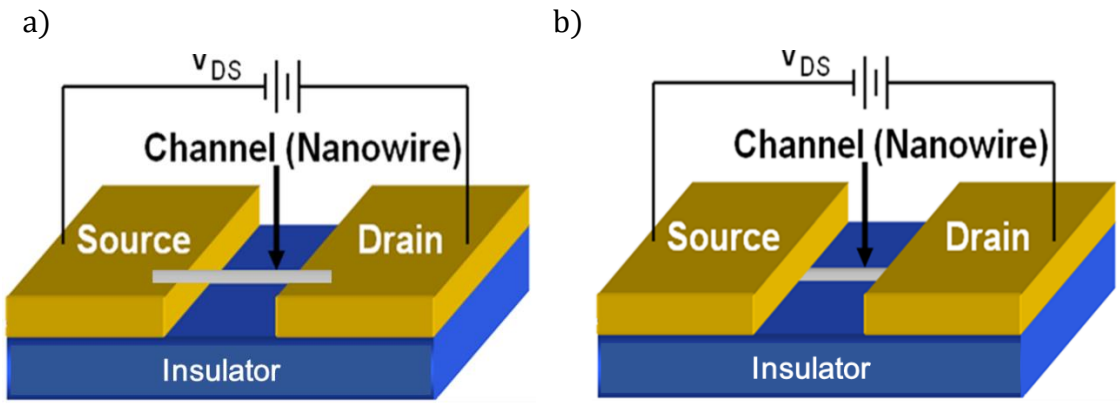

Fig. 4.6. Schematic representation of a circuit connected by a crystal in a) bottom contact mode; and b) top contact mode.[12]

In order to reduce the number of variables in the experiments, a mask was utilised to allow deposition of gold films at fixed distances. A single crystal was placed on a silicon substrate, then two adjacent apertures of the mask were positioned at the two ends of the needle. The mask apertures were filled by gold films through vapour

deposition, resulting in two gold electrodes linked by a crystal of rotaxane **4.2** (Figure 4.7).

Fig, 4.7. Gold electrodes linked by a crystal of rotaxane **4.2**.

Probes were attached at both electrodes and the variation of current was monitored upon voltage variation. The same procedure was adopted for a blank experiment, where no crystal was placed between the two electrodes, assuming that this system would not be able to show significant conductivity, given the absence of a conductive material between the electrodes (Figure 4.8).

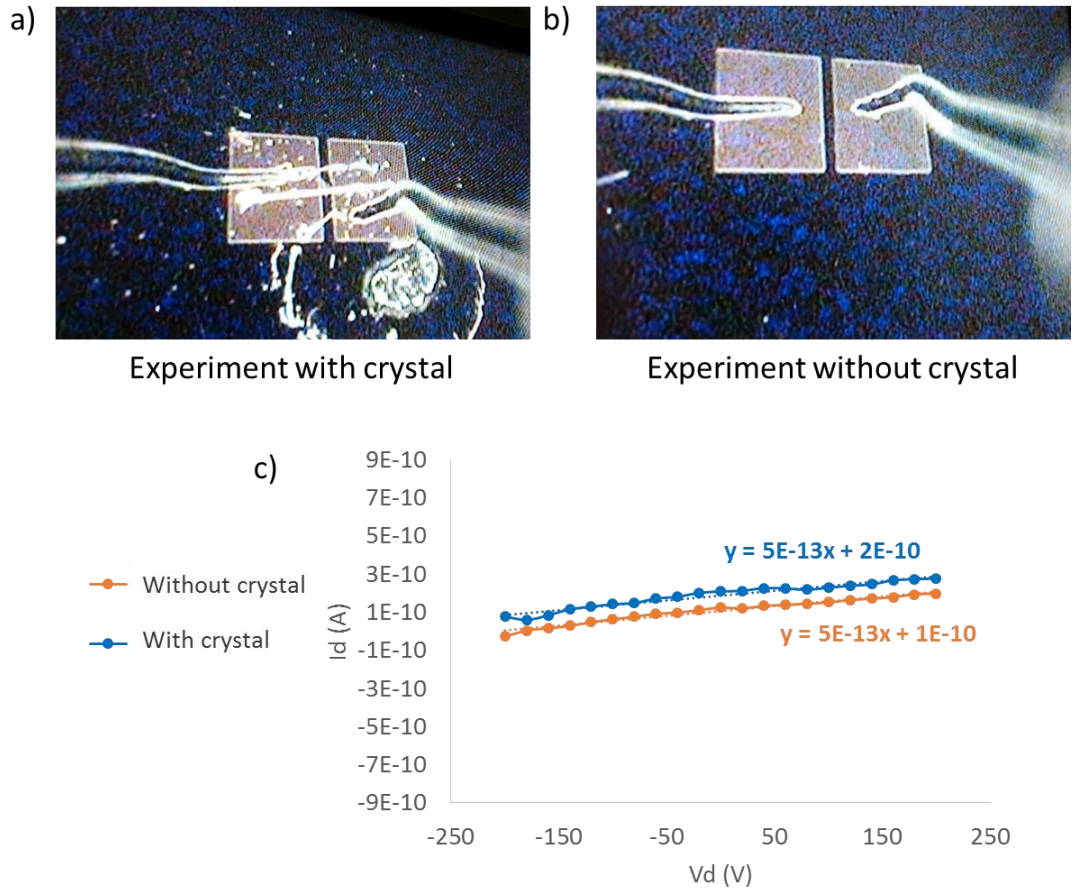

Fig. 4.8. a) Gold electrodes linked by a crystal of rotaxane **4.2**; b) gold electrodes without a crystal; and c) current-voltage characteristics of the circuits with and without a crystal.

Although this analysis was attempted using a number of different crystals, with this set-up no difference was observed in terms of conductivity between the circuits with and without the needle. Both systems showed very little current upon voltage variation, meaning that the low observed current was not related to the presence of the crystal. Why the system with the crystal provided negligible conductivity could have been related to the intrinsic inability of the material to conduct electricity, or

due to difficulties with the method. The mask, gold, and crystal deposition processes were indeed technically very difficult. Crystals were often damaged when they were transferred to the silicon plate and the positioning of the mask over the crystal was challenging due to the narrow gap between the apertures (100 μM), meaning that a good connection between the two ends of the needle and two adjacent apertures of the mask was not always achieved. In addition, the thin gold films were often scratched while attaching the probes and the crystal was not always well covered by the gold films because the thickness of the electrodes (30 nm) was almost negligible compared to the crystal diameter (approx. 20-30 μm). Given the lack of success using the above method, an alternative approach was utilised to further investigate the ability of rotaxane **4.2** to conduct electricity. A suspension containing rotaxane crystals was placed on a silicon substrate and left for the solvent to evaporate.[13] Silver paste was then placed at the two extremities of a specific crystal to act as the source and drain electrodes. The sample was again left to dry overnight and then the conductivity was measured. Initially, the experiment was very difficult and multiple tests provided inconsistent results, likely due to unwanted silver migration between close electrodes and the breaking of the delicate crystals but, after many attempts, a good experimental procedure was established. Similar to the previous experiment, the IV characteristics of this circuit were compared with one of a blank experiment consisting of silver paste electrodes without a crystal in between (Figure 4.9).

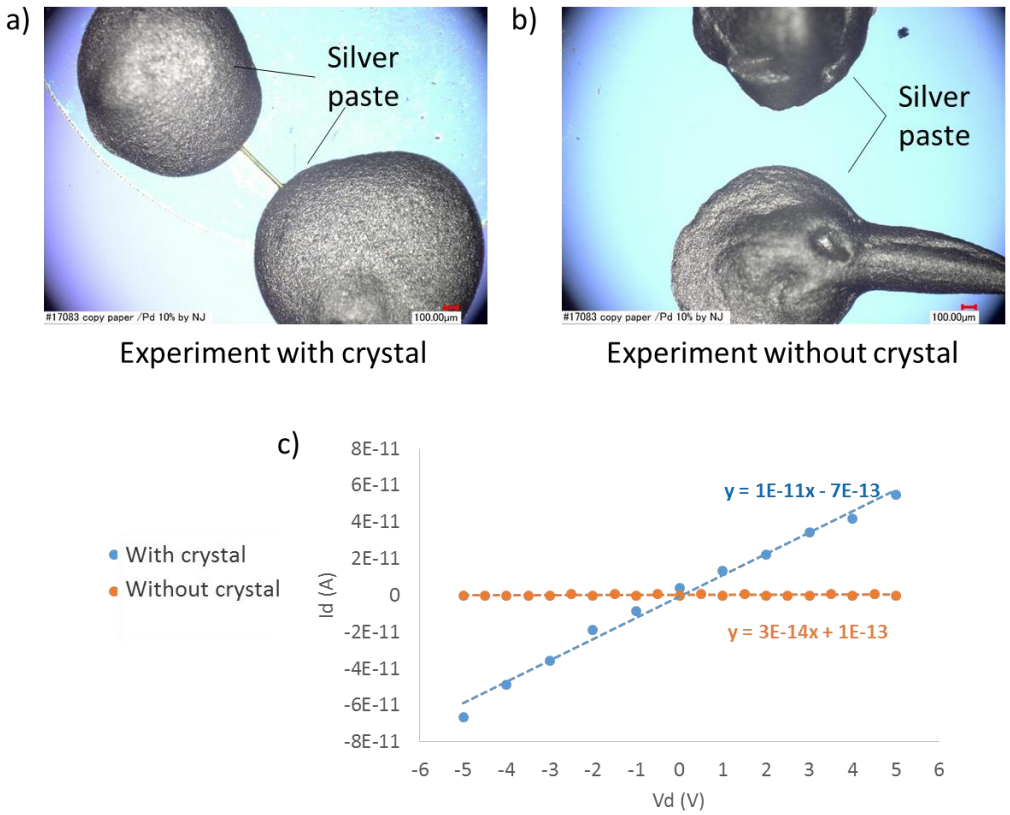

Fig, 4.9. a) Silver electrodes linked by a crystal of rotaxane **4.2**; b) silver electrodes without a crystal in between; and c) current-voltage characteristics of circuits with and without a crystal.

The experiment without the crystal showed negligible current variation upon voltage variation. The minimal slope of the curve is likely an artefact and indicates that there is effectively no conductivity between the electrodes in the absence of the crystal. On the contrary, I and V were found to be proportional in the system with the crystal of rotaxane **4.2**. This response is consistent with Ohm's law, therefore rotaxane **4.2** can be defined as an ohmic resistor.[14] According to Ohm's law, the resistance (R) of a material is obtained from the ratio between voltage (V) and

current (I) and is typically measured in Ohms (Ωs).[15] The resistance of rotaxane **4.2** was therefore calculated as the reciprocal of the slope of the IV curve, as shown below.

$$R_{\text{rotaxane 4.2}} = \frac{1}{1 \text{ x } 10^{-11}} = 1 \text{ x } 10^{11}\ \Omega$$

Having obtained the resistance of the crystal, its length (l), diameter (d) and cross sectional area (A) were estimated from the microscope image to determine its resistivity (ρ). The conductivity (σ) of the crystal was then calculated as shown below.[16]

$$\rho_{\text{rotaxane4.2}} = R\,\frac{A}{l} = 1 \text{ x } 10^{11}\ \Omega\ \frac{7 \text{ x } 10^{-6}\ \text{cm}^2}{0.08\ \text{cm}} = 8.8 \text{ x } 10^{6}\ \frac{\text{cm}}{\text{S}}$$

$$\sigma_{\text{rotaxane 4.2}} = \frac{1}{\rho} = \frac{1}{8.8 \text{ x } 10^{6}\ \frac{\text{cm}}{\text{S}}} = 1.1 \text{ x } 10^{-7}\ \frac{\text{S}}{\text{cm}} = 1.1 \text{ x } 10^{-5}\ \frac{\text{S}}{\text{m}}$$

where

σ = conductivity [S/m]

ρ = resistivity [cm/S]

R = resistance [Ω] (Ω=1/S)

A = cross sectional area [cm^2]

l = length of the crystal [cm]

The analysis was successfully replicated with a different crystal; its IV characteristics were also recorded and compared with a circuit without a crystal (Figure 4.10).

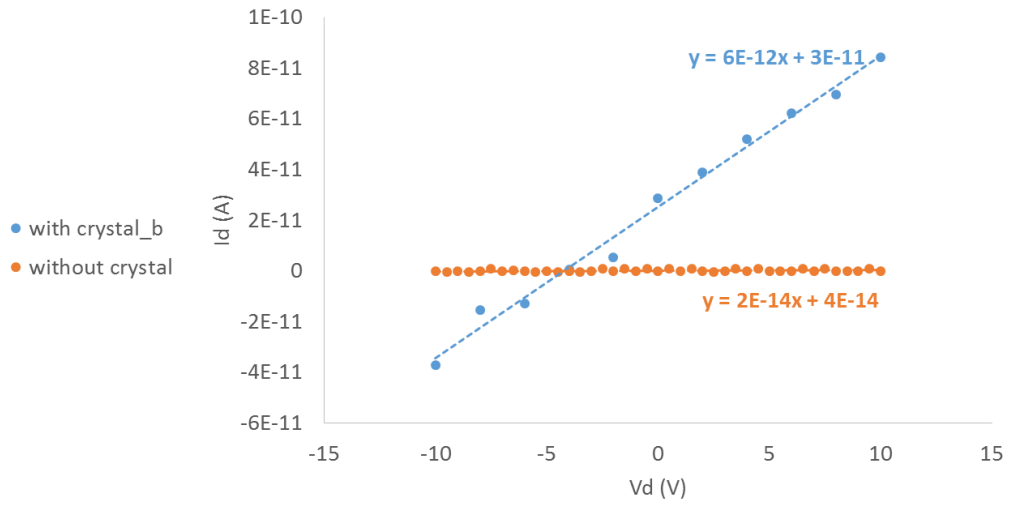

Fig, 4.10. Current-voltage characteristics of circuits with and without an alternative crystal of **4.2**.

The resistance, resistivity and conductivity of the new crystal of rotaxane **4.2** were calculated as shown below.

$$R_{\text{rotaxane 4.2\_b}} = \frac{1}{6 \times 10^{-12}} = 1.7 \times 10^{11}\ \Omega$$

$$\rho_{\text{rotaxane4.2\_b}} = R\,\frac{A}{l} = 1.7 \times 10^{11}\ \Omega\ \frac{3.1 \times 10^{-6}\ \text{cm}^2}{0.06\ \text{cm}} = 8.8 \times 10^{6}\ \frac{\text{cm}}{\text{S}}$$

$$\sigma_{\text{rotaxane 4.2\_b}} = \frac{1}{\rho} = \frac{1}{8.8 \times 10^{6}\ \frac{\text{cm}}{\text{S}}} = 1.1 \times 10^{-7}\ \frac{\text{S}}{\text{cm}} = 1.1 \times 10^{-5}\ \frac{\text{S}}{\text{m}}$$

Despite a difference in resistance and in the crystal cross section and length, the resistivity and conductivity values obtained for this crystal are the same as the ones discussed above. These results provided confidence in the reproducibility of the experiment, which was further confirmed by other tests discussed later in this Chapter, and show that electrons flow along the needles through the π-π connected dumbbells of the rotaxanes (Figure 4.11).

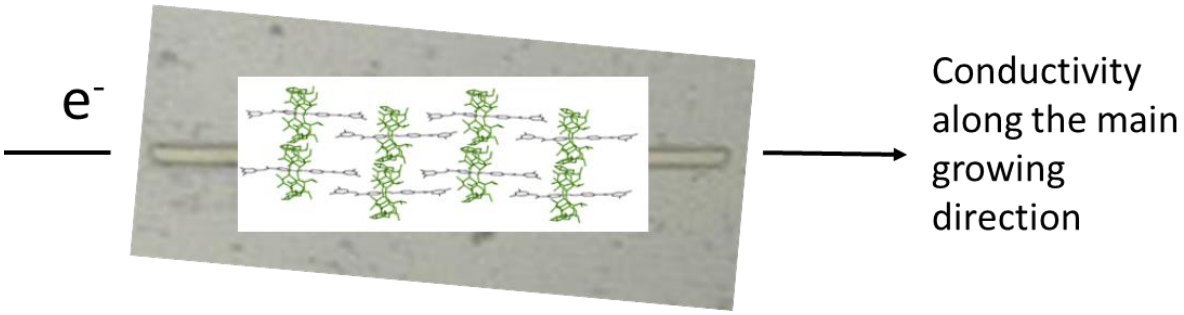

Fig. 4.11. Conductivity results and correlation between crystal structure and crystal morphology of rotaxane **4.2** based on X-ray analysis.

The conductivity value found for rotaxane **4.2** falls within the semi-conductor range (Figure 4.12)[16].

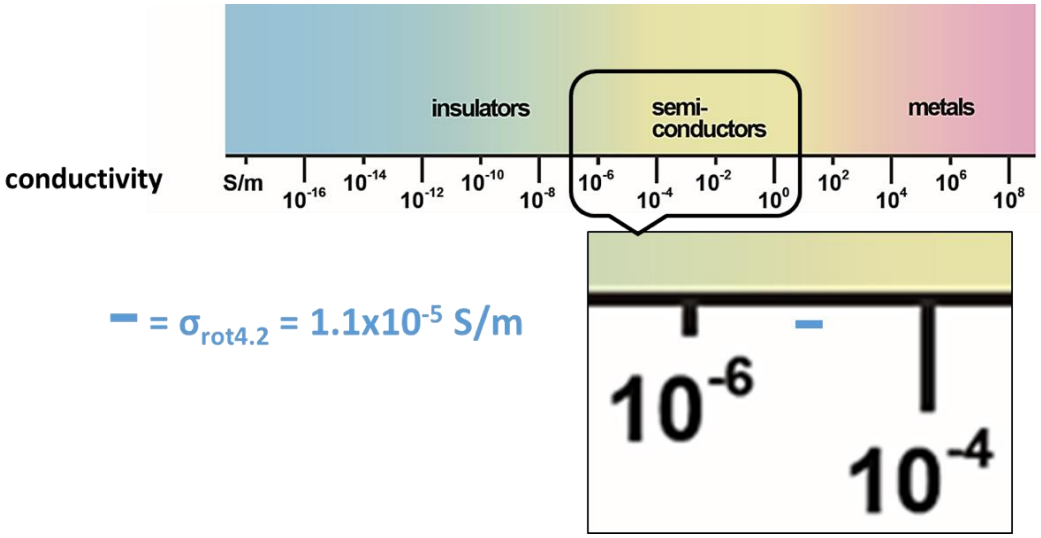

Fig. 4.12. Calculated conductivity for rotaxane **4.2** compared with a reference conductivity scale.[16]

Although previous studies have shown that electrons are able to flow through polyrotaxane-based insulated molecular wires consisting of many rings threaded onto a covalently bonded backbone string,[17] to the best of our knowledge, this is the first time that semi-conductivity has been found in an organic material where molecules are connected by weaker supramolecular interactions, which can be reversibly built and destroyed when the material is dissolved. This represents an extraordinary result, as it implies the ability to manipulate the structure of an organic semi-conductor, potentially leading to changes in the electronic behaviour of the material. This correlation will be analysed in more detail later in this Chapter.

Given the novelty of the above results, it was important to carry out control experiments and eliminate alternative explanations. In order to assess alternative

possibilities, such as that the observed conductivity was the result of silver particles migrating through or along the crystal of rotaxane **4.2** instead of being due to electrons flowing along the rotaxane **4.2** axles, cyclodextrin crystals were studied as a control. These molecules are not expected to be conductive due to the absence of conjugated guests. Crystals were grown in a vial by adding α-CD **4.11** to water to reach the saturation point and then leaving the vial uncapped to allow evaporation. Colourless blocks were obtained after a few days. The crystals exhibited orthorhombic symmetry with a single molecule in the asymmetric unit, and six ordered water molecules were observed forming hydrogen bonds with the α-CD. The X-ray crystallographic analysis showed that the molecules are organised in a herringbone arrangement (Figure 4.13).[18] This crystal packing is less than ideal as a control for the conductivity experiments, because, unlike the crystals of rotaxane **4.2**, the cyclodextrin molecules are not aligned along a single axis. Acknowledging that constraint, it was the best available system to use.

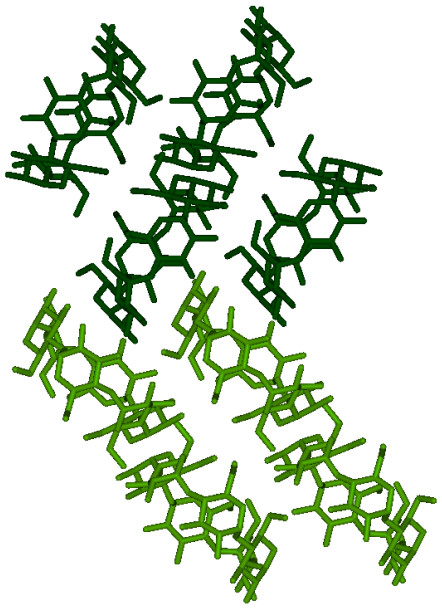

Fig. 4.13. Representation of the crystal structure of α-cyclodextrin **4.11** showing the herringbone arrangement.

The conductivity test was performed in parallel on a cyclodextrin crystal and on a bundle of crystals of rotaxane **4.2** of comparable length and cross-section (Figure 4.14).

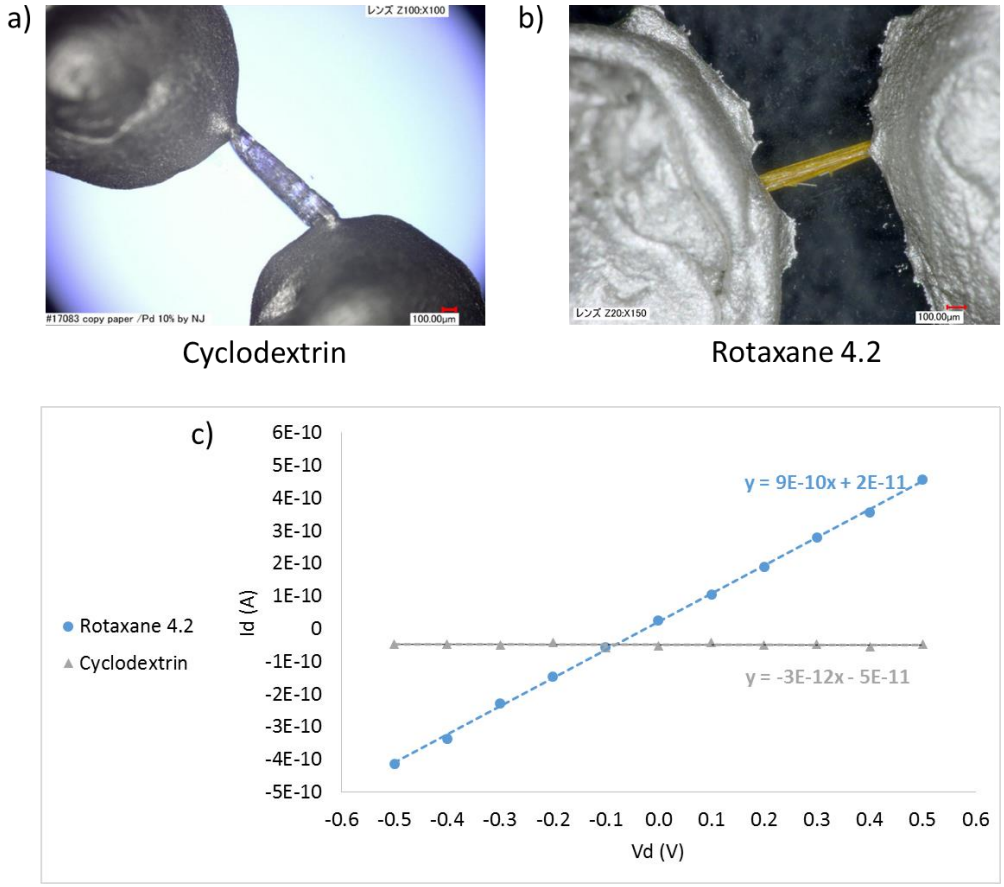

Fig. 4.14. a) Silver electrodes linked by a crystal of α-cyclodextrin **4.11**; b) silver electrodes linked by a crystal of rotaxane **4.2**; and c) current-voltage characteristics of circuits linked by crystals of α-cyclodextrin **4.11** and rotaxane **4.2**.

The system with α-CD **4.11** seemed to show a slight decrease in current upon voltage variation, which is not scientifically sensible behaviour. However, similarly to the previously discussed experiment without the crystal, the detected response was extremely low and the negative slope is likely an artefact of the data manipulation; therefore the slope is considered to be zero within experimental error. This indicates that crystals of α-CD **4.11** are not conductive. On the other hand, the bundle

of crystals of rotaxane **4.2** again showed a proportional increase in current upon voltage variation, which is consistent with the ohmic behaviour observed in the two samples discussed above. The resistance, resistivity and conductivity of the bundle of crystals of rotaxane **4.2** were calculated using the same method adopted in the previous experiments, as shown below.

$$R_{\text{rotaxane 4.2\_bundle}} = \frac{1}{9.0 \text{ x } 10^{-10}} = 1.1 \text{ x } 10^{9}\ \Omega$$

$$\rho_{\text{rotaxane4.2\_bundle}} = R\ \frac{A}{l} = 1.1 \text{ x } 10^{9}\ \Omega\ \frac{1.1 \text{ x } 10^{-4}\ \text{cm}^2}{0.07\ \text{cm}} = 1.7 \text{ x } 10^{6}\ \frac{\text{cm}}{\text{S}}$$

$$\sigma_{\text{rotaxane 4.2\_bundle}} = \frac{1}{\rho} = \frac{1}{1.7 \text{ x } 10^{6}\ \frac{\text{cm}}{\text{S}}} = 5.9 \text{ x } 10^{-7}\ \frac{\text{S}}{\text{cm}} = 5.9 \text{ x } 10^{-5}\ \frac{\text{S}}{\text{m}}$$

The conductivity value obtained for the bundle of crystals of rotaxane **4.2** is almost six times higher than that observed for the thin needles of the same material. Although experimental error can affect the results to a certain degree, other factors are also likely to contribute to this variation. These include the lower surface irregularity expected in larger crystals, as well as the potential ability to transfer current between needles of the same bundle In any case, this experiment indicates that the conductivity is dependent on the axles of the rotaxane **4.2**.

The electronic properties of crystals of rotaxane **4.2** were further studied by building a very basic Organic Field Effect Transistor (OFET).[19] In this system the

conductivity between drain and source is controlled by an electric field provided by the voltage difference between the body of the device and a gate (Figure 4.15).

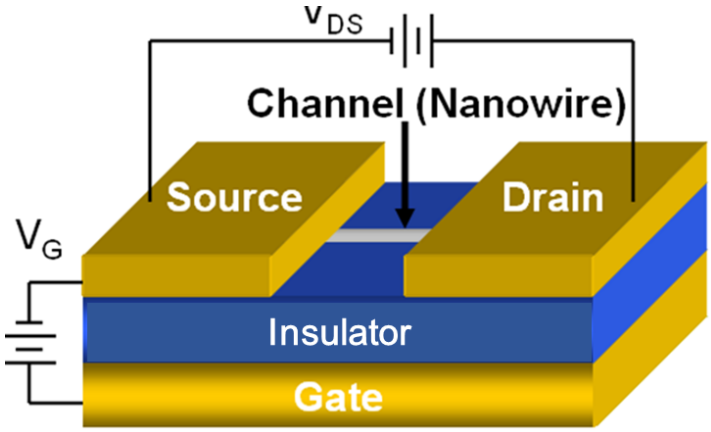

Fig. 4.15. Schematic representation of an Organic Field Effect Transistor.[12]

Typically, an OFET allows the performance of two key experiments: the electrical transfer characteristics are analysed by applying an increasing gate voltage (Vg) at constant drain voltage (Vd), while electrical output characteristics are obtained by applying an increasing drain voltage at different gate voltages. In both cases, the resulting source–drain current (Id) is plotted against the varying voltage.[20] The results obtained for rotaxane **4.2** are shown in Figure 4.16.

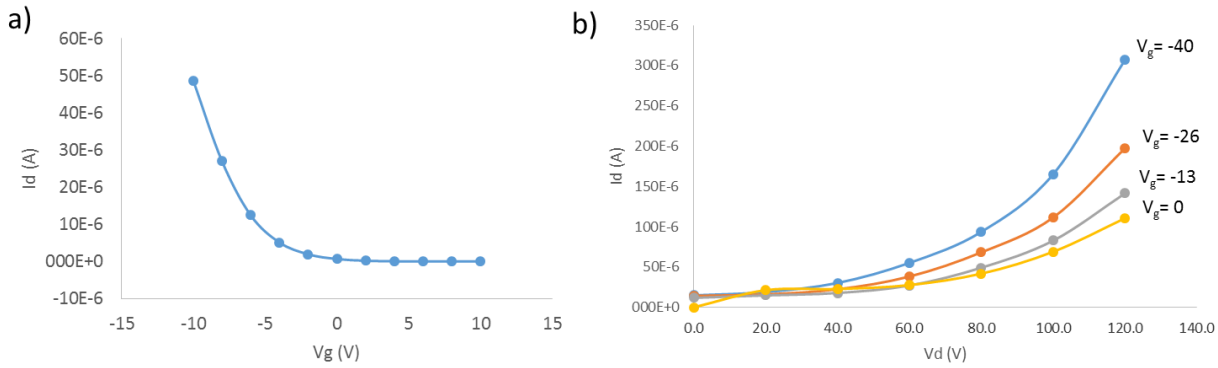

Fig. 4.16. a) Electrical transfer characteristics plot of rotaxane **4.2**; and b) electrical output characteristics plot of rotaxane **4.2**.

Both experiments showed that the source–drain current decreased when increasing gate voltages were applied, due to the induction of negative charges in the active channel facilitated by the applied voltage.[21] Further characterisation of the device, including the analysis of the electron mobility and the threshold voltage, was out of the scope of this Thesis, but could represent a valuable extension of this work.

Having observed electron flow through crystals of rotaxane **4.2**, the design, synthesis and analysis of a new rotaxane was the next aim towards the achievement of a better understanding of the potential behaviour of these types of materials as semi-conductors. Previous studies in the Easton group showed that crystal packing can be strongly influenced by changing molecular interactions using crystal engineering.[9d] In particular, it was found that applying small structural changes to rotaxane **4.2**, such as changing the capping groups from 3,5- to 2,6-dimethylanilino groups or the axle from an azobenzene to a stilbene, resulted in the loss of co-

planarity and conjugation. The new α-CD [2]rotaxane **4.13** was therefore considered, where the only difference from rotaxane **4.2** was the orientation of the amide bond, aiming to retain the key features leading to self-assembling behaviour. In rotaxane **4.2** the capping group is attached to the axle through the amide carbon, while in rotaxane **4.13** the capping group is attached to the axle through the amide nitrogen (Figure 4.17).

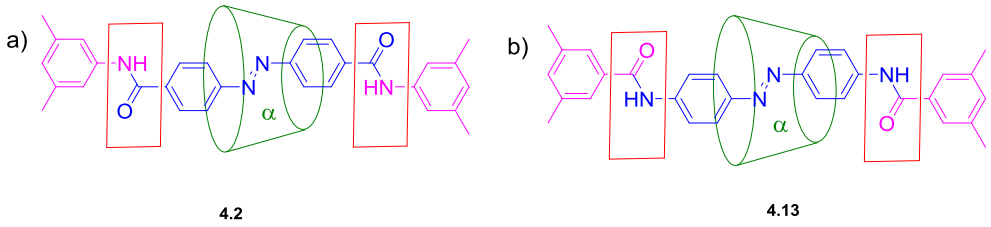

Fig. 4.17. a) Structure of rotaxane **4.2** and b) structure of rotaxane **4.13**, with the amide bond highlighted in red.

The synthesis of rotaxane **4.13** was initially carried out by treating 4,4'-diaminoazobenzene **4.14** with 3,5-dimethylbenzoic acid **4.15**, DMT-MM and Et_3N, in water containing α-CD **4.11** (Scheme 4.2).

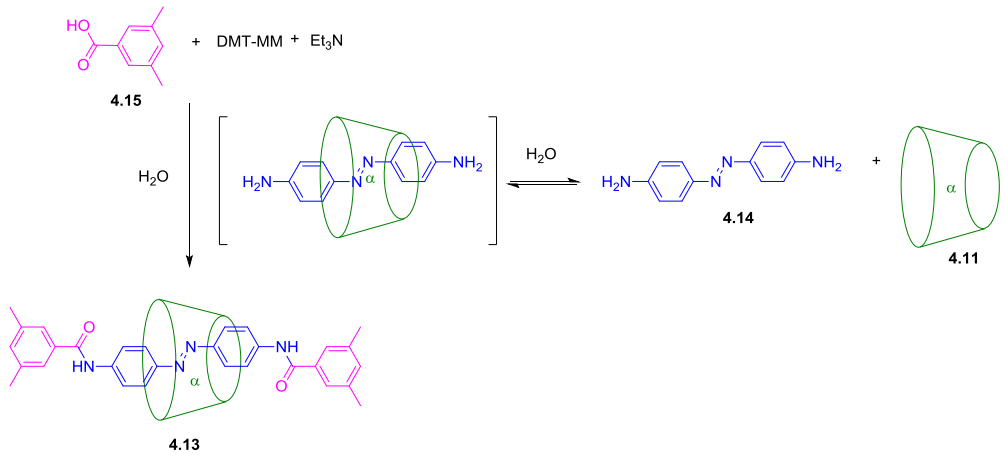

Scheme 4.2. Initial synthesis of rotaxane **4.13**.

The crude product mixture was subjected to reverse phase HPLC (Figure 4.18) and three main components were isolated and analysed by ESI mass spectrometry. The material giving rise to the major HPLC peak at 5.9 minutes showed an ion at *m/z* 1471, which corresponds to the sodiated ion of the rotaxane **4.13**. The peaks at 3.4 and 4.7 minutes each showed an ion at *m/z* 1478 which corresponds to the rotaxane **4.13** substituted with one dimethoxytriazinyl group, suggesting that two isomers were formed as by-products of the reaction. In order to minimise the DMT-MM side-reactions and in an attempt to increase the yield of the reaction, a varied synthetic procedure was carried out. The capping agent **4.15**, DMT-MM and Et_3N were left to stir in a separate vial to form the ester **4.16** and limit the presence of DMT-MM in the next reaction step. The activated capping agent **4.16** was then added to a solution containing the azobenzene **4.14** and α-CD **4.11** to form rotaxane **4.13** (Scheme 4.3).

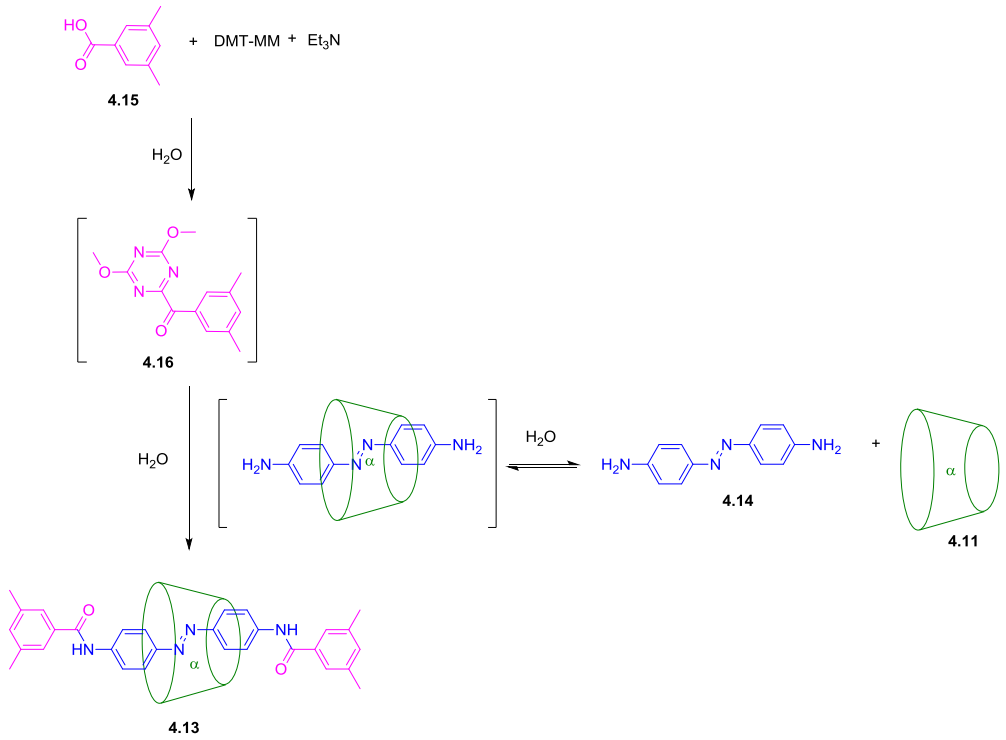

Scheme 4.3. Improved synthesis of rotaxane **4.13**.

As shown in Figure 4.18, the second method gave lower amounts of by-products.

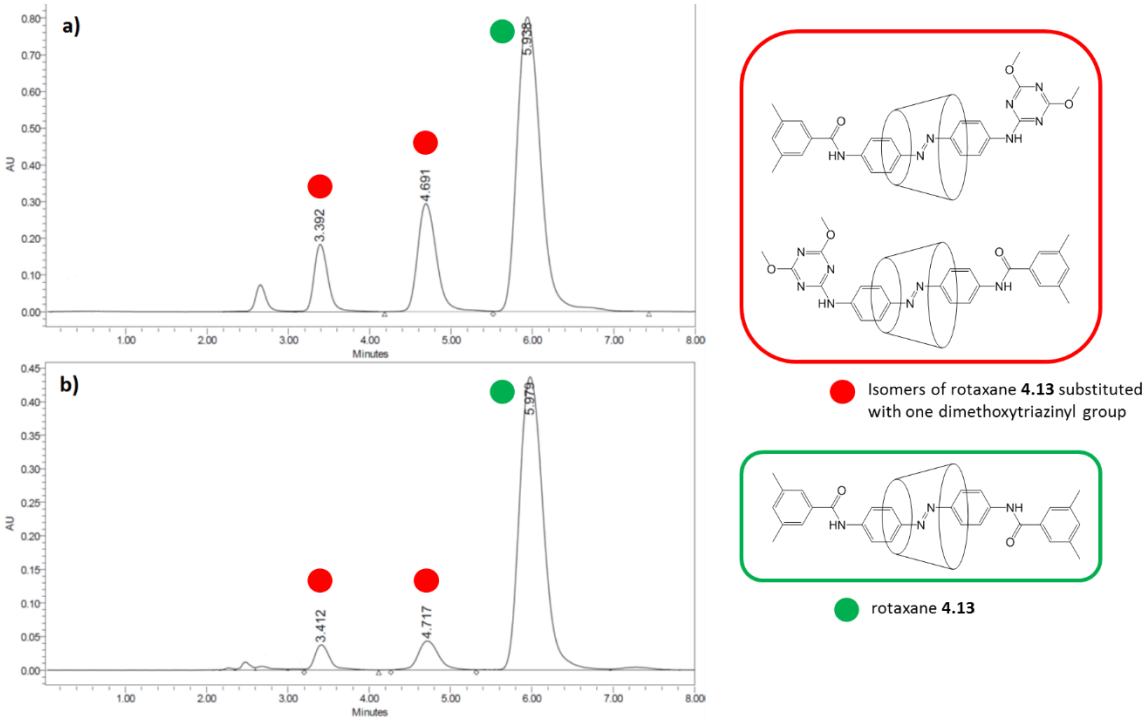

Fig. 4.18. HPLC chromatograms of the crude mixtures obtained from a) the initial synthesis of rotaxane **4.13**; and b) the improved method.

In this case, rotaxane **4.13** was again isolated by HPLC, in a yield of 5%. It was characterised using 1D and 2D NMR spectroscopy. The ^{1}H NMR spectrum confirms the presence of the distinctive features of the molecule, such as the capping group, the azobenzene and the cyclodextrin (Figure 4.19).

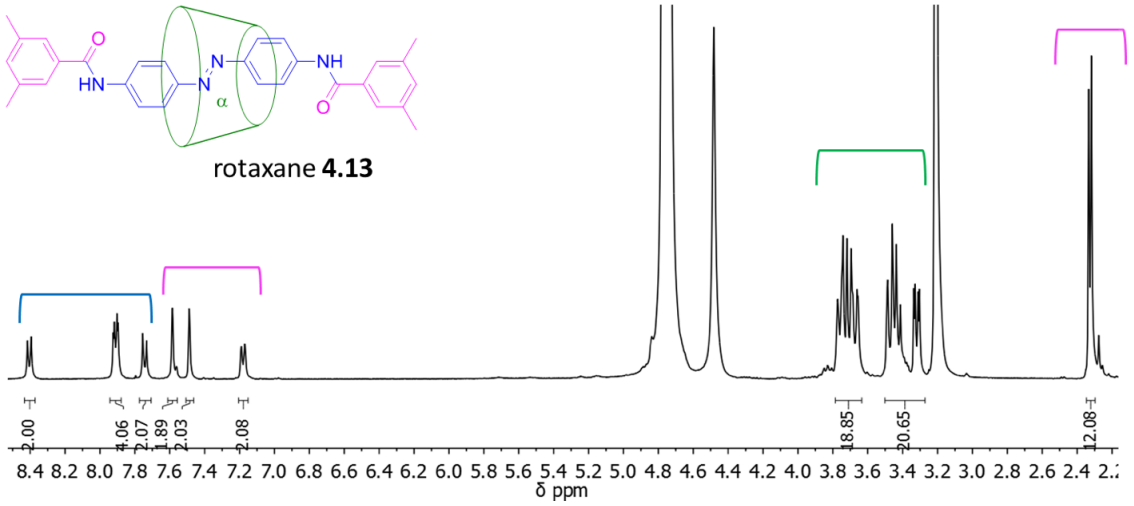

Fig. 4.19. ^{1}H NMR spectrum (400 MHz, 298 K, CD_3OD) of rotaxane **4.13**.

Following the method employed by Inoue and co-workers,[22] the 2D COSY and ROESY NMR spectra were utilised to establish the inclusion of the azobenzene in the α-CD and to investigate the position of the macrocyle on the axle. The resonances due to the cyclodextrin protons were assigned by identifying cross-peaks in the upfield region of the COSY spectrum (Figure 4.20).

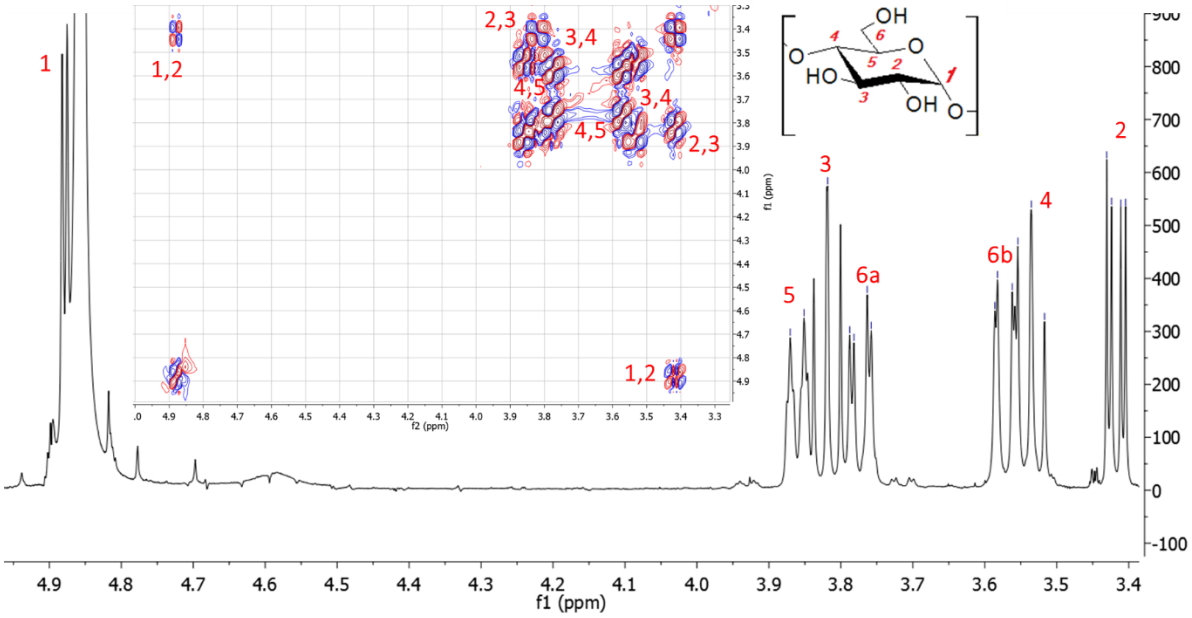

Fig. 4.20. Cyclodextrin proton resonance assignments from a section of the COSY NMR spectrum (600 MHz, 298 K, CD_3OD) of rotaxane **4.13**.

As illustrated in Figure 4.21, the COSY spectrum provided information on the correlation between the resonances of the capping group protons and between azobenzene protons of the same aromatic ring. However, it did not allow distinction between the pairs of protons of the two azobenzene aromatic rings or show correlations between the azobenzene and the capping groups.

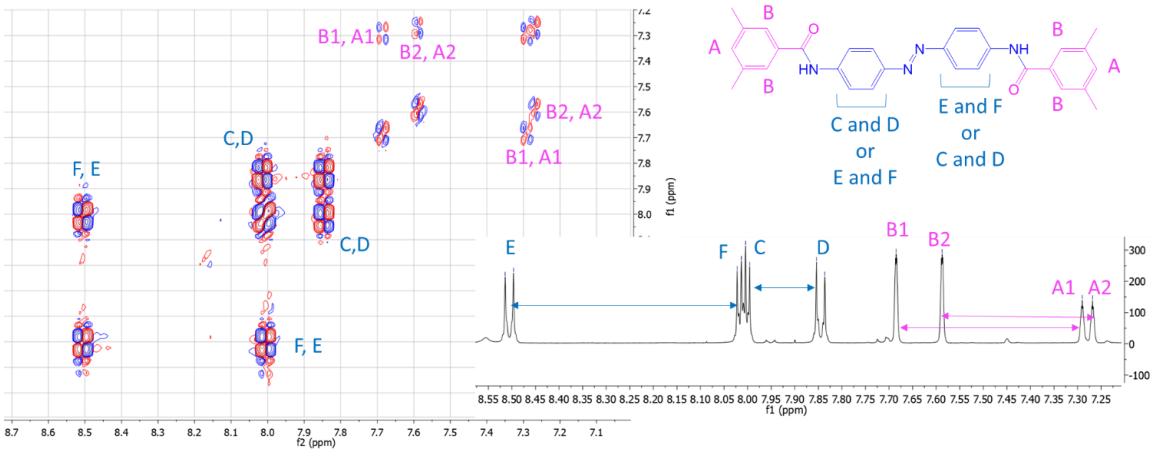

Fig. 4.21. Partial assignment of the dumbbell's protons according to a section of COSY NMR spectrum (600 MHz, 298 K, CD_3OD) of rotaxane **4.13**.

As discussed below, the ROESY spectrum (Figure 4.22) showed the inclusion of the axle in the α-CD and provided some information on their relative position.

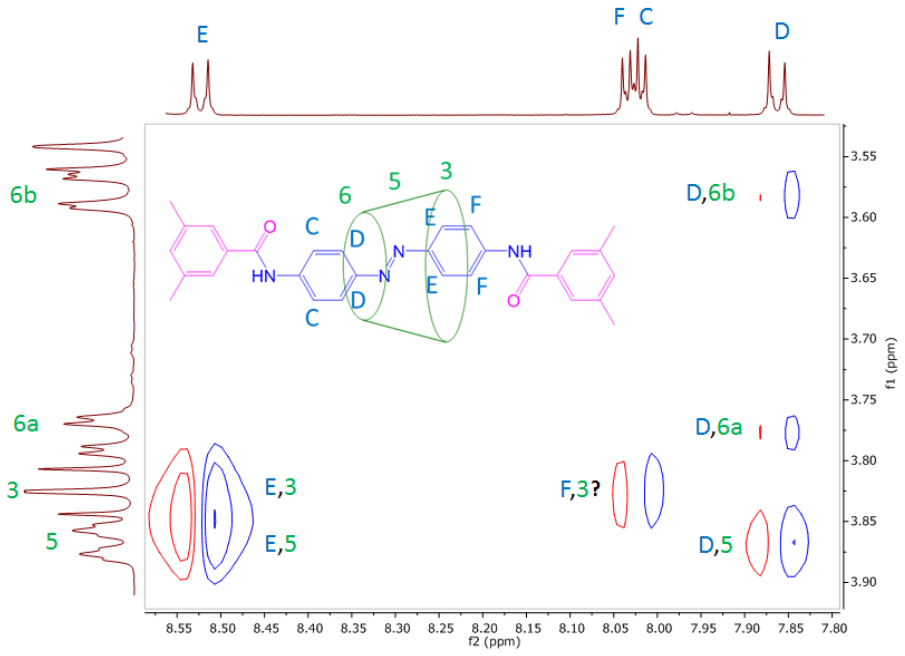

Fig. 4.22. Section of ROESY NMR spectrum (600 MHz, 298 K, CD_3OD) of rotaxane **4.13** showing NOE interactions between the axle and α-cyclodextrin protons.

The NOE interactions detected in the ROESY spectrum between the resonances of the axle and the macrocycle protons show the inclusion of the azobenzene in the α-CD. The signals of the azobenzene protons E and D show the strongest NOE correlations with the cyclodextrin, especially with the α-CD proton 5, indicating that these are probably close to the centre of the axle.

Following characterisation of rotaxane **4.13**, its self-assembling behaviour in water was analysed. As previously discussed, spectroscopic experiments on rotaxane **4.2** showed deviation from the typical linear correlation between concentration and absorbance, indicating the formation of aggregates, at concentrations higher than 10 μM.[9a] In order to investigate whether the same phenomenon occurred with the new compound, solutions of rotaxane **4.13** at concentrations ranging from 10 μM to 200 μM were prepared and analysed by UV-vis spectroscopy. All these solutions showed a linear correlation between concentration and absorbance, suggesting the absence of self-assembling behaviour at these concentrations (Figure 4.23).

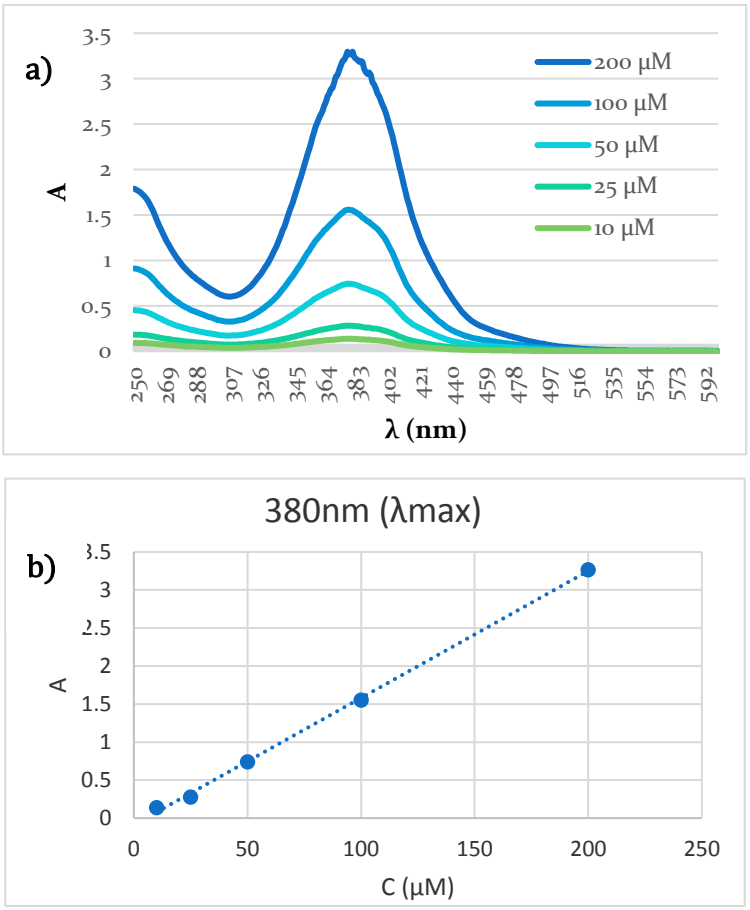

Fig. 4.23. a) The concentration-dependent UV-vis profile; and b) the correlation between concentration and absorbance at λ_{max} of rotaxane **4.13** solutions at concentrations ranging from 10 µM to 200 µM.

A similar experiment was therefore performed at higher concentrations. A 2 mM stock solution of rotaxane **4.13** was prepared and heated to 80 °C to prepare a supersaturated solution. The solution was then diluted to obtain solutions at 1 mM, 500 µM, 250 µM and 125 µM. All the solutions were left standing at 30 °C for 1 day, then their UV-vis profiles were recorded. While the more diluted solutions again provided a linear correlation between concentration and absorbance, this

behaviour was clearly not observed for the more concentrated solutions. The 2 mM solution showed only a moderate increase in absorbance at the λ_{max} compared to the 1 mM solution, while it should have been double if Beer's law had been followed. This atypical behaviour, as well as an additional absorbance band at 445 nm observed in solutions at concentrations above 500 μM, clearly indicates the formation of aggregates in solution (Figure 4.24).[9a]

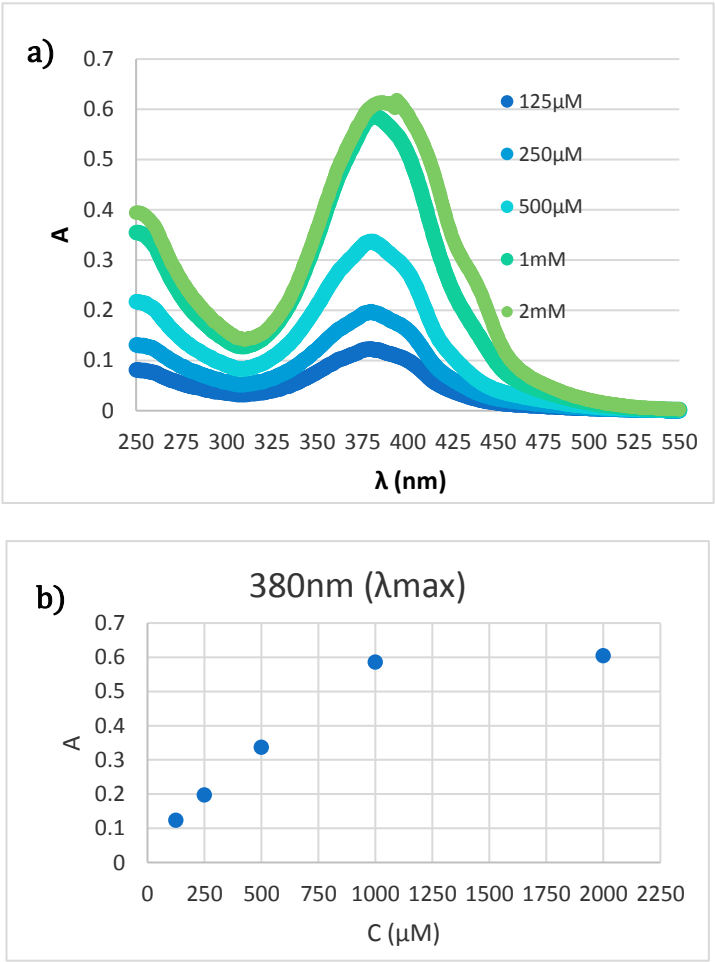

Fig. 4.24. a) The concentration-dependent UV-vis profile; and b) the correlation between concentration and absorbance at λ_{max} of rotaxane **4.13** solutions at concentrations ranging from 125 μM to 2 mM.

In order to calculate the saturation concentration of **4.13**, concentration- and time-dependent UV-vis spectroscopic experiments were carried out. As previously discussed, no significant absorbance variation was observed between the solutions at 1 mM and 2 mM, therefore any concentration within that range was likely to be supersaturated. An amorphous sample of the material was therefore dissolved in water and heated at 80 °C to prepare a 1.8 mM stock solution of rotaxane **4.13**. This solution was then diluted to obtain the following concentrations: 1.6 mM, 1.2 mM, 0.8 mM, 0.4 mM, 0.2 mM, 0,1 mM and 0.05 mM. These solutions were left to stand at 30 °C and the UV-vis spectra were recorded over time (Figure 4.25).

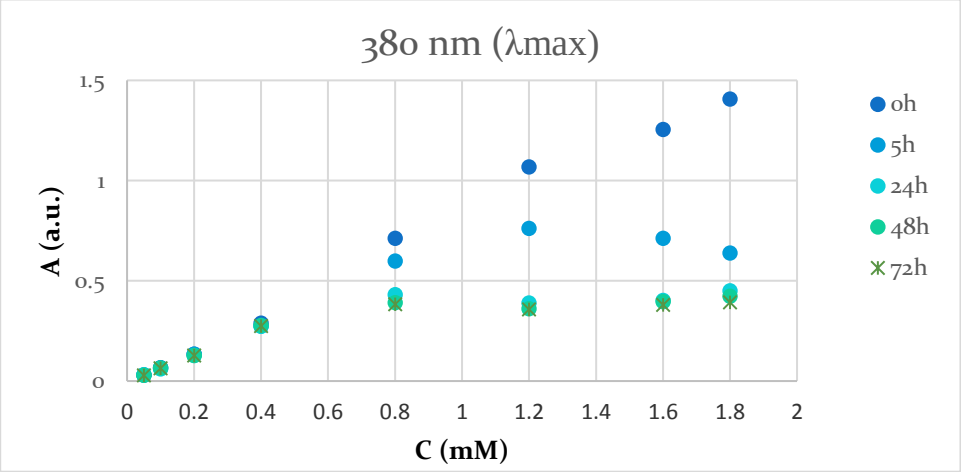

Fig. 4.25. Concentration- and time-dependent UV-vis spectroscopic studies of rotaxane **4.13** at the λ_{max} and concentrations ranging from 0.1 mM to 1.8 mM.

The solutions at concentrations higher than 0.4 mM showed the presence of little crystals after just 5 hours, resulting in a decreased absorbance of the supernatant at the λ_{max}. The supersaturated solution at 1.8 mM equilibrated to saturation

concentration within 72 hours, after which time no further change in absorbance was observed (Figure 4.26).

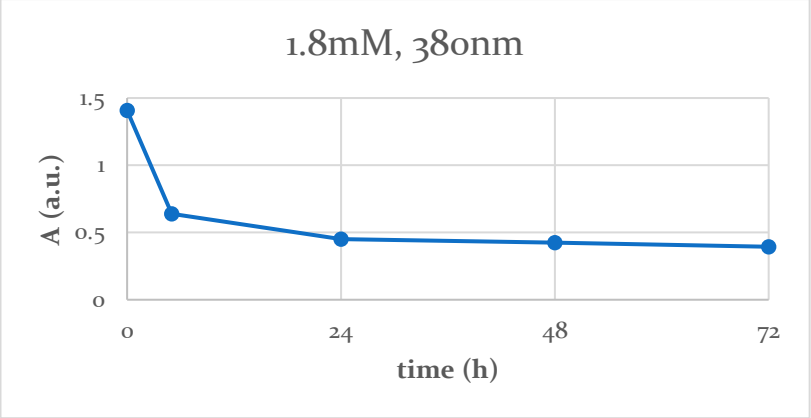

Fig. 4.26. Time-dependent variation of absorbance at λ_{max} of a solution of rotaxane **4.13** initially at 1.8 mM.

The absorbance at the saturation point was found to be 0.394 a.u. A calibration curve was then drawn with less concentrated solutions of rotaxane **4.13**, showing linear correlation between concentration and absorbance up to 0.4 mM (Figure 4.27).

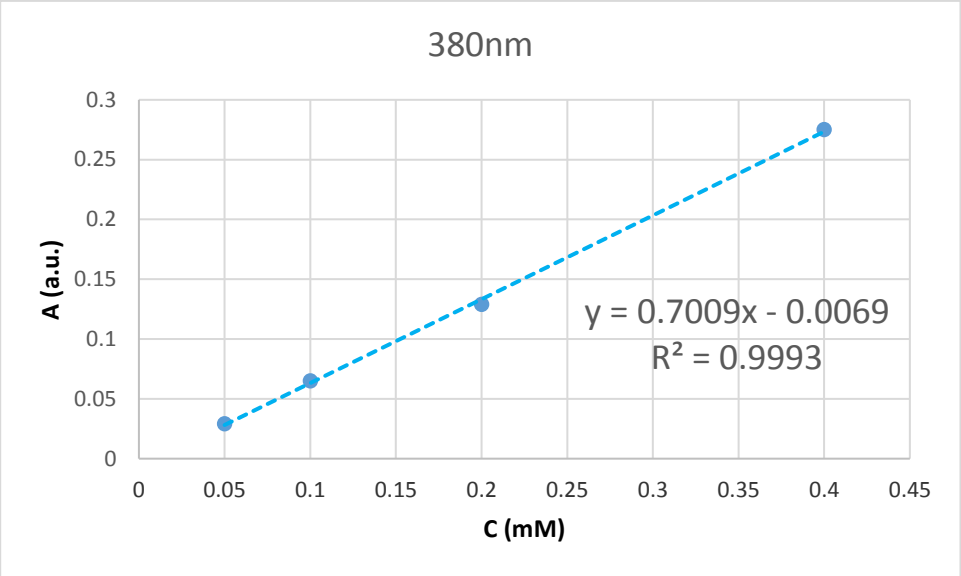

Fig. 4.27. Calibration curve at λ_{max} of solutions of rotaxane **4.13**.

The saturation concentration (Csat) was then found to be 562 μM by adding the saturation absorbance (Asat = 0.394 a.u.) into the regression equation obtained from graph in Figure 4.27.

$$Asat = 0.7009 \times Csat$$

$$Csat = \frac{0.394}{0.7009} = 0.562 \text{ mM} = 562 \text{ μM}$$

Having investigated properties of rotaxane **4.13** in solution, growing crystals was the next step towards the analysis of its conductivity behaviour. The crystallization conditions for rotaxane **4.2**, including solvent and evaporation temperature, were maintained the same as those used for rotaxane **4.13**, in order to achieve the same

evaporation rates in both experiments. Crystals were therefore grown from a supersaturated 1.8 mM solution by dissolving amorphous material in water, heating the mixture to ensure complete dissolution, then leaving the solution to evaporate at room temperature. A much quicker crystallisation process was observed compared with rotaxane **4.2**. In this case, the first crystals came out of solution after just 5 h and the crystallization appeared to be complete within 4 days, while several days were required to grow crystals from a water solution of rotaxane **4.2** and in that case crystal growth was observed for up to 11 days. The crystal structure of rotaxane **4.13** was analysed by X-ray crystallography and key similarities with rotaxane **4.2** were immediately evident. The new compound again showed aligned strands of coplanar dumbbells arranged in fibers through π-π stacking and included in α-CD molecules. As discussed for rotaxane **4.2**, this type of arrangement is a promising starting point to build insulated molecular wires. That said, while rotaxane **4.2** generated thin, needle-shaped crystals,[9a] crystals of rotaxane **4.13** were shaped more like bars. Clear differences were also observed between the crystal packing of the two systems (Figure 4.28).

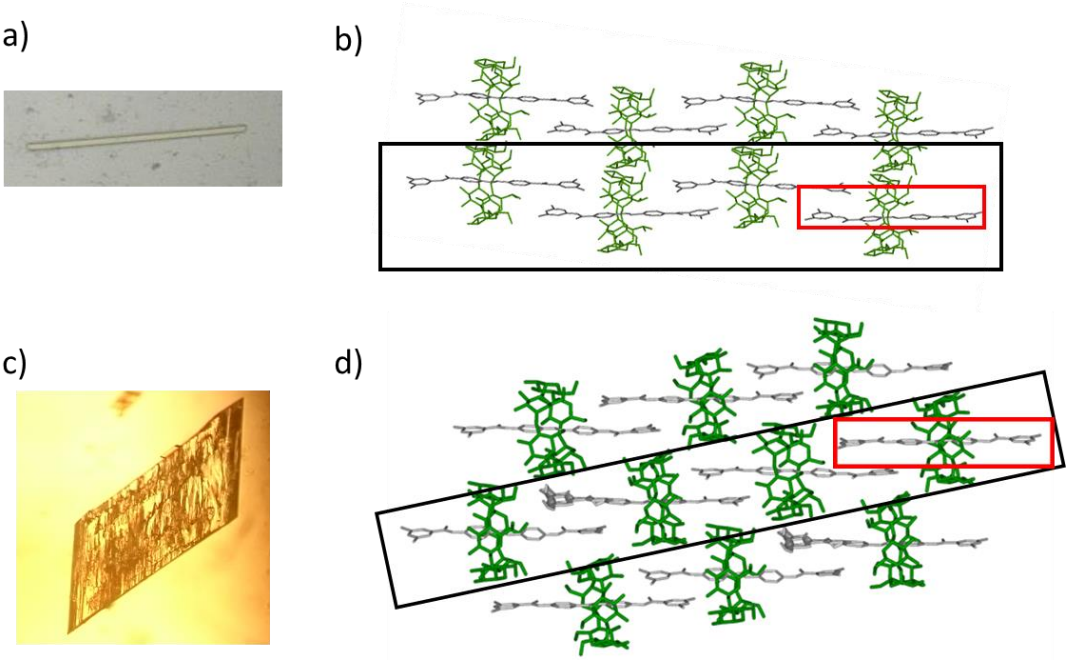

Fig. 4.28. a) Crystal shape of rotaxane **4.2**; b) crystal packing of rotaxane **4.2**; c) crystal shape of rotaxane **4.13**; and d) crystal packing of rotaxane **4.13**.

The crystal packing of rotaxane **4.2** shows that the direction of the strands of π-overlapped molecules (highlighted in black in Figure 4.28b) is parallel to the guest axis (highlighted in red in Figure 4.28b), while the axle of rotaxane **4.13** (highlighted in red in Figure 4.28d) is at an angle of approximatively 15 degrees compared to the direction of the aligned fibers (highlighted in black in Figure 4.28d). The prismatic shape of the crystals, resulting from a more two-directional growing behaviour, seems to reflect the alignment of the fibers in the crystal packing. The correlation between crystal packing and crystal morphology was investigated by mounting a single crystal on an X-ray diffractometer to perform a face analysis. As shown in figure 4.29, ten external faces were identified and indexed. The complexity of the crystal morphology, as well as the rapid desolvation of the crystals, did not provide

confidence to unambiguously determine the correlation between crystal packing and crystal morphology.

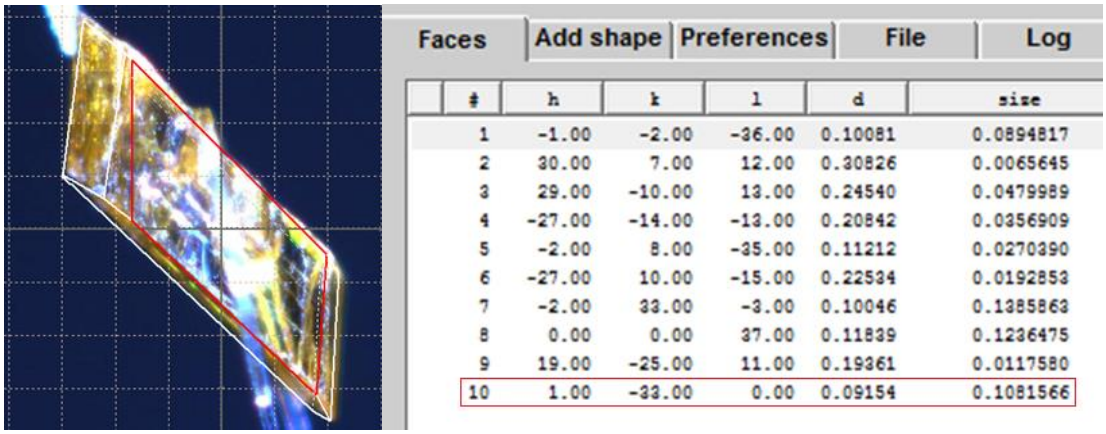

Faces | Add shape | Preferences | File | Log

#	h	k	l	d	size
1	-1.00	-2.00	-36.00	0.10081	0.0894817
2	30.00	7.00	12.00	0.30826	0.0065645
3	29.00	-10.00	13.00	0.24540	0.0479989
4	-27.00	-14.00	-13.00	0.20842	0.0356909
5	-2.00	8.00	-35.00	0.11212	0.0270390
6	-27.00	10.00	-15.00	0.22534	0.0192853
7	-2.00	33.00	-3.00	0.10046	0.1385863
8	0.00	0.00	37.00	0.11839	0.1236475
9	19.00	-25.00	11.00	0.19361	0.0117580
10	1.00	-33.00	0.00	0.09154	0.1081566

Fig. 4.29. External faces of rotaxane **4.13** and Miller indices. Face number 10 highlighted in red.

The crystal packing of rotaxane **4.13** was further analysed in order to examine the overlap between the capping groups in the two systems (Figure 4.30).

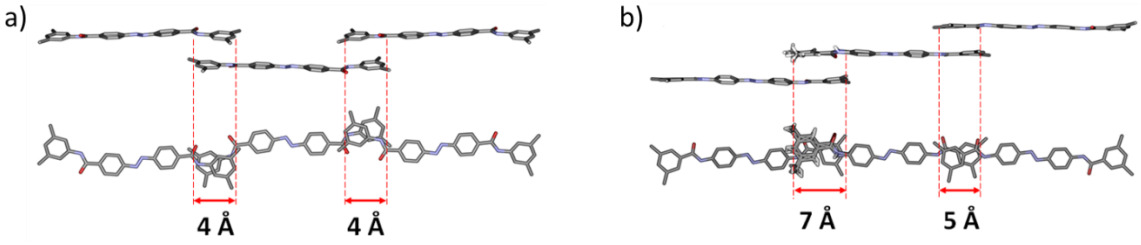

Fig. 4.30. Overlap between capping groups in a) rotaxane **4.2**; and b) rotaxane **4.13**.

As shown in Figure 4.30, in both cases the axles are nearly coplanar, with a twist angle of less than 5% between the axle and the blocking groups, allowing extended conjugation. However, in rotaxane **4.2** the overlap between the dumbbells is much less than that with rotaxane **4.13**.

The next step was to evaluate the conductivity behaviour. Aiming to reproduce experimental conditions similar to those adopted with rotaxane **4.2**, long bars of **4.13** were selected to perform the conductivity tests, and the IV characteristics were analysed in the same manner as with rotaxane **4.2**. Silver electrodes were placed at both ends of the long axis of a crystal of rotaxane **4.13** and connected to probes. Similarly to what was observed with rotaxane **4.2**, the application of increasing voltages resulted in a proportional increase in current, showing that rotaxane **4.13** is also an ohmic resistor. (Figure 4.31).

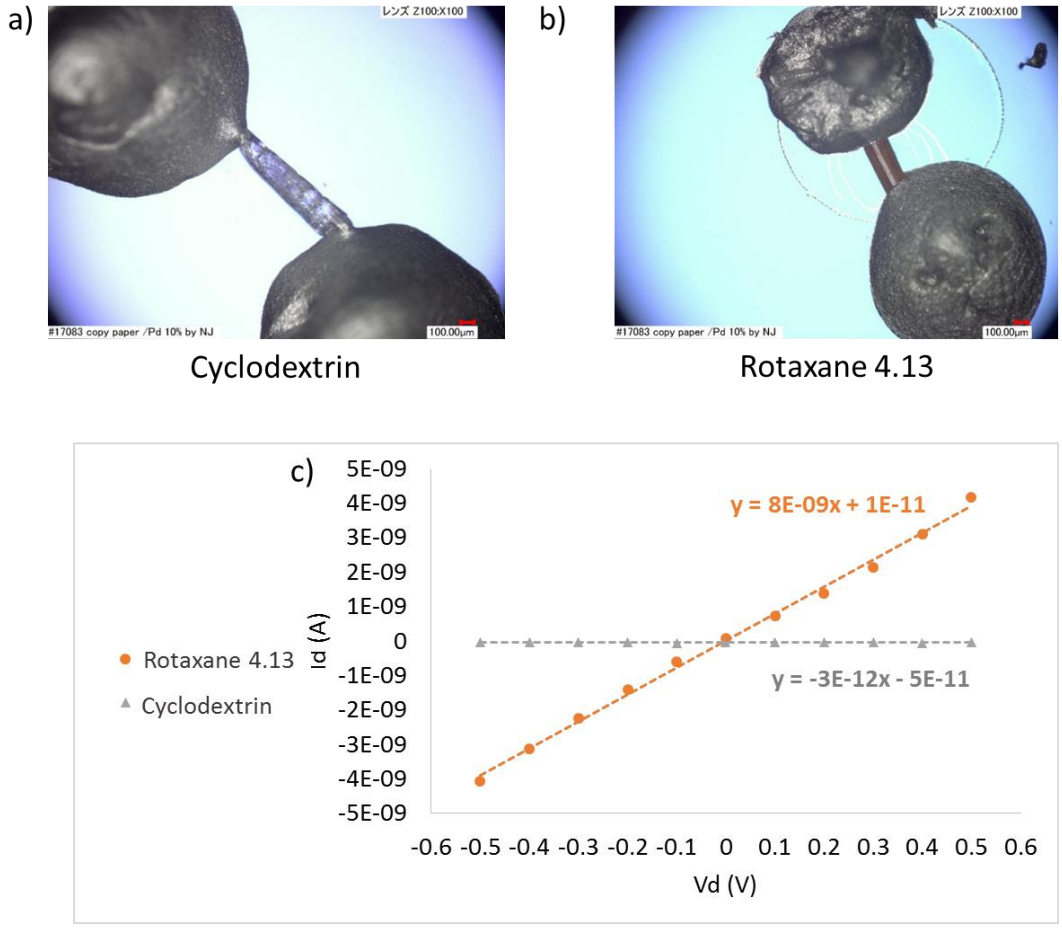

Fig. 4.31. a) Electrodes linked by a crystal of α-cyclodextrin **4.11**; b) electrodes linked by a crystal of rotaxane **4.13**; and c) current-voltage characteristics of circuits linked by crystals of α-cyclodextrin **4.11** and rotaxane **4.13**.

As shown in Figure 4.31, the crystal of rotaxane **4.13** generates a significant increase of current upon voltage variation compared to the negligible response shown by the crystal of α-CD **4.11**. Its resistance, resistivity and the conductivity were calculated using the same method applied for rotaxane **4.2**, as shown below.

$$R_{\text{rotaxane 4.13}} = \frac{1}{8.0 \text{ x } 10^{-9}} = 1.2 \text{ x } 10^{8}\ \Omega$$

$$\rho_{\text{rotaxane4.13}} = R\,\frac{A}{l} = 1.2 \text{ x } 10^{8}\ \Omega\ \frac{4.9 \text{ x } 10^{-4}\ \text{cm}^2}{0.07\ \text{cm}} = 8.4 \text{ x } 10^{5}\ \frac{\text{cm}}{\text{S}}$$

$$\sigma_{\text{rotaxane 4.13}} = \frac{1}{\rho} = \frac{1}{8.4 \text{ x } 10^{5}\ \frac{\text{cm}}{\text{S}}} = 1.2 \text{ x } 10^{-6}\ \frac{\text{S}}{\text{cm}} = 1.2 \text{ x } 10^{-4}\ \frac{\text{S}}{\text{m}}$$

The conductivity value obtained for rotaxane **4.13** is approximatively double that of the bundle of crystals of rotaxane **4.2** and one order of magnitude higher than the needles of rotaxane **4.2**. This difference could be related to a number of factors, including extended overlap between capping groups, increased charge carrier density, or simply different crystal structures. In any case, all these samples are able to conduct electricity and can therefore be classified as molecular wires. In particular, they all fall within the semi-conductor range, as shown in Figure 4.32.

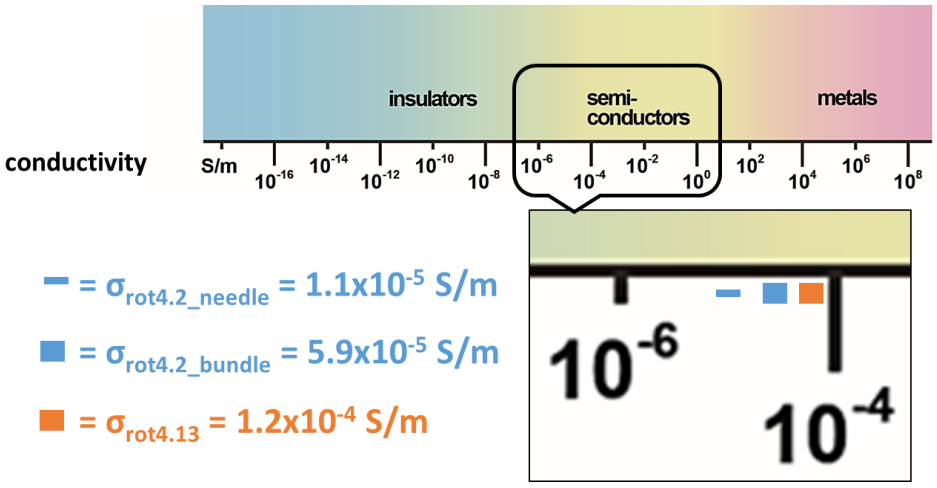

Fig. 4.32. Calculated conductivity for rotaxane **4.2** (needles and bundle), and rotaxane **4.13** compared with a reference conductivity scale.[16]

As shown below, a repetition of this experiment on a different crystal of rotaxane **4.13** provided resistivity and conductivity values close to the first experiment, showing again that the results are reproducible.

$$R_{\text{rotaxane 4.13\_b}} = \frac{1}{1.0 \text{ x } 10^{-8}} = 1.0 \text{ x } 10^{8}\ \Omega$$

$$\rho_{\text{rotaxane 4.13\_b}} = R\ \frac{A}{l} = 1.0 \text{ x } 10^{8}\ \Omega\ \frac{4{,}9 \text{ x } 10^{-4}\ \text{cm}^2}{0.05\ \text{cm}} = 9.8 \text{ x } 10^{5}\ \frac{\text{cm}}{\text{S}}$$

$$\sigma_{\text{rotaxane 4.13\_b}} = \frac{1}{\rho} = \frac{1}{9.8 \text{ x } 10^{5}\ \frac{\text{cm}}{\text{S}}} = 1.0 \text{ x } 10^{-6}\ \frac{\text{S}}{\text{cm}} = 1.0 \text{ x } 10^{-4}\ \frac{\text{S}}{\text{m}}$$

Having established that electrons are able to flow along the main axis of crystals of rotaxane **4.13**, the conductivity was also tested through a perpendicular axis of the same material. While this experiment was not possible with rotaxane **4.2** due to the needle shape of the crystals, the bars of rotaxane **4.13** allowed the attachment of the silver paste electrodes in the direction perpendicular to the long axis of the crystal. The IV characteristics of this system were compared with the ones previously discussed, where silver paste was placed along the main growing direction of the crystal (Figure 4.33).

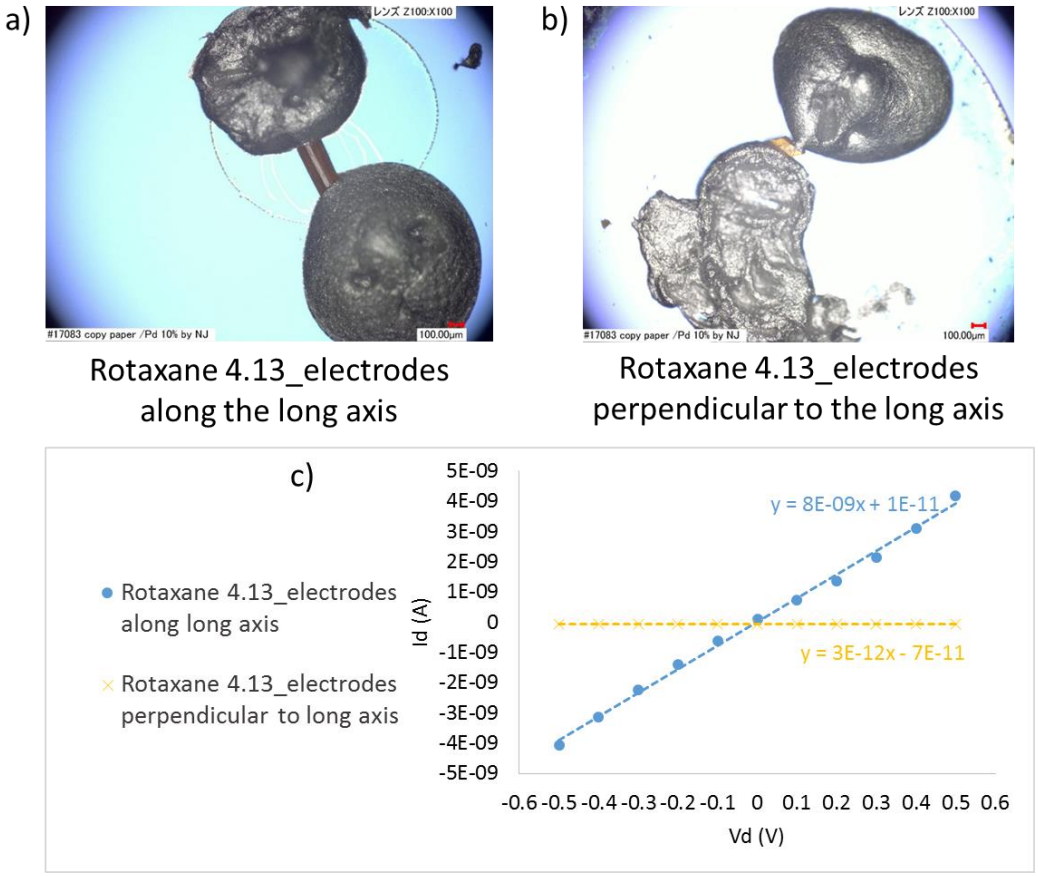

Fig. 4.33. a) Electrodes linked by a crystal of rotaxane **4.13** with silver paste along the main growing direction; b) electrodes linked by a crystal of rotaxane **4.13** with silver paste perpendicular to the main growing direction; and c) IV characteristics of circuits linked by crystals of rotaxane **4.13** with silver paste along and perpendicular to the main growing direction.

Similarly to the results obtained with the circuits without a crystal and the ones linked by α-CD **4.11**, the slope of the IV curve generated through the perpendicular axis of rotaxane **4.13** is negligible, meaning that electrons are unable to flow in this direction. The insulation observed is likely provided by the cyclodextrins surrounding the axles. Similarly, the conductivity observed in the circuit where

silver paste is placed along the crystal main growing direction is consistent with the alignment of the fibers along the long axis of the bar.

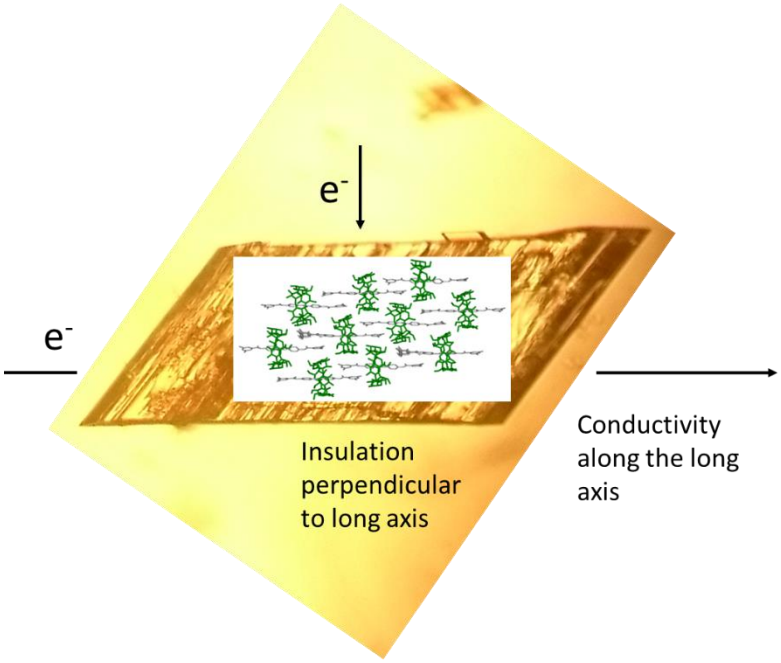

Fig. 4.34. Hypothesised correlation between crystal structure and crystal morphology of rotaxane **4.13** based on insulation and conductivity results.

The data obtained from these experiments establish the ability of crystals of rotaxanes **4.13** to act as insulated molecular wires. While the insulation could not be tested with crystals of rotaxane **4.2**, they were also proven to be molecular wires. Although the two rotaxanes had different structures and crystal morphologies, both allowed electron flow, with a similar degree of conductivity.

Further studies were focused on investigating the potential effect of co-crystallization on crystal morphology. In particular, a series of concentration-dependent crystallization experiments was performed to test the ability of rotaxanes **4.2** and **4.13** to co-crystallize in a single crystal and to evaluate the effect of this crystallization process on the crystal morphology. A supersaturated solution of rotaxane **4.2** was again utilised to drive crystal formation; however, a lower concentration compared to the previous crystallization experiments was chosen, aiming at a slower crystallization process to potentially allow the incorporation of rotaxane **4.13**. Previous studies in the group showed the formation of needle-shaped crystals from a 100 μM aqueous solution of rotaxane **4.2** heated up to 80 °C and left to stand at 30 °C for a few days to allow slow evaporation.[9d] Following this procedure, a 100 μM aqueous solution of rotaxane **4.2** was used for all the co-crystallization experiments, while different concentrations of rotaxane **4.13** were utilised to investigate the influence of the concentration on the incorporation and the crystal shape. Initially, a 1:1 mixture of rotaxanes **4.2** and **4.13** at 100 μM was prepared. After a few days of slow evaporation, needle-shaped crystals were observed (Figure 4.35).

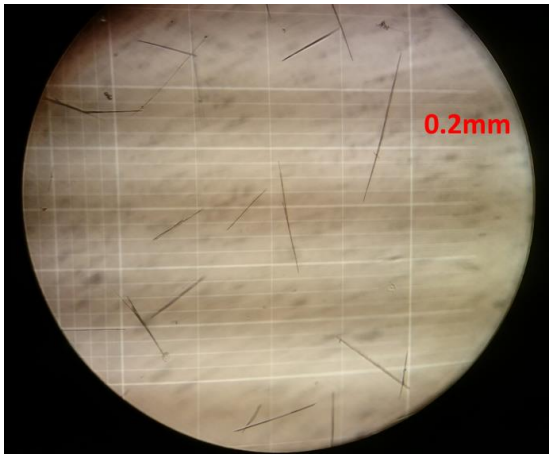

Fig. 4.35. Crystals from a 1:1 mixture of rotaxane **4.2** (100 μM) and rotaxane **4.13** (100 μM).

In order to test whether one or two species were incorporated in the crystal, HPLC analysis was performed. As a first step, the UV-vis spectra of the two rotaxanes were compared in order to identify the isosbestic point. It was found that at 368 nm the two species had the same absorption (Figure 4.36), therefore the following HPLC analysis were performed at this wavelength to allow a quantitative comparison between the two species.

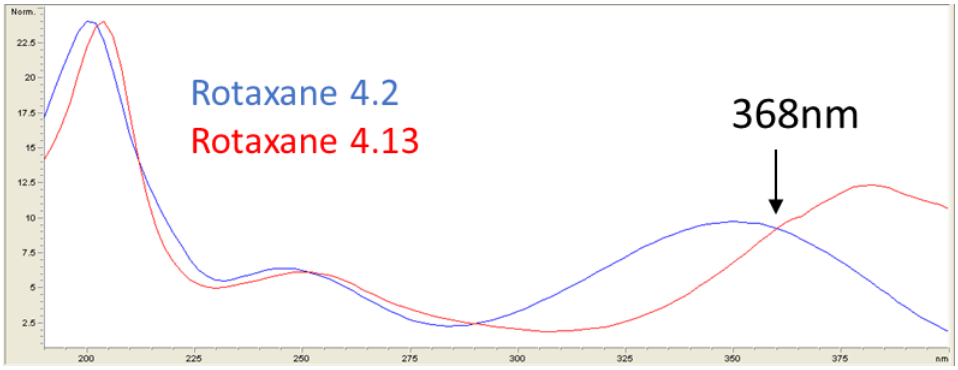

Fig. 4.36. Isosbestic point in the UV-vis spectra of rotaxane **4.2** and rotaxane **4.13**.

A single crystal from the co-crystallization was then collected, redissolved in methanol, and analysed by HPLC. The HPLC trace of this crystal showed the presence of two distinctive peaks, which were identified as the two rotaxanes **4.2** and **4.13** by comparing their HPLC profiles (Figure 4.37), indicating co-crystallization.

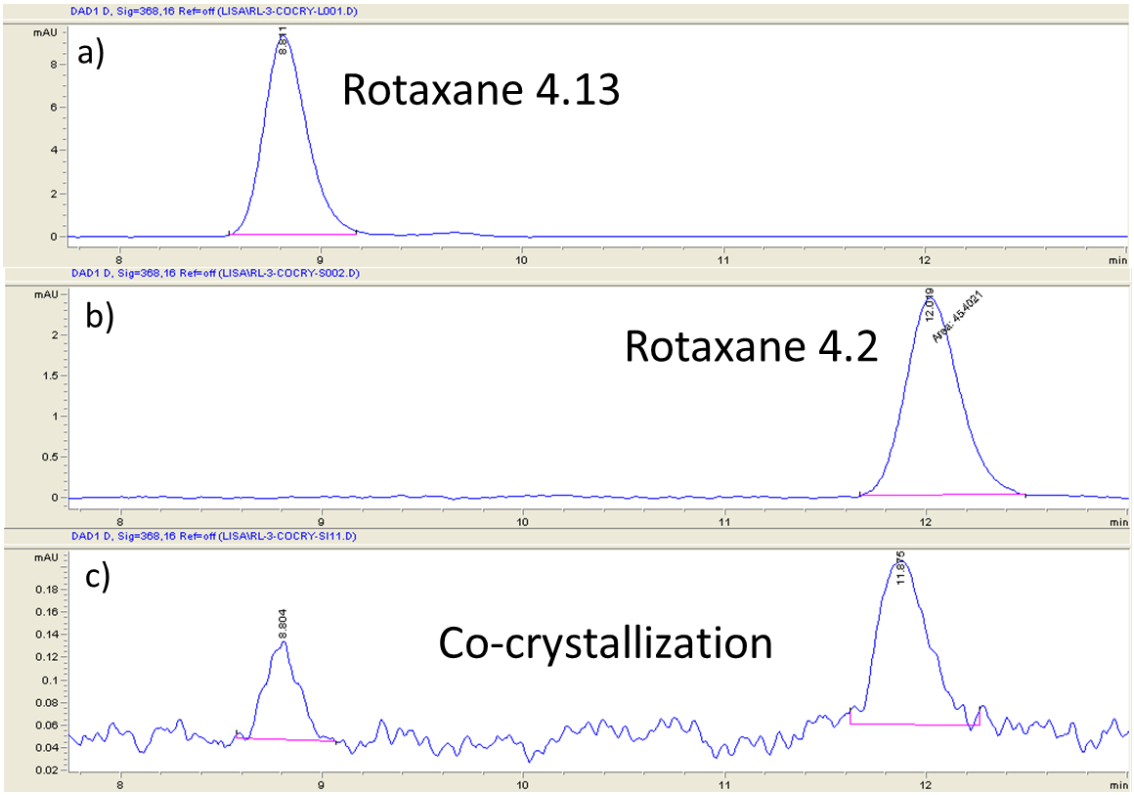

Fig. 4.37. HPLC trace of a) rotaxane **4.13**; b) rotaxane **4.2**; and c) a crystal obtained from co-crystallization.

In order to evaluate if co-crystallization would occur at different ratios between the two species, the concentration of rotaxane **4.2** was kept constant, while the following concentrations of rotaxane **4.13** were tested: 200 µM, 400 µM, 600 µM and 1000 µM.

As illustrated in Figure 4.38, both rotaxanes **4.2** and **4.13** were incorporated in single crystals for all the tested concentrations. The ratios of the two species within the same crystal were calculated from HPLC traces and analysed in relation to the crystal morphology. A needle shape of **4.2** was preserved for crystals containing up to 25% of rotaxane **4.13**. Likewise, the prismatic shape of **4.13** was preserved for crystals containing 10% of **4.2**.

Concentration of rotaxane 4.2 in the co-crystallization mixture	Concentration of rotaxane 4.13 in the co-crystallization mixture	Crystal shape of the co-crystallization crystal	HPLC trace of the co-crystallization crystal at 368 nm	Ratio between rotaxane 4.2 and rotaxane 4. 13 detected in the co-crystallization crystal
100 µM	200 µM	Needle	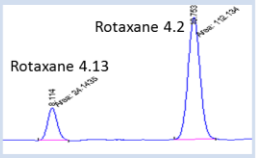	5
100 µM	400 µM	Needle		5
100 µM	600 µM	Needle		3
100 µM	1000 µM	Prismatic	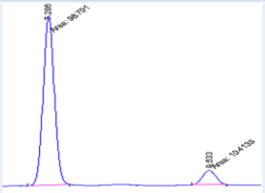	0.1

Fig. 4.38. Crystal shape and HPLC analysis of co-crystals of rotaxane **4.2** and rotaxane **4.13** at different concentrations.

These results are important from a crystal engineering perspective, as they demonstrate that the two rotaxanes **4.2** and **4.13** co-crystallize with morphologies that may be manipulated by varying the ratio between the two components.

4.3 Conclusion

In conclusion, the aim of this aspect of the project was to determine whether cyclodextrin-based [2]rotaxane self-assemblies that resemble insulated molecular fibres or coaxial cables also behave as molecular wires. IV experiments along the long axis of needle-shaped crystals of rotaxane **4.2** showed increasing current upon voltage variation. Based on the calculated conductivity, rotaxane **4.2** is classified as a semi-conductor. Preliminary experiments on a crystal of rotaxane **4.2** in an organic field effect transistor device showed again current variation upon voltage variation. Rotaxane **4.13** was also synthesized. The difference between rotaxane **4.2** and rotaxane **4.13** is the orientation of the amide groups within the dumbbells. Rotaxane **4.13** showed extended conjugation in the liquid and solid state, and the conductivity along the long axis of its prismatic-shaped crystals was similar to that observed for rotaxane **4.2**. Further conductivity experiments along a perpendicular axis of a crystal of rotaxane **4.13** showed no electron flow in that direction, demonstrating the insulating properties of the cyclodextrins surrounding the π-π stacked dumbbells. Given the current trend of miniaturization of electronic devices, this study represents a significant achievement, as it establishes the ability of rotaxanes to act as insulated molecular wires. Similar to polyrotaxane-based IMWs, these devices allow electric circuits to be scaled down to the size of macromolecules. However, unlike covalently bonded systems, the rotaxane-based IMWs exhibit a higher level of flexibility due to the reversible nature of their inter-molecular interactions

4.4 Experimental

4.4.1 General

Reagents: α-Cyclodextrin **4.11** was purchased from Nihon Shokuhin Kako Co., Japan, in 99.1% purity, and dried over P_2O_5 under reduced pressure to a constant weight before use. A reported procedure was used to prepare the rotaxane **4.2**.[9a] Other chemicals were purchased from commercial suppliers and used as received.

Freeze-drying: Solutions were freeze-dried with a Labconco Freezone 4.5 freeze-drier.

Melting Points: Melting points were determined on an Optimelt automated melting point apparatus and analysed with SRS Optimelt V. 1.107 software.

Thin-Layer Chromatography (TLC): TLC was carried out on aluminium backed 0.2 mm EMD Millipore silica gel 60 F_{254} plate. Developed plate was visualized either using UV light (254 nm) or by staining with a naphthalene-1,3-diol solution (0.1% w/v) in ethanol:water:H_2SO_4 (200:157:43), followed by heating.

High Performance Liquid Chromatography (HPLC): Analytical HPLC was carried out using a Hewlett Packard 1100 system with Agilent Chemstation software. Preparative HPLC was performed using a Waters 2996 photodiode array detector, a Waters 600 Controller, and a Waters 717 Plus Autosampler with Waters Empower 3 software.

Proton Nuclear Magnetic Resonance (^{1}H NMR): NMR spectra were acquired on Bruker Avance 400 and 600 spectrometers, using CD_3OD as solvent, and 3-(trimethylsilyl)-3,3,2,2-tetradeuteropropionic acid sodium salt as an external standard. The multiplicity of signals is reported as singlet (s), doublet (d) and multiplet (m).

Mass Spectrometry: High resolution electrospray ionisation (HR-ESI) mass spectra were recorded using a Waters LCT premier TM XE orthogonal acceleration time-of-flight (oa-TOF) mass spectrometer or ThermoFisher Scientific Orbitrap Elite™ Hybrid Ion Trap-Orbitrap Mass Spectrometer at 240k resolution.

UV-vis Spectrophotometry: UV-vis spectrophotometric data were acquired using a Shimadzu UV-2450 UV-vis spectrophotometer running with UV Probe Version 2.10 software.

Crystal data: Crystal data were collected using a SuperNova, Dual, Cu at zero, EosS2 diffractometer. The structures were solved by Dr Michael Gardiner and Dr Paul D. Carr at the Research School of Chemistry, Australian National University. Accelrys DS Visualizer 2.0 and Olex2 (OlexSys) were used to visualise crystal structures.

Microscopy: Two optical microscopes, inverted phase contrast Nikon TMS and a Nikon Alphaphot YS-2, were used to acquire microscope images.

Conductivity experiments: For the conductivity experiments, a Si wafer with a SiO_2 layer was used as gate electrode and dielectric layer, while either vapour-deposited gold films or silver paste Dotite D-550 were used for drain and source electrodes. The measurements were carried out in a N_2-filled glovebox using an Apollowave probe station microscope coupled to an external Keithley 4200-SCS semiconductor characterisation system. An optical microscope, Olympus SZ-LW61, was used to prepare samples.

4.4.2 Synthesis and characterisation

*Rotaxane **4.2***

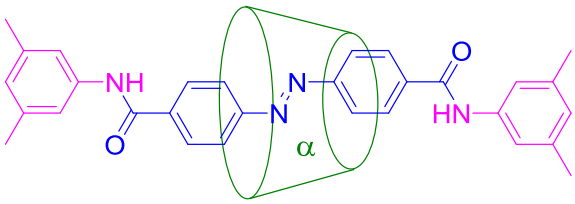

A solution of azobenzene-4,4'-dicarboxylic acid **4.10** (50 mg, 0.19 mmol), α-CD **4.11** (1.0 g, 1.05 mmol) and Et_3N (57 mg, 0.56 mmol) in water (20 mL) was equilibrated for 1 h at room temperature. DMT-MM (240 mg, 0.92 mmol) and 3,5-dimethylaniline **4.12** (57 μL, 0.45 mmol) were added to the reaction mixture, which was then stirred at room temperature overnight. The resulting solution was washed with EtOAc (5 x 25 mL). The aqueous layer was then concentrated under reduced pressure. The crude mixture was dissolved in MeOH and subjected to reverse-phase preparative HPLC. Fractions containing the product were combined, concentrated by rotary evaporation, and lyophilised to give the title compound **4.2** as an orange powder (62 mg, yield 22%).

TLC: (5:4:3:2 v/v/v/v *i*-propanol:ethanol:water:acetic acid)R_f = 0.80.

Melting point: 307-309 °C (dec.) [lit. [9a] 306-308 °C (dec.)].

^{1}H-NMR: (400 MHz, CD_3OD) δ_H 8.64 (d, *J* = 8.3 Hz, 2H, azo-H), 8.25 (d, *J* = 8.3 Hz, 2H, azo-H), 8.19 (d, *J* = 8.3 Hz, 2H, azo-H), 8.03 (d, *J* = 8.3 Hz, 2H, azo-H), 7.45 (s, 2H, aniline), 7.36 (s, 2H, aniline), 6.87 (s, 2H, aniline), 6.85 (s, 2H, aniline), 4.90–4.87 (m,

6H, CD H1), 3.85–3.38 (m, 36H, CD H2-6), 2.35 (s, 6H, Me), 2.34 (s, 6H, Me). Data consistent with lit. values.[9a]

HR-ESI-MS: (m/z) $[M + Na]^+$ calcd for $C_{66}H_{88}N_4O_{32}Na$, 1471.5279; found 1471.5261.

HPLC (Preparative): t_R = 7.0 min (column: Waters XBridge Prep C18 5 µm, 150 x 19 mm;10 mL/min MeOH/H2O 50:50 isocratic, detection wavelength: 352 nm).

HPLC (Analytical): t_R 10 min (column: Agilent Zorbax SB C18 3.5 µm, 150 x 4.6 mm; 1 mL / min MeOH/H_2O 20:80 isocratic, detection wavelength: 368 nm).

Crystal data: $C_{66}H_{102}N_4O_{42.49}$ M = 1631.43, T = 150.01(10) K, λ = 1.54184 Å, monoclinic, space group $P2_1$, a = 14.01561(8) b = 16.13656(10), c = 17.29833(10) Å, V = 3883.46(4) Å^3, Z = 2, Dc = 1.395 g cm^{-3} µ (CuKα) = 1.010 mm^{-1}, crystal size 0.30 x 0.11 x 0.05 mm. Θ_{max} = 73.860°, 61079 reflections measured, 14792 unique (R_{int} = 0.0269) which were used in all calculations. The final wR_2 was 0.0697 (all data) and R_1 was 0.0270 (I > 2(I)).

*Rotaxane **4.13***

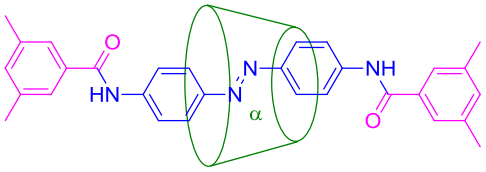

A solution of 4,4'-diaminoazobenzene **4.14** (45 mg, 2.1 × 10^{-4} mol) and α-CD **4.11** (1.4 g, 12 × 10^{-4} mol) in water (25 mL) was sonicated for 1 h, then stirred at room temperature overnight. In a separate flask, a solution of DMT-MM (230 mg, 8.4 × 10^{-}

^{4} mol) and 3,5-dimethylbenzoic acid **4.15** (130mg, 8.4 × 10^{-4} mol) in acetonitrile (50 mL) was stirred at room temperature overnight. The following day, the solution containing the activated benzoic acid was rotary evaporated, the residue dissolved in water (1 mL) and slowly added to the azobenzene solution, followed by the addition of Et_3N (57 mg, 5.6 × 10^{-4} mol). The mixture was then stirred at 40 °C overnight. The addition of DMT-MM (230 mg, 8.4 × 10^{-4} mol) and Et_3N (57 mg, 5.6 × 10^{-4} mol) was repeated and the mixture was again left to stir at 40 °C overnight. The resulting solution was washed with EtOAc (5 x 25 mL). The aqueous layer was concentrated under reduced pressure. The crude mixture was dissolved in MeOH/H_2O 40:60 and subjected to reverse-phase preparative HPLC. Fractions containing the product **4.13** were combined, concentrated by rotary evaporation, and lyophilised to give the title compound **4.13** as an orange powder (15 mg, yield 5%).

TLC: (*n*-butanol/ethanol/water 5:4:3) *R*f = 0.81.

Melting Point: 300-305 °C (dec.).

^{1}H NMR: (400 MHz, CD_3OD): δ = 8.51 (d, *J* = 8.8 Hz, 2H, azo-H), 8.01 (dd, *J* = 8.8 Hz, 4H, azo-H), 7.84 (d, *J* = 8.8 Hz, 2H, azo-H), 7.68 (s, 2H, benzoic acid), 7.59 (s, 2H, benzoic acid), 7.29 (s, 2H, benzoic acid), 7.27 (s, 2H, benzoic acid), 4.90–4.87 (m, 6H, CD H1), 3.89–3.38 (m, 36H, CD H2-6), 2.43 (s, 6H, Me), 2.42 (s, 6H, Me).

HRMS (ESI): *m/z* calcd for $C_{66}H_{88}N_4O_{32}Na$ $[M+Na]^+$ 1471.5279, found 1471.5286.

HPLC (Preparative): t_R 6 min (column: Waters XBridge Prep C18 5 µm, 150 x 19 mm; 10 mL / min MeOH/H_2O 50:50 isocratic, detection wavelength: 352 nm).

HPLC (Analytical): t_R 8 min (column: Agilent Zorbax SB C18 3.5 µm, 150 x 4.6 mm; 1 mL / min MeOH/H_2O 20:80 isocratic, detection wavelength: 368 nm).

Crystal data: $4(C_{30}H_{28}N_4O_2)\cdot4(C_{36}H_{60}O_{30})\cdot42.41(H_2O)$ M = 6561.77, T = 150 K, λ = 1.54184 Å, monoclinic, space group $P2_1$, a = 26.8301 (4) b = 23.5630 (4), c = *27.3530 (4)* Å, V = 16507.9 (5) Å^3, Z = 2, Dx = 1.288 Mg m^{-3} µ (CuK_α) = 0.95 mm^{-1}, crystal size 0.39 x 0.15 x 0.07 mm. Θ_{max} = 72.5°, 177875 reflections measured, 32838 unique (R_{int} = 0.048) which were used in all calculations. The final R[$F^2 > 2\sigma(F^2)$] = 0.130 and wR(F^2) = 0.374.

References

[1] G. Schill, H. Zollenkopf, *Liebigs Ann. Chem.* **1969**, *721*.

[2] a) S. Erbas-Cakmak, D. A. Leigh, C. T. McTernan, A. L. Nussbaumer, *Chemical reviews* **2015**, *115*, 10081-10206. DOI: http://dx.doi.org/10.1021/acs.chemrev.5b00146; b) R. A. Bissell, E. Córdova, A. E. Kaifer, J. F. Stoddart, *Nature* **1994**, *369*, 133-137. DOI: http://dx.doi.org/10.1038/369133a0; c) A. M. Brouwer, C. Frochot, F. G. Gatti, D. A. Leigh, L. c. Mottier, F. Paolucci, S. Roffia, G. W. H. Wurpel, *Science* **2001**, *291*, 2124-2128. DOI: http://dx.doi.org/10.1126/science.1057886; d) V. Balzani, M. Clemente-León, A. Credi, B. Ferrer, M. Venturi, A. H. Flood, J. F. Stoddart, *Proceedings of the National Academy of Sciences* **2006**, *103*, 1178-1183. DOI: http://dx.doi.org/10.1073/pnas.0509011103.

[3] a) C. A. Stanier, S. J. Alderman, T. D. W. Claridge, H. L. Anderson, *Angewandte Chemie International Edition* **2002**, *41*, 1769-1772. DOI: http://dx.doi.org/10.1002/1521-3773(20020517)41:10<1769::aid-anie1769>3.0.co;2-n; b) K. Yamauchi, A. Miyawaki, Y. Takashima, H. Yamaguchi, A. Harada, *The Journal of organic chemistry* **2010**, *75*, 1040-1046. DOI: http://dx.doi.org/10.1021/jo902393n.

[4] H. Onagi, C. J. Blake, C. J. Easton, S. F. Lincoln, *Chemistry – A European Journal* **2003**, *9*, 5978-5988. DOI: http://dx.doi.org/https://doi.org/10.1002/chem.200305280.

[5] R. E. Dawson, S. F. Lincoln, C. J. Easton, *Chem. Commun.* **2008**, 3980–3982. DOI: http://dx.doi.org/10.1039/B809014A.

[6] T. Girek, *J Incl Phenom Macro* **2012**, *74*, 1-21. DOI: http://dx.doi.org/10.1007/s10847-012-0112-1.

[7] F. Cacialli, J. S. Wilson, J. J. Michels, C. Daniel, C. Silva, R. H. Friend, N. Severin, P. Samori, J. P. Rabe, M. J. O'Connell, P. N. Taylor, H. L. Anderson, *Nat. Mater.* **2002**, *1*, 160-164. DOI: http://dx.doi.org/10.1038/nmat750.

[8] a) H. Onagi, B. Carrozzini, G. L. Cascarano, C. J. Easton, A. J. Edwards, S. F. Lincoln, A. D. Rae, *Chemistry* **2003**, *9*, 5971-5977. DOI: http://dx.doi.org/10.1002/chem.200305279; b) M. M. Cieslinski, P. J. Steel, S. F. Lincoln, C. J. Easton, *Supramolecular Chemistry* **2006**, *18*, 529-536. DOI: http://dx.doi.org/10.1080/10610270600837199.

[9] a) S. Maniam, M. M. Cieslinski, S. F. Lincoln, H. Onagi, P. J. Steel, A. C. Willis, C. J. Easton, *Org. Lett.* **2008**, *10*, 1885-1888. DOI: http://dx.doi.org/10.1021/ol8002145; b) C. A. Stanier, M. J. O'Connell, W. Clegg, H. L. Anderson, *Chemical Communications* **2001**, 493-494. DOI: http://dx.doi.org/10.1039/B010015N; c) J. Terao, A. Tang, J. J. Michels, A. Krivokapic, H. L. Anderson, *Chem. Commun.* **2004**, 56-57. DOI: http://dx.doi.org/10.1039/B311762F; d) H. Y. Lee, PhD thesis, the Australian National University **2014**.

[10] A. K. Mukherjee, N. Kumari, *Physics Letters A* **2018**, *382*, 1413-1418. DOI: http://dx.doi.org/https://doi.org/10.1016/j.physleta.2018.03.018.

[11] H. Yun, S. Kim, H. Kim, J. Lee, K. McAllister, J. Kim, S. Pyo, J. Sung Kim, E. E. B. Campbell, W. Hyoung Lee, S. Wook Lee, *Scientific reports* **2015**, *5*, 10220. DOI: http://dx.doi.org/10.1038/srep10220.

[12] J. S. Wan, H. Liu, in *Nanowires - Implementations and Applications*, Semiconducting Oxide Nanowires: Growth, Doping and Device application, Abbass Hashim, IntechOpen, **2011**.

[13] Y. Diao, L. Shaw, Z. Bao, S. C. B. Mannsfeld, *Energy & Environmental Science* **2014**, *7*, 2145-2159. DOI: http://dx.doi.org/10.1039/C4EE00688G.

[14] B. Mitchell, R. Ekey, R. McCullough, W. Reitz, *The Physics Teacher* **2018**, *56*, 75-78. DOI: http://dx.doi.org/10.1119/1.5021431.

[15] K. M. Tenny, M. Keenaghan, *Ohms Law*, StatPearls Publishing Copyright © 2021, StatPearls Publishing LLC., Treasure Island (FL), **2021**.

[16] A. Heeger, A. MacDiarmid, H. Shirakawa, *Conducting polymers : Nobel Prize in Chemistry* **2000**.

[17] a) T. Shimomura, T. Akai, M. Fujimori, S. Heike, T. Hashizume, K. Ito, *Synt. Met.* **2005**, *153*, 497-500. DOI: http://dx.doi.org/http://dx.doi.org/10.1016/j.synthmet.2005.07.305; b) J. Terao, Y. Tanaka, S. Tsuda, N. Kambe, M. Taniguchi, T. Kawai, A. Saeki, S. Seki, *Journal of the American Chemical Society* **2009**, *131*, 18046-18047. DOI: http://dx.doi.org/10.1021/ja908783f.

[18] Y. He, P. Fu, X. Shen, H. Gao, *Micron* **2008**, *39*, 495-516. DOI: http://dx.doi.org/https://doi.org/10.1016/j.micron.2007.06.017.

[19] H. Li, J.-L. Brédas, *National Science Review* **2020**, *8*. DOI: http://dx.doi.org/10.1093/nsr/nwaa167.

[20] C. Yumusak, M. Abbas, N. Sariciftci, *Journal of Luminescence* **2012**, *134*, 107-112. DOI: http://dx.doi.org/10.1016/j.jlumin.2012.09.003.

[21] V. P. Liyana, A. M. Stephania, K. Shiju, P. Predeep, *Journal of Physics: Conference Series* **2015**, *619*, 012029. DOI: http://dx.doi.org/10.1088/1742-6596/619/1/012029.

[22] a) Y. Inoue, in *Annual Reports on NMR Spectroscopy, Vol. 27* (Ed.: G. A. Webb), Academic Press, **1993**, pp. 59-101; b) S. Wataru, Y. Yasuhiko, I. Yoshio, C. Riichirô, T. Keiko, H. Kenjiro, *B Chem Soc Jpn* **1990**, *63*, 3175-3182. DOI: http://dx.doi.org/10.1246/bcsj.63.3175.

Chapter 5 - CONCLUSIONS AND FUTURE WORK

This Thesis presents the work undertaken towards the construction of molecular devices based on cyclodextrin host-guest inclusion complexes, with a strong focus on the synthetic strategies to build rotaxanes and daisy chains.

Molecular daisy chains were initially explored in Chapter Two as a potential platform to build molecular muscles. The work was focused on the construction of polymolecular systems because of their potential ability to amplify expansion and contraction behaviour. The *in situ* oligomerisation of self-assembled dimeric complexes was shown to be a successful method to synthesize an oligomeric series of interlocked cyclodextrin-based [c2] daisy chains. Unlike the reported stepwise approach of linking pre-formed interlocked cyclic dimers, in this method monomers are directly extended into oligomers. This one-pot reaction yielded eight distinct polymolecular species, including different types of tetramer, a hexamer, an octamer, and a decamer. These are complex supramolecular species derived from the condensation of up to sixteen molecular components and from multiple reactions, ten in the case of the decamer. Following the isolation and characterisation of the key oligomers, preliminary photochemical experiments showed reversible isomerisation of the azobenzene moieties of the tetrameric inclusion complex. The evaluation of the potential ability of the whole series to act as molecular muscles is the next logical step towards the application of these species in molecular devices. The incorporation of [c2] daisy chain rotaxanes in polymeric structures gives access

to a wide range of functional materials, including switchable nano-devices and smart nano-robots.

Rotaxanes were the focus of the following Chapters because of their intrinsic synthetic appeal and their crucial role in the development of molecular devices. Chapter Three presents an innovative synthetic method to prepare [2]rotaxane orientational isomers. While isomeric rotaxanes are usually obtained by capping a mono-capped guest included in an asymmetric host, this work demonstrates that a pre-formed, symmetric [2]rotaxane can be converted into two isomeric species through desymmetrization. Pyridinium dichlorobromate was found to be a successful bromination agent and its reaction with a previously known rotaxane gave two mono-brominated isomers, which were isolated and characterised. The NMR analysis of both compounds did not provide enough information to allow the distinction between the orientational isomers, therefore alternative approaches such as X-ray crystallographic studies would likely be useful to achieve a full structural analysis of the new species. In addition to their synthetic appeal, mono-functionalized rotaxanes can play a key role in surface modification, as well as in driving directional motion in molecular machines.

The work presented in Chapter Four focuses on the discovery of cyclodextrin-based rotaxanes as insulated molecular wires. A rotaxane previously synthesized in the group was chosen as the first candidate for conductivity experiments because of its intra- and inter-molecular co-planarity throughout the strand of the dumbbell unit.

Long needle-shaped crystals were grown and utilised to try different device settings to measure their electric properties. When a crystal was placed between two silver electrodes, a conductivity value typical of semi-conductors was detected. Blank experiments combined with X-ray crystallographic analysis established that the conductivity observed through the longest axis of the needle was the result of electron flow along the rotaxane axles. This experiment demonstrated the ability of self-assembled arrays of cyclodextrin-based rotaxanes to act as molecular wires. Crystal engineering was then utilised to design and synthesize a new [2]rotaxane, differing from the previously known rotaxane in the orientation of the amide bond. The new molecule showed extended π-conjugation in solution and a similar level of conductivity compared to the first sample analysed. Insulating properties were also found in the new rotaxane, which demonstrated its ability to act as an insulated molecular wire. Preliminary experiments on a rotaxane-based OFET showed an increasing current upon application of a negative gate voltage. The utilisation of CD-based rotaxanes as insulated molecular wires is likely to be further explored as part of the current miniaturization trend for the development of future microelectronic devices.

In conclusion, cyclodextrin-based supramolecular complexes, including daisy chains and [2]rotaxanes, have shown significant potential to build molecular devices and are therefore expected to be deployed in future applications as highly functional materials.